Department of Mechanical Engineering

Use of Air Cooling and its Effectiveness in Dry Machining Processes

Brian Boswell

This thesis is presented for the degree of
Doctor of Philosophy
of
Curtin University of Technology

June 2008

CANDIDATE STATEMENT

To the best of my knowledge and belief this thesis contains no material previously published by any other person except where due acknowledgement has been made. This thesis contains no material which has been accepted for the award of any other degree or diploma in any university.

ABSTRACT

Traditional liquid coolants used in metal machining are known to contain chemical carcinogens that could present serious health risks for machine operators and have inherent waste disposal concerns on the environment. In lessening these adverse effects, the manufacturing industry continually seeks to develop machining techniques incorporating liquid-less (dry) methods or environmentally benign coolants. Air-jet cooling is widely regarded as a viable alternative for liquid coolants in machining processes. This thesis proposes a novel air jet cooling arrangement, and assesses its thermal effectiveness and operational compatibility for specific requirements in metal cutting operation.

For tests, steel rods were machined on a standard lathe workbench at selected cutting depth, feed and speed. Type 1040 steel, which is commonly used in automobile industry, was chosen as work piece material. Instead of traditional liquid coolant, a specially designed compressed air jet is used to dissipate heat generation in the cutting zone at the tool tip. The tool tip is presented orthogonally to the work piece to maintain conformity with relevant established cutting tool theories.

A special air jet configuration based on a Ranque-Hilsch vortex tube was designed and developed for cooling the cutting zone and tool tip. The tool tip temperatures were measured by installing thermocouples at strategic locations on the tool piece and recorded on a data-logger for a range of cutting depths, feeds and speeds. The cutting power was measured with a power meter attached to the electrical power supply to the lathe. For comparison purposes, tests were also conducted with conventional single-nozzle air jets in place of the vortex-tube jets, using traditional liquid coolant and without any cooling applied to the tool tip. A thermal vision camera was also deployed for selected tests to ascertain the temperature characteristics at the tool tip.

The data was analysed to establish the thermal characteristics at the tool tip with vortex tube air jet, conventional air jet and no air jet cooling. The measured temperatures and cutting data were used to make assessments on cooling efficiency of jets used and surface finish quality of work piece. Estimates of tool life were made from the cutting theory to determine the effectiveness of the cooling systems used in the machining process.

It is found that the proposed vortex tube based air jet cooling arrangement provides a highly efficient heat removal mechanism for metal cutting and delivers thermal cooling performance very much comparable to traditional liquid coolants without the inherent chemical exposure risks to machine operators and harmful impact on the environment. With the proposed air jet cooling, the tool life is very much unchanged and the surface finish quality of work piece shows no significant change while savings will realise though lesser dependency on liquid coolant requiring careful disposal and associated costs.

ACKNOWLEDGEMENTS

The author gratefully acknowledges the assistance of the following people:

Associate Professor Tilak T Chandratilleke for all his guidance and help during the many years taken to complete this research;

Dr Ian Davies whose advice on writing this thesis was most appreciated;

The Mechanical Engineering Department technicians for their assistance during the many hours of testing and manufacturing of test equipment used is this research.

Finally, I especially thank my wife Marion Boswell without whose encouragement and help this thesis would never have been completed.

CONTENTS

APPENDIX

LIST OF FIGURES

LIST OF TABLES

NOTATION

friction surface area	A^1	mm^2
vortex cold nozzle area	A	m^2
constant	a_1	
constant	a_2	
chip cross sectional area	A_o	mm^2
constant	b	
constant	c	
cost	C	
specific heat capacity	c_p	
constant	C_t	
depth of cut	d	mm
jet diameter	D	mm
bar diameter	D_1	mm
machine diameter	D_2	mm
constant	E_1	
friction force	F	kN
feed rate	f	m/min
cutting force	F_c	kN
force perpendicular to cutting velocity	F_f	kN
percentage of full load	FL	
normal force on the shear plane AB	F_n	kN
shear force	F_s	kN
frequency	f_s	
nozzle tool tip gap	G	mm
contact length	h	mm
air enthalpy	h_a	kJ/s
crater wear depth	h_c	mm
thermal conductivity	K	W/m K
kinetic energy	KE	kJ
tool life cutting time	L	min.
latent heat evaporation	L_e	kJ/kg
cutting edge length	l_e	mm

rubbing distance	l_f	mm
mass	m	
mass of cutting fluid	m_{cf}	
motor efficiency	ME	
motor load	MP	kW
normal force at tool tip	N	kN
number of shocks	n_s	
Nusselt number	Nu	
operating hours	OH	hr
tool pressure	p	N/mm^2
air pressure	P	MPa
volumetric specific heat	ρc	$J/cm^3\ ^oC$
potential energy	PE	kJ
heat quantity	Q	
chip equivalent	q	
resultant force	R	kN
radial distance from centre of jet	r	mm
ideal gas constant	R	
chip ratio	r_c	
Reynolds number	Re	
tool nose radius	r_ε	mm
thermal number	R_T	
surface roughness	R_y	μm
specific heat of material	S	J/kg K
system entropy	S	kJ
cutting distance	S_{cd}	mm
tool temperature	T	K
feed/rev.	t_1	mm/rev
chip thickness	t_2	mm
absolute temperature	T_a	K
temperature rise in the shear zone	T_{AB}	^oC
mean temperature rise of chip	T_c	^oC
cold air exit temperature	T_c	^oC
temperature of the friction surface	T_f	^oC

tool flank	T_{flank}	K
hot air exit temperature	T_h	^oC
air inlet temperature	T_i	^oC
interface temperature	T_{int}	^oC
maximum rise at tool chip interface	T_m	^oC
mean chip interface temperature	T_s	^oC
shear zone temperature	T_{sz}	^oC
tool thermocouple temperature	T_{th}	K
tool temperature	T_{tool}	K
work temperature	T_w	^oC
system internal energy	U	kJ
specific energy during cutting	U_c	J/m^3
cutting velocity	V	m/s
air velocity	V_a	m/s
spindle speed	N	rpm
flank wear	VBb	mm^3
chip velocity	V_c	m/s
shear velocity	V_s	m/s
chip width	w	mm
tool wear	W	
wear rate due to abrasion	W_a	
wear rate due to brittle fracture	W_b	
wear rate due to other mechanism	Wi	
wear rate due to rate processes	Wr	
wear rate	w_s	
adjusted wear rate	w_{s1}	
distance between air stream	z	m
mass flow rate	$\dot{m}$	kg/s
heat flow rate	$\dot{Q}$	kJ/s
system work	$\dot{W}$	kJ/s
rake angle	α	deg
abrasive resistance of the tool	σ_a	
resistance to brittle fracture	σ_s	

thermal diffusivity	α_t	mm^2/s
average shear plane temperature	β	^oC
shear strain	γ	
heat conducted into the work	κ	W/m K
friction angle	λ	deg
friction co-efficient	μ	
cold fraction	μ_{cf}	
density of the work material	ρ	kg/m^3
volumetric specific heat	ρc	$J/cm^3\ ^oC$
side cutting edge	σ	deg
abrasive resistance of the tool	σ_a	
resistance to brittle fracture	σ_s	
shear strength of the work material	τ	MN/m^2
shear angle	ϕ	deg
tool sharpness	ψ_T	

CHAPTER 1

INTRODUCTION

1.1 Overview Of The Machining Process

Since the beginning of the industrial revolution metal cutting manufacturing processes have involved the removal of unwanted material. Metal removal continues to be the principal method of manufacturing. The advent of rapid prototyping machines capable of producing the most complicated of shapes still does not reduce the volume of machining necessary today. Interestingly, in 1971, the Delphi Type Forecast [1] for the International Institution for Production Engineering predicted that machining would remain the principal method of metal product manufacturing. The popularity of machining throughout the world however ignores one major problem: the enormous amounts of liquid cutting fluid needed to prolong tool life gives rise to serious environmental issues as well as health concerns for the machine operators. Being aware of this, manufacturers worldwide have been trying to minimise or eliminate the use of liquid coolant during metal cutting. This has given rise to manufacturers incorporating a limited amount of dry machining into the manufacturing processes. The aeronautical industry relies on dry machining for most of its metal cutting processes due to the machinability of lighter and softer materials. On the other hand the automotive industry is desperate to achieve dry machining for economic and environmental (green manufacturing) reasons. Unfortunately, the materials used in this particular industry are harder and tougher, and are not as easy to machine as aluminium alloys used in the aerospace industry. A brief history of the metal cutting process and its investigation can be found in ‘The Mechanics of Machining” by Armarego and Brown [2], and a more detailed review in an article by Finnie [3].

1.2 Machining Process

1.2.1 Metal cutting chip formation

Fundamentally, machining is a material removal process where a layer of material is removed in the form of chips from the workpiece by the action of a wedged shaped

cutting tool. The first studies of chip formation were qualitative in nature and investigated the material flow (deformation) in the chip formation. Rosehain and Sturney [4] attempted to classify the process according to the type of chip produced. These authors classified the chip as “shear”, “tear”, and “flow chips”. This classification was used until 1938 when Ernes [5] presented his classical observation of chip formation. They were:

(a) Discontinuous Chip

Figure 1.1 shows a segmented discontinuous chip, which exhibits some deformation even though it is broken at fairly regular intervals by fracture across the width and thickness of the chip. The associated machine surface is rough and irregular.

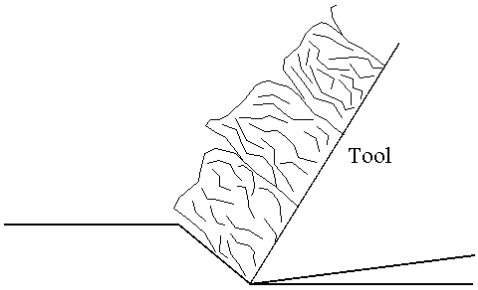

Figure 1.1: Discontinuous chip

Shown in Figure 1.2 is a continuous chip. As the name suggests, the chip is formed as a continuous ribbon when machining ductile materials under ideal cutting conditions. This chip is the result of continuous plastic deformation leading to steady cutting forces and a smooth machined surface.

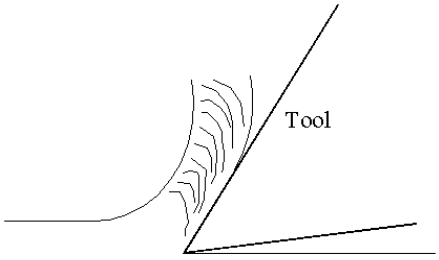

Figure 1.2: Continuous chip

(b) Continuous Chip with Built-up Edge

This type of chip is formed when machining ductile materials under certain cutting conditions, and is shown in Figure 1.3. The chip is continuous, but at the cutting edge on the tool face there is a build up of deformed material. Ernest [5] was also able to show that the build up and breakdown of this deformed material was cyclic in nature. The breakdown was such that part of the build-up material attached itself to the machined surface, while the other part attached itself to the back of the chip. Due to the short cycle time the associated machined surface is rough and irregular.

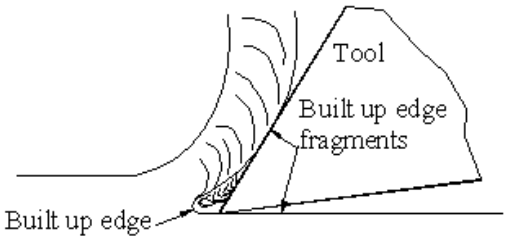

Figure 1.3: Continuous chip with built up edge.

1.2.2 Metal cutting

The normal and most common metal cutting condition is known as oblique machining, which is the cutting process when turning, milling and drilling. Figure 1.4 shows metal being removed by a typical oblique turning process.

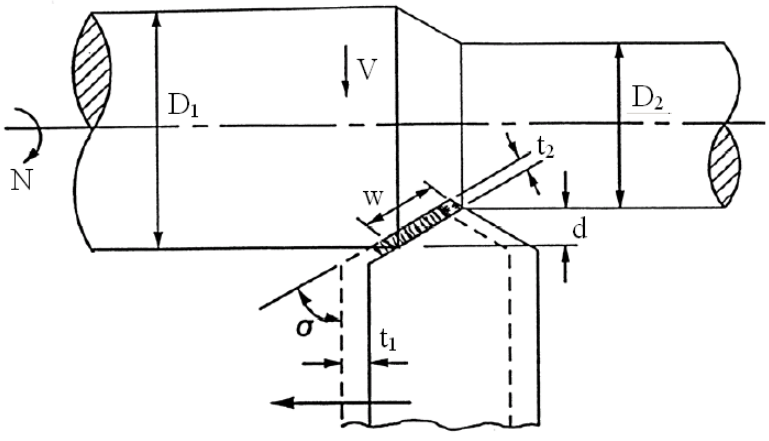

V = cutting speed, d = depth of cut, w = chip width, t_2 = chip thickness, t_1 = feed/rev, N = spindle speed, σ = side cutting edge, D_1 = bar dia, D_2 = machined dia.

Figure 1.4: Metal removal by oblique turning process.

Oblique machining is a complex machining process due to the shape of the cutting edge. Attempts have been made to analyse the process Lin and Oxley [6], although this results in a complex solution to analyse. Figure 1.5 shows a simplified metal cutting process known as orthogonal machining. The orthogonal cutting process is normally the analysis used by researchers as it eliminates a number of variables that can affect the cutting theory. For this reason the orthogonal model is used for the analysis of the machining process in this research.

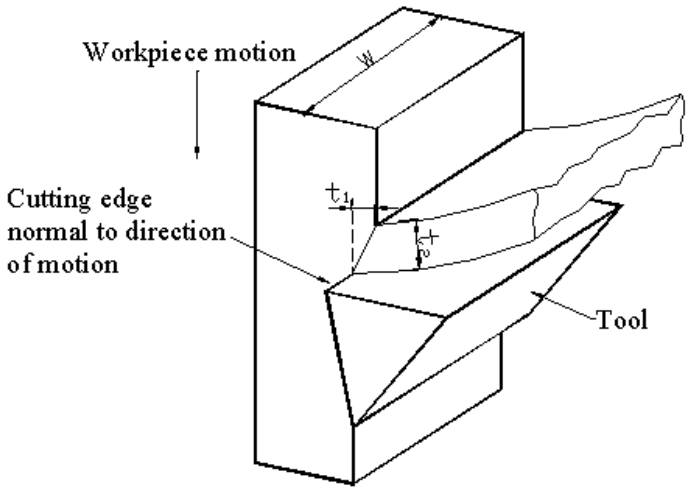

Figure 1.5: Metal cutting configuration needed for orthogonal machining.

In orthogonal machining the cutting edge of the tool is set perpendicular to the direction of the cutting, and parallel to the surface being machined, as shown in Figure 1.5 and 1.6. Also, the tool must overlap the cutting surface such that the metal removal is only done on the primary surface. If the width of cut is very much larger than the depth of cut shown in Figure 1.5 $t_1 < w$, then the flow of the material approximates to that of plane strain: that is the flow is in two directions only.

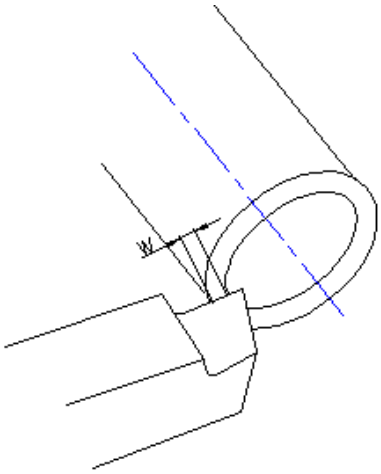

Figure 1.6: Special cutting conditions needed on a lathe to obtain orthogonal machining.

Under certain conditions on the lathe the machining processes can be considered as approximately orthogonal. These conditions are that the feed must be small relative to the depth of cut - making most of the cutting taking place in the direction of the feed, and the cutting on the nose of the tool will be negligible (Mikell P. Groover [7]). The special machining conditions that allow orthogonal analysis to be used were employed in determining the set feed rate and depth of cut on the engine lathe.

1.3 Generalisation Of Tool Life

Information available for establishing tool life is largely generalised and empirical in nature. This is fundamentally due to the cutting process, as the changing of one parameter will result in a new set of data. For example, the classification of material and processes in the Machining Data Handbook [8] is wide and varied. When considering low carbon steels, it is noted that as many as twenty different steels are found in that group, and suggests cutting conditions for different operations are only in the form of “first try” conditions. Such data can in fact have a variability of as much as 50 percent to 100 percent. Also, the tool life expected is stated at 30 to 60 minutes for a throw-away carbide tool tip for continuous cutting. This is in fact another generalisation because there is also great variability in the shape/type of tips and grades of tips. Just how large is the variability cannot be estimated; that in turn reduces the reliability of the available data.

In order to overcome these difficulties and provide more reliable data, many countries have set up Machining Data Banks [9] based on information on the machining process collected from various sources. In conjunction with this available machining data, it is apparent that appropriate tool life tests need to be carried out for the material and tool tips used in this research. This will allow this research to determine the effectiveness of air-cooling of the tool tip, by comparing air-cooling test data against reliable tool life data.

1.4 Tool Tip Heat Generation

Manufacturers know that the hotter the tool becomes the quicker the tool tip will break down and need to be replaced. Clearly it is essential for modern manufacturing to prolong tool life to maximise production. The main parameters that are known to have influence on the tool tip temperature are the tool tip material, the material being cut, and the cutting velocity. Figure 1.7 shows typical temperatures that can be generated in the cutting zone. As the yield strength of the material is approached, the heat helps the separation of the chip from the work piece.

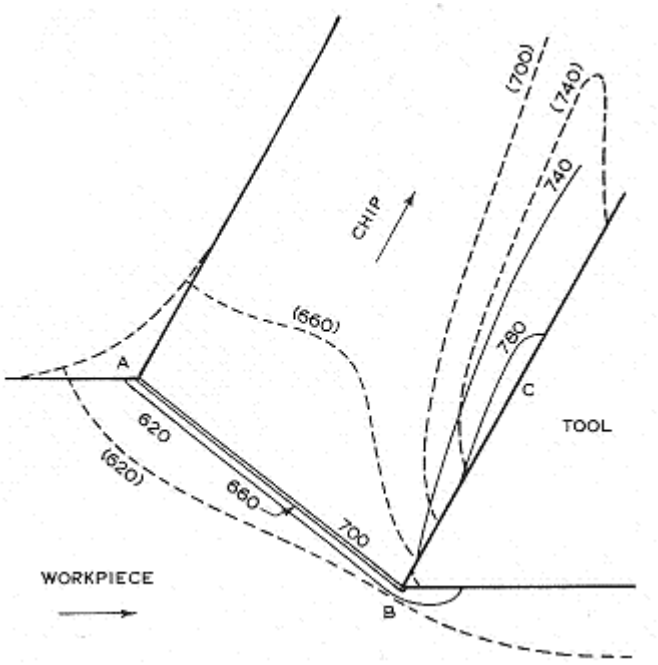

(obtained from G. Bothroyd) [10]

Figure 1.7: Temperatures at shear plane AB.

The more heat in the primary cutting zone the easier the chip will separate. However, with too much heat the tool tip material will also want to separate from the tool tip, vastly reducing its tool life. Traditionally, the approach to prolong tool life is to supply large amounts of liquid cutting fluid to the cutting zone to cool the tool tip. The consequence of this is to add additional cost to the product, and appropriate costly disposal preparations must be in place for the contaminated cutting fluid. Therefore, exploiting the potential of dry machining is economical and environmentally necessary for modern manufacturing.

1.5 Environmental Cost Of Liquid Coolant

Manufacturing industries in industrial nations throughout the world are now both coerced by government legislation and the growing awareness of society to ensure that their manufacturing processes do not harm the environment. For this reason increased attention is now paid to the environment and health impact of industry activities. In the case of the metal cutting process, manufacturers are encouraged to find ways to reduce the use of liquid coolant during machining. Over the years other methods of cooling the tool tip have been tried with some degree of success. CO_2 was used in the mid-nineteen fifties and hailed as the greatest solution to the cooling of tool tips. However, it was soon discovered by those companies who adopted this method of cooling to be expensive and relied on a large amount of auxiliary equipment. Today this method of cooling would not be considered on environmental grounds, as CO_2 is a “greenhouse gas”, and would promote this phenomenon. In more recent times, the use of cryogenic cooling has been used with some success, but this method also depends on large amounts of auxiliary equipment available to supply the liquid nitrogen, and this is expensive to use. In addition the machine tool operators safety is of concern, as care must be taken in using this very cold fluid.

As more attention is being focused on the role of cutting fluids in machining, there is a new ISO 14000 international environmental management system standard to guide manufacturers. The aim here is to help manufacturers reduce the environmental burden produced by manufacturing. An environmental burden analysed by H. Narita *et al.* [11] that considers all aspects of the machining process shows that liquid coolant alone contributes to 0.98 kg-CO_2/L equivalent CO_2 emission intensities. This is the amount of greenhouse gas that has been produced during the making of the

liquid coolant and from using it. So the machine tool energy efficiency and the impact of the process waste have a negative effect on the environment D. Dudzinski [12]. These CO_2 emission values clearly show why dry machining is being considered more and more for applicable machining processes.

1.6 Coated Tungsten Tool Tips

Recent advances in tool tip coatings have proven to be most effective in improving the performance of dry cutting by reducing the ability of the cut material to stick to the tool tip. Figure 1.8 shows a tungsten coated tool tip with three layers. This tool tip has outstanding wear resistance and toughness and is:

- suitable for fast and dry machining;
- suitable for mass and large batch production;
- suitable for unmanned machining.

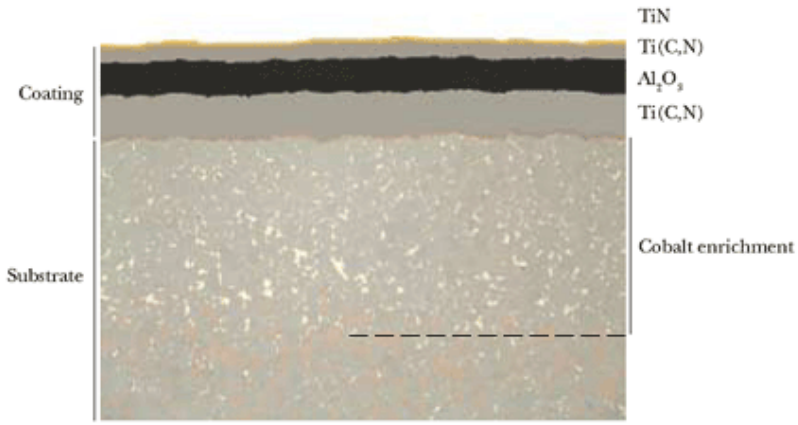

(Picture from Seco web site on the 6th Dec. 2005) http://www.secotools.com/template/start

Figure 1.8: Typical materials used to produce tip insert.

However, even with the improvements to tool tip materials, tool life will always be reduced due to the higher working temperatures of dry machining K. Causton [13]. As previously outlined, the use of dry machining can be considered as a “green” manufacturing process as there is no pollution generated waste with the cutting of the material. The significance of using dry machining can be highlighted when we note that, in Australia alone, millions of litres of liquid coolant are consumed each year. This has been estimated to constitute about 7 to 17 percent of the total machining

costs. The equivalent CO_2 emissions contributed by the disposal of the liquid coolant can be evaluated as 0.192 kg-CO_2/L. Research has shown that dry machining is preferably carried out at high speed N.A. Abukhshim *et al.* [14]. Although cutting metal at high speeds is associated with high temperatures, most of the additional heat generated is removed by the chips.

1.7 Objective of Research

The object of this research is to show that dry machining with air-cooling can be shown to be as effective as - if not better than - traditional wet machining of metals. Dry machining alone eliminates the use of coolant and the waste burden on the environment, therefore reducing machining costs. Unfortunately, dry machining by itself reduces the life expectancy of the cutting tool due to the high temperatures involved in machining. Dry machining with the addition of air-cooling extends tool life during machining. Air-cooling reduces the temperature at the tool interface, it is readily available and environmentally friendly, it is easy to work with, and it is also cost effective. However, just applying a jet of air does not simply provide the solution. The challenge is to ensure that air-cooling can be made to be as effective as traditional wet machining methods of cooling the tool tip during machining. Also, the performance of the air-cutting process should not produce an inferior surface finish in comparison to one produced by traditional coolant.

CHAPTER 2

REVIEW OF PREVIOUS WORK - MACHINE TOOL COOLING

2.1 Introduction

Metal cutting theory and tool cooling approaches are presented in this literature review to obtain a sound understanding of the metal cutting process. From the analysis of these theories the most important parameters are identified that affect the tool tips performance. The major detrimental parameter to the tool performance is the generation of heat at the tool interface. This increased temperature at the tool interface has proved to have an enormous effect on the wear mechanisms. To reduce the wear on tool tips it is essential to dissipate the generated heat at the cutting zone. An understanding of how the heat is generated and what affects it has on the tool tip is essential in any development of an efficient new air-cooling system for the tool tip. Measuring meaningful tool tip temperature during machining has always been extremely difficult. An attractive alternative approach has been the development of mathematical models that enable you to calculate the tool tip temperature. The earlier analytical work on steady-state temperatures generated during metal cutting was developed by Chao and Trigger [15], although there are other analytical models including the model by Boothroyd [10] as modified by Oxley [16].

2.2 Mechanics Of Metal Cutting

2.2.1 Cutting theory

Most analytical studies of chip formation have been restricted to continuous chip formation due to the steady state conditions under which the chip is formed. The type of chips that were formed during the experimental tests in this research were all of this type. Based on observations of the chip formation process, Ernst [17] derived the geometrical configuration as shown in Figure 2.1, resulting in the shear plane model for the chip formation.

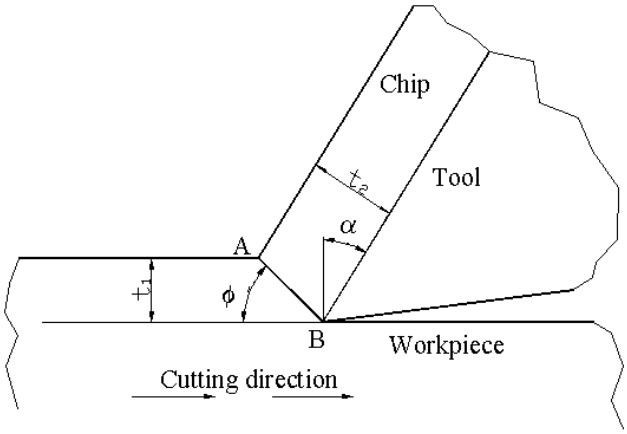

Figure 2.1: Shear plane model of chip formation

However, it has long been known that the actual process of chip formation is in two separate shear zones Christopherson *et al* [18]: a primary shear zone in front of the tool, and a secondary deformation zone at the tool chip interface as shown in Figure 2.2. Ernest derived the model by neglecting the secondary deformation zone and idealising the primary shear zone by a plane.

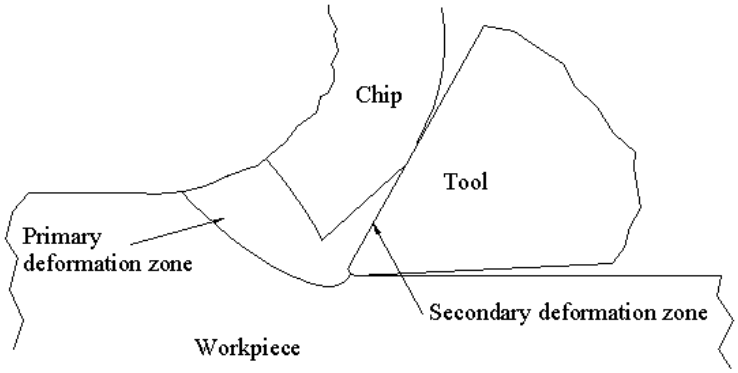

Figure 2.2: Actual plastic shear zone of chip formation

It also assumes that the tool is perfectly sharp and the chip curl is neglected. The chip is assumed to be formed by simple shear on a shear plane "AB", as shown in Figure 2.3 which is at the shear angle, ϕ, to the cutting velocity, V. The shear angle is the defining parameter for the geometry of the shear plane model. The model assumes that the work material approaches "AB" with the cutting velocity. This implies a discontinuity in the tangential velocity along "AB" called the shear velocity, V_s, which is acceptable as only the velocity normal to "AB" must be continuous.

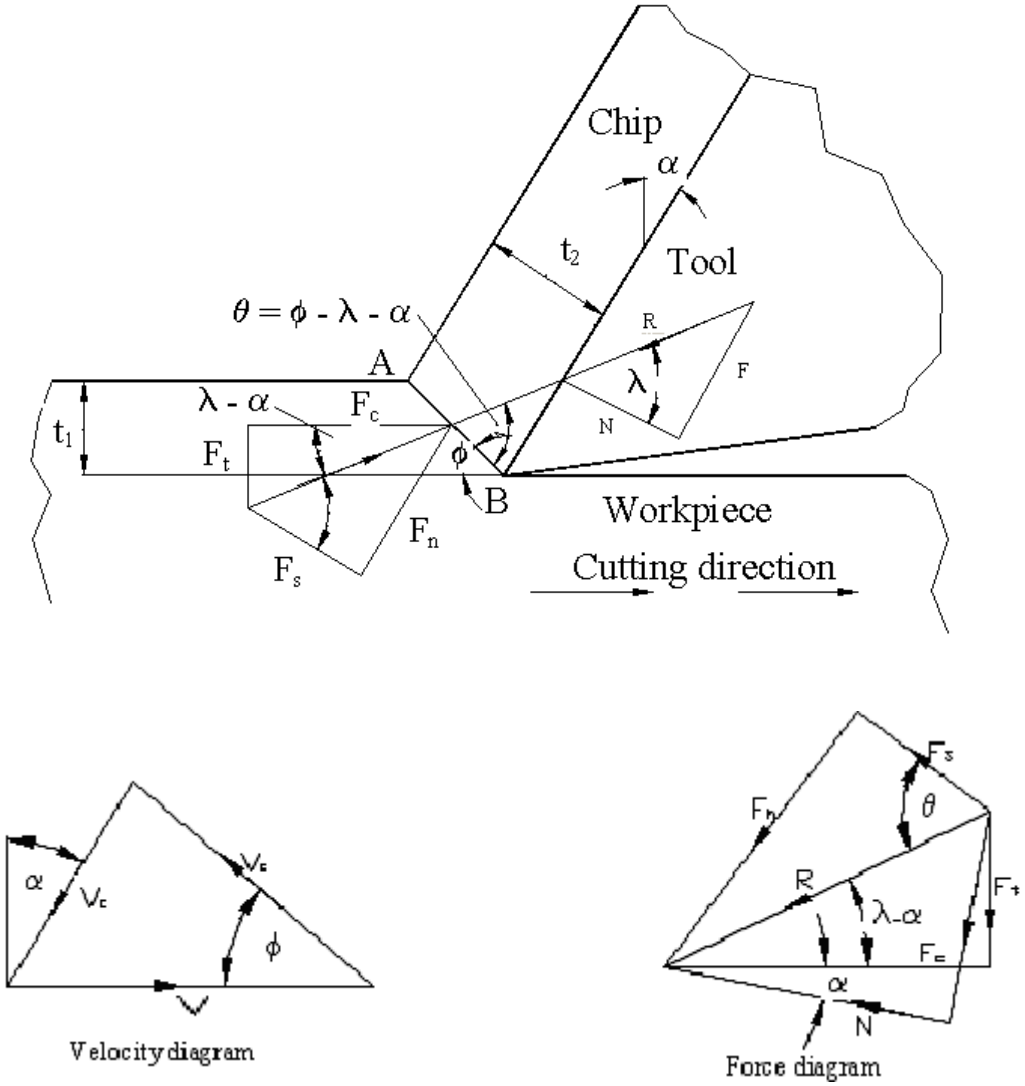

Figure 2.3: Shear plane model of chip formation showing force and velocity.

From Figure 2.3 it is observed that the cutting velocity, shear velocity and chip velocity, V_c, can be related by the equations (2.1) and (2.2) obtained from Altintas [19]:

$$V_c = \frac{V \sin \phi}{\cos(\phi - \alpha)} \tag{2.1}$$

$$V_s = \frac{V \cos \alpha}{\cos(\phi - \alpha)} \tag{2.2}$$

The total shear strain for chip formation can be calculated by assuming that the chip formation process is in pure shear, in the direction of V_s as shown in Figure 2.4.

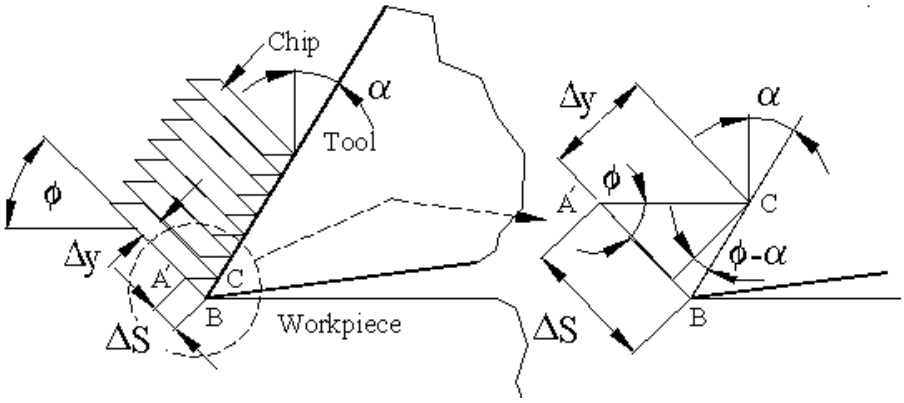

Figure 2.4: Block slip model for total shear strain of chip formation.

The shear strain, γ, is defined as the ratio of the tangential displacement of an element of the material to its height and is given as:

$$\gamma = \frac{\Delta s}{\Delta y} = \frac{\cos\alpha}{\sin\phi\cos(\phi-\alpha)} \tag{2.3}$$

Ernest and Merchant [17] produced a set of equations relating to force, angle and velocities for cutting from basic geometry, as shown in Figure 2.3. They assumed that the chip was in equilibrium under the action of two forces, one transmitted from the plane "AB" and the other coplanar force transmitted to the chip by the tool, which is the resultant force, *R*. This force can be resolved into the following components, as shown in Figure 2.3: where *F* is the friction force, *N* is the normal force at the tool chip interface, F_s is the shear force, F_n is the normal force on the shear plane "AB", F_c is the cutting force parallel to the cutting velocity, and F_f is the force perpendicular to the cutting velocity. The angle λ, between *R* and *N*, is defined as the friction angle:

$$\tan\lambda = \frac{F}{N} \tag{2.4}$$

Calculation of the cutting forces can only be made when the cutting conditions for the tool are known. Therefore it is necessary to know the tool rake angle, α, the

undeformed chip thickness, t_1, and the cutting velocity, V. The geometry of the cutting process would be incomplete without the shear angle, ϕ, or chip thickness, t_2, included. Without this information the cutting forces or temperature may be estimated. In order to obtain a solution for ϕ, Ernest and Merchant made use of the fact that "AB" is in the direction of maximum shear strain-rate and it is infinite in this direction as a result of the velocity discontinuity. Based on this the authors defined the two cutting forces F_f and $F_{c,}$ in terms of ϕ, λ and α, allowing the shear stress along "AB" to be calculated using the equations (2.5 and 2.6):

$$F_c = \frac{t_1 w \tau_{AB} \cos(\lambda - \alpha)}{\sin\phi \cos(\phi + \lambda - \alpha)} \tag{2.5}$$

$$F_f = \frac{t_1 w \tau_{AB} \sin(\lambda - \alpha)}{\sin\phi \cos(\phi + \lambda - \alpha)} \tag{2.6}$$

where, t_1 and w, are the undeformed chip thickness and width of cut. It was assumed that ϕ would be such as to make "AB" a direction of maximum shear stress:

$$\frac{\partial \tau_{AB}}{\partial \phi} = 0 \tag{2.7}$$

which derives equation (2.8).

$$\phi = \frac{\pi}{4} + \frac{\alpha}{2} - \frac{\lambda}{2} \tag{2.8}$$

2.2.2 Heat generated by plastic deformation and friction

During machining heat is generated as the chip travels over the top face of the tool as shown in Figure 2.5. The primary heat is caused by the chip undergoing plastic deformation with secondary heat being generated from friction as the chip moves over the tool.

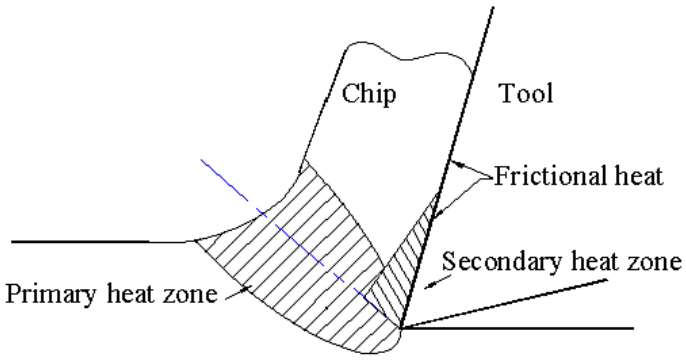

Figure 2.5: Heat generating areas in chip.

The mean temperature rise in the shear zone T_{AB} can be estimated by considering the plastic work done in the zone which gives rise to the equation:

$$\Delta T_{AB} = \frac{(1-\kappa)F_s \cos\alpha}{\rho S t_1 w \cos(\phi - \alpha)} \tag{2.9}$$

Where κ is the proportion of heat conducted into the work,

ρ is the density of the work material (kg/m^3),

S is the specific heat (J/kg K).

and F_s is the shear force derived from the equation (2.10)

$$F_s = F_c \cos\phi + F_f \sin\phi \tag{2.10}$$

By representing the shear zone with a plane uniform heat source along AB, and by making other simplifying assumptions, Weiner [20] obtained a theoretical solution for the proportion of heat conducted into the work, κ as a function of $R_T \tan\phi$ where R_T is a nondimensional thermal number given by equation (2.11):

$$R_T = \frac{\rho S \mathrm{V} c t_1}{\mathrm{K}} \tag{2.11}$$

K in this equation is the thermal conductivity (W/m K). Experimental values of κ obtained by Boothroyd [10], who measured shear zone temperatures using infrared photography, confirmed the form of Wiener's Theoretical results but showed that in general the theory underestimates κ. In view of this Stevenson and Oxley [21] used empirical equations for κ based on Boothroyd's [10] experimental data which gave:

$$\kappa = 0.5 - 0.35\log(R_T \tan\phi) \quad \text{for } 0.04 \leq R_T \tan\phi \leq 10.0 \tag{2.12}$$

$$\kappa = 0.3 - 0.15\log(R_T \tan\phi) \quad \text{for } R_T \tan\phi \geq 10.0 \tag{2.13}$$

Due to substantial temperature rises occurring in the shear zone, the values of specific heat and thermal conductivity will change significantly. This was allowed by using the following empirical temperature dependent functions for specific heat of work material *S*, and the work material thermal conductivity *K*.

$$S = 0.109 + 0.00009T \tag{2.14}$$

$$K = 2.79 + 0.0017T \tag{2.15}$$

Where S is in (J/kg K) and K is in (W/m K)

The allowance for temperature effects on *S* and *K*, which appear in equations (2.9) and (2.11) meant it was necessary to use the iterative process to obtain the temperature rise ΔT_{AB} from equation (2.9). The actual temperature of T_{AB} was obtained for the given values of F_c, F_f, ϕ, etc., by adding the initial workpiece temperature T_w, onto the calculated value for ΔT_{AB}. Therefore:

$$T_{AB} = \Delta T_{AB} + T_w \tag{2.16}$$

By using the distortion along the tool chip interface, Stevenson and Oxley [21] determined the value of δ the ratio of the thickness of plastic zone along the interface to the chip thickness to be approximately 0.125, and subsequently used this value in calculations. They used the Boothroyd [10] method to determine the temperatures at

the tool chip interface given in equation (2.17). In this method the mean temperature rise of the chip, T_c is found by considering the frictional work along the interface. The maximum rise in temperature at the tool chip interface, T_m, is then obtained by multiplying T_c, by a factor which is determined on the thickness of plastic zone, δt_2. The mean chip interface temperature, T_s is the average shear plane temperature and β (approximately equals 0.7) is an empirical correction factor that accounts for temperature variation along the chip tool contact zone.

$$T_{\text{int}} = T_s + \beta T_m \tag{2.17}$$

In calculating T_{int} an iterative procedure was once again used, as the specific heat S was not known independently of T_{int}. The maximum temperature rise in the chip, T_m, is calculated once the thickness of the tool chip interface δt_2, and tool chip contact length, l_c are found.

From Boothroyd's results Stevenson and Oxley derived an empirical equation relating T_m and T_c to give equation (2.18)

$$\log\left[\frac{T_m}{T_c}\right] = 0.06 - 0.195\delta\sqrt{\frac{R_T t_2}{h}} + 0.5\log\left[\frac{R_T t_2}{h}\right] \tag{2.18}$$

The average temperature rise, $T_{c,}$ can be calculated by equation (2.19), where F is the frictional force as the chip moves over the tool face and can be calculated by equation (2.20). For an accurate analysis, both the plastic layer thickness $\delta t_{2,}$ and total contact length h, must be measured with a microscope that has a large magnification. The contact length h can be estimated approximately by using equation (2.21), assuming that the resulting cutting force acts in the middle of the contact length and parallel to the stress free chip boundary.

$$T_c = \frac{F\sin\phi}{\rho S t_1 w\cos(\phi - \alpha)} \tag{2.19}$$

$$F = F_f\cos\alpha + F_c\sin\alpha \tag{2.20}$$

$$h = \frac{t_2 \sin(\phi + \lambda - \alpha)}{\sin\phi \cos\lambda} \tag{2.21}$$

From experimental data from a variety of work materials Cook [22] derived equation (2.22) for determining the tool interface temperature using dimensional analysis, and agreed with the iterative methods developed earlier.

$$\Delta T = 0.4 \frac{U}{\rho c} \left[\frac{V_c t_1}{\alpha_t} \right]^{0.333} \tag{2.22}$$

Where U is the specific energy during cutting, ρc is the volumetric specific heat, and α_t is the thermal diffusivity of the work material and is obtained from:

$$\alpha_t = \frac{k}{\rho c} \tag{2.23}$$

From Cook's equation (2.22) the actual tool interface temperature T_{int} is:

$$T_{\text{int}} = \Delta T + T_w \tag{2.24}$$

Haci Saglam *et al. [23]* investigated the effect rake and approach angles have on cutting forces and tool tip temperature during different cutting conditions. The theoretical forces were calculated using machine theory, and were found to have an average deviation of 0.37 percent between the measured cutting forces. The tool temperature was calculated using Stevenson and Oxley's empirical equation (2.18), and the actual temperature was measured using a pyrometer. However, the correlation between the calculated temperature and the measured temperature was found to have a deviation of 43 percent for the same experiments. The reason the measured value produced such a large error from the empirical equation temperature (2.18), was due to the measurement of the tool temperature during machining not being close enough to the cutting edge of the tool. This highlights one of the major challenges of measuring the temperature at the tool tip during machining, and shows

the benefits of being able to calculate the tool tip temperature by using material properties.

2.3 The Effect Of Coolant On Tool Performance

2.3.1 Traditional liquid coolant

Cutting fluids have been extensively used in metal cutting operations as the preferred method of removing the heat generated at the tool tip during machining. In addition to cooling the cutting tool the coolant also:

- reduces the friction wear,
- improves tool life,
- improves surface finish,
- reduces the shear strength of the work material, and
- removes the chips from the cutting zone.

Dependent on the type of machining operation the cutting fluid needed may be a coolant, a lubricant, or both. The effectiveness of the cutting fluids depends on a number of factors, such as the type of machining operation, tool and workpiece materials, cutting speed and method of application. Primarily, cutting fluids are thought of as coolants, and are in fact referred to as such. As the coolant flows over the tool, chip, and work piece, it removes the heat from the cutting zone as shown in Figure 2.6. The effect of temperature on tool wear is discussed in Chapter 3 where it shows the effect temperature has on the wear mechanisms. In general, a reduction on tool temperature increases the tool life. This is due to the tool material initially being harder and so more resistant to abrasive wear at lower temperatures Secondly, the diffusion rate of constituents in the tool material is less at lower temperatures.

Cutting fluids unfortunately do not flow over the tool and workpiece as a simple steady stream. Varying geometry and properties of the tool, chip and workpiece lead to a complex heat transfer mechanism. The rate of fluid flow, its thermal conductivity, and its specific heat and latent heat all affect the rate of heat transfer from the cutting zone. A coolant strategy on tool performance for high speed machining concluded H.A. Kishawy *et al. [24]* that the coolant application method

has only a limited influence on the flank wear, but is crucial in controlling the volume of material adhesion. Researchers have shown that there are several mechanisms to explain cutting fluid access to the tool chip interface, as shown in Figure 2.6 and 2.7.

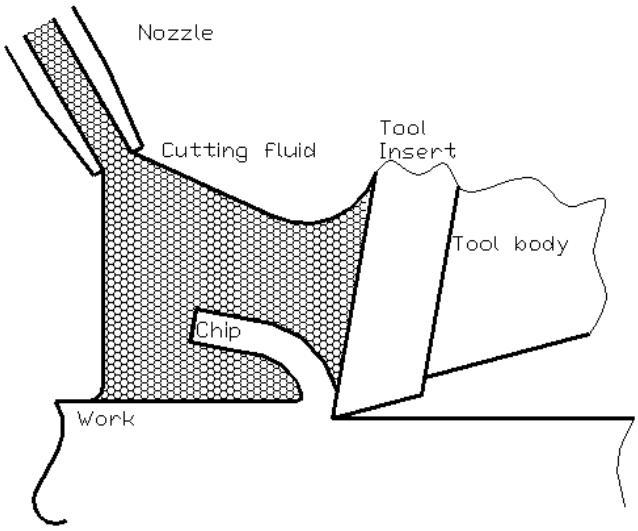

Figure 2.6: Tool tip cooled by traditional cutting fluid.

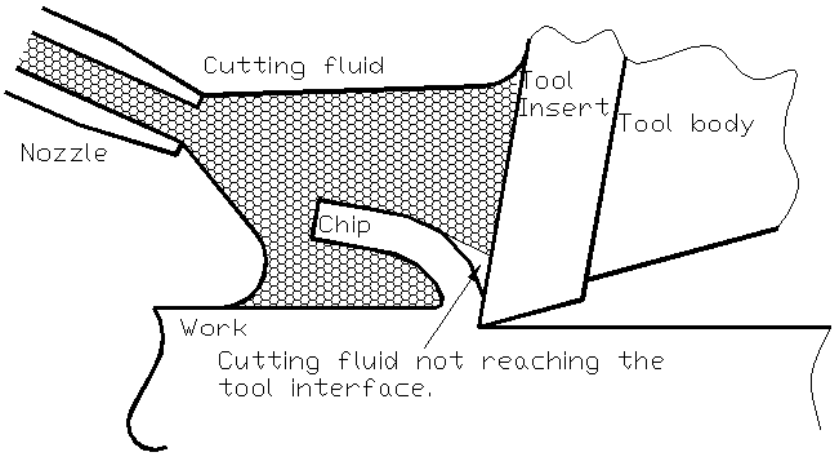

Figure 2.7: Traditional cutting fluid not reaching the tool tip interface.

Merchant *et al.* [25] suggested penetration of the cutting fluid down the capillaries between the back of the chip and the tool, and in the process this forms a lubrication film by physical and chemical absorption on the capillary wall. The lubrication

action of the coolant requires the cutting fluid to penetrate the capillaries of the cutting zone, and also the penetration time must be less than the capillary lifetime for this to be effective. However, the relative inaccessibility of the tool point to receive coolant has shown that the capillary action breaks down near the tool tip, but not actually at the tool tip. The advantage of having liquid coolant close to the cutting zone is that not only does it reduce the temperature of the tool tip, it also reduces the force required to shear the work material. The reduction of shear stress in the plastic zone is know as the Rebinder effect, and involves the penetration of the cutting fluid into the work piece via small surface cracks due to machining.

There are four basic methods used in practice in applying the coolant Kalpakjian and Schmid [26]. The main method of application is by flooding the cutting zone. However, by using this approach, coolant penetration is more likely to be as shown in Figure 2.7 where the coolant does not reach the tool chip interface during cutting.

Devising a simple heat transfer experiment which may be directly related to the cutting conditions when comparing coolants has led some researchers, Shaw, Cook and Smith [27], to list temperature zones of interest, and in order of increasing temperatures as follows:

(i) The workpiece as it approaches the shear plane.
(ii) The chip as it leaves the shear zone.
(iii) The tool work interface (clearance face).
(iv) The tool chip interface (rake face).

These four temperature zones were used to assess the cutting fluids during machining, even though the significance to the cutting process of these temperatures is not fully understood. Eugene [28] found from interface temperature measurements that, at a cutting speed of 15 m/min, there was a remarkable linear relationship between the cooling effect of the five fluids tested and the specific heat of these fluids. His results for two steels tested are given in Table 2.1. At higher speeds Eugene found, as had Shaw, Pigott and Richardson [29], that the situation changed beyond a cutting speed of 24 m/min. He found that the cooling effect of all fluids

decreased markedly, and that for tempered steel the fluids had no effect on the interface temperature.

Table 2.1: Influence of various cutting fluids on the tool chip interface as measured by the tool work thermocouple

Composition	Specific heat of medium	Temperature decrease, %	
		Steel A (tempered)	Steel B (annealed)
Compound oil, low viscosity	0.489	3.9	4.7
Compound oil, high viscosity	0.556	6	6
Aqueous solution of wetting agent	0.872	14.8	8.4
Aqueous ”soda product” solution, 4%	0.923	-	13
Water	1.00	19	15

Table obtained from E.J.A. Armarego and R.H. Brown [2]

Cutting conditions: Turning operation, high-speed tool, depth of cut 4.8 mm, feed rate of 0.4 mm/rev, cutting speed 15 m/min, rake angle 20^{o}, Temperatures measured during dry cutting were: steel A, 804 ^{o}C; steel B, 726 ^{o}C

These results show that cooling measured at the chip tool interface temperature may be directly related to thermal properties of the fluid for a range of cutting speeds. With variation in speed this correlation is lost, due to the influence of other effects, e.g., friction reduction at low speeds, or insufficient heat flow into the fluid at high speeds and feeds.

2.3.2 Environmental concerns of using coolant

For environmental and economic reasons there has been a continuing worldwide trend to minimise or eliminate the use of cutting fluids since it is known that coolant used in the machining process is toxic and harmful to both the environment and human health. In addition, the coolant is further contaminated during the machining operations, and bacteria organisms are produced in the coolant as it ages. This makes it necessary to dispose of the coolant in a way that meets with the appropriate environmental regulations. For this reason the disposal costs account for up to 17 percent of the cost to the metal cutting manufacturing industry as researched by

Shaw C. Feng [30]. This increasing cost and health issue is encouraging the metal cutting industry to adopt “Green Manufacturing” or dry machining where possible.

2.4 Alternative Methods To Liquid Coolant

2.4.1 Dry machining

Dry metal cutting has only been made possible due to the technological innovations of tool materials, with the most recent being the coating of the tool tip to help reduce the friction over the rake face P. Zelinski [31]. Even with these developments there is still an enormous amount of heat generated in the cutting zone, giving rise to a search for alternative ‘green’ cooling methods to reduce tool tip temperature to help prolong the working life of the tool tip.

It may also be noted that there are some machining operations that are better to be carried out under dry conditions. For example, when considering medical implants such as a ball joint for the hip, coolant would be undesirable due to the fear of contamination. Workpiece material is also a contributing factor to the suitability of dry machining. For example, most aluminium alloy as well as most carbon steels can be dry-machined, as they allow most of the generated heat to be carried away with the chips F. Georgia [32]. However, to obtain optimum dry cut conditions, Anselmo Eduardo Dinz and A. Jose de Oliveira [33] compared wet and dry rough turning. They found that it is only possible to obtain dry tool life time compatible with wet cutting when the following cutting conditions are met:

- increase the feed rate to, 0.4 mm/rev,
- recommended cutting speed for a ISO P15 tip 290 m/min,
- reduce the depth of cut: the maximum depth of cut to be 1 mm.

Based on their results, dry machining is not suitable for high values of depth of cut as the tool life obtained was too short to be of use. For this reason dry cutting in rough turning operations is restricted to those components with small stock removal Anselmo Eduardo Dinz and R. Micaroni [34]. Figures 2.8 and 2.9 show the comparison of the mean value of tool life for a P15 carbine tool tip under wet and dry cutting conditions.

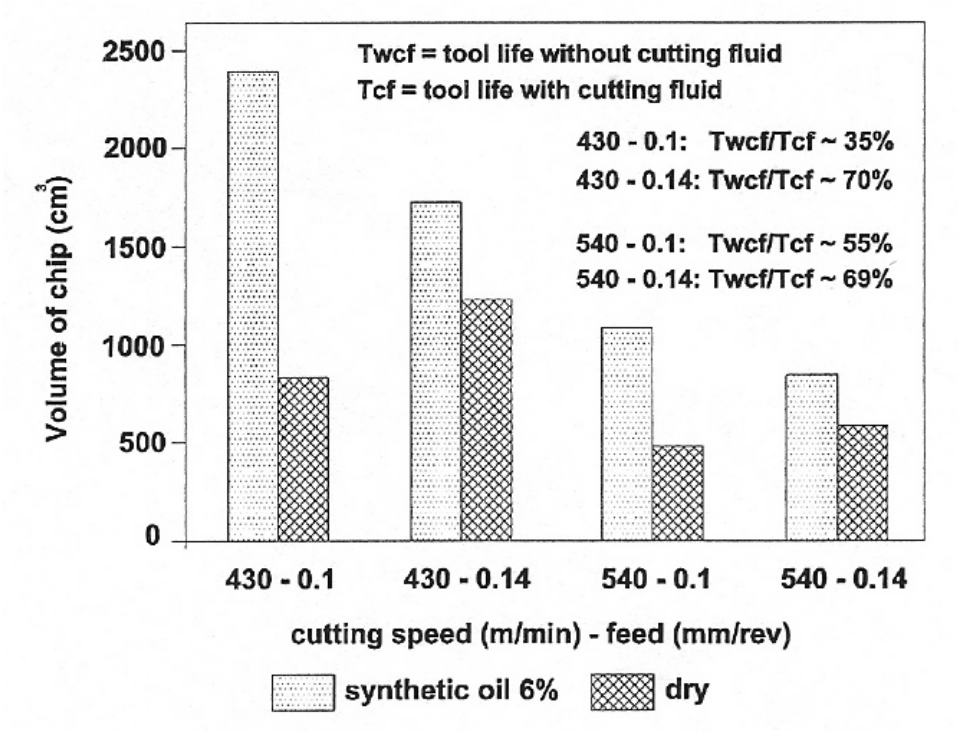

Obtained from Anselmo Eduardo Dinz and Ricardo Micaroni [35]

Figure 2.8: Volume of material removal per tool life for a depth of cut of 1mm.

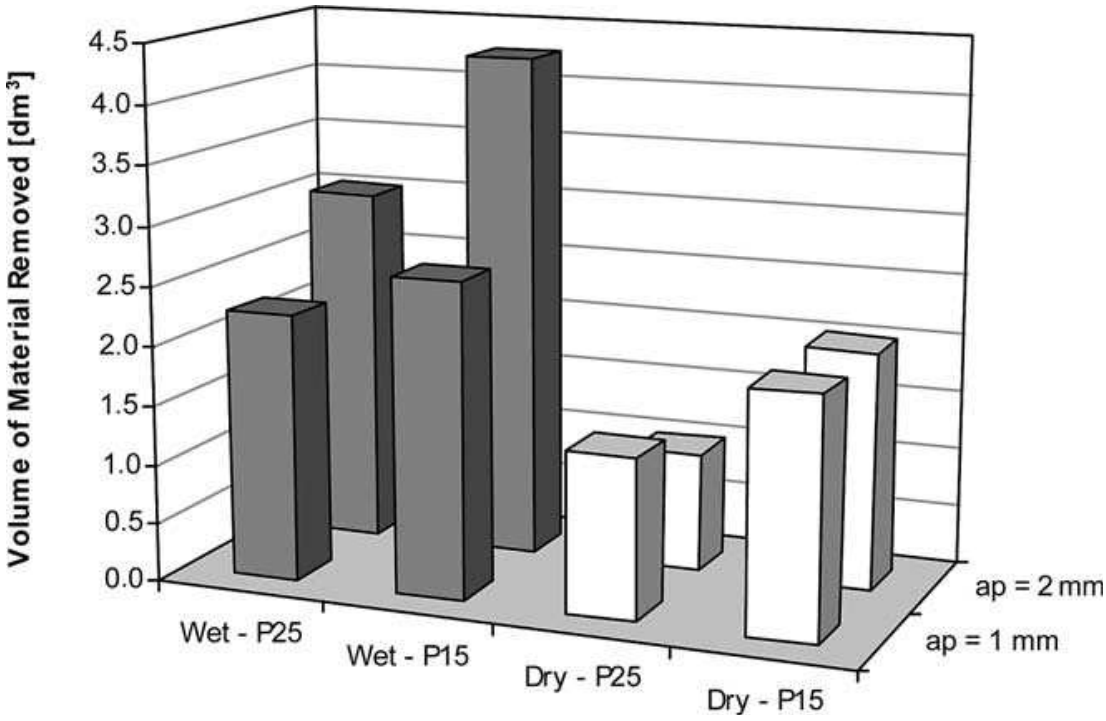

Obtained from Anselmo Eduardo Dinz and Adilson Jose de Oliveira [33]

(cutting speed of 350 m/min and feed of 0.4 mm/rev)

Figure 2.9: Volume of metal removed for 0.3 mm flank wear.

The main type of wear found in the tool tips was flank wear, as shown in Figure 2.11 and is caused by abrasion between the tool and workpiece. Figures 2.10 and 2.12 show the flank wear VB_B against volume of material removed. The graphs relating to dry cutting with the cutting speed V = 290 m/min Figure 2.10 are above those related to cutting with abundant fluid, showing that tool wear is faster for dry cutting at this speed. But when V is increased to 350 m/min, all the graphs were mixed, and it can be said that the rate of tool wear increase was very similar for both dry cutting and cutting with coolant. Figure 2.13 shows the contrast of dry and wet surface finishes obtained from finish turning as found by Anselmo Eduardo Dinz and Ricardo Micaroni [34].

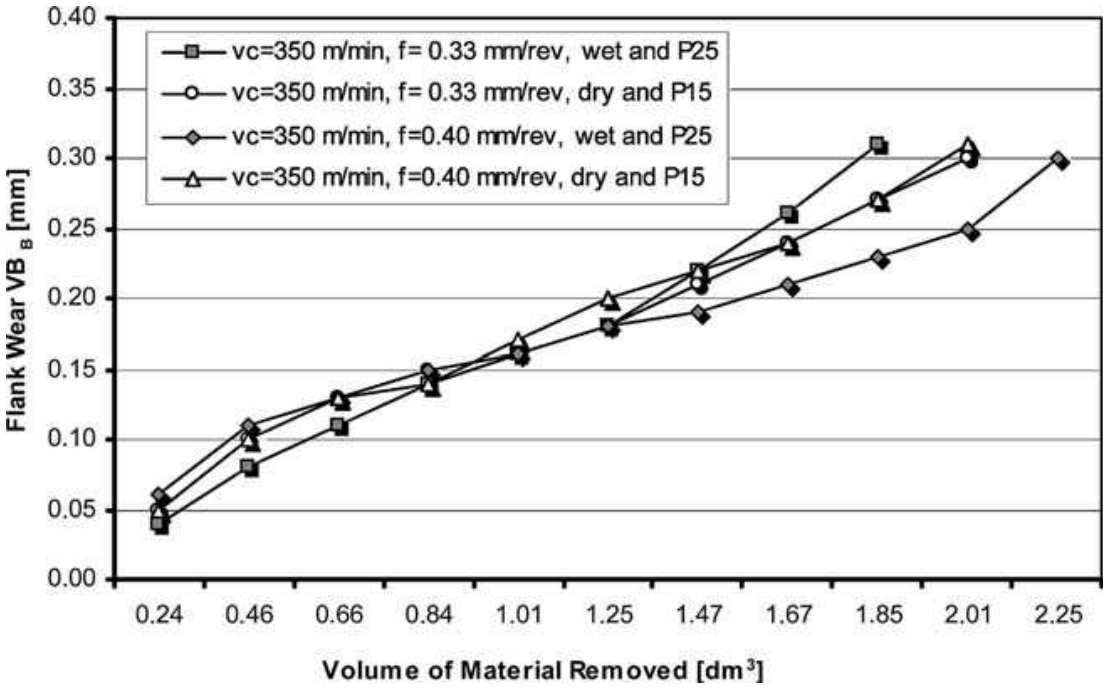

Obtained from Anselmo Eduardo Dinz and Adilson Jose de Oliveira [33]

(For a cutting speed of 350 m/min and 1 mm depth of cut.)

Figure 2.10: Flank wear (VBb) volume of metal removed.

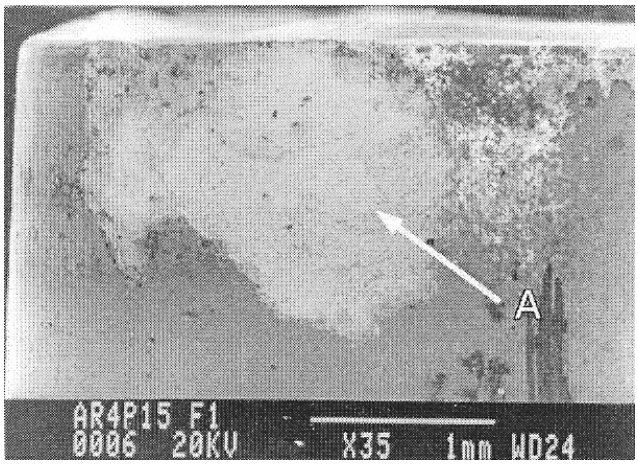

(For a cutting speed of 350 m/min and feed of 0.4 mm/rev.)

Obtained from Anselmo Eduardo Dinz and Adilson Jose de Oliveira [33].

Figure 2.11: Arrow "A" identifies flank face wear on the tool tip.

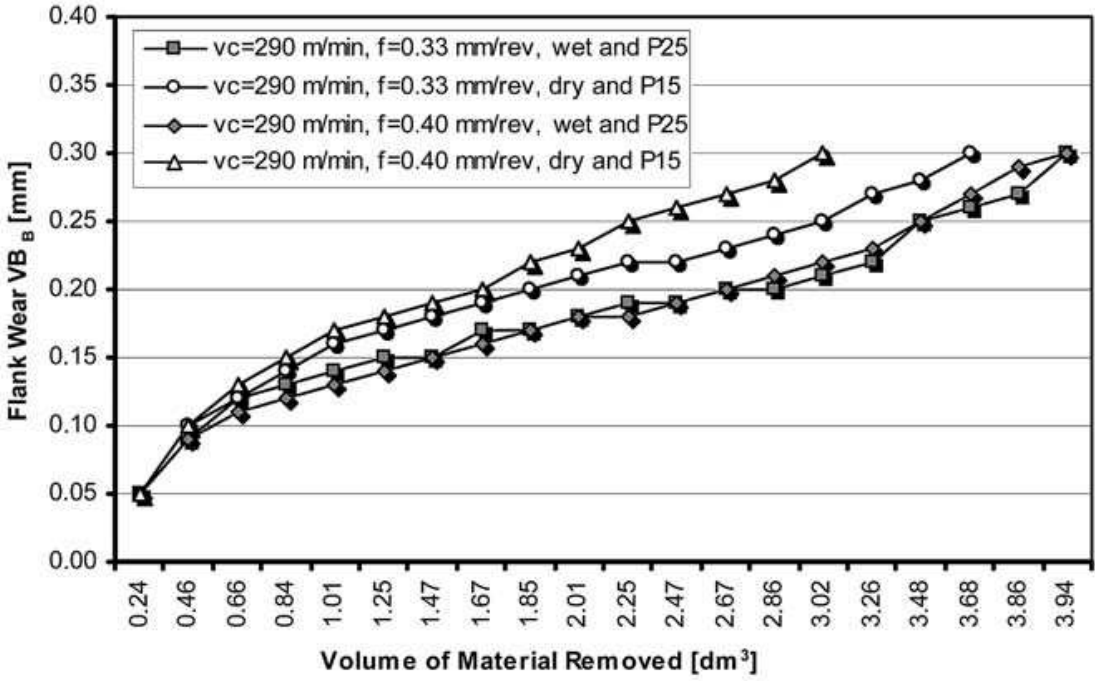

(For a cutting speed of 290 m/min and 1 mm depth of cut.)

Obtained from Anselmo Eduardo Dinz and Adilson Jose de Oliveira [33].

Figure 2.12: Flank wear (VBb) volume of metal removed.

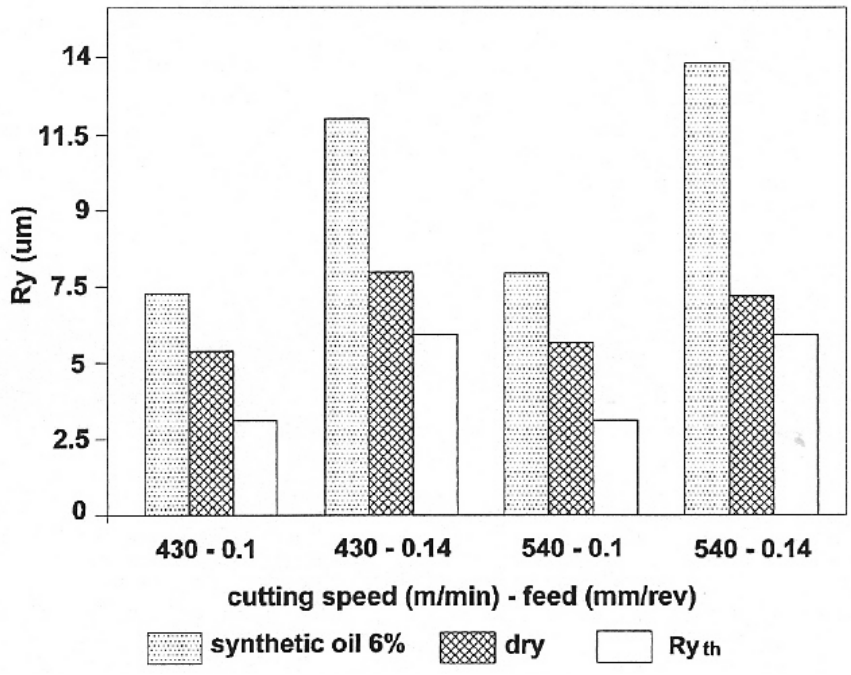

Obtained from Anselmo Eduardo Dinz and Ricardo Micaroni [34]

(The surface roughness (R_y), tool nose radius r_ϵ = 0.4 mm)

Figure 2.13: Surface roughness (Ry) for all conditions.

The R_y theoretical value is expressed by the equation (2.25):

$$Ry = \frac{f^2}{8r_\varepsilon} \tag{2.25}$$

Figure 2.14 shows how the tool tip radius affects the tool life under wet and dry finish turning over the two cutting speeds used. As expected, the tool life is always longer for wet cutting, although when the cutting speed is increased with dry cutting, the tool tip temperature gets closer to wet machining temperatures. Similarly, the larger the tool tip radius (r_ϵ = 0.8 mm) is the cooler the tool tip is as shown in Figure 2.14.

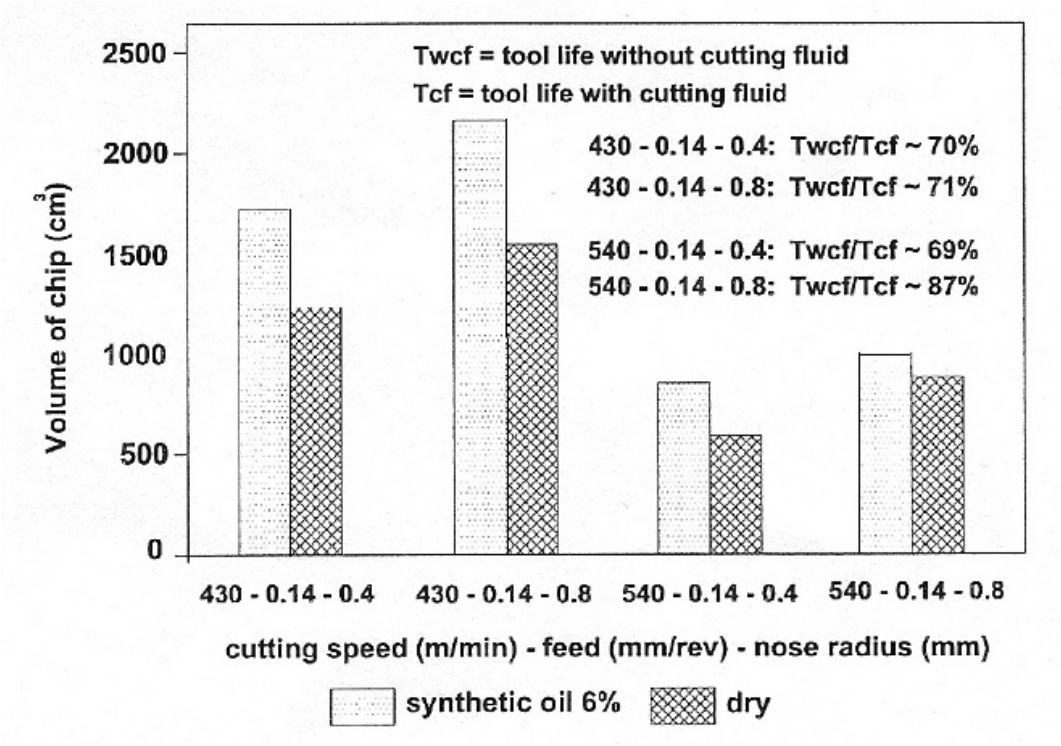

Obtained from Anselmo Eduardo Dinz and Ricardo Micaroni [34]

with r_ϵ 0.4 mm and 0.8 mm and a feed of 0.14 mm/rev

Figure 2.14: Tool life in volume of chip removed

2.4.2 Minimum quantity lubricant (MQL)

This method of cooling the tool tip uses a fine mist of air-fluid mixture containing very small amounts of cutting fluid delivered to the cutting zone through the spindle of the machine tool. Typically this is sprayed through a 1 mm diameter jet at a pressure of 600 kPa, and at a rate of 1 to 100 cc/hr, which is approximately one ten-thousandth of that used in using traditional coolant.

An investigation by A.S. Varadarajan *et al.* [36] compared the use of wet turning with MQL turning, with the coolant being supplied from a jet directed onto the flank face of the tool at an injection pressure of 20 MPa, delivering 2 ml/min of coolant. Higher cutting ratios were achieved during minimal application than during dry turning and conventional wet turning. This was due to MQL achieving better lubrication properties at the tool chip interface than traditional coolant. The cutting temperatures comparing MQL with wet and dry turning is shown in Figure 2.15 and 2.16.

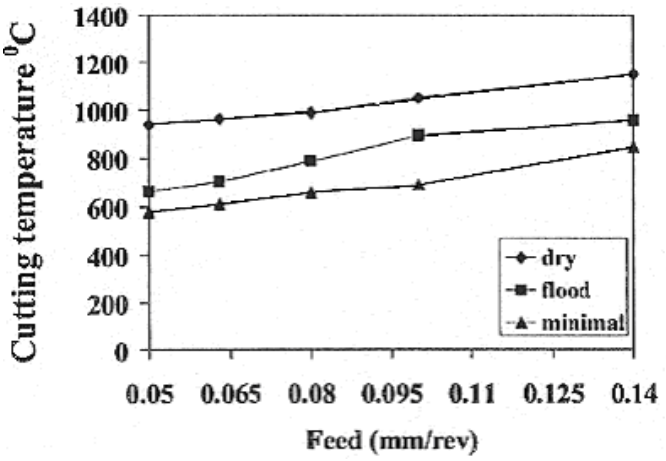

(For a cutting speed of 80 m/min, various feed rates and depth of cut of 1.25 mm)

Obtained from A.S. Varadarajan et al [36].

Figure 2.15: Temperature comparison of MQL and wet and dry turning.

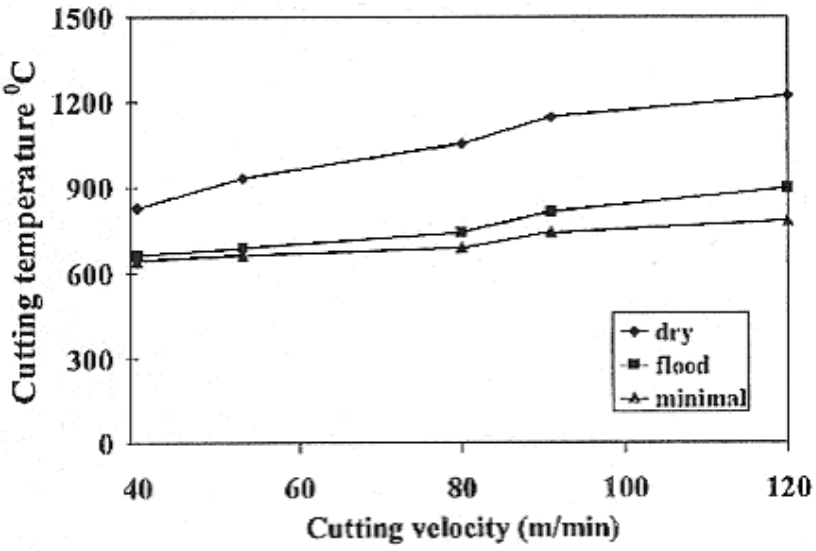

(For a feed rate of 0.1 mm/rev, various cutting speeds and depth of cut of 1.25 mm)

Obtained from A.S. Varadarajan et al.[36]

Figure 2.16: Variation of cutting temperature during MQL, wet and dry turning.

The cutting temperature is the dominant factor in tool wear as all the wear mechanisms are accelerated at high cutting temperatures. During conventional wet turning the quantity of heat, *Q*, extracted by convective heat transfer is given by:

$$Q = m_{cf} c_p \Delta T \tag{2.26}$$

where Q is the heat quantity, m_{cf} is the mass of cutting fluid, c_p is the specific heat capacity and ΔT is the temperature reduction. For MQL application, cooling occurs due to both convection and evaporative heat transfer. The evaporative heat transfer is improved by the atomisation of the liquid.

$$Ql = Q + mL_e \tag{2.27}$$

where m is the mass of evaporation fluid and, L_e, is the latent heat of evaporation.

Since the evaporation enthalpy of water is approximately equal to 2000 kJ/kg, evaporation of even a very small quantity of water is sufficient to create significant cooling. The cutting fluid droplets by virtue of their high velocity, can penetrate the blanket of vapour formed and reach the hot tool interface facilitating more efficient heat transfer than is possible with conventional wet turning, where the adherent firm of lubrication retards the heat transfer. The reduction of cutting temperature and shortening of the tool chip contact length during MQL should also produce a better surface roughness as shown in Figure 2.17.

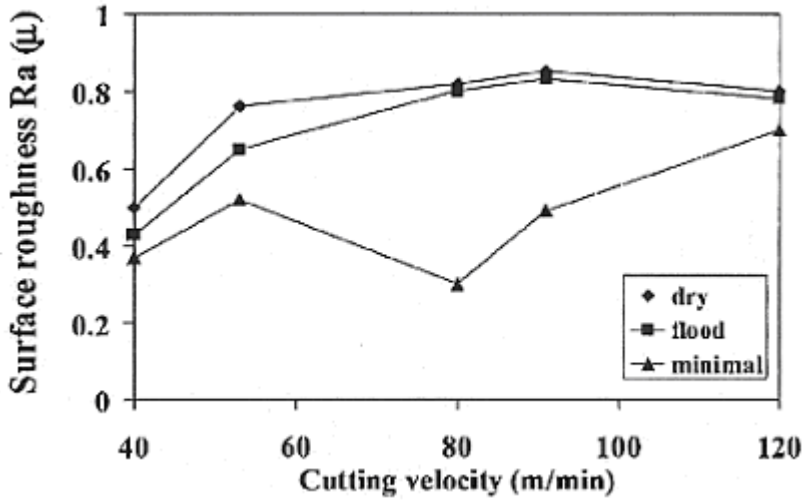

(For a feed rate of 0.10 mm /rev, various cutting speeds and depth of cut of 1.25 mm.)
Obtained from A.S. Varadarajan *et al. [36]*

Figure 2.17: Surface roughness during MQL, wet and dry turning.

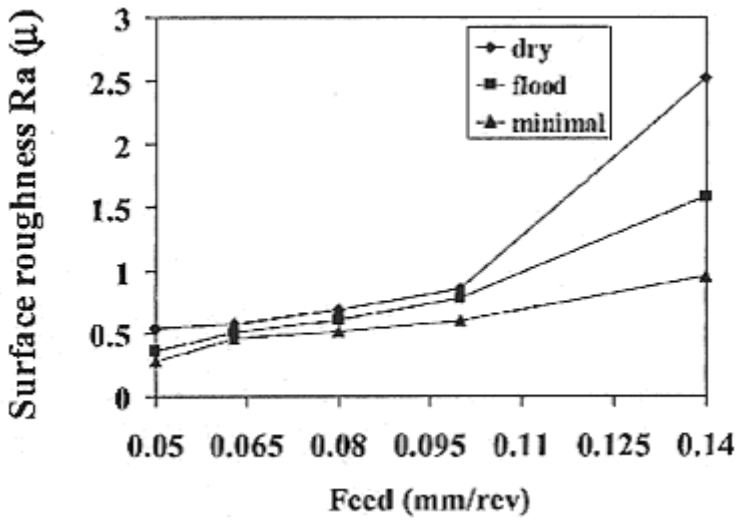

(For a cutting velocity of 80 m/min, various feed rates and depth of cut of 1.25 mm.)

Obtained from A.S. Varadarajan *et al.*

Figure 2.18:Variation of surface roughness during MQL, wet and dry turning.

M. Rahman *et al.* [37] evaluated the effectiveness of MQL during milling operations and demonstrated similar benefits as found in turning.

2.4.3 High pressure jet-assisted cooling

Ultra-high-pressure cooling in turning operations has shown to be another effective method of cooling the tool tip and was first investigated in 1952 by Pigott and Colwell [38]. This cooling process has been widely used in so-called “hard to machine materials” such as high-temperature alloys and titanium, as these materials cannot be machined effectively without cooling Dahlman and Escursell [39].

In the 1990s, Podgorkv [40] and Godelvski [41] proposed a new green machining system consisting of water vapour as the coolant and lubricant during the cutting process. The water vapour produced in the vapour generator is first passed through the quadric heater for drying, before the vapour flow is directed on to the cutting zone through the jet. Temperatures are monitored as the water vapour passes through the quadric heater and jet since this is critical to the effectiveness of the cooling vapour. Results obtained from this process show that the cutting force, the friction coefficient, and the cutting temperature were all reduced and improved the surface

finish. Figure 2.19 shows a typical water vapour generator delivering system that provides a high-pressure water spray to the cutting zone.

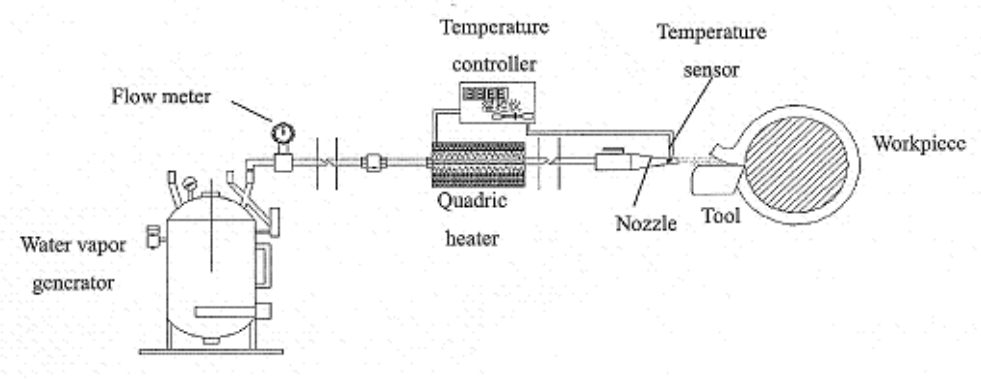

Obtained from Junyan Liu *et al.* [42]

Figure 2.19: Diagram of a vapour generator device and vapour feeding system.

For the same cutting conditions the high pressure water vapour process was compared against dry cutting, compressed air and oil water emulsion. The cutting tool temperature reduction for the water vapour cooling is shown in Figure 2.20 and the surface finish is shown in Figure 2.21.

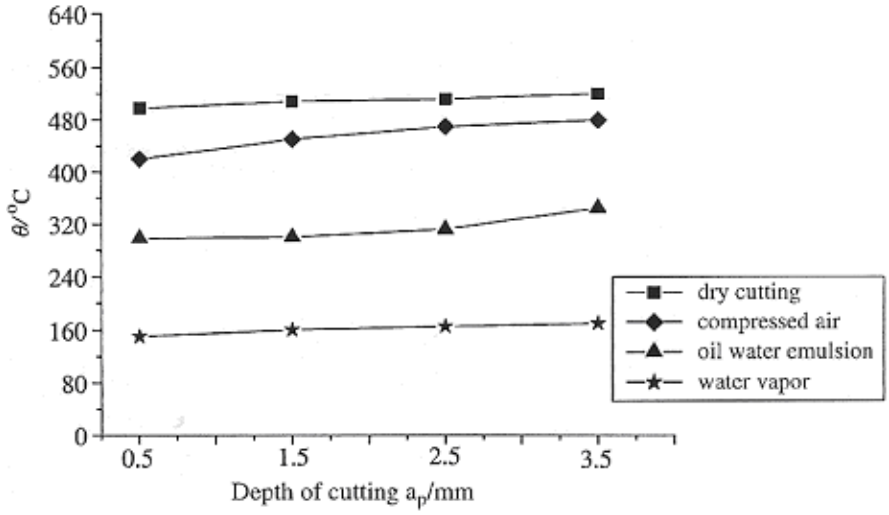

Obtained from Junyan Liu *et al. [42]*

Figure 2.20: The cutting temperature comparison of dry, compressed air, oil and emulsion and water vapour.

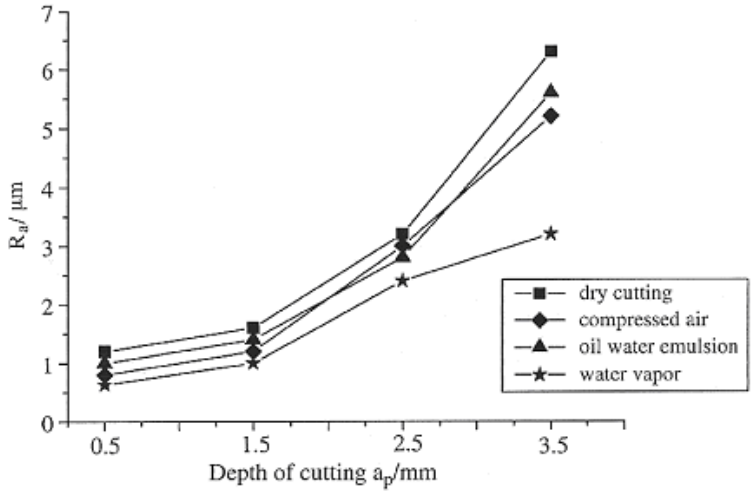

Obtained from Junyan Liu *et al. [42]*

Figure 2.21: The surface roughness comparison of dry, compressed air, oil and emulsion and water vapour.

2.4.4 Cryogenic cooling

Cryogenic cooling consists of using liquid nitrogen to reduce the temperature at the cutting zone. Liquid nitrogen as a cryogenic coolant has been investigated intensely in recent years as a method of cooling for hard to machine materials, Shane Y. Hong and Yucheng Ding [43].

They considered three methods to cool the cutting zone:

1. cryogenically freezing the workpiece;
2. heat conduction using a cold chamber under the tool tip;
3. and spraying liquid nitrogen onto the tool tip.

Cryogenic freezing of the workpiece consists of submerging the workpiece into liquid nitrogen preceding the machining process. Similarly, another approach is to submerge the tool in liquid nitrogen before machining. However, these methods are not suitable for all materials as the material structure can be altered, for example, thermal cracking to the surface of the tool. Obviously this method of cooling does not lend itself to modern manufacturing practices due to time involved in submerging tools in liquid nitrogen, and the useful operating time of the tool is short.

The second cryogenic cooling approach is to conduct the heat away from the tool tip by locating a liquid nitrogen filled chamber under the tool tip as shown in Figure 2.22.

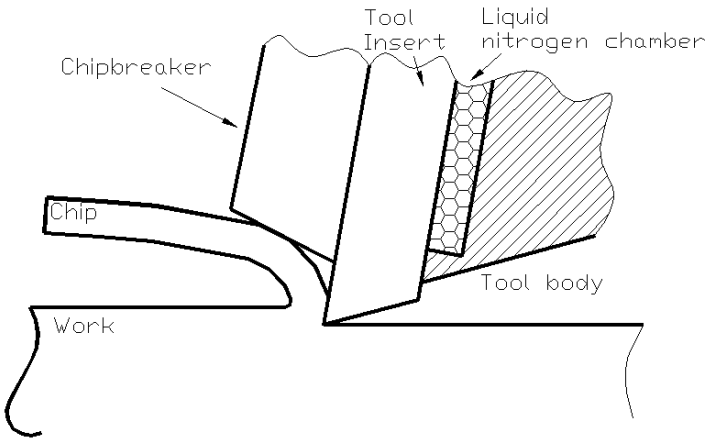

Figure 2.22: Tool tip cooled by nitrogen chamber positioned under the tool tip.

An adequate cooling effect can be expected from this cooling method when there is a large area of the tool insert in contact with the liquid nitrogen, if the tool tip material is highly conductive thermally, and if the tip insert thickness is suitable for the heat transfer.

The third method consists of liquid nitrogen being sprayed onto the tool tip. The challenge here is to have enough liquid nitrogen reaching the cutting zone before evaporation. Another research paper by Shane Y. Hong *et al.* [44] examined the lubricational properties of liquid nitrogen between the chip and the tool rake face. Like the first method, some material may develop thermal cracking on the surface. The isothermal contours of temperature distributions showing the various cooling effects for dry cutting, wet cutting and cryogenic cooling is shown in Figures 2.23 to 2.27. A comparison of the isothermal contour of the "emulsion cooling tool" Figure 2.24 and the "cryogenic tool rake cooling" Figure 2.27 shows the difference in temperature to be within 40 ^{o}C with respect to the cooling nitrogen. Where the liquid nitrogen makes contact on the tool face positions DC and BC the temperatures are far colder, which would lead to thermal cracking of the tool. The workpiece material used in generating these isothermal contours was Ti-6Al-4V, at a cutting speed of 90 m/min, depth of cut of 1.27 mm and feed rate of 0.25 mm/rev.

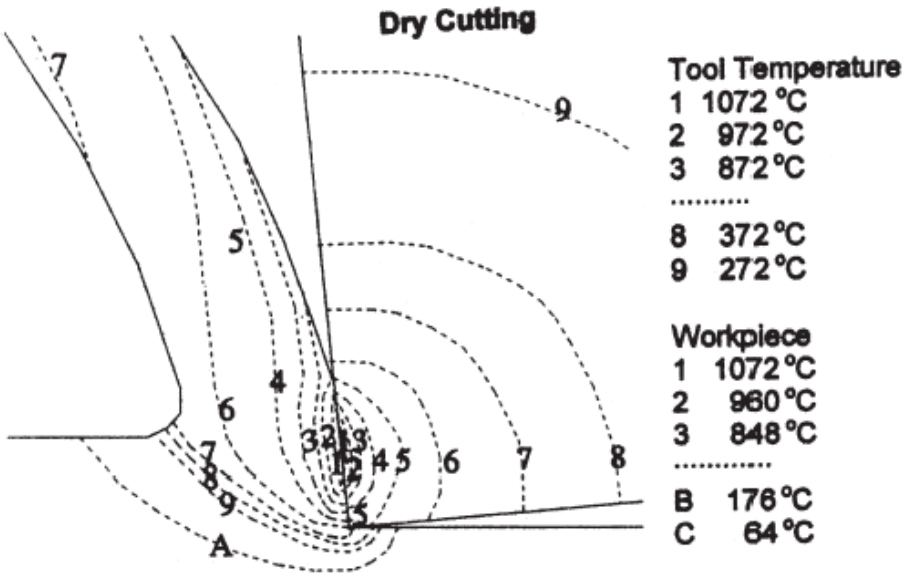

Obtained from Shane Y. Hong *et al.[43]*

Figure 2.23: Isothermal contour for dry cutting.

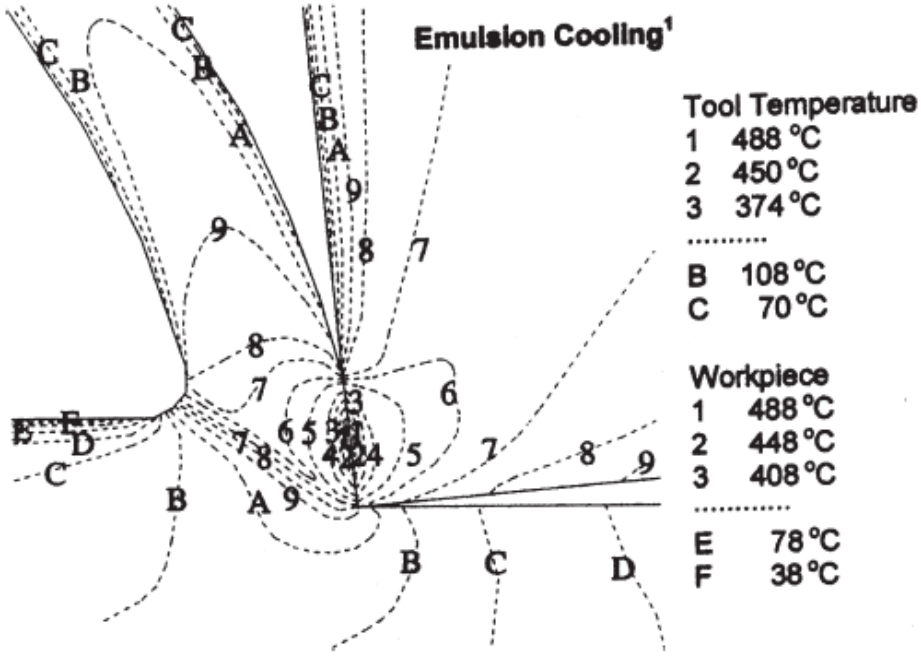

Obtained from Shane Y. Hong *et al.[43]*

Figure 2.24: Isothermal contour for wet cutting.

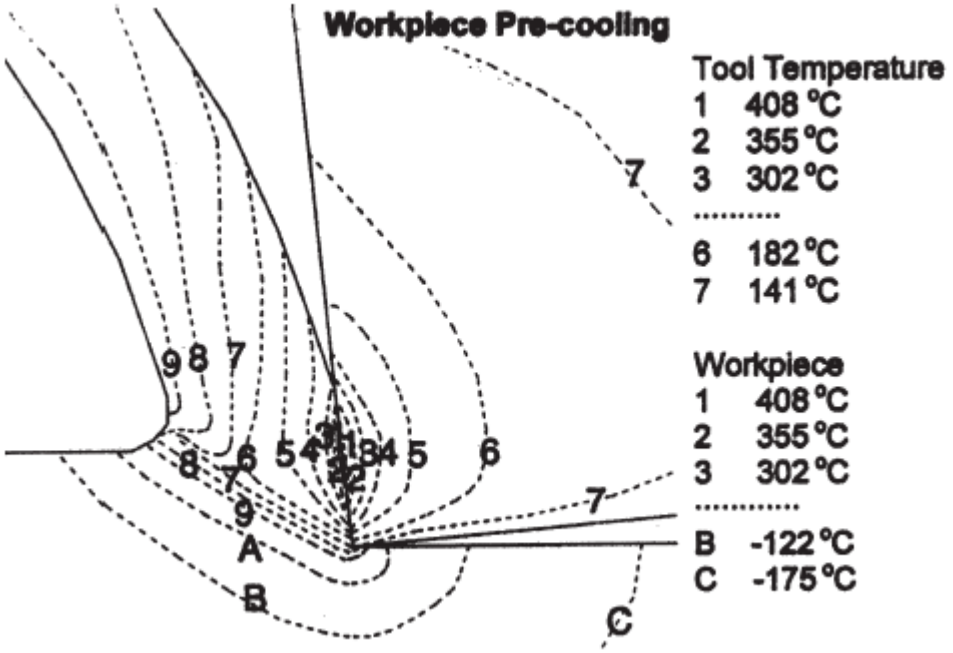

Obtained from Shane Y. Hong *et al.* [43]

Figure 2.25: Isothermal contour for workpiece precooling.

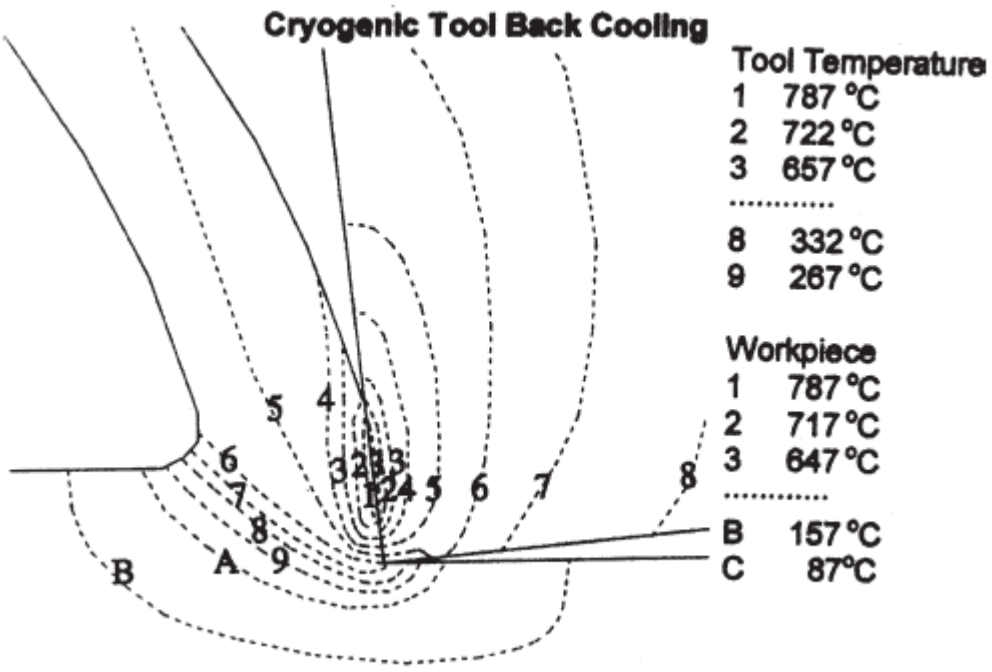

Obtained from Sane Y. Hong *et al.* [43]

Figure 2.26: Isothermal contour for tool back cooling.

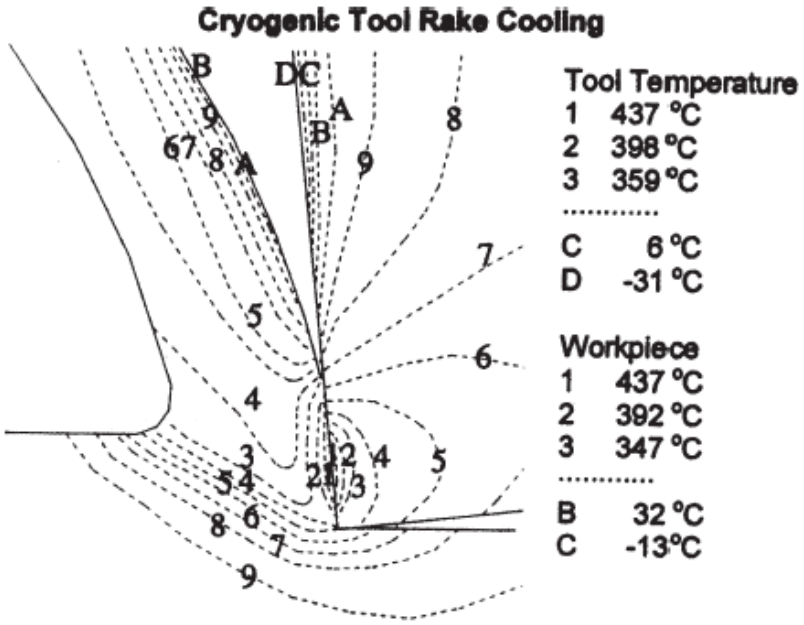

Obtained from Shane Y. Hong *et al.* [43]

Figure 2.27: Isothermal contour for liquid nitrogen sprayed on tool face.

Figure 2.28 clearly shows that the most efficient cooling of the tool tip is achieved by cooling both the top rake face and the flank face of the tool.

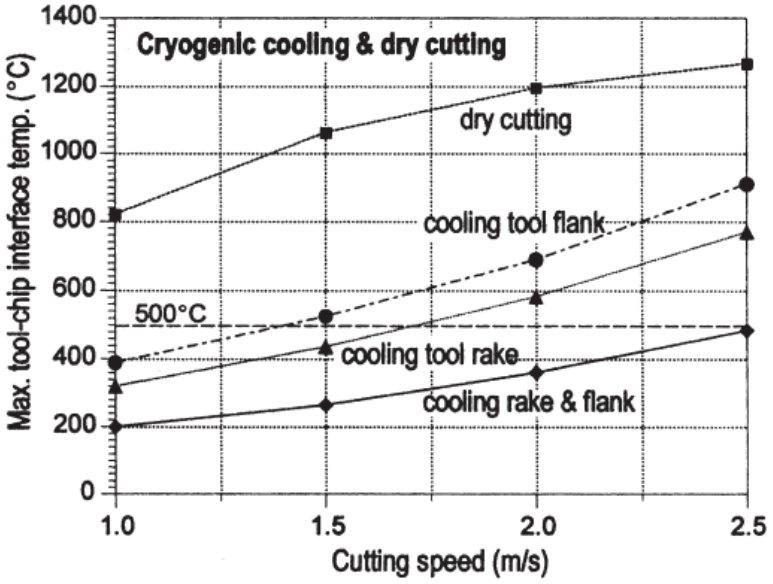

Obtained from Shane Y. Hong *et al.* [43]

Figure 2.28: Tool temperature verses cutting speed.

CHAPTER 3

TOOL LIFE

3.1 Introduction To Tool Life

Tool life is defined as the point when a tool has reached the end of its useful life. This is when the tool can no longer perform the task for which it is required, *eg*. produce the appropriate surface finish or dimensional accuracy. However, this does not imply that the tool is no longer able to remove work material; only that it is unsuitable for continued use. Therefore tool life is based on a definition that is application dependant, and so often varies from one application to another. This variation in definition makes tool life data from different sources difficult to compare because of the different criteria used. The criteria used as a measure of tool life includes such parameters as the total volume of metal removed to failure (*i.e*. end of useful life), the total time to failure (often used in interrupted cutting applications such as milling), total length of tool path to failure, and the number of components produced to failure. Another criterion of tool life that has often been used – particularly in the development of empirical functions of tool life is the concept of cutting speed for a given time to failure, *eg.* the cutting speed that results in a 60 minute tool life. It is generally undesirable to allow a tool to remain in service until complete failure of the cutting edge occurs because of the total loss of the tool and possible damage to the component being machined. For this reason tools are generally removed from service just prior to total failure, and are often defined in terms of a definite amount of tool wear.

Wear may occur on either the rake face of the tool or the clearance face of the tool as shown in Figure 3.1. Wear occurs on the rake face in the form of a small depression called a crater, situated just back from the cutting edge. The physical dimensions of this crater can be used to define tool failure.

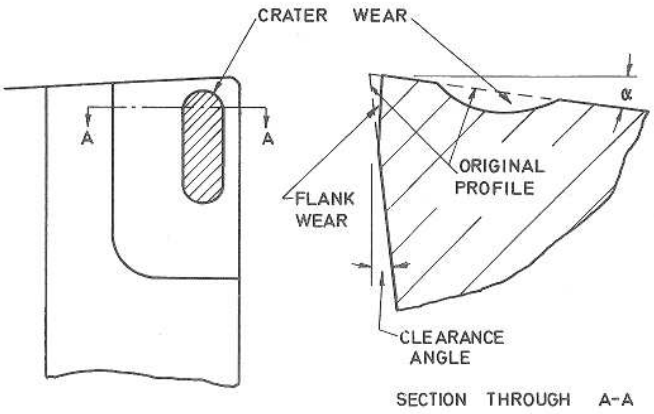

as shown in ISO 3685:1993(E)

Figure 3.1:Typical crater and flank wear on lathe tools.

Wear on the clearance face, called flank wear, appears as a land immediately below the cutting edge, the average or maximum width of which may be used to define the tool life. These failure criteria may be used independently or together depending upon the application. Since crater wear does not always occur to an appreciable extent, it is more common to use flank wear as a measure of tool life. For this reason it is essential to be able to use the tool life as the major measurement in establishing the effectiveness of tool tips. The test procedures used in determining tool life were in accordance with "Tool-life testing with single-point turning tools" ISO 3685:1993(E). The following important aspects of tool life are now considered.

3.2 Tool Life Analysis

3.2.1 Empirical tool life relationships

The ability to predict tool life from conditions under the control of the machine operator, e.g. feed, speed, and width of cut, allied with knowledge of the wear characteristics of the tool, would be highly desirable. However, due to the difficulties involved in analysing such a complex process, many researchers attempted to determine empirical relationships between the machining parameters and tool life as defined by some suitable criterion. The best-known work on tool life is that of F.W. Taylor [45] who fitted a power law to the observed dependence of tool life on cutting speed and obtained the equation:

$$VL^{a1} = C_t \tag{3.1}$$

where V is the cutting velocity, L is the cutting time (tool life) and, a_1 and C_t are constants. The Taylor equation is still perhaps the most commonly used tool life formula today. Experience has shown that for the conventional speed range, equation (3.1) is a good predictor of the variation of tool life with cutting velocity, but it has definite disadvantages as a 'universal' tool life formula. The constants, a_1 and C_t, must be determined for each tool/work combination for a given range of cutting conditions, and then strictly applied only for that range of speed, undeformed chip thickness, depth of cut and tool geometry. Practical expediency, though, often dictates that these values of the constants are used for other cutting conditions. Accuracy, however, requires a new determination of the constants, a_1 and C_t, if anything other than the cutting speed is altered. Despite these problems, much of the tool life data available in tool engineers' handbooks are based upon Taylor's tool life equation, or some general form of the equation. J. Taylor [46] comments that in view of the large experimental errors involved in tool life testing to determine a_1 and C_t, it is difficult to say whether equation (3.1) is intrinsically true, or is a close approximation to a more basic relationship. Recent developments in the theory of wear mechanisms and the study of tool life suggest that the latter is true.

Equation (3.1) has been extended to include other variables in an attempt to incorporate the effects of feed rate and width of cut on tool life. The extended formula is:

$$LV^{a2} f^{b} w^{c} = C_t \tag{3.2}$$

where f is the feed rate, w is the width of cut and, a_2, b, c and C_t,, are constants. There have been many variations of this equation proposed including the general tool life equation of F.W. Taylor, which was proposed in 1907. This equation, much too complex for practical use, included terms for feed rate, depth of cut and tool radius together with several empirical constants Taylor [45]. The term for the tool nose radius was included because Taylor used tools having large nose radii, and he found it necessary to account for this fact in his formula. Woxen [47] overcame this

problem by introducing the use of another equation for tool life that used a parameter he called the “chip equivalent”.

The “chip equivalent” is defined as the total engaged cutting edge length, *le*, divided by the undeformed chip cross-sectional area, A_o, in Figure 3.2.

$$q = \frac{l_e}{A_o} \tag{3.3}$$

The equation derived by Woxen [47] is another variant of the Taylor equation, based on studies by Woxen [47] of experimental tool life data and tool temperature measurements. From his studies, Woxen [47] came to the conclusion that the chip equivalent was a physical quantity that - together with cutting speed and material properties - determines the temperatures at the cutting edge.

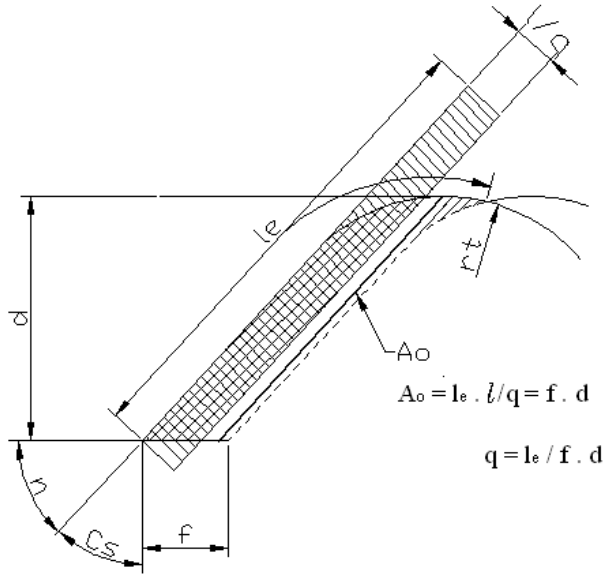

as proposed by Woxen

Figure 3.2: The chip equivalent.

Colding [48] in his research on tool life made extensive use of the chip equivalent concept to derive a generalised equation based on experimental tool life data. Applying dimensional analysis to the problem, Colding derived two dimensionless groups based on the assumption that tool life was a direct function of temperature.

The two dimensionless groups contained the chip equivalent, the thermal diffusivity, cutting speed and the tool life as variables. Colding [48] compared his derived tool life equation with Taylor's equation, and showed the influence of the chip equivalent on the Taylor constant *V*. However, Colding's equation, like Taylor's equation, would require extensive experimental studies to accurately determine the various empirical constants in the equation. Appling dimensional analysis to determine the tool life with respect to tool temperature and work piece properties, together with experimental data, produced two related dimensionless groups. The two groups took into account the following variables:

- Cutting temperature,
- Cutting speed,
- The area of cut,
- The specific cutting energy,
- The thermal conductivity of the work material (the volume specific heat of the work material), and an
- Experimental constant.

It can be noted that the effect of the above variables correlate reasonably well with tool temperature and tool life from previous work. From this dimensionless analysis it can be concluded that the Taylor equation (3.2) applies when the temperature is constant. This implied that, for the Taylor equation to hold, variations in cutting speed would affect the tool life but not the tool temperature. In discussing Taylor's research, Armerago and Brown [2] made two comments. The first comment was that the constancy of temperature of Taylor's equation was not valid, as the cutting speed did not affect the tool temperature. Secondly, Armerago and Brown point out that since the temperature is shown to depend upon all the other properties used in the tool life analysis, it follows that temperature need not be included as a separate variable in the analysis.

To reduce the time taken to carry out tool life tests using the same cutting conditions that are used with Taylor's equation, some researchers have found that the factorial experimental design method can give reliable results. This method was investigated

by Axinte *et al.* [49] and Dos Santos *et al.* [50], where they presented the case in favour of the optimal experimental design, which used the ongoing calculation of the values produced in the testing to check the convergence of the coefficient and their confidence intervals. The advantage of using the fractional factorial method is that it provides a way to produce the extended Taylor's theory with the minimum number of tool life tests. Researchers who have used this method have considered it to be efficient and to give good results. An example which illustrates the saving of time by using this method of tool life testing can be seen when carrying out tests for two cutting conditions (e.g. wet and dry). This would need four different sets of conditions carried out three times each, resulting in 24 tests to be completed. If the tool life test had been carried out simply by using Taylor's extended theory, the number of tests needed would have been 96, increasing the cost and time.

3.2.2 Tool life and wear mechanisms

In the preceding discussion all of the researchers derived empirical equations for tool life based on experimental data. No mechanism of wear was suggested or required, and the equations and constants were entirely empirical in nature. It has been suggested by a number of researchers from their experimental work and temperature analysis that the tool life is directly related to the tool temperature, with the tool life/temperature relation given by the following equation:

$$L = E_1 T^{-F} \tag{3.4}$$

where, L is the tool life, T is the tool temperature, and E_1 and F are constants. Woxen [47] and Colding [48] have established this equation for the clearance (flank) face wear, whilst Trigger and Chao [51] derived the same form from considerations of rake face wear. The equations from these analyses were all based on the common assumption that diffusion mechanisms were the dominant cause of tool wear.

Sata [52] examined tool life – as defined by a specific amount of tool wear - in light of the several wear mechanisms involved. He established the independence of rake face crater wear on cutting temperature, specific wear rate of the cutting tool,

frictional stress and chip-tool rubbing distance. Based on previous frictional wear studies on virgin surfaces, he expresses the tool wear by the following relationship:

$$W = w_s T_f \, pA^1 l_f \tag{3.5}$$

Where W is the total wear rate, w_s is the specific wear rate, T_f is the temperature of the friction surface, p is the contact pressure, A^1 the friction surface area, and l_f is the rubbing distance. Because of the assumption of Coulomb friction, equation (3.5) becomes:

$$W = w_s^1 T_f \tau A^1 l_f \tag{3.6}$$

where $w_s^1 = \frac{w_s}{\mu}$ with μ the friction co-efficient, and τ the shear stress on the friction face. By considering rake face conditions, Sata obtained the equation for crater wear depth h_c as:

$$h_c = w_s^1 T_c \tau_c l_c \tag{3.7}$$

where T_c is the chip/tool temperature, τ_c is the rake face shear stress and lc is the frictional sliding distance of the chip given by:

$$l_c = VLr_c \tag{3.8}$$

where V is the cutting velocity, L is the cutting time and, r_c is the cutting ratio, (i.e. t_1 / t_2).

From experimental data, Sata [52] showed that the rate of crater wear was dependent on the value of specific wear rate w_s^1. By estimating the tool face temperatures using the method of Lowen and Shaw [53], he further showed the dependence of specific wear rate on temperature as shown in Figure 3.3, and this provided the link between crater wear and rake face temperature. Sata [52] concluded from his crater wear

results that a high correlation exists between specific wear rate and rake face temperature, that in turn was proportional to rake face shear stress and frictional rubbing distance.

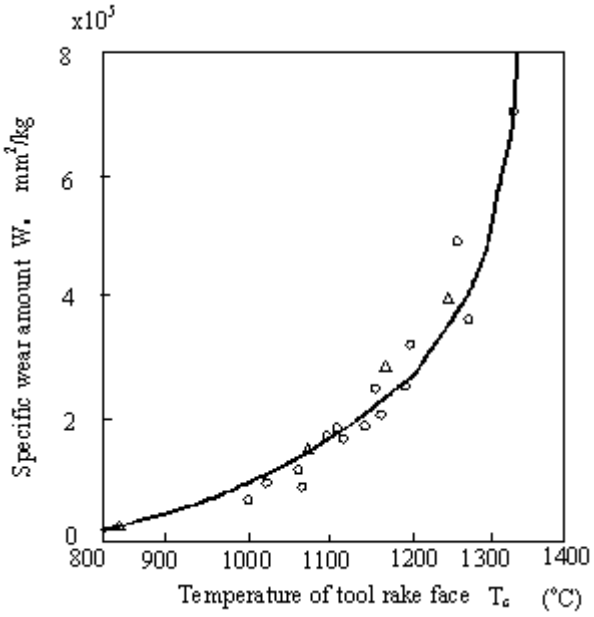

as given by Sata [52].

Figure 3.3: Relationship between the specific wear rate and tool temperature.

Trigger and Chao [51], by using the laws of adhesion wear in combination with the theory of rate processes, established the same general dependence of crater wear on temperature.

Takeyama and Murata [54] followed up the observations of Sata [52] on the dependence of the wear process on cutting temperatures on the fundamental mechanisms of tool wear. Extending their theory of rate processes to the problems of flank wear made an important contribution to the knowledge of tool wear, in that flank wear is now the most commonly used criteria of tool life. Expressing the total tool wear as the sum of wear due to brittle fracture, mechanical abrasion, rate processes (eg. diffusion) and any other mechanism not accounted for by the above, they obtained the expression:

$$W = W_b(n_s, \sigma_s) + W_a(S_{cd}, \sigma_a) + W_r(T_a, t) + W_i \tag{3.9}$$

where W is the total wear, W_b is the wear due to brittle fracture, W_a is the wear due to abrasion, W_r is the wear due to rate processes, W_i is the wear due to any other mechanism, σ_s is the resistance to brittle fracture of the tool material, σ_a is the abrasion resistance of the tool, n_s is the number of shocks, S_{cd} is the cutting distance, T_a is the absolute temperature of the cutting edge, and t is the cutting time. Neglecting the term W_i, which should be small compared to the other mechanisms, and assuming that in continuous cutting the term W_b can also be neglected equation (3.9) becomes:

$$W = W_a(S_{cd}, \sigma_a) + W_r(T_a, t) \tag{3.10}$$

on the basis that fresh abrasives in the workpiece continually abrade the tool and their distribution would be fairly uniform, W_a will be proportional to the cutting distance and independent of the temperature, W_r, the rate term, can be assumed to be proportional to $e^{-E/RT}$ where E is the activation energy, R is the universal gas constant, and T_a is the absolute temperature. From this the total wear becomes:

$$\frac{dW}{dt} = V(T_a, f)A_1 + B_1 e^{-E/RT} \tag{3.11}$$

where V, is the cutting velocity, A_1 and B_1 are constants associated with the work material and f, is the feed.

Using experimental cutting data for ISO P15 carbide tools, Takeyama and Murata [54] were able to evaluate the constants in equation (3.12), and thus show Figures 3.4(a) and (b) that below a certain cutting temperature the wear was independent of temperature, *i.e.* the first term of equation (3.11) predominated, but above a certain temperature (about 1200 K for the tool/work combination used) the wear was highly temperature dependent.

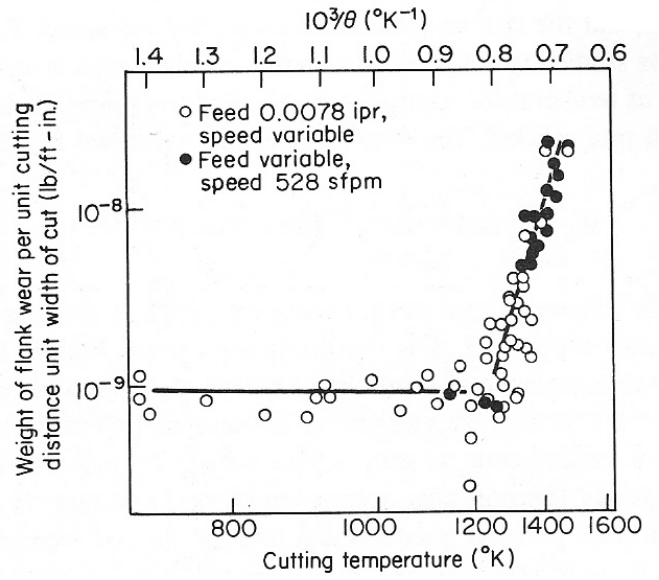
$10^3/\theta$ (°K^{-1})
1.4 1.3 1.2 1.1 1.0 0.9 0.8 0.7 0.6
Feed 0.0078 ipr, speed variable
Feed variable, speed 528 sfpm
Weight of flank wear per unit cutting distance unit width of cut (lb/ft – in.)
10^{-8}
10^{-9}
800 1000 1200 1400 1600
Cutting temperature (°K)

(a)

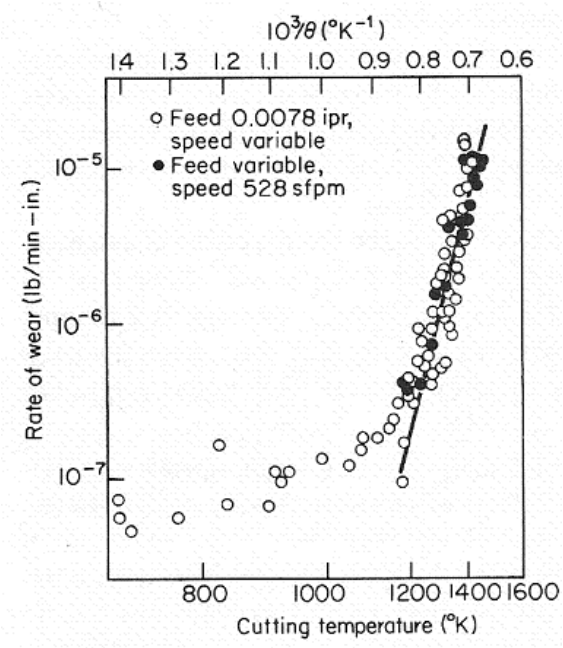
$10^3/\theta$ (°K^{-1})
1.4 1.3 1.2 1.1 1.0 0.9 0.8 0.7 0.6
Feed 0.0078 ipr, speed variable
Feed variable, speed 528 sfpm
Rate of wear (lb/min – in.)
10^{-5}
10^{-6}
10^{-7}
800 1000 1200 1400 1600
Cutting temperature (°K)

(b)

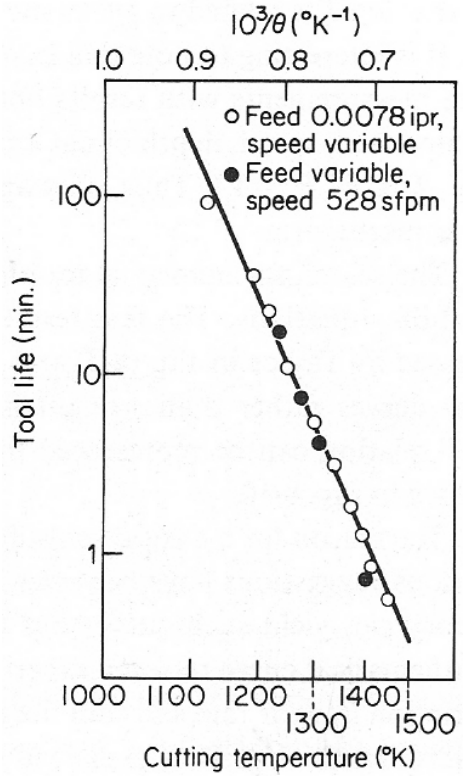

(c)

as given by Takeyama and Murata [54].

Figure 3.4(a-c): Tool wear and tool life data as functions of the measured cutting temperature when machining stainless steel with carbide tools.

From the work done by Takeyama and Murata [54] it would seem as though there are two principal mechanisms involved in the wear of carbide tools. At low cutting speeds, when the cutting temperature is low, the wear is abrasive and dependent only on the cutting distance. At higher speeds, and also higher cutting temperatures the temperature dependent mechanism diffusion predominates. Under normal commercial cutting conditions in lathes (*i.e.* high temperatures) this latter term would be expected to be the one controlling tool life, with the rate of tool wear proportional to $e^{-E/RT}$ for a given tool/work combination regardless of the other cutting conditions. Takeyama and Murata [54] concluded by showing that, for a given tool/work material combination, it is possible to predict tool life from a knowledge of the cutting temperature only using graphs such as that shown in Figure 3.4(c).

3.2.3 Temperature dependency on tool life

From the results of Takeyama and Murata it can be seen in Figure 3.4(c) that for a

given tool/work material combination, tool life is a function of temperature. If this is the case, then it should be possible to use the temperatures from the predictive machining theory used in section 2.2 to determine tool life. Oxley, Hastings and Stevenson [55] investigated the possibility of predicting the tool life, making use of the experimental results of Takeyama and Murata [54]. They derived the following tool life relationship:

$$L = 10^{71.75}(T_{tool})^{-22.82} \tag{3.12}$$

where L is the tool life in minutes for 0.6 mm flank wear, and T_{tool} is the cutting tool temperature in ^{o}K. In the tool life experiments the side cutting edge angle σ was not zero in all cases as it should be for orthogonal conditions, and the tool had a nose radius of 0.8 mm, which meant that cutting was not on a single straight cutting edge. In making predictions of temperature, however, the process was assumed to be orthogonal with allowance made for the effective increase in width of cut by:

$$w^1 = \frac{w}{\cos\sigma} \tag{3.13}$$

The errors involved in neglecting the nose radius were assumed to be small. Oxley *et* al [55] simply assumed that the life would be a third of the value given by equation (3.12). This supposes that the flank wear against time graph is a straight line passing through the origin which in general is an oversimplification of the actual relation. However, it was sufficiently accurate for their purposes. In making tool life predictions T_{tool} was found from:

$$T_{tool} = T_{flank} = 0.89T_{\text{int}} \tag{3.14}$$

where T_{flank} is the temperature at the flank and T_{int} (interface temperature) was calculated from equation (3.14). This equation was derived from the experimental work of Boothroyd *et al*. [56], and shows that the ratio of flank to interface temperature (^{o}K) varies between 0.82 and 0.95 with an average value of 0.89.

The predicted tool life results given by the full lines in Figure 3.5(a) were derived from equations (3.12) and (3.14). T_{int} values were used, obtained from the earlier version of the predictive machining theory for the cutting conditions used in the tool life tests [63]. It can be seen that the theory predicts the correct trends in tool life with changes in cutting speed, V, feed, t_1 and side cutting edge angle σ, and also that the quantitative agreement is good. The predicted line of tool life against cutting speed Figure 3.5(b) is slightly curved and not straight as assumed in the well known Taylor tool life relationship. This is in agreement with the experimental findings of a number of researchers. There is considerable scatter in the experimental results given in Figure 3.5(c), which is typical of tool life tests, and an explanation for this scatter was given in light of the theory presented. Hastings and Oxley [57] stated that if tool life is considered to be a function of the flank land temperature, then the scatter in the tool life results reflects either:

(i) a variation in the tool wear rate at constant temperature,
(ii) or a significant variation in the flank land temperature.

However, data by Takeyama and Murata [54] and Sata [52] for wear rate versus temperature indicates that the variations in wear rate for a given temperature are less than the measured variations in tool life evident in Figure 3.5(a). This therefore suggests that there is another mechanism causing the variation in tool life. On the basis of the assumed total dependence of tool life on cutting temperature, this can only be caused by variations in the cutting temperature.

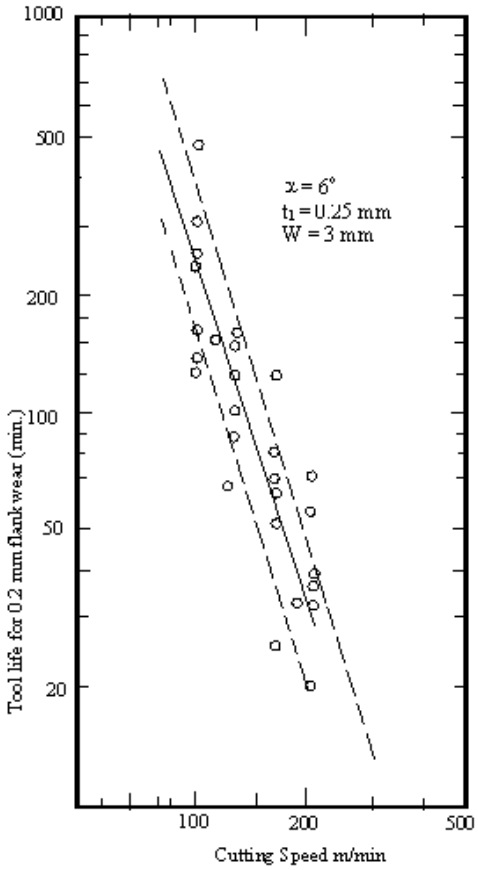

for the machining of XCsteel with an ISOP10 carbide grade tip

As found by Hastings and Oxley [55]

Broken line represents predicted variation in tool life.

Figure 3.5(a-c): Predicted and experimental tool life results

Chao and Trigger [58] give data for the variation of cutting temperature with cutting speed; Brinell gives data for hardness. From their results it can be seen that the temperature increases with an increase in hardness.

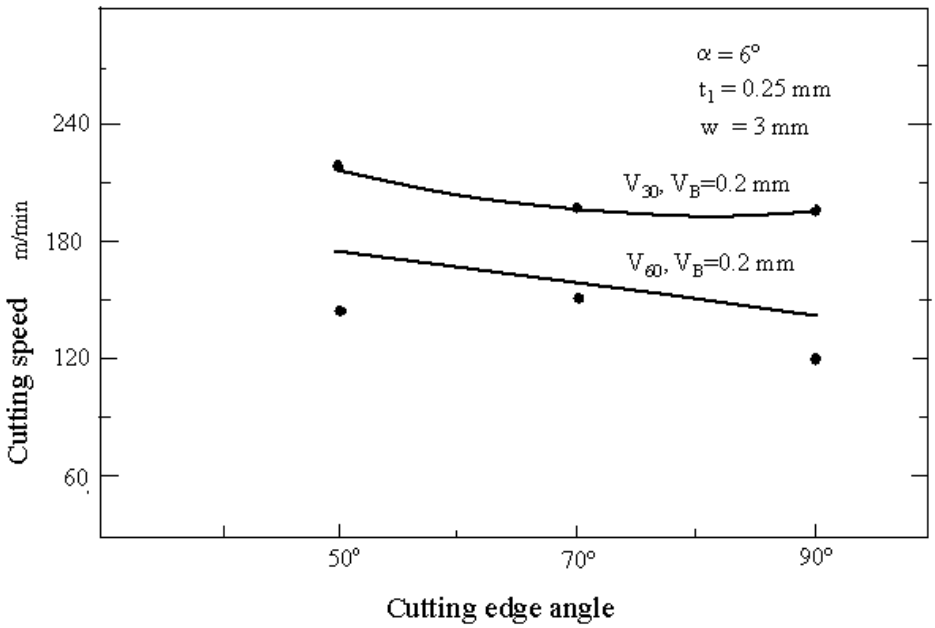

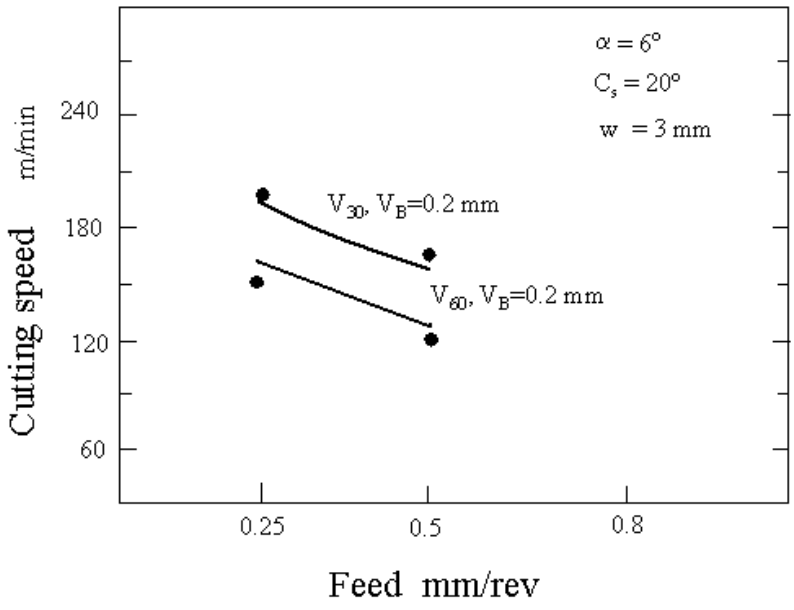

As found by Hastings and Oxley

Figure 3.5(b and c): Showing the influence of tool cutting edge angle and undeformed chip thickness.

Following a suggestion by Oxley *et al.* [55] an alternative method was used by Hastings and Oxley [57] to determine tool life. The method involved using the experimental values of tool life in conjunction with values of temperatures predicted by the machining theory to obtain the constants in equation (3.14), which is opposed to using experimentally measured temperatures as in equation (3.12). This would be analogous to finding the constants in the Taylor tool life equation, but the resulting

function would be applicable to a much wider range of conditions, and would enable the influence of feed and tool shape to be taken into account in addition to the cutting speed. A preliminary investigation of this kind, in which a set of four tool life tests for various speeds and feeds in Figure 3.6(a-d) were used to determine the constants in equation (3.5), was carried out by Hastings and Oxley [57]. The original tests were done using En8 steel with a P30 grade triangular insert in a standard tool holder.

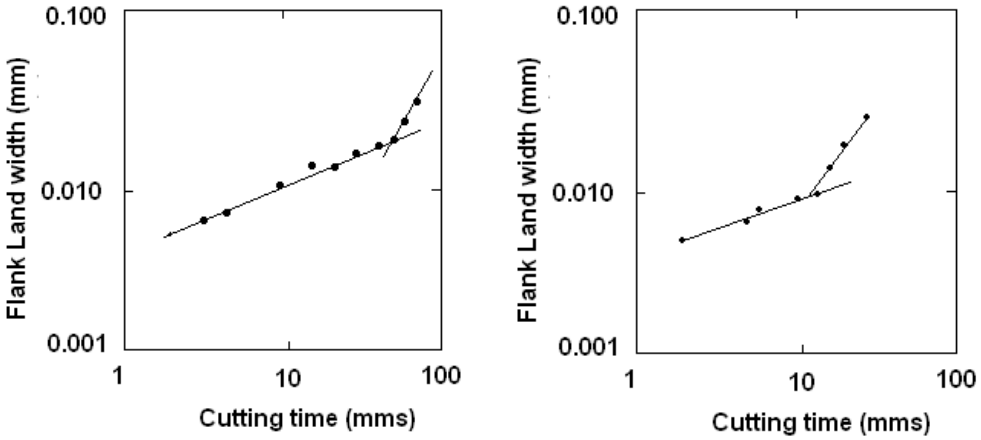

(a) V = 122 m/min, $\alpha = 5^o$, $t_1 = 0.28$ mm/rev, $T_{tool} = 1180$ K

(b) V = 122 m/min, $\alpha = 5^o$, $t_1 = 0.53$ mm/rev, $T_{tool} = 1228$ K

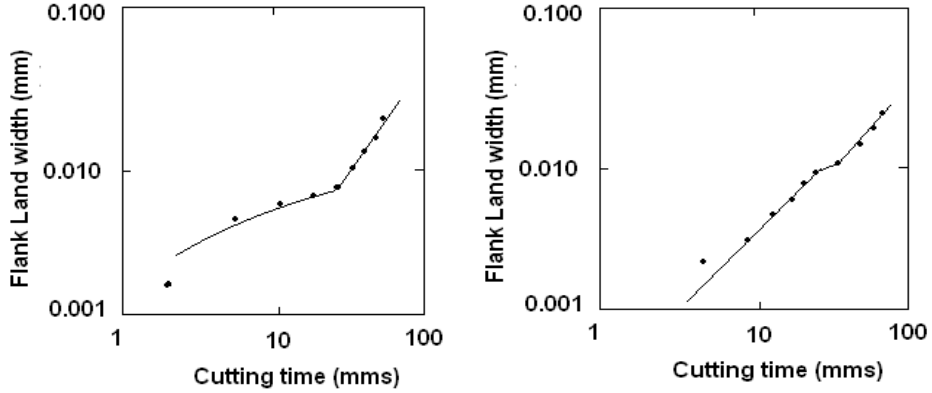

(c) V = 163 m/min, $\alpha = 5^o$, $t_1 = 0.132$ mm/rev, $T_{tool} = 1201$ K

(d) V =63 m/min, $\alpha = 5^o$, $t_1 = 0.53$ mm/rev, $T_{tool} = 1120$ K

Obtained from Bruce.

Figure 3.6(a-d):Tool life cutting times for various cutting speeds and undeformed chip thickness.

Using a tool wear limit of 0.2 mm for the tool life test, the tool tip temperature is now plotted as a function of the corresponding predicted temperature, and a

regression line calculated for the results as shown in Figure 3.7. This gave the following equation relating to tool life, in the same form as equation (3.12), to the predicted tool life,

$$L = 10^{50.38}(T_{tool})^{-16.06} \tag{3.15}$$

with L equal to the tool life for 0.2 mm wear, and T_{tool} in this case taken as 0.89 T_{int} in the same form as equation (3.14) temperature in K. The results are plotted in Figure 3.8, together with the estimated tool life band obtained by taking into account the material variability as explained above.

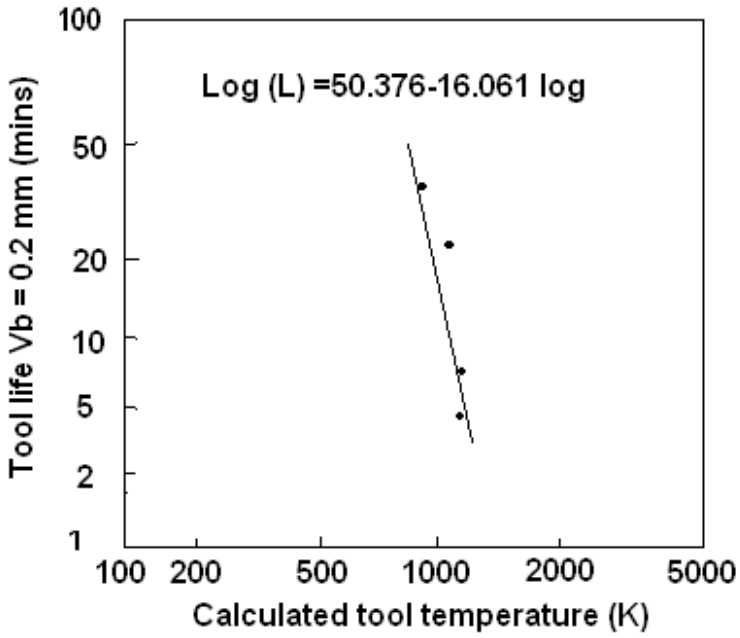

Figure 3.7:Tool data of (Figure 3.6) plotted as a function of the predicted cutting temperature from Bruce.

While not as good as the results shown in Figure 3.7, it can be seen that the agreement between predicted and experimental tool life values is again encouraging. Richardson, Hastings and Oxley [59] presented results for tool life for high-speed steel cutting tools for a plain carbon steel work material of 0.5 percent carbon content using the above method.

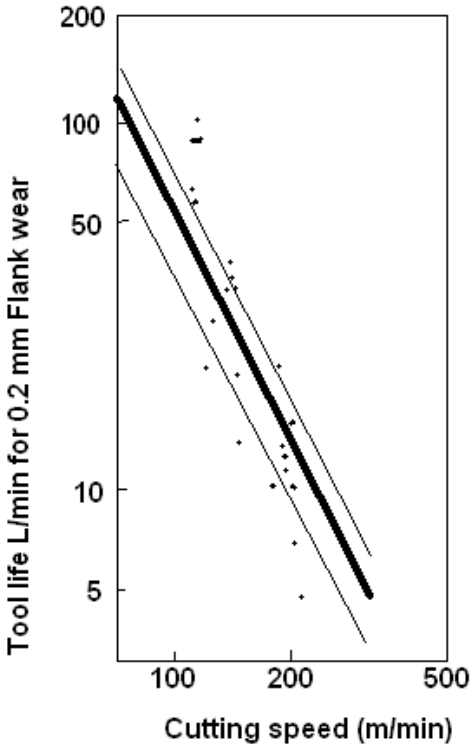

t_1 =0.25, w = 3 mm, α = 6°.

Data calculated by using the relationship given by equation (3.15)

XC45 steel with ISO P30 grade carbide tool tip.

Figure 3.8: Predicted and experimental tool life for machining

It was found that for the conditions where built-up edge did not occur, the temperature index for equation (3.4) was -21.56, which did not vary greatly from the index (-22.82) obtained *by* Takeyama and Murata [54] in the diffusion range. It was also found that the equation derived by them gave a significantly better fit with experimental tool life data than that given by the empirical equation (3.2), which is again encouraging. It can be concluded from these investigations that the predicted temperatures can be used to determine tool life, with account taken of variations in work, material, properties, and cutting conditions, far more effectively than with the usual empirical methods.

3.2.4 Tool Wear Rates

Research carried out by Hastings *et al.* [60] presented results relating to tool life, by relating tool wear rates to the reciprocal of the temperature. In this way the more fundamental relation given in equation (3.11), as derived by Takeyama and Murata

[54], can be investigated using temperatures predicted from the machining theory. In the paper by Hastings *et al [57]*, the first term of equation (3.11) was neglected on the grounds that, for carbide tool materials at cutting temperatures in excess of 700°C to 800°C, the predominant wear process would be a diffusion wear process, and the first term which is due to abrasion would not significantly affect the total wear.

The work by Takeyama and Murata [54] expressed the total wear rate $\frac{dW}{dt}$ as the rate of weight of flank removed per unit time, and in the work by Hastings *et al.* the wear rate was defined as the rate of growth of flank land.

In determining temperatures from the machining theory Hastings *et al.* [57] used a somewhat different approach to that described above. It will be recalled that in the earlier work, the interface temperature T_{int} was taken as the maximum temperature in the chip, as given by equation (3.12) and equation (3.14) used to determine the tool temperature. In the work by Hastings *et al.* the interface temperature was calculated using equation 3.16.

$$T_{\text{int}} = T_w + T_{sz} + \psi_T T_m \tag{3.16}$$

where T_w is the work temperature, T_{sz} is the shear zone temperature rise, T_m is the maximum temperature rise in the chip, and ψ_T ($0 < \psi_T \leq 1$) is a factor which allows for T_{int} being an average value (ψ_T for a sharp tool = 0.7).

Research carried out on flank wear by Hastings *et al.* [60] has shown that the flank wear rates have been related to the predicted temperatures instead of experimental temperatures. The problem which arises as with the earlier research on tool life [57] is the question of which estimated temperature to use. Obviously, the tool wear rates are temperature dependant; therefore the temperatures of interest are those on the wearing surfaces of the tool. Due to the difficulties in obtaining the average flank land temperature, Hastings et *al.* [60] adopted to use the theoretical estimates of the average tool chip interface temperature (T_{int}). This was achieved using a modified version of the predicted theory of machining with a constant value of $\delta = 0.02$ being used, which may at first appear an inappropriate choice. There is, however, some experimental evidence by Bothroyd [56] and Zakaria [61] to show that there is a

good correlation between the average interface temperature and the average flank land temperature, as shown for example, by equation (3.14).

Results of experimental wear rates plotted against the reciprocal of temperature are given in Figure 3.9. In this figure the full lines represent linear regressions of the experimental wear rates with the reciprocal of temperatures, while the broken lines are the 95 percent confidence intervals for the regressions.

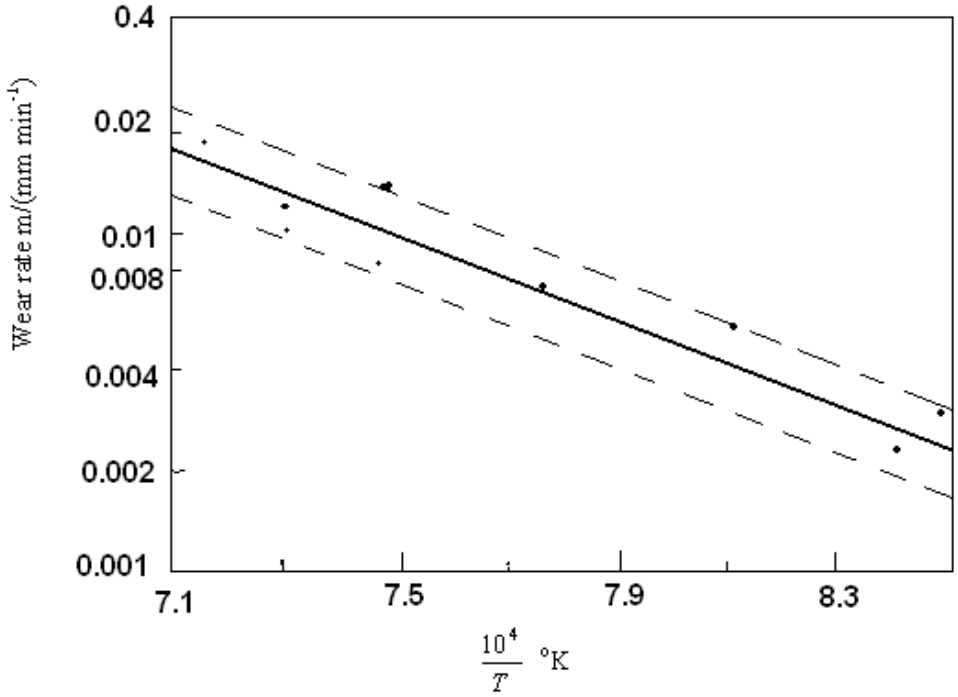

as obtained by Hastings *et al.* [60]

Figure 3.9: Results of wear rate against reciprocal of tool temperature for two rake angles.

It should be noted that the results given in Figure 3.9 show trends which are consistent with known tool wear behaviour: with increases in cutting speed and undeformed chip thickness, and decreases in tool rake angle resulting in higher wear rates, and with cutting speed having the largest effect and rake angle the least. It can be seen from the results in Figure 3.9 that the majority of the experimental points fall within the confidence interval bands, indicating that the log of the tool wear rate is inversely proportional to the estimated tool temperature within the variability of the experimental data. In Figure 3.9 there is some apparent separation of positive and negative rake angle points, but the sample is too small for the separation to be

significant. The results clearly indicate that the tool wear mechanism is temperature dependent, with the diffusion equation consistently followed. Figure 3.10 shows the effect of using two different grades of carbide tool materials, the harder wear resistant finishing grade giving lower wear rates than the tougher general purpose grade of carbide as would be expected.

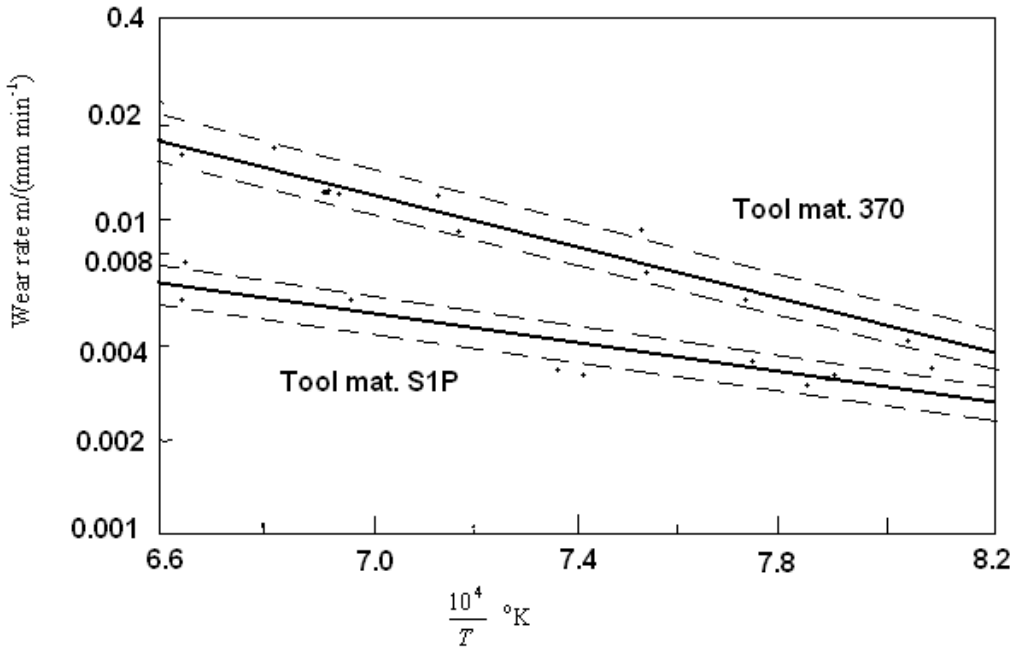

(α =-5^o , t_1 = 0.11 mm, 0.24 mm and 0.54 mm)
as obtained by Hastings *et al.[60]*

Figure 3.10: Wear rate for two tool materials when machining axle steel of 0.41 percent carbon content.

The results given in Figure 3.11, which show the wear rates for a given tool material with two different work materials, are interesting in that, for a given temperature, the low carbon steel gives higher wear rates than the medium carbon steel. However, the points marked A and B in Figure 3.11 indicate the wear rates for the same cutting conditions, *i.e.* speed, undeformed chip thickness, etc, and it can be seen that the medium carbon steel gives the higher wear rate which is the expected result.

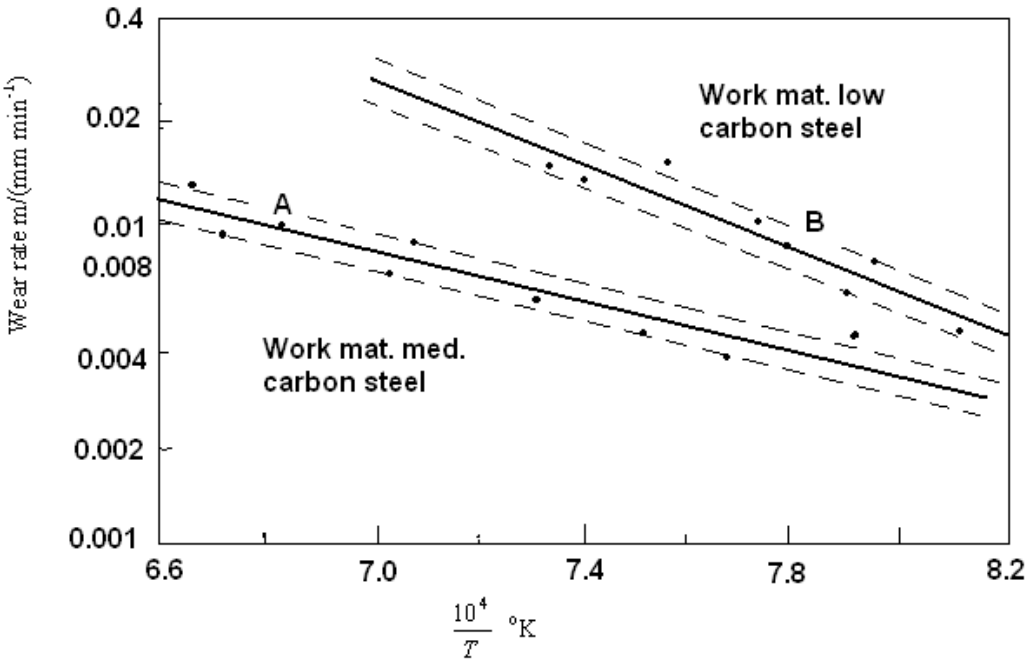

(α =-5^o , t_1 = 0.11 mm, 0.21 mm and 0.41 mm)

as obtained by Hastings *et al.* [60]

Figure 3.11: Wear rates for two work materials when machining with K45 material.

A possible explanation given by Hastings *et al. [60]* for the higher wear rate of the low carbon steel for a given temperature is as follows. Due to the high temperatures in the interface contact zone, work material in this zone will be transformed to austenite, having a carbon content approximately equal to that of the work material. Carbon which is highly soluble in austenite will diffuse more rapidly from the high carbon content tool material into the low carbon steel than it will into the medium carbon steel. Loladge [62], in discussing carbon diffusion, provides an equation for diffusion of carbon into austenite as a function of the austenite carbon content, and when applied to the two work materials used here, gives diffusion rates which are at least ten times greater for the low carbon steel. This high rate of diffusion of carbon however, is not the direct cause of the observed differences in wear rate, as it requires the removal of the large atomed heavy metals present in the tool material for wear to be observed. The diffusion of carbon from the tool results in a carbon depleted layer on the surface of the tool, and this gives rise to the formation of complex metallic carbides at the tool/work material interface Suzuki [63]. The removal of this by workpiece and chip is believed to give rise to the observed tool wear Yamamoto [63]. The higher rate of carbon diffusion for the flow carbon

material results in a greater rate of formation of the complex carbides, and at a higher wear rate, as evidenced by the experimental results of Narutaki and Yamane [64].

3.3 Concluding Remarks

The use of Taylor's equations (3.1 and 3.2) has considerable disadvantages since the information necessary to define constants in these equations requires a large number of tool life tests. Nevertheless, this approach is still widely applied with many books and computer programs available for tool data references to determine tool life. However, due to the enormous expense involved in accumulating data and the limited applicability of data once collected, considerably more effort needs to be directed towards the understanding of the complex nature of tool wear in an effort to develop more theoretically based methods of tool life estimation. Consideration of the turning process when the tool temperature is sufficiently high for diffusion to occur (as discussed in Section 3.2.2.), shows that a diffusion based equation can be used to effectively relate the wear rate of a carbide tool to the temperature of the tool. This is in addition to considering the diffusion method to reduce the number of tool life tests. The use of the fractional factorial experimental design method will also substantially reduce the number of tool life tests.

Diffusion is clearly the basic mechanism involved in wear for the conditions considered, and is basically the transference of atoms from a region of high density to a region of low density. For diffusion to occur in machining there must be transference of atoms from the tool to the workpiece, which accelerates as the tool tip temperature increases, accelerating tool wear. From the previous discussion, it can be concluded that tool life can be used as a measurement for determining the effectiveness of the cooling system, as we know the wear mechanisms are increased at elevated temperatures.

Knowing the temperature in the cutting process is of great importance to this research in order to determine the most effective method of cooling the tool tip. Tool life can be calculated from the temperature, so minimises the time needed for determining the effectiveness of the different air-cooling methods.

In conclusion, the results obtained in this investigation support the findings obtained by other researchers such as Takeyama and Murata [54] and Bertil N. Colding [48], that during cutting conditions using carbide tools, diffusion seems to be the dominant factor controlling tool wear rates and therefore tool life. For accurate predictions of tool life to be made it is clear that accurate estimates of temperature are essential. With this in mind, it is essential that the predicted theoretical temperatures and experimental temperatures are reliable for accurate tool life predictions.

CHAPTER 4

CHARACTERISTICS OF AIR COOLING

4.1 Overview Of Air Cooling

Air-cooling of cutting tools has struggled to be taken seriously by the manufacturing industry during the machining processes when liquid coolant has been available. The object of this research is to prove that air-cooling can be improved to the point that it can replace traditional cutting fluid, without any reduction in tool life or reduction to quality of work piece surface finish.

Air-cooling is certainly not a new idea, and has been used in many industrial applications over the years, such as dissipating the heat generated by electronic equipment or reducing the temperature inside buildings. There are many examples of air being used as the cooling method. During the late 1950's there were a number of people who thought the answer to the problem of cooling tool tips during machining was by directing refrigerated carbon dioxide at the cutting zone. However, it soon became clear that this was not an economical proposition, resulting in the central refrigerating carbon dioxide plant either being left unused or dismantled. Using refrigerated gases was examined by Walter [65] where he showed that the use of these fluids can be economic in certain situations. Hollis [66] found that carbon dioxide can be particularly effective in reducing crater wear on carbide tools when machining titanium alloys and other difficult to machine materials. Since carbon dioxide is a greenhouse gas this method of cooling would no longer be acceptable to today's manufacturing industry.

A comparison of using refrigerated compressed air with ambient compressed air was conducted by Pahlitzsch [67], where he found that there was a 400 percent increase in tool life for air at –40 ^{o}C to –56 ^{o}C, while even at –8 ^{o}C, a 40 percent increase occurred when the tests were made with steel machined at 30 m/min. Since Pahlitzsh proved that refrigerated air increases tool life, the challenge is to provide a very cold air stream to the tool tip during machining. Heat dissipation at the tool tip when cooled by air is limited in comparison to liquid coolant. In an attempt to increase the

effectiveness of air cooling, a number of methods have tried to improve the conductivity of the air before presenting the air to the cutting zone. Currently, the cooling methods used involve liquid nitrogen evaporation refrigeration, vapour-compression refrigeration, adiabatic expansion refrigeration and semiconductor refrigeration with vapour compression refrigeration. All of these methods are able to reduce the temperature of the cutting zone. Unfortunately, they all need additional energy to be used to be able to supply the cool air to the tool tip adding to the environmental burden. Therefore, the ideal air cooling method is one that only needs the supply of compressed air, eliminating the need to rely on any primary cooling system. Attempts using “Impinging Air Jets” have been made in a variety of industrial applications. Although this cooling method does not reduce the temperature of the air presented to the tool, the impinging air jet increases the effectiveness of removing heat from a surface. It seems reasonable then to investigate how effective this type of cooling method may be in cooling the tool interface during machining. The metal cutting tests (Chapter 6) show that the nozzle position was critical to the efficiency of the impingement cooling process, making this method of cooling impractical for use in the workshop. Another method of improving the heat dissipating effects of the air is by using a “Ranque-Hilsch Vortex Tube”, a device that can produce cold air and provide a cold jet of air to the tool interface. For workshop use it is found to be a simple device providing cold air to the cutting zone requiring no finicky adjustment. The mechanism producing the temperature separation of cold air and hot air when passing through the vortex tube is examined in Section 4.3.

Obviously the use of an air jet is highly desirable as there are no environmental issues associated with its use, except for the usual safety procedures necessary for compressed air. Normally modern machine tools have compressed air readily available to operate any additional auxiliary equipment, making it ready for use in cooling. For these reasons, the use of air-cooling is convenient to use for cooling the cutting zone.

4.2 Jet Impingement Cooling Process

4.2.1 Introduction

When a velocity air jet impinges vertically on a flat plate it hits the plate and spreads either side of the point of impact. At the point of impact (directly below the air jet) a stagnation point occurs. The highest level of cooling occurs here. As you move away from the stagnation point the velocity of air at the flat plate increases to a secondary maximum, and then decreases again. It is over the area between the stagnation point and the point of secondary maximum air velocity that the majority of cooling occurs. It is for this reason that the distance to the secondary maximum air velocity would have to be maximised. Changing the distance between the air jet and the plate (h_j) will alter the distance to the secondary maximum air velocity. Consequently, the major focus of this research is to ascertain the effectiveness of the impingement process (what effect is there if any on distance h_j and secondary maximum air velocity) when applied to the tool face.

4.2.2 Jet impingement cooling mechanism

The theory explaining how altering the jet height h_j affects the velocity of the airstream and the heat transfer, and the behaviour of the airstream as it leaves the jet and hits the flat wall has to be determined. Figure 4.1 shows the impinging air jet having a diameter D at a distance h_j from the flat plate. As the air leaves the jet it is assumed to have a uniform velocity in a direction perpendicular to the flat plate. This interaction of the air with its surroundings begins to slow the air, causing a linear expansion of the width of the air jet. As the jet strikes the flat plate it separates either left or right of the point of impact.

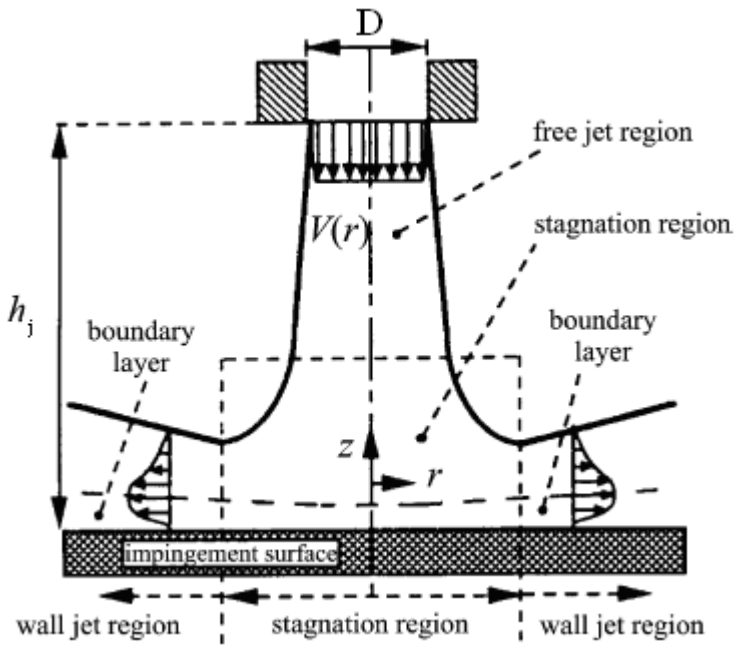

as given by M.Angioletti *et al.* [68]

Figure 4.1: Flow regions for air impinging free-surface jet.

The point on the flat plate that is vertically in line with the centre of the jet is known as the stagnation point. At this point air velocity is zero (stagnation), and the value of *r* is zero (*r* is the measured distance from the stagnation along the flat plate). That is, *r* is the radial distance from the centre of the jet.

Other shaped surfaces have been researched. Hee Lee *et al.* [69] presented results of jet impingement cooling. However, it is necessary to consider additional factors in this application, such as the shape of the tool tip surface and the speed of rotation of the workpiece, as these will have an effect on the impinging jet as shown in Figure 4.2.

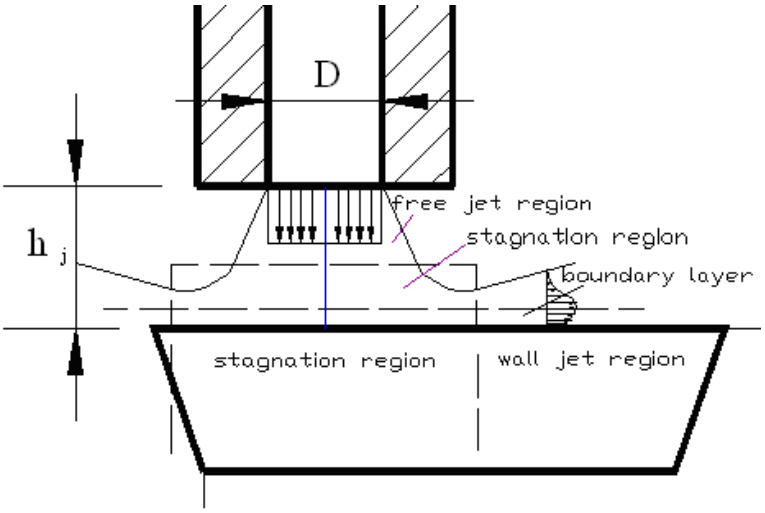

Figure 4.2: Flow regions for air impinging jet on the top face of a tool tip.

As the air stream moves into the wall jet region shown in Figure 4.1 it begins to slow, due to the friction of the flat plate. This is due to the velocity boundary layer. As particles make contact with the flat plate they assume zero velocity. These particles then act to retard the motion of the particles in the adjoining fluid layer, which in turn slow the motion of the particles in the next layer. This occurs until the particle has a negligible effect on the velocity of the adjoining particle. At this point the particles have the velocity of the free stream. Figure 4.3 below shows a diagram of the effect of the boundary layer.

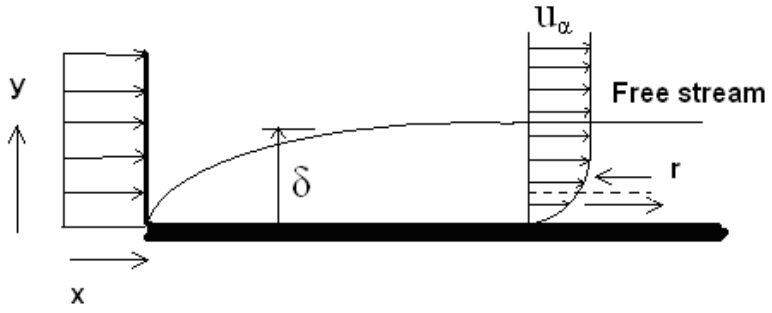

Figure 4.3: Laminar Boundary Layer.

The value δ represents the distance from the wall where the particle velocity becomes 99 percent of the free stream velocity, and is known as the boundary layer thickness. Greater fluid velocity means a greater heat transfer, thus a thinner boundary layer results in a greater heat transfer across the surface. Creating a

turbulent air stream induces vortices within the air stream. The vortices act to 'break up' the boundary layer, hence increasing the amount of heat transfer, as the boundary layer is thinner. In order to operate in the turbulent region, the velocity of the air stream leaving the jet has to be sufficiently high. Determining the minimum velocity required for turbulence is discussed in M. Angeioletti *et al.* [70] where it is shown that the swirls are vortices that are induced by the turbulent motion of the air stream as shown in Figure 4.4.

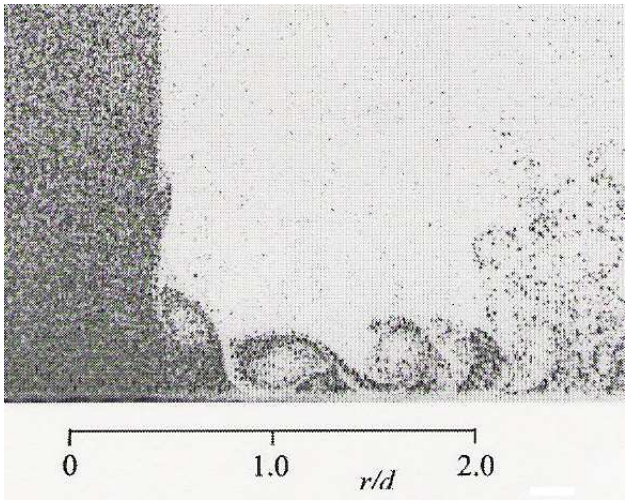

Taken from M.Angioletti *et al.*

Figure 4.4: Visualised flow of an impinging jet.

Figure 4.5 shows a simplified view of a cross section of a typical air jet, showing the physical contour of the air stream. It is well known that air leaves the jet at a uniform velocity and it begins to expand away from the jet centre. When it strikes the flat plate, the air stream spreads away from the stagnation point. The air stream has a high velocity when it leaves the jet, and as it strikes the wall it is forced to change direction. During this process the momentum of the air stream perpendicular to the wall causes the jet stream to compress; this compression is shown by the dotted line in Figure 4.5. It is shown that the maximum air stream velocity at the flat plate occurs when the air stream is the thinnest, making the air move faster to maintain the same mass flow rate Hee Lee [71]. It is the same theory that is used in standard throttling applications. This velocity is the secondary velocity maximum as the maximum velocity occurs at the jet exit.

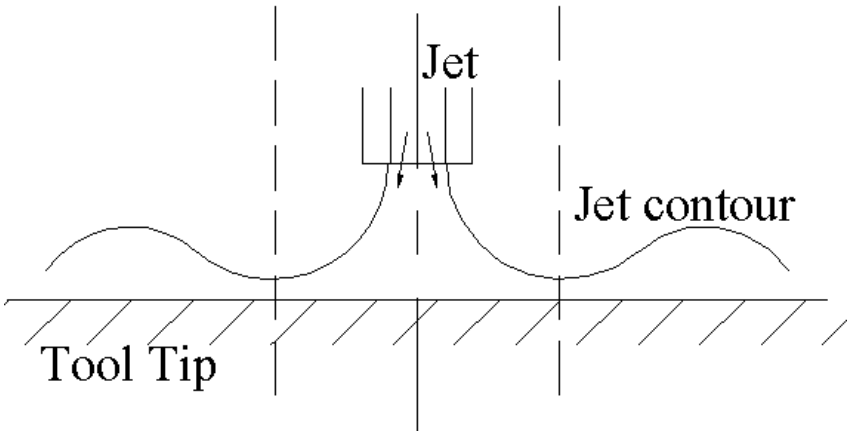

Figure 4.5: Simplified flow contour and velocity profile of an impinging jet.

The heat transfer at the flat plate is very much dependant on the velocity of the air flow past the plate. Therefore, the greatest heat transfer will occur at the points of maximum air velocity.

The most common method of determining the effectiveness of heat transfer is by using the Nusselt (Nu) number, which is a number developed to directly measure the heat transfer at a surface. If the Nusselt number is known at all points on the flat plate then the heat transfer across the flat plate is known.

The Nusselt number is defined as the dimensionless temperature gradient at the surface of an object and as defined as (4.1):

$$N_u = \frac{h_T}{k_f} \tag{4.1}$$

where h_T is the local convection coefficient, L_P is the plate length in m.

Incropera [72] developed a theoretical model that predicts the behaviour of the Nusselt number during jet impingement on a flat plate. Figure 4.6 shows these predictions.

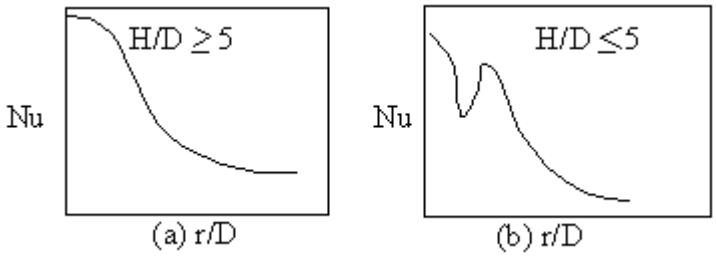

Figure 4.6: Variation of Nusselt number on a flat plate during jet impingement.

Taken from Incropera

Both diagrams in Figure 4.6 show how the local Nusselt number varies as the distance *r* from the jet centre is increased. The left side of the diagrams indicates the jet centre. Figure 4.6(a) shows a typically expected Nusselt number distribution. The peak occurs directly below the centre of the jet (at the stagnation point), and the Nusselt number decreases as the distance from the jet centre increases.

Figure 4.6(b) above shows a differing expected Nusselt number distribution. It differs because there is a secondary peak Nusselt value away from the stagnation point. This secondary peak would increase the cooling undertaken, causing a desirable effect. The reason this secondary peak is produced is due to turbulence in the air stream.

If there is a sharp rise in the level of turbulence, which occurs as the air jet flows along the stagnation region to the wall, then vortices may be induced in the stagnation region Figure 4.1. These vortices act to increase the air velocity, and so increase the heat transfer experienced. Thus a secondary Nusselt number maximum occurs.

As the $\frac{h_j}{D}$ value decreases, the stagnation region increases, and the rise in the level of turbulence across this region would increase. Incropera suggests that all $\frac{h_j}{D}$ values below 5 produce a large enough rise in the level of turbulence to induce the secondary Nusselt number maximum.

The measured local Nusselt number is dependent on the local velocity of the fluid. The Nusselt number is dimensionless, so to allow for a more versatile set of results a dimensionless velocity measure would be advantageous. The Reynolds number was developed as a measure of the fluid velocity characteristics and is dimensionless; therefore it makes a perfect number to measure the fluid velocity characteristics. The Reynolds number definition is the ratio of inertia to viscous force and is defined as:

$$R_e = \frac{\rho V_a D}{\mu} \tag{4.2}$$

Jung- Yang et al. (1996) used a fixed ratio of 2, and varied R_e and the jet diameter to see how it affected the average Nusselt number. Their conclusion was that as the jet diameter increased, and all else remained constant, the average Nusselt number would increase. This increase does not have a linear relationship, and they indicated that increasing the jet diameter beyond 5 - 6 mm would have little effect on the average Nusselt number. Hence the selection of the jet diameter is crucial to the final results.

Jung-Yang San et al. [73] discovered that altering the jet diameter with all other factors constant would alter the measured value for the Nusselt number. They also noted that as the jet diameter reached 5 - 6 mm, further increasing the jet diameter would have a lesser effect on the Nusselt number. The jet diameter used for cooling the tool tip during machining ranged from 1 mm diameter to 4 mm diameter. Jets greater than 5 mm are shown not to have a largely increased Nusselt number according to Jung-Yang San *et al.* [73].

4.3 Ranque-Hilsch Vortex Tube

4.3.1 Introduction to Ranque-Hilsch vortex tube

The Ranque-Hilsch vortex tube is a device that is able to separate airflow into two different streams simultaneously, one hotter than the inlet air and the other cooler as shown in Figure 4.7. Having no moving parts makes the vortex tube remarkable. This device has been referred to as “Maxwell’s demon,” a fanciful means of separating heat from cold without work. The vortex tube basically consists of three

pipes and a supply of compressed air to achieve a moderately low temperature at the cold outlet.

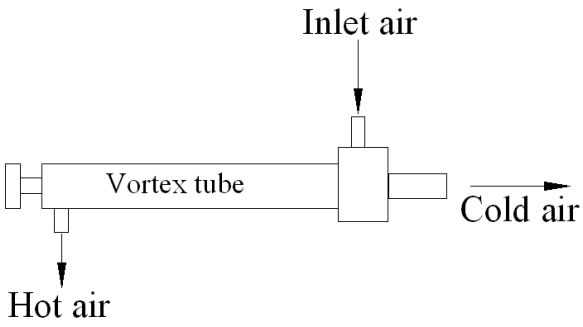

Figure 4.7: Schematic diagram of showing split of hot and cold air.

The origin of the device is obscure. The principle was first discovered in 1928 by accident by a Frenchman, George Ranque [74], a French physics student. He was experimenting with a vortex-type pump that he had developed when he noticed warm air exhausting from one end and cold air from the other. Ranque attempted to exploit the commercial potential for this strange device that produced hot and cold air with no moving parts. Unfortunately this venture failed and the vortex tube slipped into obscurity until 1945 when Rudolph Hilsch, [75], a German physicist, made some improvements on the Frenchman's design, but found that it was no more efficient than conventional methods of refrigeration in achieving low temperatures, and subsequently has not been used substantially since this time.

The mechanism underlying the energy transfer from the cold to the hot flow remains elusive. There is great debate even as to the basic physics of the phenomenon. The majority of researchers suggest that the mechanism is based on the interactions of turbulence, compressibility, and shear work as shown by Deissler and Perlmutter [76] analysis. There are a significant number of researchers who consider acoustic effects as responsible for the exchange in energies Kurosaka [77]; this is far more inconclusive than the energy conservation analysis results have shown.

Recent research has been divided into two categories. The first category termed as 'external studies' was concerned with the performance of the tubes. The most commonly varied parameter is the dimensions of the tube. Research involving the

study of the efficiency of a tapering tube has had conflicting results, whereas varying the length of the tube and diameter of the diaphragm is shown to affect its performance. It was found by Gulyaev [78] that the minimum ratio of the length of the tube to that of its diameter is thirteen. Other research suggests a ratio of forty to fifty for optimum operation. As for the diaphragm, the optimum dimension is a ratio of 2:3 for the diaphragm diameter to tube diameter. Other interesting research includes the effect of cooling the exterior of the tube to improve its efficiency. Another idea was rotating the hot tube in sympathy with the air in an attempt to create a temperature inversion in the tube. It was found that cooling the tube actually reduces the temperature of the cold flow, which increases the efficiency of the tube if it were to be used for cooling applications.

4.3.2 Vortex tube energy transfer process

Currently the working mechanism of a vortex tube is not fully known, and an explanation why the vortex tube operates as it does needs further investigation. The process itself is straightforward, as outlined by Stephan *et al.* [79]. Compressed air in the range of 0.72 to 0.76 MPa is supplied to the vortex generator, through the tangential inlet nozzle which produces the high speed rotating airflow inside the vortex generator. Subsequently, there is a radial temperature gradient increasing from the inner core of the tube to the outside wall of the tube. This is primarily because of the potential energy of the compressed air converting to kinetic energy, due to the forced vortex caused by the external torque near the tangential air inlet. Therefore the high-speed swirling flow inside the tube and away from the walls will be created. The existing air inside the vortex hot tube is normally at the atmospheric temperature and so, when the rotating flow enters the vortex tube, it expands - and its temperature drops to a temperature lower than the ambient temperature. The difference between these two temperatures will lead to a temperature gradient along the tube producing colder peripheral air than the core air. As a result, the central air molecules will lose heat to those in the outer region as shown in Figure 4.8(a). It is notable that this system is a dynamic system due to the nature of the airflow in the tube, and therefore will not reach equilibrium. The result of this is that the peripheral outer air has a higher kinetic energy than the inner air which has lost its kinetic energy, and is now a cold air stream.

- This process is called radial convection.
- Forced vortex: In a forced vortex, the velocity is directly proportional to the radius of the vortex.
- The closer to the centre, the slower the velocity.

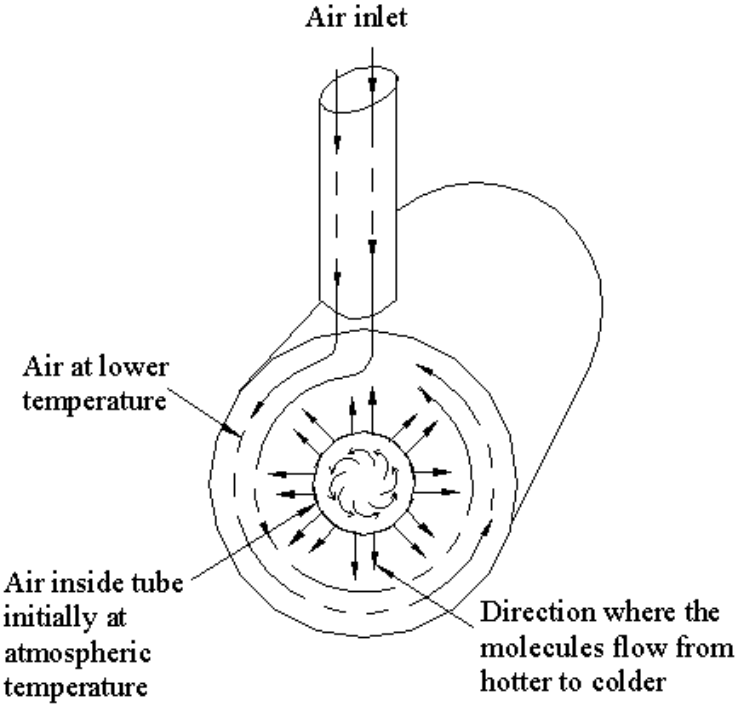

Figure 4.8(a): Radial heat convection in vortex tube due to the expansion of the compressed air.

The existence of a major pressure gradient due to the forced vortex in the radial direction will provide a centripetal force for circular swirling, and therefore it will lead to high pressure at the tube wall and low pressure at the centre. When the air enters the peripheral region (A), and then it expands, the outer air will be cooled due to its expansion. Consequently, the inner core air (B) will get warm because it is compressed by the expansion of the peripheral air. Heat is then transferred from the inner core (B) to the outer core (A). As the inner air is being compressed, it naturally tries to push against the periphery by expanding. Work is therefore done on the outer core air, which then gets heated. The difference in pressures results in the expansion and contraction of the air, which causes work to be done on the peripheral air. Therefore, heat is transferred radially outward as shown in Figure 4.8(b).

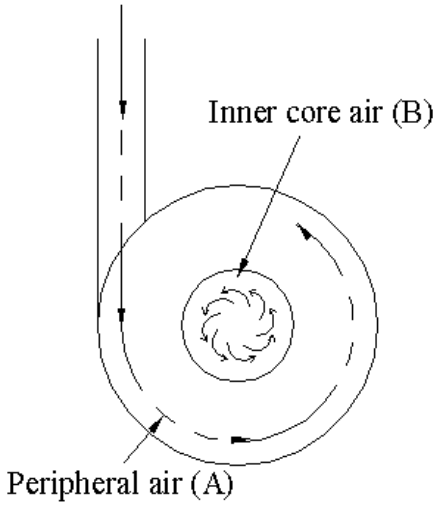

Figure 4.8(b): Schematic positions of the peripheral and inner core air.

When the air continues to swirl along the tube the more energy separation will occur by axial convection while it moves towards the hot end. During this progression, the heat will be transferred from the core air to the outer air. As the airflow reaches the hot end, a fraction of the air will exhaust through the conical valve which is located at the hot end. The remaining air flow will spin back towards the cold end due to the adverse pressure gradient near the centre, as shown in Figure 4.9. The remaining portion of the warm air preserves its direction of motion in the vertical flow that is either in a clockwise or anticlockwise manner around the circumference of the tube. Furthermore, this air stream resides at the inner air column of the tube where the air pressure is lower.

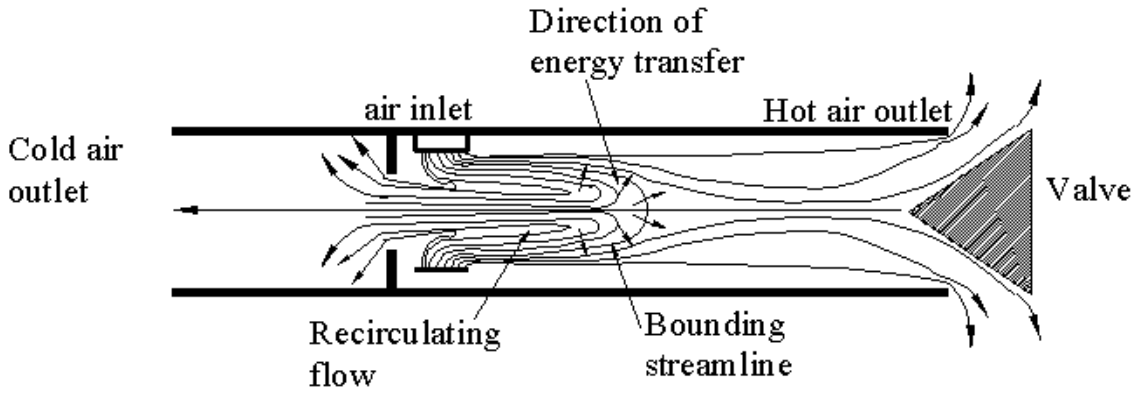

Figure 4.9: A diagram of the airflow pattern in vortex tube.

If the angular velocities of both the air streams are preserved, it means that any two particles taken from both the air streams will take the same time to complete a revolution around the circumference of the tube. From the principle of conservation of angular momentum, it seems that the angular velocity of the inner air column molecules would increase by the equation:

$$mr^2\omega = constant \tag{4.3}$$

The equation implies that in the inner air column, where the value of r (radial distance measured from the centre of the tube to the particular molecule in concern) is small, there should be a corresponding increase in the molecule's angular velocity, *w*, to allow for the conservation of the total angular momentum in the system. This is assuming that there is negligible mass difference, *m*, between any two-air molecules in the tube. However, the angular velocity of a particular molecule in the inner air column remains unchanged. This means that angular momentum has actually been lost from the inner air column of the vortex tube. Angular momentum of the inner column is not preserved or more specifically decreases, due to heat transferred to the outer core. This results in the transfer of energy from the inner air column to the outer air column. The loss in heat energy from the inner core air heats up the air molecules in the outer air stream. The outer air column becomes hotter and the inner air column becomes cooler Lewins *et al.* [80]. Upon reaching the hot end, the hotter peripheral air escapes through the small openings between the conical valve and the tube wall (hot outlet). However, the central air, which is cooler, is deflected by the tapered valve spindle and continues its travel from the hot end towards the cold tube. Only the innermost air molecules pass through the diaphragm and exit through the cold end where it is collected. As a result, the air molecules are separated into a hot stream and cold stream through the hot and cold ends of the vortex tube respectively.

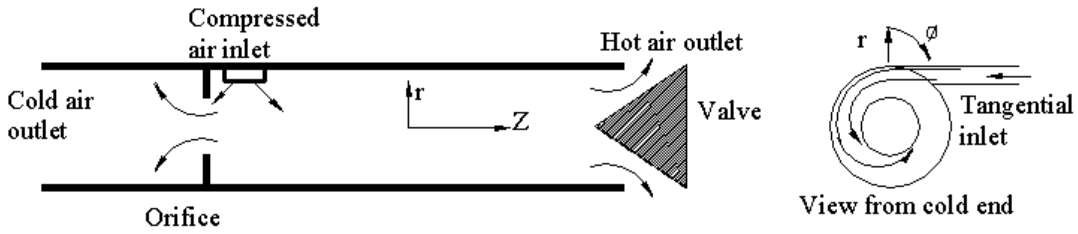

Figure 4.10: Schematic vortex tube diagram showing tangential air inlet.

The Figure 4.10 shows a good view of the vortex tube. It is important to note that separation takes place specifically at the hot end tube. The purpose of the tapered spindle (conical valve) is to direct the cold air to the axial region of the tube in a counter flow. The diaphragm (orifice) on the other hand, is used to block the peripheral air, so that the central flow will escape through the cold end.

4.4 First Law Of Thermodynamics Implications In Vortex Tube

4.4.1 First Law analysis

The absence of moving parts in the vortex tube may create a wrong supposition that this phenomenon is violating thermodynamics law. The fact that without doing any work at room temperature, a stream of air that can be divided into two different streams, one cooler and one hotter, seems to contradict the second law of thermodynamics. However, it is important to mention that despite this misleading belief the physics remains intact. Although, the physics of the vortex tube is complicated, the study of the basic principles of thermodynamics can help to gain a better understanding of what is happening inside a vortex tube.

The first law of thermodynamics deals with the conservation of energy, and according to this law the reaction between the vortex tube and the ambient is exactly equal to the energy that is lost from the vortex tube to the ambient. This energy can be seen in two different states: Heat and Work. Hence, for every thermodynamic system with a specific control volume:

$$\dot{Q}_{C.V} + \sum \dot{m}_i (h_i + \frac{v_i^2}{2} + g z_i) = \sum \dot{m}_e (h_e + \frac{v_i^2}{2} + g z_e) + \dot{W}_{c.v} \qquad (4.4)$$

where $\dot{Q}_{cv}$ is the rate of heat flow, which transfers through the control volume boundary, and $\dot{W}_{cv}$ is the work that can be done by the system on it's ambient, $\dot{m}$ is the mass flow rate, *h* is the enthalpy of the air stream, *v* is the stream velocity, *z* is the distance between the air stream and a source point, and the subscripts i and e refer to inlets and outlets streams.

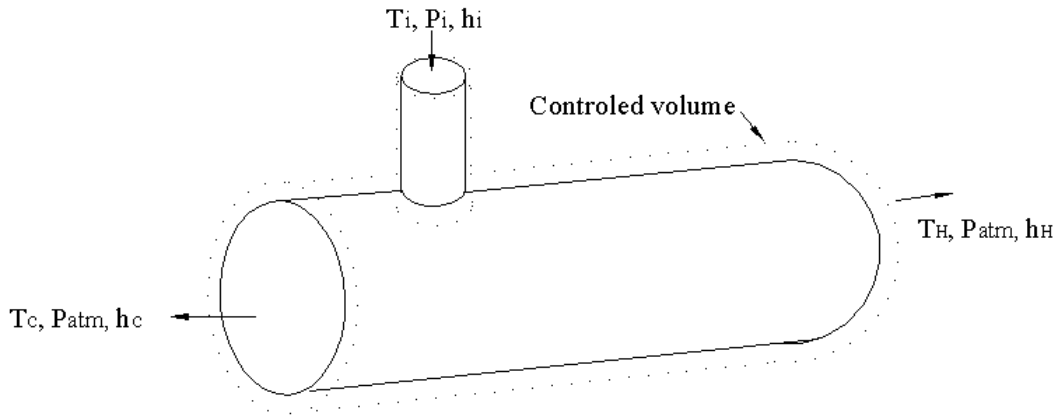

Figure 4.11: Schematic control volume of a vortex tube.

Assuming that the vortex tube is well insulated, then the heat transfer between the system and the ambient can be taken as $\dot{Q}_{cv}$ equal to zero with v_i and v_e also equal to zero as is the work W. Considering the control volume as shown in Figure 4.11 for the vortex tube, then equation (4.4) can be simplified as:

$$\sum \dot{m}_i h_i = \sum \dot{m}_e h_e \tag{4.5}$$

The expanding air can be treated as ideal gas and it can be assumed that it obeys the ideal gas laws, and having constant specific heat capacity c_p, you can write:

$$h = c_p T \tag{4.6}$$

$$\dot{m}_i c_p T_i = \dot{m}_c c_p T_c + \dot{m}_h c_p T_h \tag{4.7}$$

by defining μ_{cf} as the cold fraction:

$$\mu_{cf} = \frac{\dot{m}_c}{\dot{m}_i} \tag{4.8}$$

from the continuity equation:

$$\dot{m}_c + \dot{m}_h = \dot{m}_i \tag{4.9}$$

Combining equations (4.7), (4.8) and (4.9) gives the relationship between inlet stream temperature and cold stream temperature, (hot stream temperature and cold fraction). So the equations can be written as:

$$T_i = \mu T_c + (1-\mu)T_h \tag{4.10}$$

by assuming;

$$\Delta T = T_h - T_c \tag{4.11}$$

$$\Delta T_c = T_i - T_c \tag{4.12}$$

$$\Delta T_h = T_h - T_i \tag{4.13}$$

where ΔT is the difference between the hot and the cold stream temperatures, ΔT_c is the temperature difference between the inlet and cold streams, and finally ΔT_h is the temperature difference between the inlet and hot streams. The equation can be written as:

$$\Delta T = \Delta T_h - \Delta T_c \tag{4.14}$$

Combining equations (4.10) and (4.14) allows you to determine ΔT_c and ΔT_h theoretically by measuring the cold fraction, μ_{cf}, and total temperature difference, ΔT. Therefore:

$$\Delta T_c = (1-\mu_{cf})\Delta T \tag{4.15}$$

$$\Delta T_h = \mu_{cf}\Delta T \tag{4.16}$$

Equation (4.15) and equation (4.16) can be used to show the consistency of the first law of thermodynamics for tests carried out on the vortex tube.

4.4.2 Temperature separation

There are two theoretical temperature separations of the air in the vortex tube that have been investigated. The first method considers temperature separation in the vortex tube by using a general dimensionless analysis approach. The second method investigates the relationship between the variation of different parameters in the vortex tube and energy destruction. Both these methods are used to show the consistency of the experimental testing of the vortex tube.

Eiamsa-ard and Promvonge [81] have worked together to derive a mathematical model of the thermal separation in the vortex tube to help predict the energy separation. The general mathematical formulations such as the continuity equation, viscous equation, thermal energy equation and the equation of states are used.

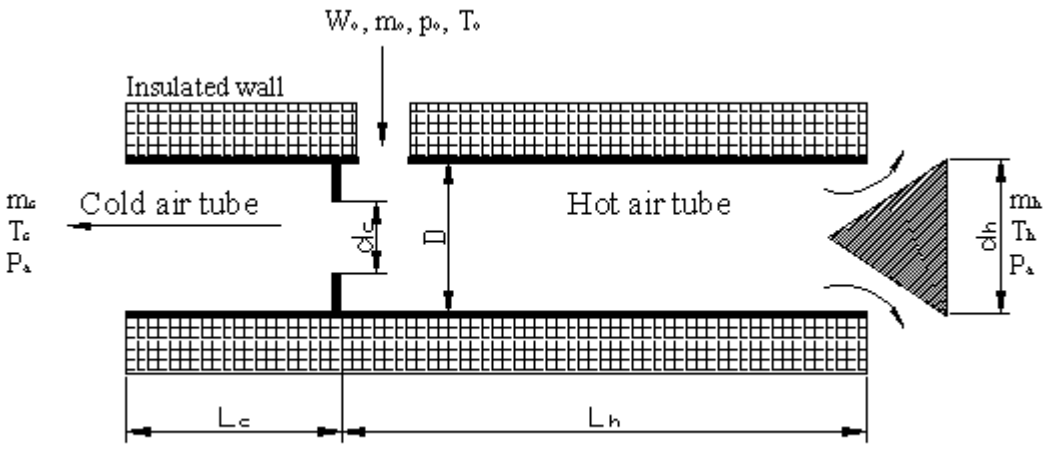

Figure 4.12: Ranque-Hilsch vortex tube parameters.

The phenomenon under consideration here is in a steady axis symmetrical compressible flow system, where the body force and any energy source are neglected, which is depicted in Figure 4.12. It is proposed that the vortex tube is well insulated and the air flowing through the tube is considered to be an ideal gas (air). Therefore, by using the method of dimensional analysis the continuity equation can be written as:

$$\frac{1}{r}\frac{\partial}{\partial r}(\rho r v_r)+\frac{\partial}{\partial z}(\rho v_z)=0 \tag{4.17}$$

The mass flow rate at the vortex tube inlet was separated into two air streams, one is the cold mass stream at the cold tube, and the other is the hot mass stream at the hot tube, which can be expressed as follows:

$$\dot{m}\left(c_{pc}T_c+\frac{v_{zc}^2+v_{\theta c}^2}{2}\right)+\dot{m}_h\left(c_{pc}T_h+\frac{v_{zh}^2+v_{\theta h}^2}{2}\right)=\dot{m}_o\left(c_{po}T_o+\frac{w_o^2}{2}\right) \tag{4.18}$$

The temperature drop at the cold tube exit is one of the important variables that must be considered in determining the energy separation in the vortex tube. This relationship can be used for predicting the temperature reduction of the cold air tube of any similar vortex tube, which is useful when considering the prototype air-cooled tool tip. The most important parameter indicating the vortex tube's performance is the cold mass fraction. As it is a ratio between a mass flow rate in the cold tube and a mass flow rate of the air inlet, the function relationship can be written as follows:

$$\mu_c+\mu_h=1 \tag{4.19}$$

Experimental results indicate that the cold mass fraction μ_c varies from 0.0 to 1.0 when other parameters are kept constant. From equation (4.20) the temperature reduction at the cold air stream is shown to be a function of cold mass fraction.

$$\frac{\Delta T_c}{\Delta T_{c.\max}}=g(\mu_c) \tag{4.20}$$

It is useful that equation (4.20) can be used to compare vortex tubes that are geometrically similar to each other.

4.4.3 Transfer of vortex tube temperature by energy method

A useful thermodynamic model which can be used to optimise the dimensions and operating conditions of a vortex tube is the energy model. Saidi and Allaf Yazdi [82] derived an equation for the rate of entropy generation; this equation is used to model the irreversibility term. Energy is a property whose magnitude identifies the maximum useful work potential of a system. Specifically, energy is the useful work that can be extracted from a system which executes a reversible process between its initial state and a dead state. A reversible process is a totally loss-free process. Defining *Ex* as a symbol for energy, the quantitative definition of energy is:

$$Ex = (U + KE + PE - Uo) + Po\,(V\text{-}Vo) - To\,(S - So) \tag{4.21}$$

where *U* is internal energy of the system at its initial state, *KE* is kinetic energy of the system in its initial state, *PE* is potential energy of the system in its initial state, *V* is volume of the system in its initial state, S is entropy of the system in its initial state, U_o internal energy of the system at the dead state, *Po* is pressure of the system at the dead state, V_o is volume of the system at the dead state, T_o is temperature of the system at the dead state, and S_o is entropy of the system at the dead state. Consider the two states 1 and 2, neither of which is the dead state, where the energy changes by the following expression:

$$Ex2 - Ex1 = (U2 - U1) + (KE2 - KE1) + (PE2 - PE1) + Po(V2 - V1) - To(S2 - S1) \tag{4.22}$$

In thermodynamics expression (*Ex2 - Ex1*) are equal to:

$$Ex2 - Ex1 = Energy\ transfers - Energy\ destruction \tag{4.23}$$

By using the first law and the second law of thermodynamics, it shows that the equation (4.23) can be written as:

$$Ex2 - Ex1 = \int_2^1 \left(1 - \frac{T_o}{T_b}\right) dQ - \left[W - P_o\left(V_2 - V_1\right)\right] - T_o \dot{S}_g \tag{4.24}$$

where T_b is system boundary temperature, dQ is a very small heat transfer in each step between state 1 and 2 during a reversible process, W is work and $\dot{S}_g$ is entropy production.

In equation (4.24), term $\int_2^1 \left[1-\frac{T_o}{T_b}\right] dQ$ is energy transfer accompanying heat transfer;

term $(W - P_o(V_2 - V_1))$ is energy transfer accompanying work transfer, and finally term $T_o\dot{S}_g$ is called energy destruction.

Saidi and Allaf Yazdi [82] have shown that if the conditions of flow in a vortex tube can be assumed adiabatic, a steady state having no heat and work interaction with the environment exists, then the first law can be written as:

$$(1-y)(T_h - T_c) + (T_c - T_i) = 0 \tag{4.25}$$

Also, using the second law of thermodynamics:

$$\left(\dot{S}_g\right)_{vortex-tube} = \dot{m}_i\left[(1-y)(S_c - S_h) + (S_i - S_c)\right] \tag{4.26}$$

where y is cold mass fraction and subscripts c, h and i are cold stream, hot stream and inlet stream respectively.

By combining equations (4.25) and (4.26) and using ideal gas (air) behaviour, then:

$$\left(\dot{S}_g\right)_{vortex-tube} = \dot{m}_i\left[c_p \ln\frac{\left(T_h/T_c\right)^{(1-y)}}{1+(1+y)(T_h/T_c - 1)} + R\ln\frac{P_i}{P_c}\right] \tag{4.27}$$

By using $T_o\dot{S}_g$ as energy term in equation (4.26), the rate of vortex tube total irreversibility can be presented as:

$$i = T_o\dot{m}\left[c_p \ln\frac{\left(T_h/T_c\right)^{(1-y)}}{1+(1-y)(T_h/T_c - 1)} + R\ln\frac{P_i}{P_c}\right] \tag{4.28}$$

Using equation (4.28) will help in determining the energy destruction versus cold mass fraction changes. This is used to determine the optimum region for operating the vortex tube at different inlet pressures, therefore allowing the most efficient cooling to take place for a particular condition.

4.4.4 Vortex tube efficiency

In refrigeration it is so important to determine the coefficient of performance of the cooling device. Hence, it seems only logical to determine the coefficient of performance of the vortex tube and compare it with the conventional refrigeration coefficient of performance to determine its efficiency in use. The vortex tube can be used as a refrigeration device when the cold pipe wall is used to reduce the temperature of an enclosure or as a heating device when the hot pipe wall is used to increase the temperature of an enclosure. It should be noted that opposite to what is normally viewed in thermodynamics, the vortex tube in this case is an open control volume device. If the system was assumed to be steady state, then from the first law of thermodynamics:

$$\Delta \dot{H} = \dot{Q} \tag{4.29}$$

where $\Delta \dot{H}$ is the system enthalpy change and $\dot{Q}$ is the heat exchanged between the system and its surroundings. Let us assume that $\dot{Q}$ is approximately zero, even though the cold tube may have frost on it and the hot tube is very warm. If this is the case, then:

$$\Delta H = \Delta H_c + \Delta H_H = 0 \tag{4.30}$$

where ΔH_c is the enthalpy change of the cold stream, and ΔH_H is the enthalpy change of the hot stream. Assuming the air as an ideal gas, the total enthalpy change can be written as:

$$\Delta H = m_c c_p \left((T_c - T_i\right) + m_h c_p \left(T_h - T_i\right) = 0 \tag{4.31}$$

where m_c is mass flow rate at cold tube, m_h is mass flow rate at hot tube, T_c is cold air temperature, T_i is inlet air temperature, T_h is hot air temperature, and c_p is specific heat of air at constant pressure, and assumes the process as reversible and adiabatic. By applying the second law of thermodynamics to the above:

$$\Delta S = \int \frac{1}{T} dq = 0 \tag{4.32}$$

where ΔS is total entropy change, q is heat transfer and T is absolute temperature. The actual entropy change of the control volume at steady state is:

$$\Delta S = \Delta S_c + \Delta S_h \tag{4.33}$$

where ΔS_c and ΔS_h are the entropy change from entrance to exit of the portion of entering air which leaves the cold tube, and the portion of entering air which leaves the hot tube respectively. For an ideal gas (air) with constant specific heat, the entropy change can be written as

$$\Delta S = \frac{\dot{m}_c}{\dot{m}_i}\left[c_p \ln\frac{T_c}{T_i} + R\ln\frac{P_i}{P_c}\right] + \frac{\dot{m}_h}{\dot{m}_i}\left[c_p \ln\frac{T_h}{T_i} R\ln\frac{P_i}{P_h}\right] \tag{4.34}$$

where the subscripts I, c and h are respectively inlet stream, cold stream and hot stream, and R is the ideal gas (air) constant.

Since the appearance of a cold (or hot) effect upon the pipe wall without moving parts would attempt to consider this device as competition for a refrigerator (or heat pump), it is useful to estimate its coefficient of performance (COP).

$$COP = \frac{\Delta \dot{H}_c}{\dot{W}} \tag{4.35}$$

where $\Delta \dot{H}_c$ is obtained from:

$$\Delta \dot{H}_c = \dot{m}_c (T_i - T_c) \tag{4.36}$$

where $\Delta \dot{H}_c$ is equal to the heat that is transferred to the cold stream through the cold pipe wall (like a heat exchanger) from some source (like the cold box in a refrigerator), and $\dot{W}$ in the present case is the work done to compress the air from atmospheric pressure, and temperature to the inlet conditions of the tube. Assuming reversible compression (isentropic, minimum work), $\dot{W}$ is then obtained from:

$$\dot{W} = \frac{\dot{m} R (T_2 - T_1) n}{n-1} \tag{4.37}$$

where T_2 is the compressor exit temperature, and T_1 is the compressor inlet temperature (reversible, polytropic process; air: n = 1.4). Considering the complete system, P_1 and T_1 are the atmospheric pressure, and temperature P_2 and T_2 are the compressor exit conditions.

$$\left[\frac{P_2}{P_1} \right]^{\frac{n-1}{n}} = \frac{T_2}{T_1} \tag{4.38}$$

After the air is compressed, it is kept in the high-pressure tank where it cools down to the atmosphere temperature T_1, so the inlet temperature of the sonic jet T_i, is equal to T_1, noting that:

$$\frac{Rn}{n-1} = c_p \tag{4.39}$$

Equation (4.37) can be simplified to:

$$\dot{W} = \dot{m}_i c_p (T_2 - T_1) \tag{4.40}$$

with T_2 is calculated from equation (4.38). This is an ideal work value so it is less than the actual work needed to drive the compressor. By considering the above equations and using the equation (4.35), the coefficient of performance of the vortex

tube can be determined. In Chapter 6 the performance of the vortex tube developed for cooling the tool tip during machining will be compared with the impingement method of cooling to establish the most efficient method of air-cooling when machining.

4.5 Vortex Cooling Effect

4.5.1 Elements of the vortex tube

Unlike the impingement process, there has been little research undertaken on the vortex tube. The vortex tube shown in Figure 4.13(a) was produced for cooling the tool tip during machining, and was designed from the original concepts of the Ranque-Hilsch Tube. A vortex tube consists of three important parts. The mid-section is normally where the air enters the vortex generator, which may have a spiral section to increase the speed of the air. It is also the part that is connected to the cold tube and the hot tube as shown in Figure 4.13(b). When compressed air enters the inlet it is directed tangentially to the vortex generator, causing it to spin around producing a spiral airflow. To the left hand of this section is the hot tube, as shown in Figure 4.13(b). Normally the hot tube is about 350 mm long, and at the end there is a conical valve which controls the amount of air escaping. On the right side of the vortex generator is the cold tube, which is approximately 100 mm long. The diameter of both of the tubes is 13 mm. Between the Vortex Generator and the cold tube there is a diaphragm fitted - with a central hole which can be easily altered - allowing diaphragms with large or small holes to be used. This adjustment to the vortex tube can increase or decrease the temperature obtained at the cold exit.

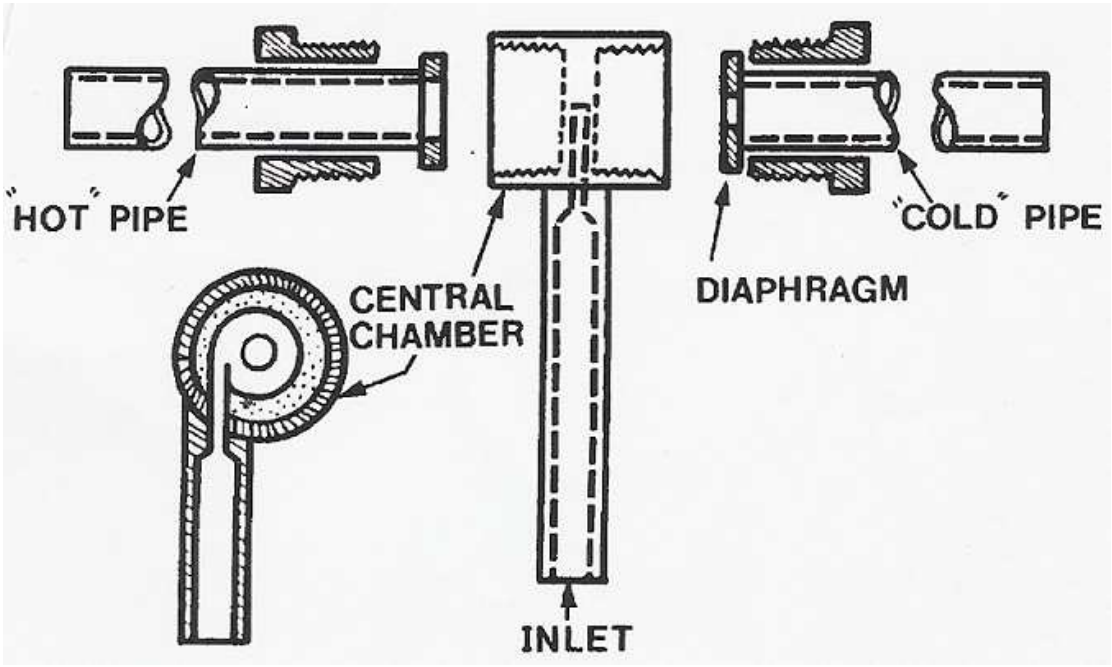

Figure 4.13(a): Schematic diagram of Hilsch Tube Showing diaphragm.

Taken from The Wirbelrohr's roar [83]

Considering the above geometry of the vortex tube, the compressed air is supplied circumferentially into the tube at sonic speed, and creates a cyclone (vortex) spinning at a million revolutions per minute. The air is forced to spin inward to the centre where it then escapes up along the hot tube, as this path presents the least resistance to the airflow. The air continues to spin as it travels along the tube until it meets the conical valve, where it turns part of the spinning air column (vortex) inside itself Figure 4.13(b). The slower moving air inside the column of spinning air gives up its heat to the faster spinning outside column of air. The cold air travelling down the spinning air is now directed out of the cold end of the vortex generator, while the hot air is exhausted out of the hot exit end of the vortex tube. The volume and temperature of these two air streams can be changed by adjusting the conical valve built into the hot air exhaust exit. It was possible to obtain temperatures as low as -46 °C and as high as +127 °C when using the vortex tube shown in Figure 4.13(b) under test conditions.

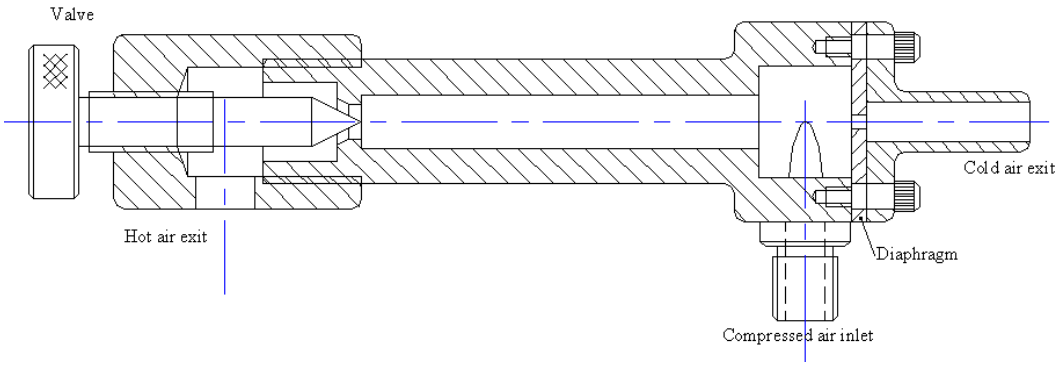

Figure 4.13(b): Sectional view of the vortex tube showing the conical valve.

4.5.2 Experimental analysis on vortex tube configurations

The vortex tube which was produced is shown in Figure 4.13(b), where the hot tube length was made shorter than the diameter length ratio specified to allow convenient use on the lathe. Therefore, experimental analysis is necessary to determine the performance of this vortex tube, as there are many gaps in the theoretical knowledge as to what makes an effective vortex tube. The pre-machining cooling tests on the vortex tube were carried out systematically as outlined in Table 4.1 to 4.2.

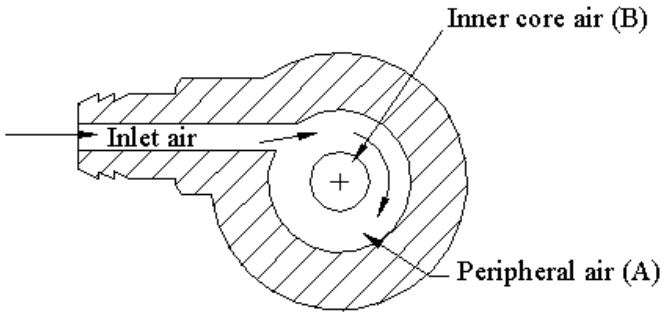

Vortex Generator G1

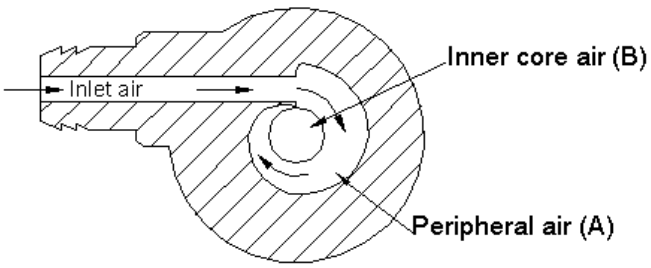

Vortex Generator G2

Position of peripheral and inner core air (A & B)

Figure 4.13(c): Sectional view of vortex generators internal shape.

Table 4.1: Vortex test parameters

	Diaphragm			Generator			Hot tube length	
Inlet pressure (MPa)	0.275	0.275	0.275	0.275	0.344	0.344	0.275	0.275
Orifice diaphragm (mm)	3	5	7	3	3	3	3	3
Vortex generator	G1	G1	G1	G2	G2	G1	G1	G1
Hot tube length (mm)	140	140	140	140	140	140	250	360

Table 4.2: Vortex tube optimum configuration

Inlet pressure (MPa)	0.206	0.275	0.344
Orifice diaphragm (mm)	3	3	3
Vortex generator	G1	G1	G1
Hot tube length (mm)	140	140	140

A test-rig was used to assist with tests of the numerous vortex configurations and different operating conditions to determine the optimum configuration to use when air-cooling the tool tip. The test-rig Figure 4.14 indicates the positions of the thermocouples, compressed air inlet T_i, cold outlet T_c, hot outlets T_h, and the fourth thermocouple located outside the vortex tube which measures the ambient temperature during the vortex tube tests.

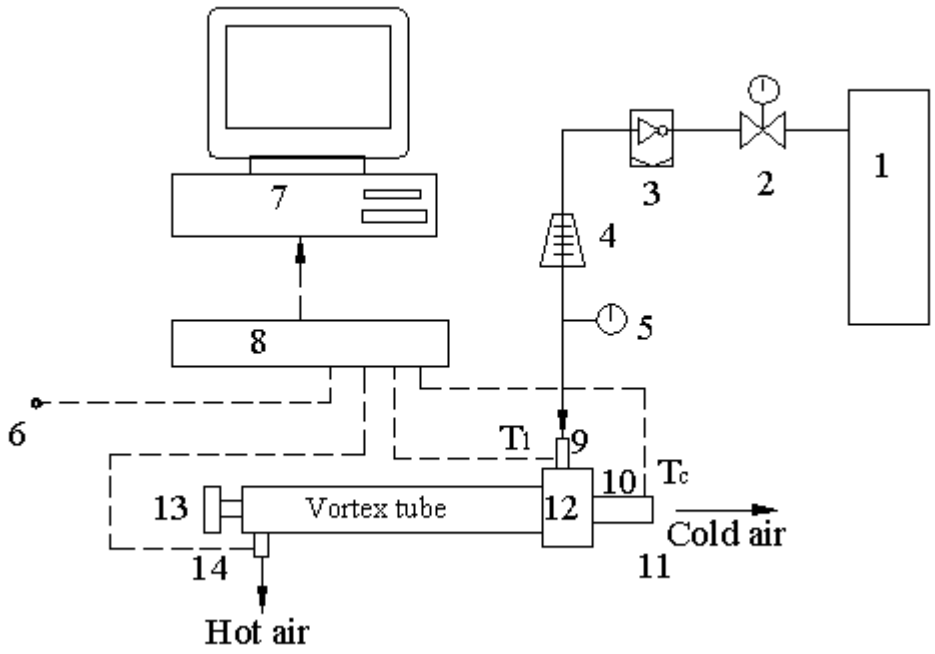

The experimental rig consists of the following apparatus: 1. Air compressor, 2. Control valve, 3. Air dry filter, 4. Flow meter, 5. Pressure gage, 6. Thermocouples 9,10 & 14, 7. Computer, 8. Data logger, 11. Cold nozzle, 12. Vortex generator, 13. Conical valve adjustment.

Figure 4.14: Block diagram of vortex tube testing changes to the vortex tube.

Further aspects of the test procedure can be found in Appendix A.

The results obtained from the tests are presented in Figures 4.15 to 4.24. These experiments on the vortex tube configuration show the effects each has on the vortex tube exit temperature. To help compare the vortex tubes it is useful to use the cold mass fraction, as this can be contrasted over the range of vortex tube tests.

It is important to note that the air mass flow rate at the hot end of the tube varies from its maximum value (which is equal to the mass flow rate of the compressed air) to its minimum value (which is equal to zero), and is shown on Figures 4.15 to 4.24 as the horizontal axis on the graphs. By the law of the conservation of mass, the mass flow rate at the cold end is equal to the difference of the inlet mass flow rate and the mass flow rate at the cold end. Therefore, by varying the mass flow rate at the hot end, you effectively control the mass flow rate at the cold end from its minimum to its maximum value.

$$\text{Cold Mass Fraction} = \frac{\dot{m}_c}{\dot{m}_{in}} = \frac{\dot{m}_{in} - \dot{m}_h}{\dot{m}_{in}} \tag{4.41}$$

Where $\dot{m}_c$ = mass flow rate at cold end

$\dot{m}_h$ = mass flow rate at hot end

$\dot{m}_{in}$ = mass flow rate of compressed air at inlet

Cold mass fraction is the percentage of input compressed air that is released through the cold end of the tube. Generally, the less cold air being released, the colder the air will be. Adjusting the control valve will vary the cold mass fraction. High cold mass fraction would give a greater airflow, but does not give the lowest possible temperature. The high cold mass fraction combination of airflow and cold temperature produces the maximum refrigeration capacity. A low cold mass fraction on the other hand means a smaller volume of air coming out that is very cold. In short, the less air to be released, the colder the air becomes. The effect of velocity on the temperature drop at the cold end is important since, if the velocity that produces the lowest temperature drop is known, then the compressed air pressure and the cold jet diameter could be optimised. A decrease in the jet diameter would also force the air to flow towards the direction of the hot end, and would lead to an improvement in the vortex tube efficiency to some extent.

$$\dot{m}. = \frac{\rho AL}{t} = \rho Av \tag{4.42}$$

$$v = \frac{\dot{m}}{\rho A} \tag{4.43}$$

The compressed air pressure is set at 0.206 MPa, 0.275 MPa, and 0.344 MPa respectively to investigate how air pressures affect the vortex tube performance. Obviously, the higher the air pressure the higher the cost of producing the compressed air. Therefore the parameters that use the lowest pressure while producing the coldest temperature should be used to aid reductions in the operating cost of air-cooling. The coefficient of performance estimation for any cooling device

can be used to give a good measure of the practical refrigeration performance of the cooling system. This can therefore be used in determining the performance of the vortex tube, which can in turn be compared with a conventional refrigeration system. The vortex tube's coldest airflow from the previous test needs to be used in determining the coefficient of performance for this vortex tube. In this case, the lowest cold temperature is obtained from the vortex tube with a 3 mm diameter jet, vortex generator one (G1), length 360 mm and inlet air pressure 0.275 MPa. The lowest temperature measured was T_c = -16.8 ^oC. The related values for this temperature are given in Table 4.3:

Table 4.3:Recorded readings from test

Parameter	Value
Cold Mass Fraction	0.605
Inlet Temperature (^oC)	22.4
Ambient Temperature (^oC)	22.6
Hot Outlet Temperature (^oC)	66.6
Inlet Volumetric Flow Rate (SLPM)	1095
Hot Outlet Volumetric Flow Rate (SLPM)	425
Cold Inlet Volumetric Flow Rate (SLPM)	651

To determine the coefficient of performance of the vortex tube for the previous conditions, it is necessary to calculate the compressor exit temperature T_2 (314 K) by using equation (4.37) when:

$P_1 = P_{Ambient}$ = 101.325 kPa, $T_1 = T_{Ambient}$ = 296 K, P_2 = 376.35 kPa and n =1.4

The coefficient of performance for the vortex tube can now be calculated by using equation (4.37), which gave a value of 1.38.

4.5.3 Experimental data and analysis

The diaphragm plate used between the vortex generator and the cold nozzle allowed different orifice diameters to be quickly tested. Table 4.1 gives the orifice diameters used in the tests. The test data for the three orifice diameters is shown in Figure 4.15

and 4.16 respectfully. Experimental data has shown that the vortex tube cold air stream temperature decreases with respect to the cold air mass fraction, which can be obtained from equation (4.20). The biggest temperature drop was obtained when a 3 mm diameter orifice (diaphragm) was used, as shown in Figure 4.13(b). This orifice had the smallest diameter between the vortex generator and the cold tube air exit.

It can be concluded that the smaller the diameter of the orifice at the cold exit from the vortex generator, the greater is the reduction in temperature. Examination of Figures 4.15 to 4.24 shows a trend, in that the lowest temperatures occur at the low cold mass fraction. Unfortunately, the flow meter was not capable of measuring the cold mass fraction near zero. Therefore it was not possible to find the exact cold mass fraction where the lowest temperature occurs, although from the graphs it is possible to assume that this value will be between 0 and 0.1. The biggest temperature decrease at the cold air outlet and the corresponding highest hot air outlet temperature was shown to have cold mass fraction between 0.6 and 0.7 when using orifice one (G1) as shown on Figure 4.15.

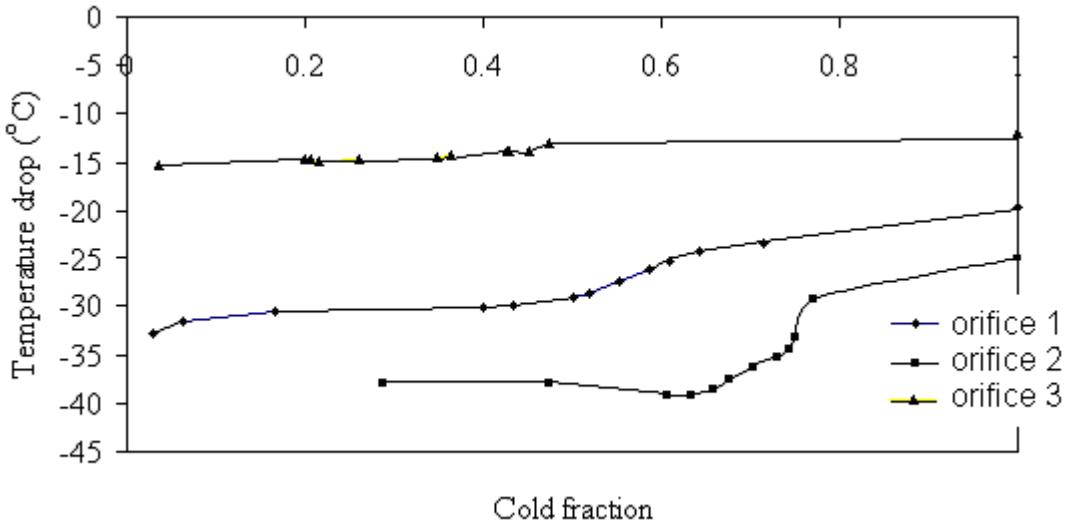

Figure 4.15: Cold airflow temperatures with respect to cold fraction.

The trend for the hot exit temperature reflects the different orifice diameters as shown in Figure 4.16, also corresponding with the cold fraction between 0 and 1. For their respectful orifice diameters the temperature starts increasing to the highest point

and then there is a sudden decline in temperature as the conical valve is adjusted past the optimum point.

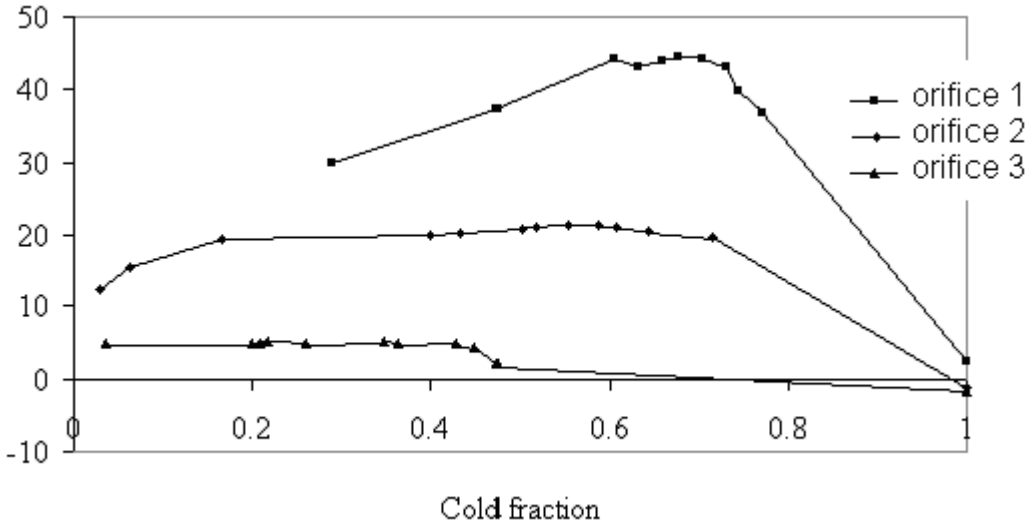

Figure 4.16: Orifice diameter effects on hot exit temperature.

This was predictable as it is known that at low cold mass fraction, a high fraction of inner swirling air-flow joins the outer airflow at the hot outlet, and therefore the temperature of the hot air stream decreases. Opening the conical valve beyond its optimum position allows additional air to escape through the hot exit with a reduced temperature. At this position the conical valve has less airflow moving towards the cold end, causing the temperature to increase as shown in Figure 4.15.Comparing the temperatures of the hot exit and the cold exit it is apparent that there is a relationship between the two streams of air, and can be clearly seen by examining Figure 4.15 and 4.16.

In an attempt to improve the temperature difference between the hot air and the cold air, a redesigned vortex generator was produced (Figure 4.13(c)), to try and increase the speed of the vortex air. It was anticipated that the spiral shaped vortex generator two (G2) would generate a larger temperature drop due to its spiral shape. However, after carrying out tests, it was found that the larger temperature drop and higher temperature increase was not obtained by using this vortex generator. Figure 4.17 and 4.18 shows the effect of the vortex generator shape.

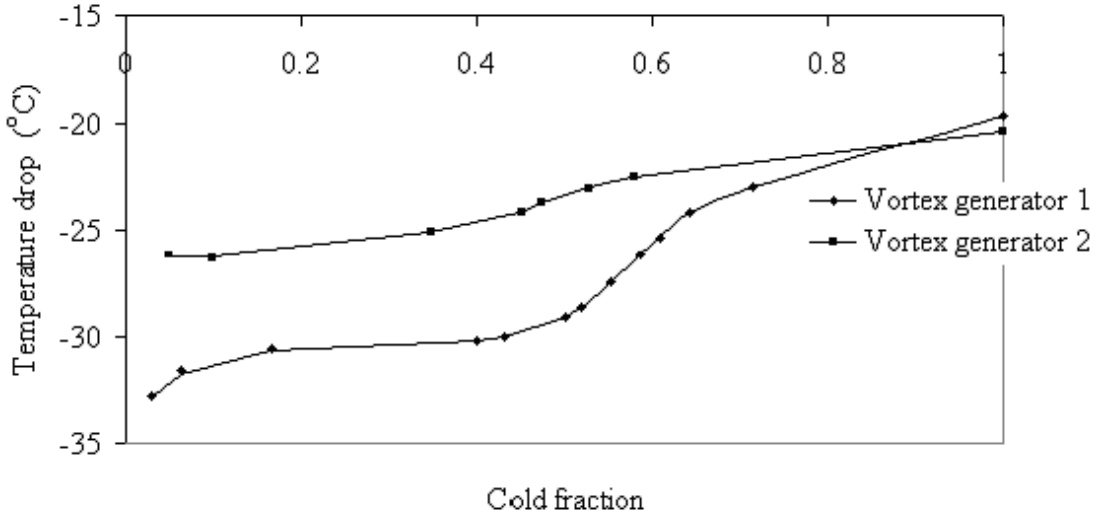

Figure 4.17: Vortex generator shape effect on temperature at cold exit.

It was discovered that the spiral shaped vortex generator two (G2) was unable to increase the acceleration of the airflow any more than vortex generator number one. Figure 4.17 shows that, by increasing the cold mass fraction, the temperature drop will be reduced; this is also shown in Figure 4.18.

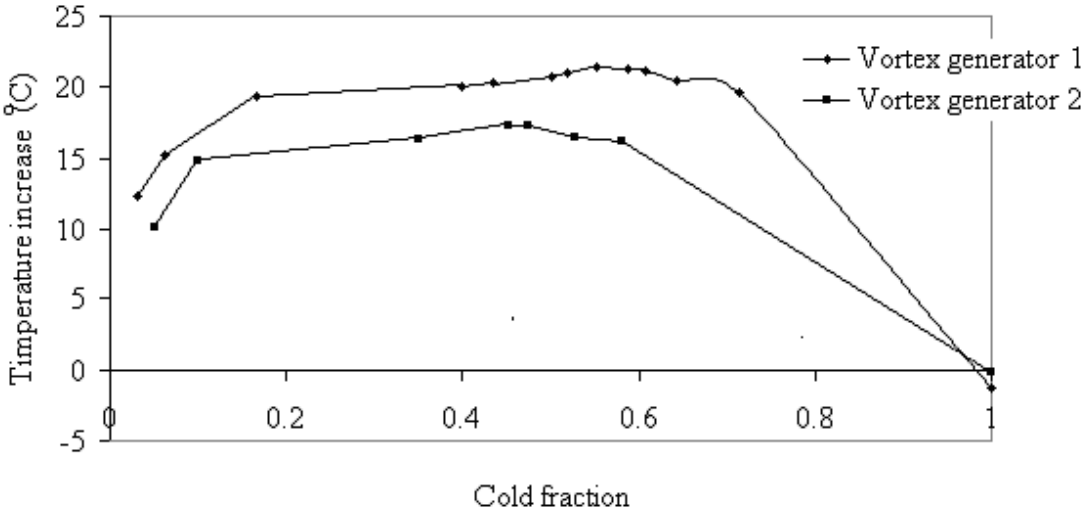

(Insulated vortex tube)

Figure 4.18: Vortex generator shape effect on temperature at hot exit

Substantial research would be necessary to obtain the optimum design for a spiral shaped vortex generator used in conjunction with a small hot tube length.

The length of the hot tube is shown to have an important effect on the energy separation of the vortex tube, as observed by the temperature reduction as the hot tube length increases. This is due to the air inner flow having more time to transfer energy to the outer airflow. Therefore, the 360 mm tube length as shown in Figure 4.19 achieved the highest temperature reduction. However, beyond the optimum length of the hot tube, the temperature decreases again as was found when tests were carried out on a very long vortex tube. This reduction in temperature is due to the energy transfer becoming inversed beyond this optimum length, allowing the outer hot airflow to start warming up the inner airflow. When the inner airflow hits the conical valve, it is directed back towards the cold end at a higher temperature.

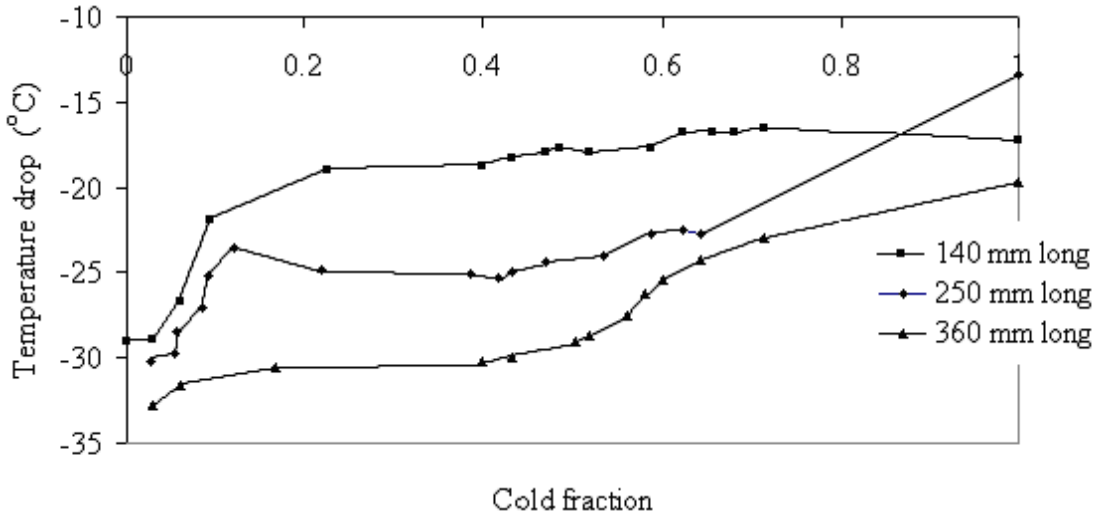

Figure 4.19: Temperature decrease at cold exit with respect to tube length.

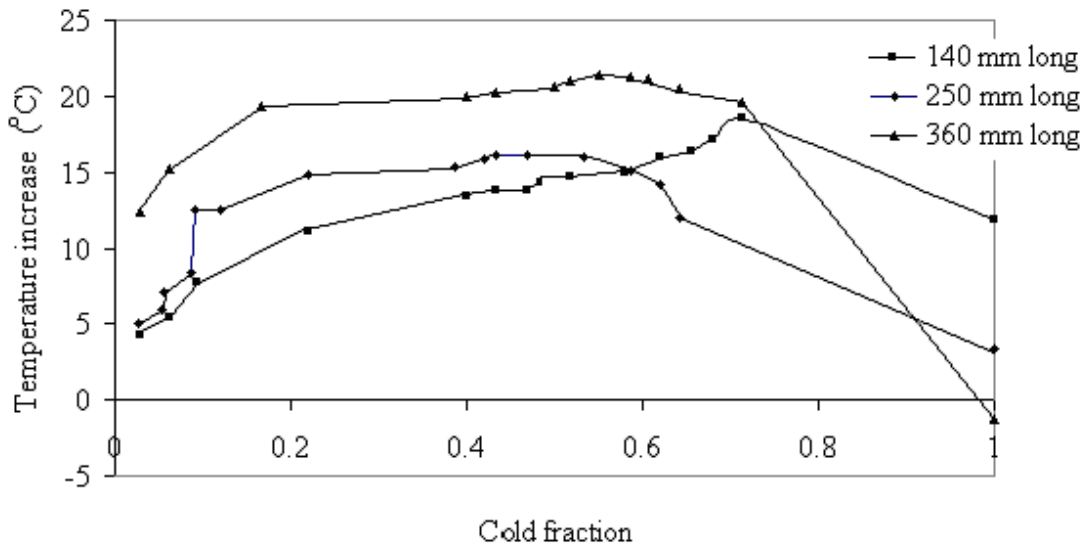

Figure 4.20: Temperature increase at hot exit with respect to tube length.

From the tests it can be concluded that the greatest temperature increase can be obtained by the longest tube or by reducing the orifice diameter from the vortex generator as shown in Figure 4.16. Once again the maximum temperature increase for all lengths can be achieved by the cold mass fraction between 0.4 and 0.7. One of the most important effects on the vortex tube is pressure, as shown in Figure 4.21 and 4.22 which shows that by increasing the pressure, there is a reduction in the temperature at the cold exit. In fact it is noticeable that both detailed graphs show that 0.206 MPa pressure gives slightly higher values for temperature reduction and temperature increase. Tests carried out at above 0.8 MPa air pressure have demonstrated that the temperature decrease at the cold exit, and the temperature increase at the hot exit, increases dramatically.

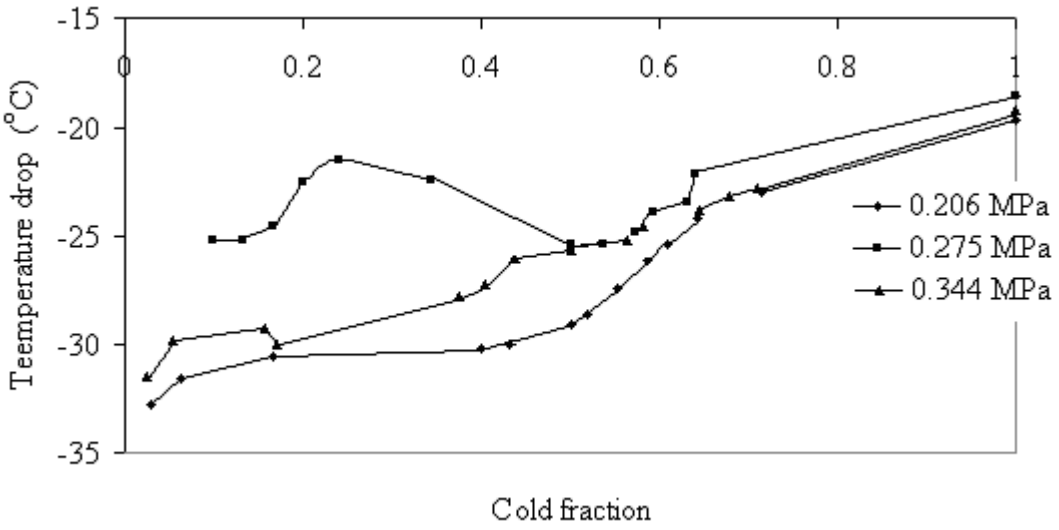

Figure 4.21: Cold exit temperature decrease with respect to pressure.

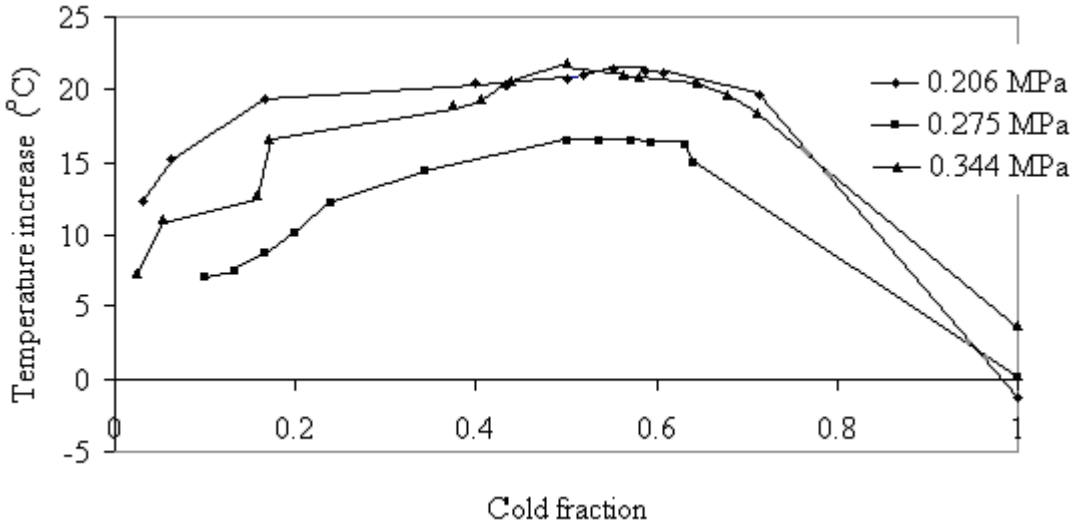

Figure 4.22: Hot exit temperature increase with respect to pressure.

The trends obtained in Figure 4.22 are similar to those that Stephan, [79] obtained from his experiments, except the highest and lowest temperature values which were found for different pressures. The maximum values that Stephan [79] obtained for his temperature increase were between a cold mass fraction of 0.8 and 0.95, whereas the maximum cold mass fraction achieved with the vortex tube under test were 0.5 and 0.7. These differences are due to the geometrical parameters of the vortex tubes that were used in the different tests.

One of the assumptions made for the operating conditions of the vortex tube was that there is no heat transfer between the vortex tube and its surroundings, as shown in Figure 4.23. Even for the cold mass fraction of values between 0 and 0.1, it is better not to use insulation. At this low cold mass fraction a high portion of the airflow moves towards the hot end, and at the same time the temperature of the outer airflow increases because of the insulation. This allows the outer airflow to start warming up the inner airflow, causing the heat transfer process to become reversed, increasing the temperature of the cold air stream.

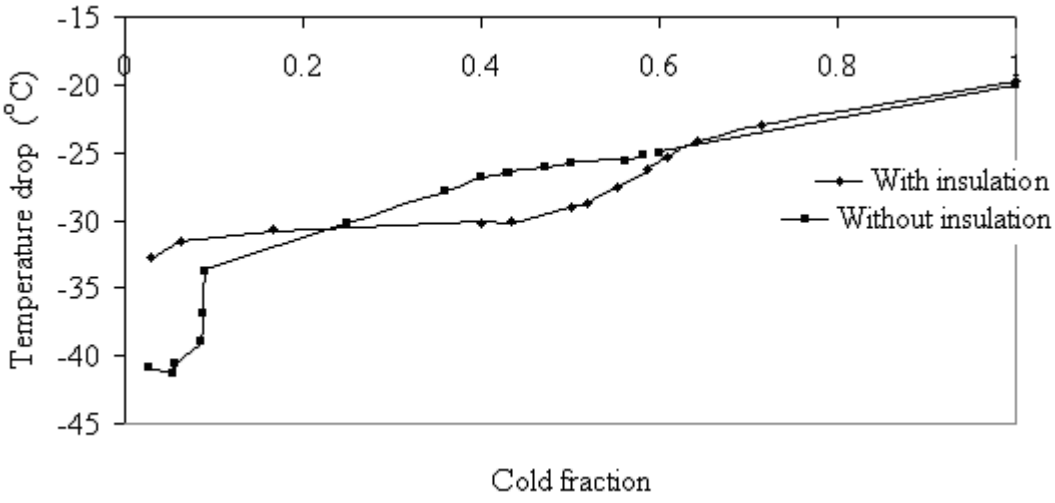

Figure 4.23: Comparison of vortex tube temperature decrease at the cold air exit with and without insulation.

Examination of Figure 4.24 illustrates how using insulation can noticeably increase the temperature of the hot air stream. In fact, this result was predictable as insulation minimises the heat transfer to the ambient, and hence the temperature of the hot airflow increases.

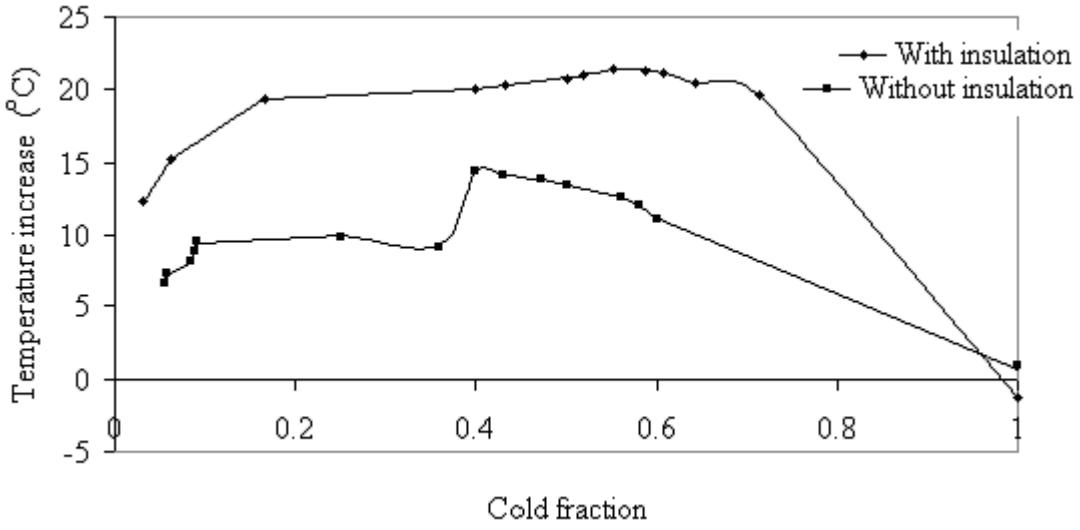

Figure 4.24: Comparison of vortex tube temperature at the hot exit with and without insulation.

CHAPTER 5

TOOL TIP TEMPERATURE MEASUREMENT

5.1 Overview

At first glance being able to measure the actual temperature at the cutting zone looks like an easy task. However, it is only when considering the position that the temperature has to be measured, that the enormity of the task is realised. Many researchers have investigated different methods of obtaining the cutting zone temperature with different degrees of success. In Chapter 2, the use of metal cutting theory and dimensional analysis was used to predict the tool tip temperature during dry machining. These theories proved to give excellent results when compared to the experimental temperatures for dry machining. When air-cooling is applied during machining the indirect method proved to be unreliable for determining the tool tip temperature. For this reason, the tool tip temperature is better obtained by a direct measurement to provide a more accurate temperature. Therefore, to obtain the best direct method of measuring the tool tip temperature, a review of the following temperature measuring processes was investigated.

The temperature measurement processes can be grouped into the following categories:

(a) Thermo-chemical;
(b) Radiation thermometry;
(c) Thermo-electrical;
(d) Indirect method.

These methods were investigated and used to determine the tool tip temperature during the air-cooling cutting process. Consideration of accuracy, effectiveness, and ease of use are all of prime importance when selecting a method for measuring the tool tip temperature during machining. The generation of the chip shown in Figure

5.1 illustrates the challenge of obtaining the tool tip temperature, as the chip is always present at the point where the temperature needs to be measured.

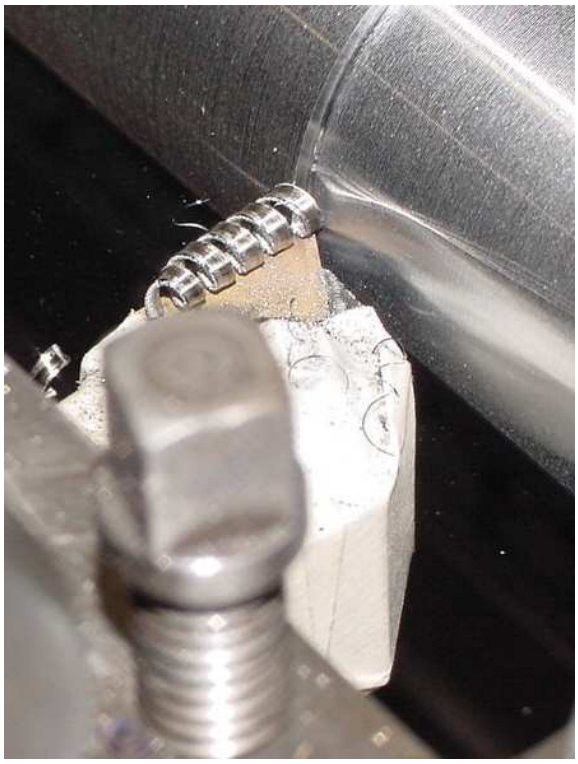

Figure 5.1: Generation of a continuous ribbon chip.

5.2 Temperature Measurement Methods

5.2.1 Thermo-chemical

Thermo-chemical temperature measurement relies on the appearance of the chip or tool surface produced during machining. This can be categorised into two distinct techniques, one relying on the application of a temperature indicator, and the other examining the changes in the tool material.

- the effect of temperature on special substances know as thermo colours which exhibit colour variation for different temperature values;
- the effect of temperature on the metallurgical structure of the tool material or chip.

The first technique simply relies on applying paint onto the surface of the tool, and by examining the change in colour of the paint after machining you are then able to determine the temperature reached in the tool. The second method is similar in that you are examining the tool using a microscope in order to identify changes in colour

and structure within the tool tip material. As these methods depend on good surfaces, they are not always effective for use in the shear zone or with the chip because of irregularities in the deformed surface.

The colour change of the chips can also be used to indicate temperature at the tool tip as shown by S.H.Yeo and S.H. Ong [84]. When using this method it is important that the tip coating is known as this has an effect on the thermal behaviour of the tool. The cutting temperature for different cutting conditions can be quickly assessed by referring to Figure 5.2, which shows the range of temperature for a given colour, chip generation and tool type.

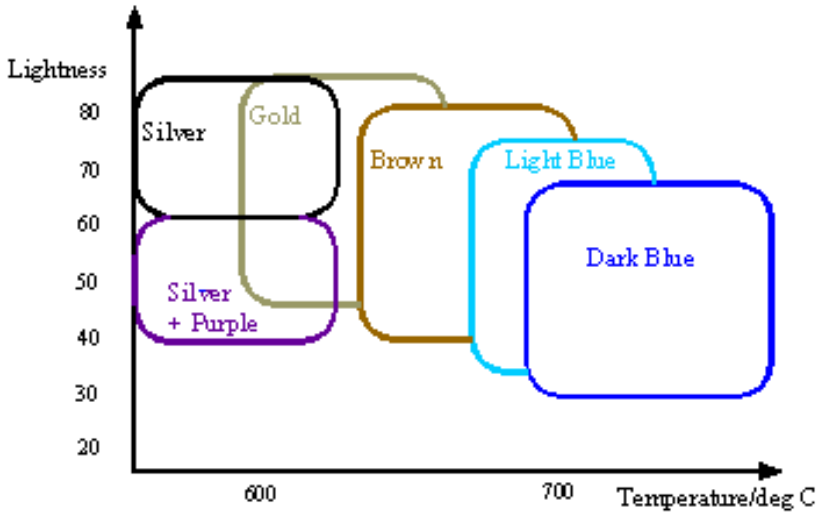

Figure 5.2: Chip colour as a function of tool-chip temperature.

Knowing the transition temperature for each colour the isothermals can be inferred for the methods described above. These methods should only be used as a general guide to temperature due, to the low sensitivity of the thermo-colours and the range of transition temperatures involved. Also, owing to the subjective term used to describe the relative colours on the tool surface or chip, temperatures recorded are not as accurate as obtained by other methods. From an understanding of metallurgical properties and phase changes of different carbides in a tool, Trent [85], [86] and [87] estimated the isothermals around the tool interface by examining the formation of the crater wear on the rake face, which he related to the temperature of fusion between the carbide tip and the work piece. Wright and Trent [88] studied the changes in the structure and hardness that occurred in molybdenum grade high speed

steel (HSS) cutting tool material for temperatures between 600 ^{o}C and 900 ^{o}C. With this gathered data they obtained isothermals in the tools of this material, by examining metallographic sections through worn tools in a plane normal to and near the middle of the cutting edge. An accuracy of +/- 25 ^{o}C was stated for their work. More modern work using this technique involves using a Scanning Electron Microscope (SEM) to detect the various phase changes in the HSS cutting tools. This method is good for measuring temperature distribution along the tool interface, as the machining process is not interfered with in any way. The disadvantage of this technique is that it has a limited temperature range, time consuming preparation, interpretation of the metallographic sections, and limited number of tool materials that can be examined in this way.

The second method considered in this thermo-chemical grouping is the examination of chips produced when using a coated carbide tool under a microscope to determine if there is a formation of a thin layer of FeO (wustite) on the surface of the chip. This indicates that these chip particles have absorbed much of the energy from the cutting process when reaching their high temperature. Under close examination, it is observed that small white particles (5 to 10 μm across) have adhered to the surface of the chip during contact with the tool. Investigation of these white particles with the microscope proves that they are αAl_2O_3 and TiO_2 as found by C. Costable, *et al* [89]. It is well known that Al_2O_3 can adopt several phases dependant upon the method and temperature of production. Other composite tool tips have shown phase changes, and are useful with respect to failure mechanisms of the tool tip as investigated by D. Jianxin *et al.* [90]. Blue chips have a presence of αAl_2O_3 on the surface suggesting operating temperatures in excess of 1000 ^{o}C. However, for the cutting tests during air-cooling, the chips produced were light blue in colour indicating that this temperature is more in the region of 650 ^{o}C.

5.2.2 Radiation thermometry technique

All objects emit thermal radiation, whether they are at a low temperature or high temperature. At low temperatures mainly infrared radiation (radiant heat) is given off; while at elevated temperatures the object begins to glow (emitting visible light) as the amount of thermal radiation emitted increases with temperature. These techniques are used to investigate the tool tip cutting temperature during chip

formation in a non-invasive manner, as there is no contact necessary during the radiation thermometry processes. With the thermographic technique the radiation from the tool, the work piece, and the chip are measured to establish the temperature zone on the outside of the surfaces of these regions. Radiometric methods involve the use of pyrometers (radiation thermometers) or infrared photography to measure the infrared or total radiation that is given off from a body. Radiation thermometers can have a temperature range from –50 ^{o}C to 3000 ^{o}C, which is ideally suited for the temperature reached during metal cutting.

As with all measuring equipment it is necessary to calibrate the pyrometer to allow the correct temperatures to be measured. Great care must be taken when calibrating these instruments as the quantity of radiation emitted by a hot object depends on its emissivity, which can be affected by the reflectivness of the object. As a result, radiation thermometers will indicate different temperatures readings from objects with different emissivities, even when they are at the same temperature. Therefore, when calibrating radiation pyrometers it's necessary to have a source with a very well known emissivity. This is usually achieved using a blackbody source.

One of the first researchers to use this technique for determining the temperature at the surface of the tool and workpiece was Schwerd [91], who developed a radiation pyrometer where the radiations were beamed onto a thermocouple with an optical condenser. Another approach used in calibrating a pyrometer was by Y.K. Potdar and A.T. Zender [92] who were recording the temperature in transient metal cutting. Normally there is a lack of knowledge of some of the parameters involved, such as emissivity as a function of temperature due to the varieties of tool tip surfaces. However, this can be obtained experimentally: Y.K. Potdar and A.T. Zender [93] followed the next procedure. A calibration specimen (tool tip) was prepared to the same surface finish as the actual test tool tip. Two K-type thermocouples separated horizontally by 5 mm are spot welded to the surface of the specimen. The calibration specimen is kept in the same position as the actual test specimen, with the same surface to which the thermocouples are attached facing the detectors. The detectors are focused on the region between the attached thermocouples. The specimen is heated from behind the face - on which there are no thermocouples - by a heat gun,

and the infrared radiation is recorded as the specimen cools down. From this data a second-order best-fitting curve was obtained to use for calibration.

Reichenbach [94] drilled holes through a workpiece normal to the surface being machined, and then measured the radiation emitted from the hole by a lead sulphide cell placed at the hole beneath the workpiece. He attempted to measure shear plane angle and tool flank temperatures as the line of sight of the hole moved along the shear plane and then along the tool flank, but had difficulty in measuring the radiation due to burring of the hole. However, he reported that the observed temperature increased the larger the undeformed chip thickness was made. Due to the difficulty encountered by Reichenbach in obtaining the tool temperature, he does not recommend this as a suitable method.

Chao, Li and Trigger [95] used a lead sulphide photoconductive cell assembly to measure the flank face temperature. The whole assembly was accommodated in an axial slot (38 mm wide and 76 mm long) provided in the wall of a tubular workpiece on which orthogonal machining was performed. The radiant energy emitted at the tool flank was detected by the cell through a 2.38 mm diameter hole drilled axially in the tube wall with a hypodermic needle. Using a conductive paper electrical analogue, the authors Chao, Li and Trigger [95] inferred the temperature Figure 5.4 and the heat flux distribution along the tool interface from the measured flank temperature distribution Figure 5.3.

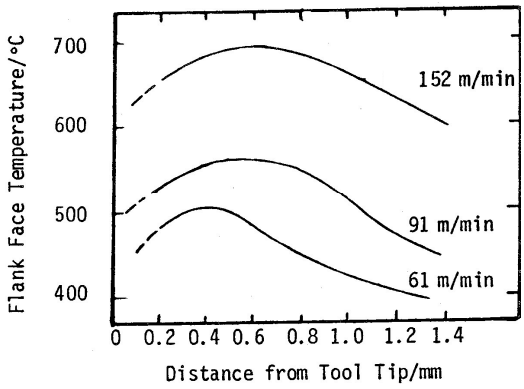

As obtained by Chao *et al.* [95] for AISI52100 work material; K3H carbide tool material; 7° rake angle; 0.14 mm/rev feed rate.

Figure 5.3: Experimental flank face temperatures.

The maximum temperature at the interface occurs at about 0.6 to 0.7 of the total contact length as shown in Figure 5.4. This agrees well with the results of Arndt and Brown [96]. More recent researchers E. G. Ng *et al.* [97] have modernised the Reichenbach method of drilling holes by using a pyrometer in conjunction with optical fibres. The advantage of this arrangement shows that it is possible to register transient heat generation in high-speed discontinuous cutting.

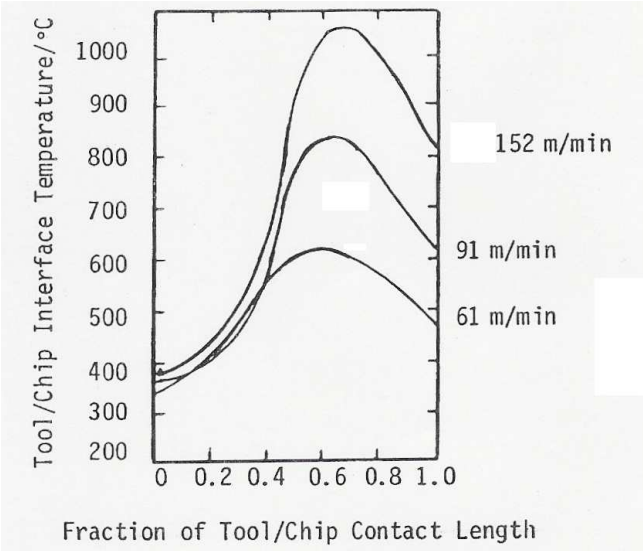

As obtained by Chao *et al* [95]. for AISI 52100 work material; K3H carbide tool material; 7^{o} rake angle; 0.14 mm feed rate.

Figure 5.4:Experimental chip interface temperatures

Figures 5.3 and 5.4 show the temperature distribution at the tool interface that was measured directly with considerable success by Lenz [98] using a pyrometer. He drilled a 0.2 mm diameter hole through the tool, and by changing the position of this hole to different locations of the chip contact length, was able to measure the radiation emitted from the underside of the chip surface using a lens assembly. In order to maintain an open hole, Lenz [98] found it necessary to provide a hole of 1 mm diameter and 0.2 mm deep around the hole at the rake face.

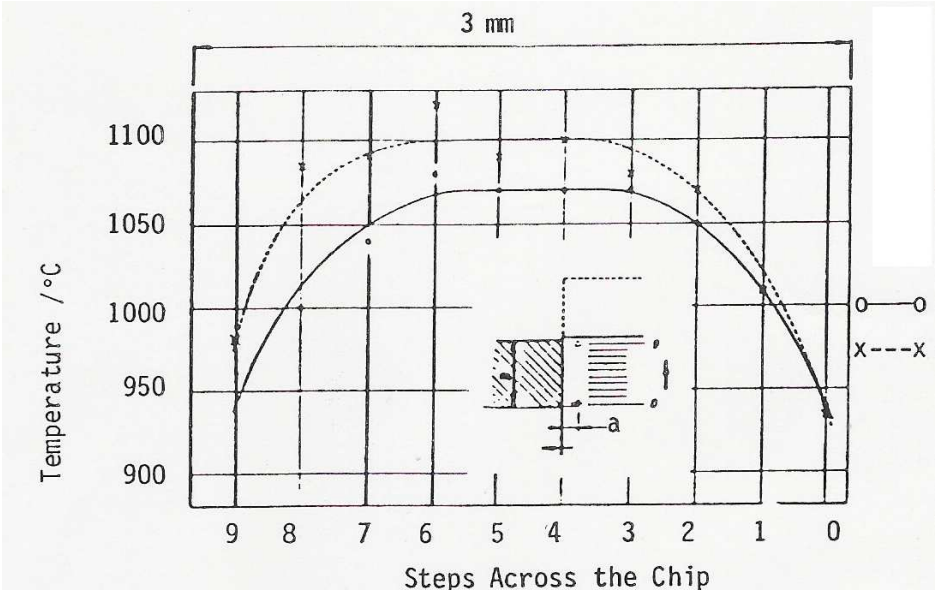

(a) For CK 60N steel working material; P10 carbide tool; -10^{o} rake angle; 95 m/min cutting speed.

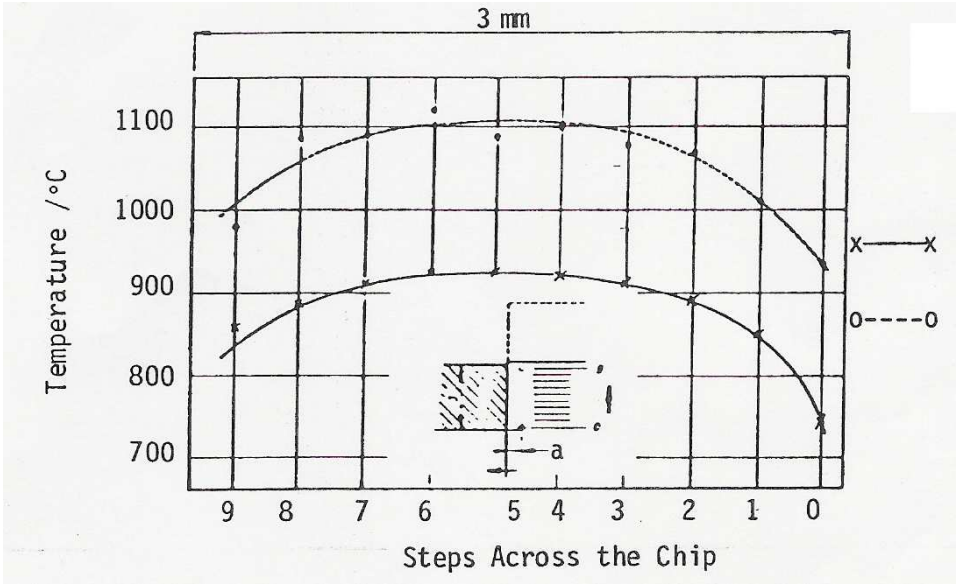

(b): For XC 45 steel working material; P10 carbide tool; -10^{o} rake angle.

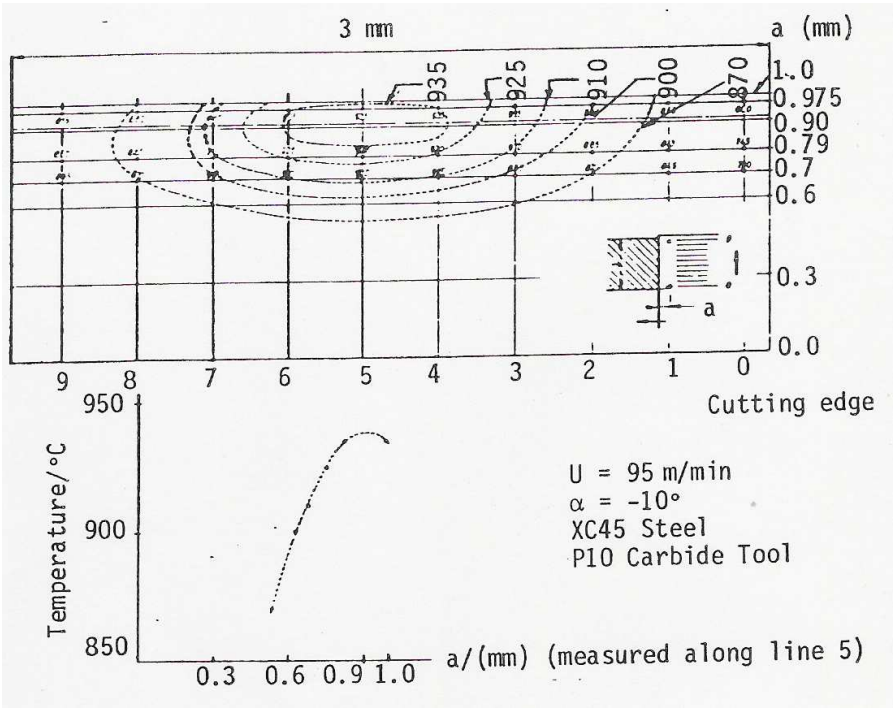

(c): For XC 45 steel working material; P10 carbide tool; -10^{o} rake angle.

He investigated the effects of speed and rake angle on interface temperature and found that it increased with speed and decreased in rake angle, as shown in Figure 5.5(d). The isotherms created about the contact area were shown to be non-symmetrical about the centre line of the contact area line 5. This was attributed to the fact that while air was at the left end of the tool around line 9, there was still conductive tool material on the right around line 0, as shown in Figure 5.5(a-c). Also shown in Figure 5.5(c) is the interfacial temperature distribution along line 5, which gives the maximum temperature close to the end of contact.

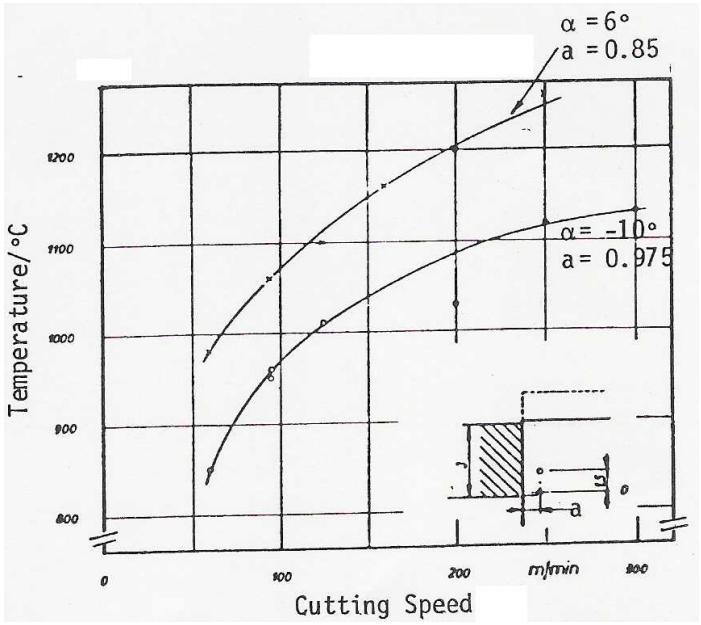

(d): For XC 45 steel working material; P10 carbide tool; 6^{o} rake angle.

Figure 5.5(a-d): Temperature distribution across the tool interface for separate distances from the cutting edge.

As obtained by Lenz. [98]

Friedman and Lenz [99] developed a pyrometric device to measure the temperature field on the upper surface of the chip, which, together with those obtained by Lenz [98], provided a more comprehensive picture of the overall temperature field in the chip. They showed that the temperature did not vary greatly across the chip although the temperature increased slightly at the chip edges as shown in Figure 5.6.

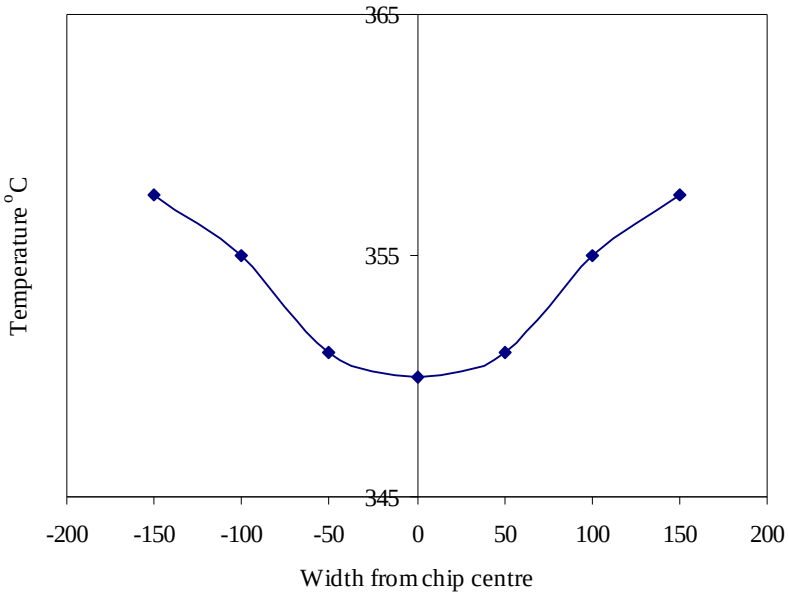

(data from Friedman and Lenz [99])

Figure 5.6: Lateral distribution of chip temperature at a distance of 1mm from the cutting edge.

This was attributed to the simultaneous decrease in chip thickness at the edge of the chip. Figure 5.7 shows the temperature distribution along the chip velocity direction for different feeds, and from this it can be concluded that a reduction of feed results in an increase in temperature. The higher temperature in the upper chip surface for the inner chips is due to a reduction in the cross-sectional area of the chip, since the heat generated is dissipated in this smaller area resulting in an overall temperature increase.

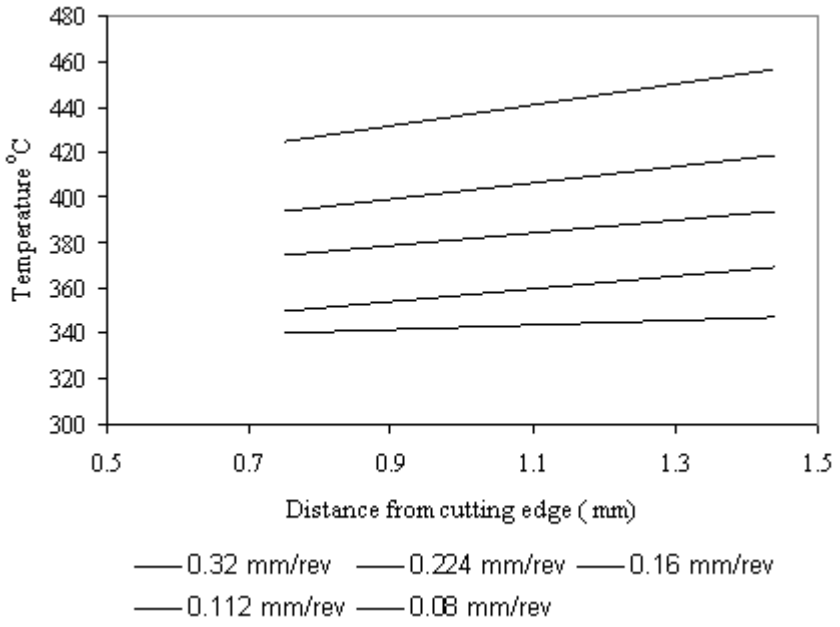

data from Friedman and Lenz [99]

Figure 5.7: Influence of undeformed chip thickness (feed t_1) on the upper chip surface temperature.

Boothroyd [10] used infra-red photography to record the radiation emitted from the sides of the chip, workpiece, and tool. Using a microdensitometer to detect variations in the optical density of the photographic plate, Boothroyd [10] plotted temperature distribution for various cutting conditions in the chip, workpiece, and tool. A typical example of the temperature distributions obtained is shown in Figure 5.8. It shows that the temperature rises steadily while going through the shear zone, and that the maximum interface temperature lies somewhere in the middle of the tool chip interface contact length.

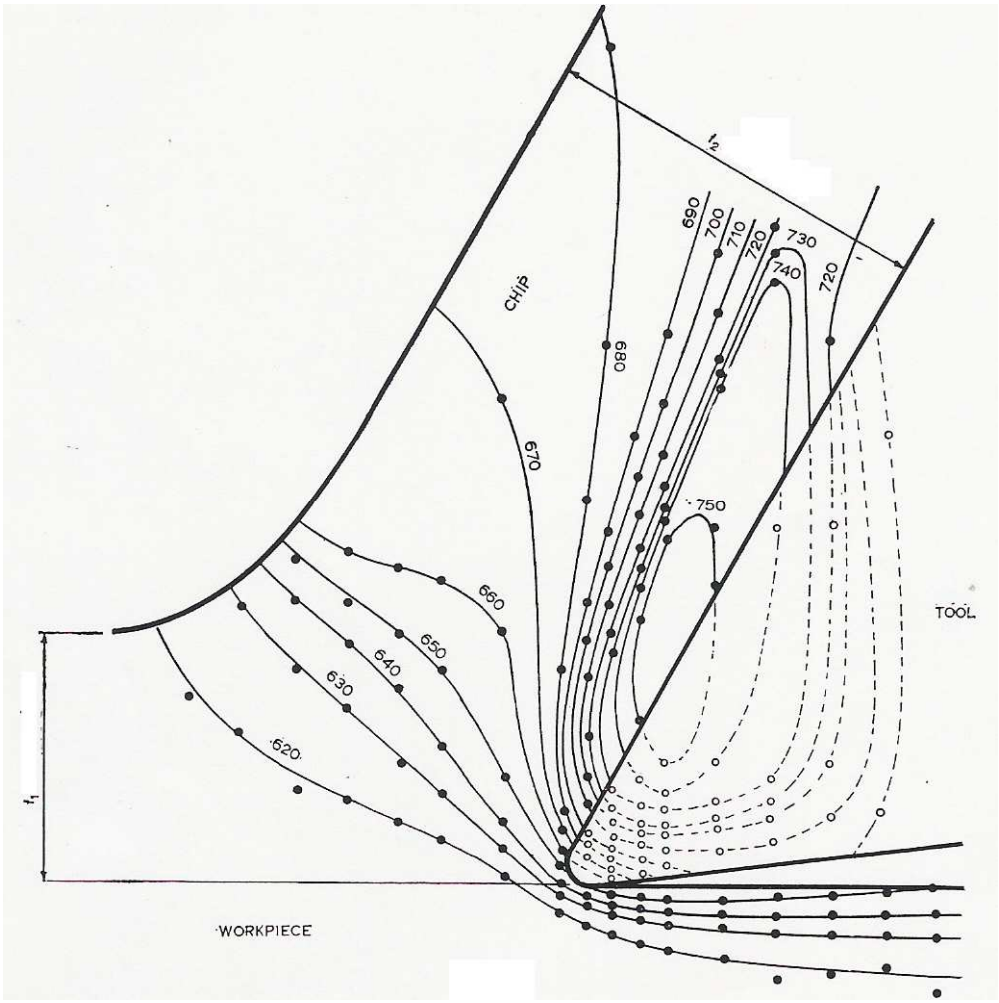

Obtained by Boothroyd [10]

Figure 5.8: Isotherm pattern (^{o}C) in chip, tool and workpiece.

It is also noticeable that the temperatures are very high. This was due to preheating of the work piece, which was necessary to obtain sufficient radiation for the infrared photography. This constitutes a weakness in this method, as it is not normal machining practice to preheat the workpiece to such a high temperature. Also, such preheating would affect the strength of the work material and therefore alter the mode of deformation and temperature distribution that would normally be obtained during conventional machining. A further weakness in this method is the fact that the temperature distribution on the sides of the chip, workpiece and tool may not be representative of the distributions away from the sides as found by Arndt and Brown [96] and Figure 5.9. In Jeelani [100] the technique used by Boothroyed was extended to measure the temperature at the tool contact zone without having to preheat the workpiece. This was due to the extended sensitivity of the high speed infra-red film

now available, and it was able to detect temperatures as low as 371 ^{o}C. Jeelani [100] confirmed that the proportion of heat (β) conducted into the workpiece decreases with an increase in cutting speed as suggested by other researchers.

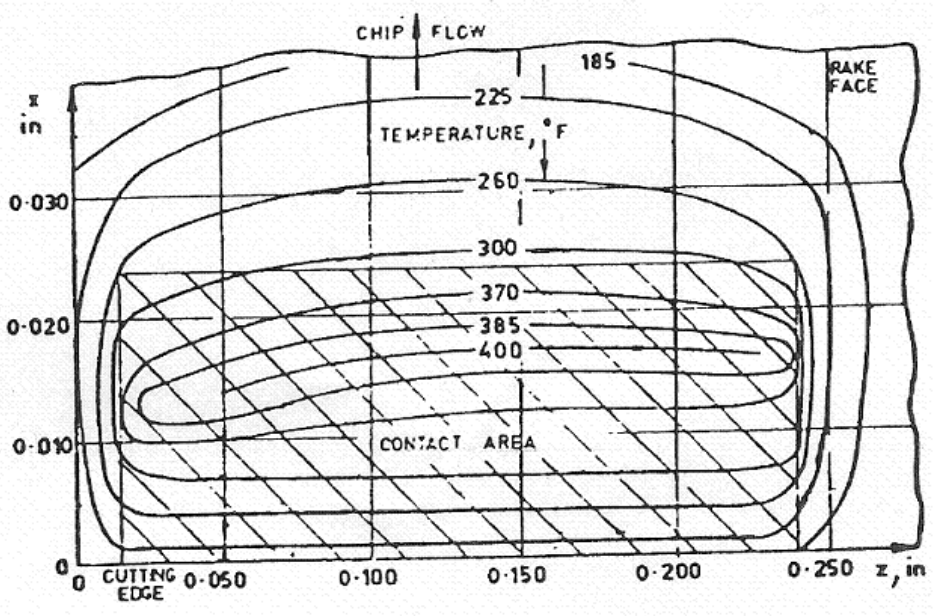

Obtained by Arndt and Brown [96] (note temperatures are in degrees Fahrenheit)

Figure 5.9: Experimental rake face isotherms.

A more recent method of temperature measurement has been the use of an infra-red sensitive camera as shown in Figure 5.10. In this test the temperatures at the three spots were also measured by imbedded thermocouples to verify the infrared camera measured temperature distribution of the tool.

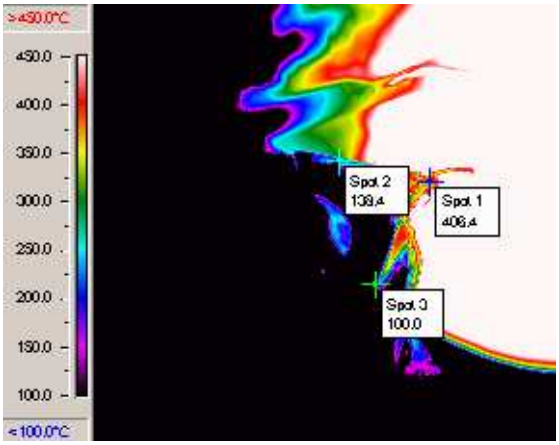

Figure 5.10: Example of the temperature zone measured by an infrared camera during tool test.

A technique using the infrared camera for measuring the steady state tool chip interface temperature was developed by Kwon *et al.* [101] who measured the transient cooling behaviour on the rake surface after the feed motion was halted. The tool tip temperature falls rapidly when the cutting action stops due to the removal of the heat sources. Using the infrared camera after the feed is stopped only measures the dissipation of the heat from the last point in the cutting operation. This therefore makes the infrared approach of measuring the tool tip temperature unsuitable for use during air-cooling tests.

It can be assumed that temperatures measured on the side face were approximately the same as the values found in the middle of the tool. Examples of the temperature distribution are shown in Figure 5.9. Again it shows that the trends are the same as observed by other researchers, that the maximum temperature of the tool chip contact length occurred somewhere in the middle of the contact length. A general temperature decrease is also observed as the depth from the heat source increases. Sutter *et al.* [102].

At first, using the infrared camera to measure the tool tip temperature looked like the most promising method, as there is no apparent interference to the cutting process, and the temperatures recorded would be at real time. Also, having an infrared picture of the cutting process should provide an excellent opportunity to visually analyse the air-cooling system. Unfortunately, it became apparent that this method of measuring the tool tip temperature was not suitable, as the temperature of the chips was influencing the infrared picture of the cutting zone as shown in Figure 5.11. The white area shows the chip forming on the top of the rake face, covering the view of the tool tip during machining.

To save the camera lens from being scratched by the chips during machining an optical gold coated mirror (which has no effect on the temperatures recorded by the infrared camera) was used. The mirror fixture was designed to hold the mirror directly above the cutting zone, and remained in this position for the whole machining operation as shown in Figure 5.11.

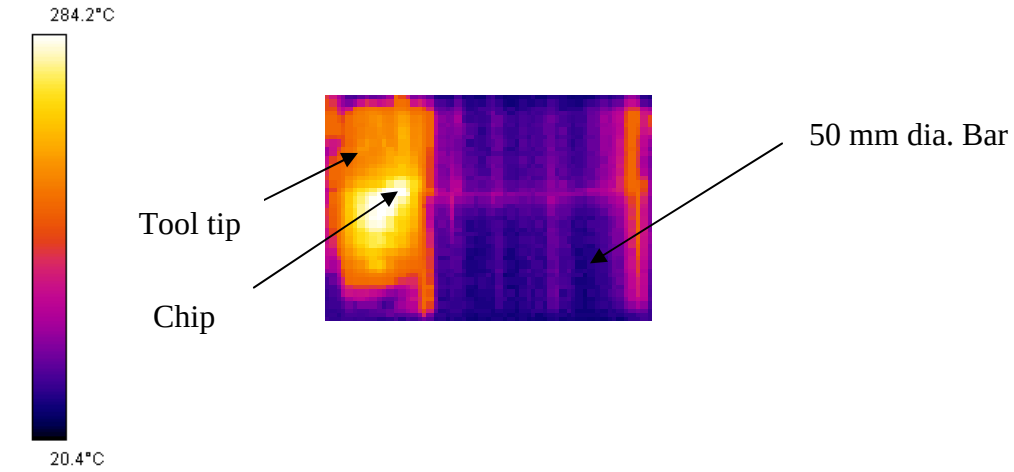

Figure 5.11: Infrared picture of the cutting zone

If it was possible to remove the chip from the area of interest then this method would be easy to use and give accurate results when calibrated correctly. Kwon *et al.* [101] used this measurement procedure where he adopted to have no chip present and interrupted the cutting process to take an infrared picture. Allowing the chip to be removed from the view of the thermal camera apparently allows you to determine the temperature of the tool tip without chips interfering. The problem with this is it was found that the tool tip rapidly cools as soon as the cutting action stops, resulting in the tool tip being measured at a far cooler temperature than when machining, as shown in Figure 5.12.

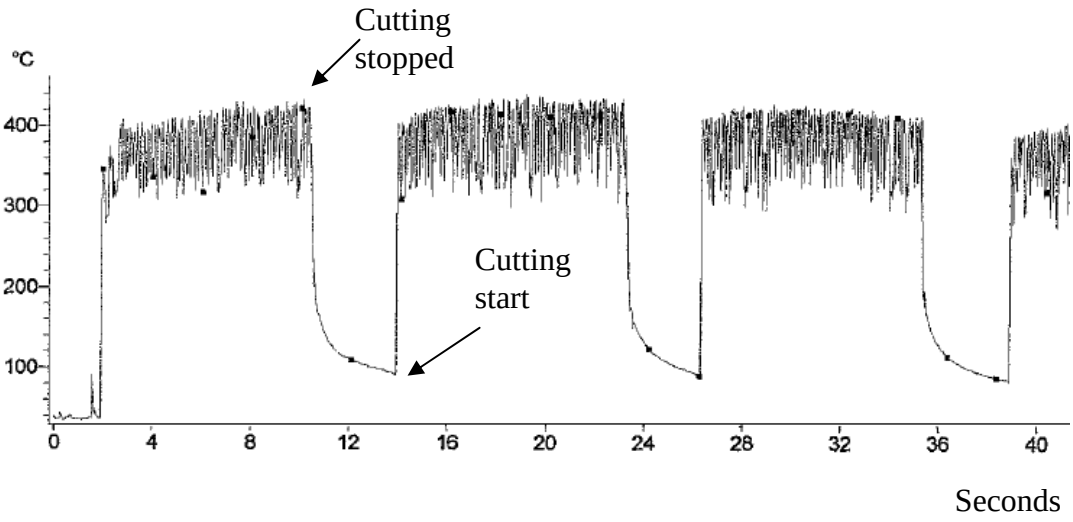

Figure 5.12: Temperature reduction when cutting stops

5.2.3 Thermo-electrical techniques

Thermo-electric methods essentially use thermocouples to measure temperatures. The thermocouple is recognised as a simple technique for measuring the tool interface temperature without interfering with the machining process. Essentially this consists of making the tool chip interface the hot junction of the thermocouple and measuring the potential difference generated. Herbert [103] was among the first to employ this technique and he encountered two basic challenges. The first was the difficulty of calibration since the interface consisted of an extremely clean surface pressed together by extremely high pressures. The second challenge was that of determining what temperature was being calibrated against the thermal generated e.m.f. during the machining process (maximum, minimum or average). Some researchers were of the opinion that the calibration temperature was some sort of integrated mean value. However, additional analysis to determine which temperatures were really consistent with the potential values obtained, concluded that the temperatures calibrated against the potential values were slightly below the average values.

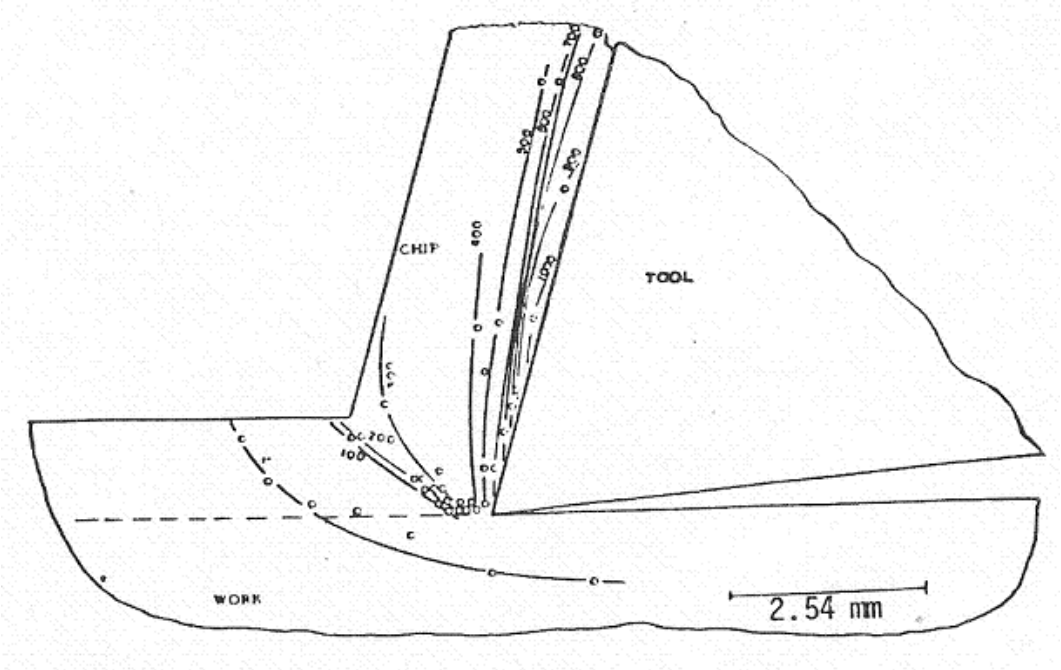

Obtained by Reichenbach [94] for a 1020 steel at a cutting speed of 45 m/min and feed of 1.27 mm/rev

Figure 5.13: Temperatures found by using imbedded thermocouples.

By using an arrangement of very small thermocouples in the measurement circuit, and making corrections for the interface pressure distribution, he was able to obtain temperature distributions along the interface. Reichenbach [94] embedded thermocouples in the side of the workpiece at several depths below the uncut surface and hence measured temperature in the chip and work piece. From these various measured temperatures Reichenbach [94] was able to sketch the temperature field in the chip and workpiece as shown in Figure 5.13.

Balint and Brown [104] developed an interesting thermo-electric method, which employed the point contact between a traversing probe and the face of a tool of dissimilar material as the hot junction. The probe is passed along the surface of the tool and the e.m.f. generated is measured by an oscilloscope, allowing the temperature distribution of the exposed rake face to be obtained. The isothermals obtained were extrapolated into the tool chip interface region, taking the heat balance into consideration. This technique ensured good electrical and thermal contact at the hot junction, and it did not interfere with the machining process. However, the necessary extrapolations in obtaining the tool interface temperature are dependent on the temperature gradient at the tool interface as they can be quite large. Arndt and Brown [96] extended the traversing thermocouple probe technique to measure the temperature distribution in the tool chip contact region by directly cutting a V-shape groove in the work material (with a V-shaped tool set at 180 ^{o}C) ahead of the main tool. This split the chip as it moves up the rake face of the main tool, enabling the probe to be traversed over the interface along the V-groove. They found it necessary to have a gap of 0.356 mm in the chip in order to traverse inside the split chip. An example of the temperature isotherms they obtained is given in Figure 5.8. In conjunction with this, Arndt and Brown [96] were measuring the average interface temperature using a tool/work thermocouple to investigate the nature of the transient temperature rise during machining. It was found that the initial temperature rise is very rapid in the first second of cutting and thereafter it continues to rise at a steadily decreasing rate for several minutes. They attributed the temperature rise after the first few seconds of cutting to heat conduction. To standardise their measurements, they commenced all probe traverses 20 seconds after the start of cutting. Arndt and Brown compared their experimental results with the temperature distribution obtained from analytical solutions proposed by Chao *et al.* [105] and Rapier [106]. They found

while the average interface temperature as measured by the tool-work thermocouple agreed well with the analytical values, the measured interface temperature distribution was far below (about 205 ^{o}C to 260 ^{o}C) the theoretical distributions. Arndt and Brown suggested that this discrepancy was probably due to the high temperature gradient from the sides of the chip and in the asperities on the tool face with which the probe made contact. The form of their experimental distribution along the interface, however, agreed well with that calculated by Chao *et al* [105] analytical method, with a maximum occurring within the contact length. Although the location of the maximum temperature was 71 percent of the contact length from the cutting edge compared with a value of 89 percent for the analytical distribution.

More recently Young [107] used a highly sensitive infrared detector to determine the temperature of the chip back section during orthogonal cutting of AISI 1045 steel. He showed a rapid increase of temperature corresponding to a sudden breakdown of the cutting edge. The method of embedded thermocouple temperature measurement is one of the most extensively used methods of determining the tool tip temperature today. Kitigawa *et al.* [108] used this technique to investigate the influence of temperature on the tool wear during high speed turning. This method allowed the edge of the wire to be exposed on the rake face by grinding. The chip sliding on this rake face breaks the insulation to create a hot junction between the wire and the exposed site on the tool tip. The reported tool tip temperatures recorded were close to 1200 ^{o}C at a cutting speed of 150 m/min. O'Sullivan and Cotterell [109] measured the temperatures in turning using two thermocouples in the work piece. They also indicated that an increase in cutting speed resulted in a decrease of the temperature as previous researchers had found. They attributed this reduction to the higher metal removal rate, which results in more heat being carried away by the chip and therefore less heat being conducted into the workpiece. Ay and Yang [110] used a technique with K-type thermocouples to analyse temperature variations in carbide tool tips in cutting various materials. They observed oscillation in temperature near the cutting edge, which was more marked for ductile material and less in hard-machining materials. These observations were attributed to the chip formation, which raises the local temperature upon its contact with the work material. Obikawa [111] and Usui *et al*. [112] both inserted thermocouples into several holes at different locations in the interior of the tool tip, with some of them as close to the surface as possible.

However, with this method a high number of drillings are required to determine the distribution of the temperature at the tool tip interface to give a reliable picture of the temperature distribution across the tool tip.

5.2.4 Indirect measurement of tool interface temperature

Measurement of the tool interface face temperature is always extremely tricky to accurately achieve due to the dynamic cutting conditions that the tool tip operates within. In an attempt to simplify this process a series of experiments making use of the effect of conductivity of the heat travelling through the tool were carried out. The aim here was to establish a mathematical model for the heat travelling through the tool tip. Using this model would then allow a temperature measurement to be taken at any point on the tool tip, preferably one out with the cutting zone to be used to determine the tool interface temperature. This series of experiments was carried out on the engine lathe using an electrical inductive furnace to heat up the workpiece, with the temperatures along the bar being monitored. The cutting tool was pressed hard against the end of the workpiece to ensure good thermal conductivity between the tool and the workpiece. The temperature was then measured as it progressed through the tool tip. From the recorded temperatures as shown on Figure 5.14 a mathematical model was found.

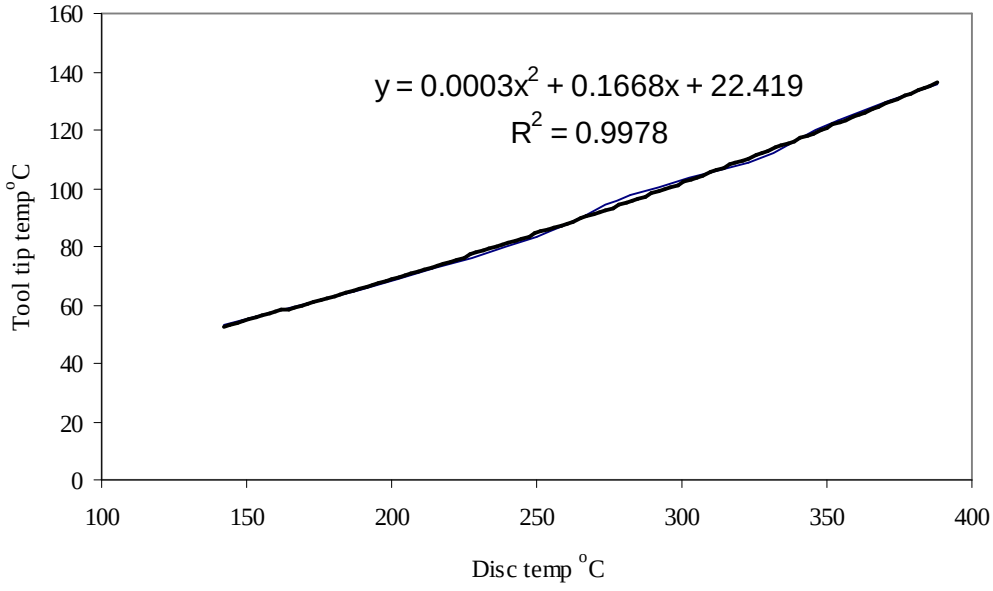

Figure 5.14: Graph showing temperatures in a copper disc placed between tool tip and work piece.

$$T_{tip} = 0.0003x^2 + 0.1668x^2 + 22.419 \quad (5.1)$$

Unfortunately, the derived mathematical model when compared with the cutting theory proved to be unreliable, and was quickly rejected as an unsuitable method. The reason the model failed was that it did not take into account the distinctive way that the heat is generated in metal cutting, as was discussed in Chapter 2.

5.3 Tool Tip Temperature Measurement

5.3.1 Thermocouple method

A review of commercially available data logging instruments revealed the most suitable with respect to data capture speed was the National Instruments TC-2196 data logger and National Instruments software. The data was then recorded on the computer for analysing as shown in Figure 5.15.

Figure 5.15: Data logger and computer used for analysing tool tip temperatures.

The K-type thermocouple to be used with the data logger needs each hot-junction (thermocouple wire ends) suitably prepared to ensure electro-conductivity when inserted into the tool tip. This involved welding the two wires together resulting in a

welded bead being created of approximately 10 to 15 percent of the wire diameter. As there are a number of thermocouples in use it is necessary that the thermocouples are all connected using a zone box. This is a region of uniform temperature used to ensure that all connections made within it are at the same temperature. The zone box is an integral part of the National Instruments TC-2196 data logger. The National Instruments software allowed for changes to be made to the measured output from the hot junction, from degrees centigrade to mV. This is very useful as it allows a table of thermoelectric voltages Appendix B to be used for calibration purposes. The procedure involved inserting the thermocouple into an ice bath and adjusting the output to give 0 ^{o}C if necessary. A block diagram of the temperature measuring procedure used is shown in Figure 5.16, which shows a thermocouple being calibrated.

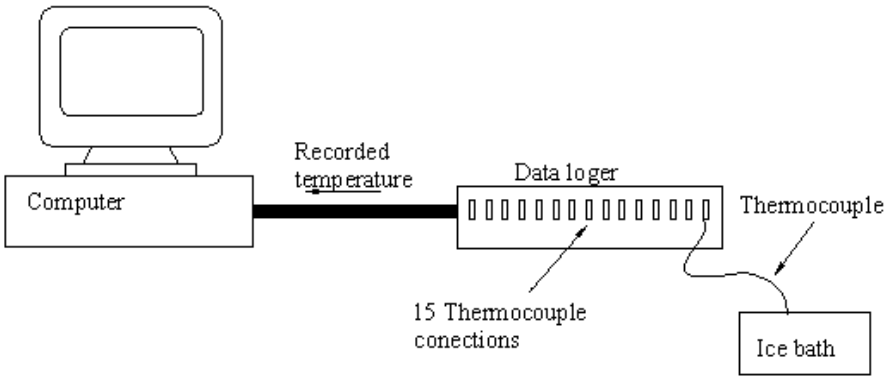

Figure 5.16: Block diagram for reading multiple thermocouples.

Other aspects to consider when calibrating is that all the wiring should be checked, and the voltage on the reference thermocouple channel should be close to zero before the reference thermocouple is put into the ice-bath, and should correspond to the zone-box temperature as shown in Figure 5.17.

Figure 5.17: Zone-box combined with data logger.

Having the capability to measure a number of thermocouples at the same time was found to be extremely useful in analysing the tool tip temperature, as this allowed additional temperatures to be recorded, such as the cold air leaving the vortex tube jet.

Considerable time and effort was spent to establish a suitable method of inserting the thermocouples into the tool tip. Thermocouples need to be placed at the correct position to measure the temperature at the tool interface, as well as providing suitable protected from the chips. Also, it is essential that thermo-conductivity between the thermocouple and the tool tip is made to ensuring accurate temperatures. This was achieved by using thermal paste when inserting the hot-junction into the small holes in the tool tip. Figure 5.18 shows an early attempt at protecting the thermocouples. Machining was obviously not successful as on this occasion the thermocouple was destroyed after just one pass of the cutter. This graphically illustrates the hostile environment in which thermocouples have to record the tool temperature. The introduction of a removable metal guard solved the problem of protecting the thermocouples, and allowed easy access to the imbedded thermocouples. Using this method of protection enabled the tool tips to be used until the end of their useful tool life. Herchang Ay and Wen-Jei Yang *et al* [110] have made similar use of embedded thermocouples.

Figure 5.18: Effect of the cutting environment on the thermocouple.

5.3.2 Machining tests

In order to test the temperature measuring process it is first necessary to verify the measured temperature against predicted temperatures obtained from the machining theory in Chapter 2. This requires the power used during machining to be measured to allow Cook's [22] equation (2.22) to be used to determine the tool interface temperature. Figure 5.19 shows the power analyser used to measure the lathes power during machining.

Figure 5.19: Power analyser being used to measure the power during machining.

A number of lathe power readings were recorded for different cutting conditions as given in Table 5.1.

Table 5.1: Cutting conditions used during power readings

	Cutting speed (m/min)	Feed rate (mm/rev)	Depth of cut (mm)	Work material	Tool tip grade	Rake angle
Power reading 1	175	0.23	1	AISI1030	P15	10
Power reading 2	175	0.23	2	AISI1030	P15	10
Power reading 3	175	0.28	1	AISI1030	P15	10
Power reading 4	175	0.28	2	AISI1030	P15	10
Power reading 5	190	0.23	1	AISI1030	P15	10
Power reading 6	190	0.23	2	AISI1030	P15	10
Power reading 7	190	0.28	1	AISI1030	P15	10
Power reading 8	190	0.28	2	AISI1030	P15	10

- The cutting tool body was a Seco CTGPR 2020-16 with a triangular tip

With the selection of the experimental conditions completed, the tool tips were prepared with the embedded thermocouples and calibrated. The metal cutting tests were carried out under orthogonal conditions as outlined in Chapter 2. A record of at least 20 seconds of metal cutting was made for each cutting condition ensuring that steady-state heat transfer conditions were obtained during the cutting test. Cook's [22] equation was used to calculate the tool interface temperature for comparison with the experimental measurements.

The temperatures recorded for the tool tests when a constant feed is used while varying cutting speeds, produced an isotherm pattern which showed an increase in temperature as the cutting speed increased. Examining the temperatures produced when the cutting speed is constant and the feed rate is varied, shows that an increase in temperature occurs for an increase in feed rate. It was observed that the hot spot for increased cutting speed moved closer to the cutting edge, and for the higher feed rate moves further away from the cutting edge due to the proportional increase in the undeformed chip thickness, t_1, as shown in Figure 5.5(b). It is interesting to note that the observations and temperatures recorded were similar to those observed by previous researchers. Using the present cutting conditions a comparison can now be made between the maximum interface temperature measured and one calculated from the predictive theory of machining described in Chapter 2. These results are shown in Figure 5.20.

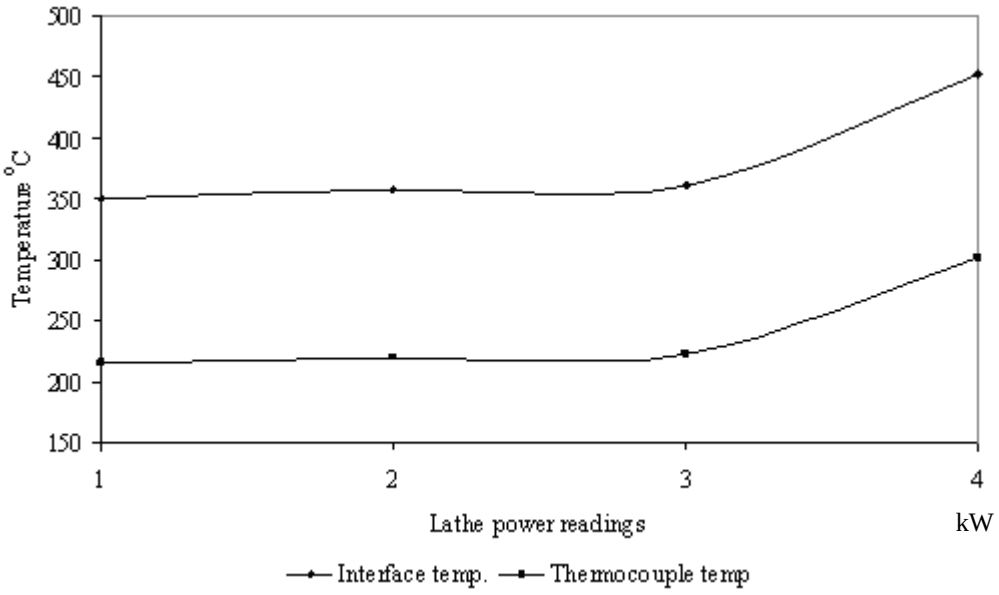

(cutting speed of 175 m/min. feed 0.23 mm/rev and 1mm depth of cut)

Figure 5.20: Contrast of predicted interface temperature and calculated temperature at thermocouple position in tool tip.

The calculated temperature for the thermocouple positioned in the tool tip compared reasonably well with the experimental temperature obtained during dry cutting, as shown by the experimental temperature given in Figure 5.20. Also, any changes in cutting conditions show the calculated values still gave good agreement. For both the

cutting speed and undeformed chip thickness the calculated results show an increase in temperature. The difference between the actual magnitudes of the theoretical and experimental temperatures is not surprising, considering that Cook's [22] equation establishes the temperature at the tool interface while the thermocouple is positioned 1 mm from the edge. It can be clearly seen from the experimental results of Arndt and Brown in Figure 5.9 that the temperature at the edge can be much higher than the position where the thermocouples are placed due to an attempt not to reduce the strength of the cutting edge.

5.4 Discussion

It has been shown that there is considerable difficulty in obtaining the temperature at the tool interface. This results in a variety of methods of determining the tool tip temperature, each with their own degree of difficulty and success. Experimental techniques used so far have been wide and varied in obtaining the temperature distributions of the tool tip. Each of the methods discussed have advantages and disadvantages associated with them, as described earlier. The following criteria should be used when selecting a method of temperature measurement for the tool tip:

- the predicted tool chip interface temperatures predicted from theory need to be verified experimentally;
- the method used must be able to detect temperature variations up to 1000 ^{o}C;
- the method chosen must not interfere with the machining process in any way;
- the method chosen must be able to produce a distribution of the temperature variation over the region under observation.

Using the above criteria helps identify the best method of measuring the tool tip temperature for this particular application. Determining tool tip temperature during air-cooling clearly identifies the imbedded thermocouple technique. The recorded temperatures should be as close as possible to the cutting edge, and must indicate the actual variations due to any change in cutting conditions (eg. cutting speeds, air-cooling being used). Preliminary experiments showed that the tool tip temperatures measured during cutting indicated all changes in operating conditions of the tool tip. Although the tool interface temperature is not measured directly, it is possible to

determine this temperature from the temperatures that are measured, and by recording the power used during cutting. Recording the actual temperatures at different positions on the tool tip in conjunction with measuring the power used during cutting, allowed the tool interface temperature to be calculated, as shown in Figure 5.21. This graph conformed closely to previous research by Friedman and Lenz [99] Figure 5.7, and showed that the temperatures measured a short distance from the tool interface would be much reduced.

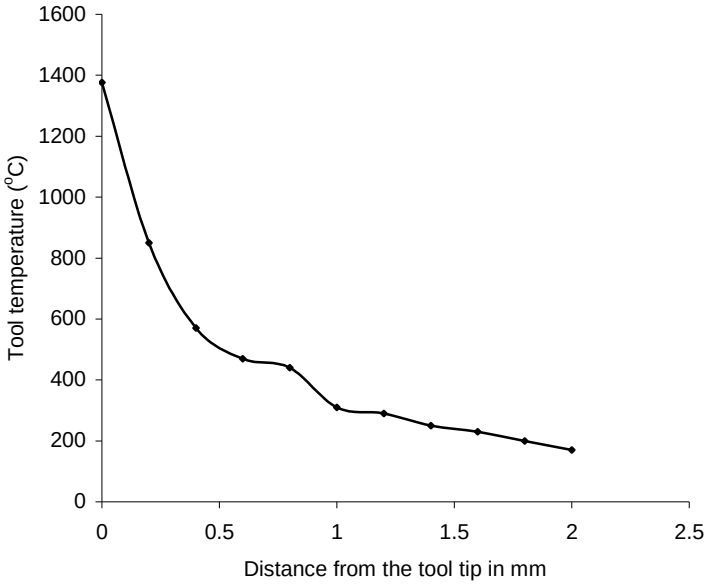

(for a cutting speed of 175 m/min and feed rate of 0.23 mm/rev)

Figure 5.21:Temperature distribution over the tool tip rake face.

However, temperatures obtained by Chao *et al.* [95] produced far higher temperatures as shown in Figure 5.3 at a compatible cutting speed and lower feed rate, and must bring to question the use of the photoconductive cell method used to measure the flank face.

For practical purposes it is impractical to position the thermocouple closer than 1mm to the tool interface, due to this weakening the tool tip to a point that no machining would be possible without the tool tip breaking. Therefore a compromise between tool tip strength (tool life) and measuring the temperature as close to the tool tip interface has to be made. Figure 5.22 shows the position of thermocouples in the tool

tip and illustrates the compromise that was made with respect to tool life and temperature measurement at the tool tip.

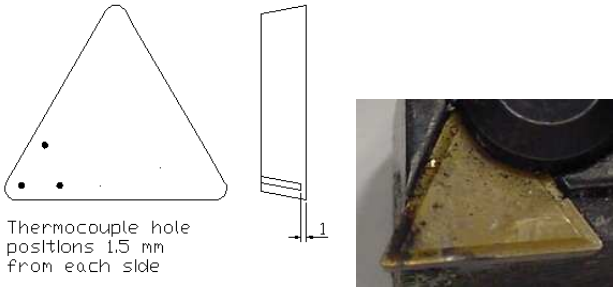

Figure 5.22: Position of thermocouples in tool tip.

Obviously, the temperatures that are measured during the metal cutting will not be as high as the tool interface temperature due to the position of the thermocouples. However, this compromise worked well as the tool tips had a reasonable tool life, and the temperatures recorded reacted to any changes to the machining conditions, as well as showing the effect of air-cooling when applied to the tool tip.

CHAPTER 6

AIR-COOLING OF TOOL INTERFACE

6.1 Overview Of Cooling Tool Cutting Zone

Research has shown that getting traditional liquid coolant to the tool interface is never achieved (as discussed in section 2.3.1), due to the movement of the chips rubbing over the top rake face. Potentially the penetration of cold air at the tool interface is superior due to the smaller molecular structure of a gas (air). The challenge for air-cooling is to obtain cutting temperatures at the cutting zone that are as close to - or better - than traditional wet cutting. Chapter 4 examined the theories of jet-impingement cooling and of the Ranque-Hilsch vortex tube. These theories are now applied to the metal cutting process to help establish an effective cooling system for the tool interface. Jet-impingement was selected first to provide air-cooling to the tool interface as this method has proven to have been effective in heat removal in many other applications. The Ranque-Hilsch vortex tube on the other hand has had limited practical application, and therefore provides the biggest challenge in obtaining the optimum air-cooling system. For both air-cooling systems a number of tool cutting tests are required to determine how effective they are compared to a traditional wet cooling method.

To determine the effectiveness of the air-cooling systems it is necessary to have a clear set maximum temperature and minimum temperature at which the tool cuts metal. Dry cutting will produce the upper temperature limit, while traditional wet cutting produces the minimum cutting temperature as shown in Figure 6.2. The positions of the imbedded thermocouples are shown in Figure 6.1, with the closest to the tool interface being measured by the thermocouple on channel 13 (Ch13).

The test procedures used were in accordance with ‘Tool Life Testing” with single-point turning tools ISO 3685: 1993(E). Effectiveness of the air-cooling system can be shown by measuring the tool tip temperatures during machining, or by examining the flank wear on the tool under an optical microscope.

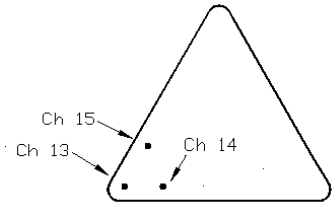

Figure 6.1: Thermocouples channel positions in tool tip.

The steady state cutting temperature for dry cutting is reached in approximately 10 seconds and for traditional wet cutting in approximately 5 seconds, as shown Figure 6.2.

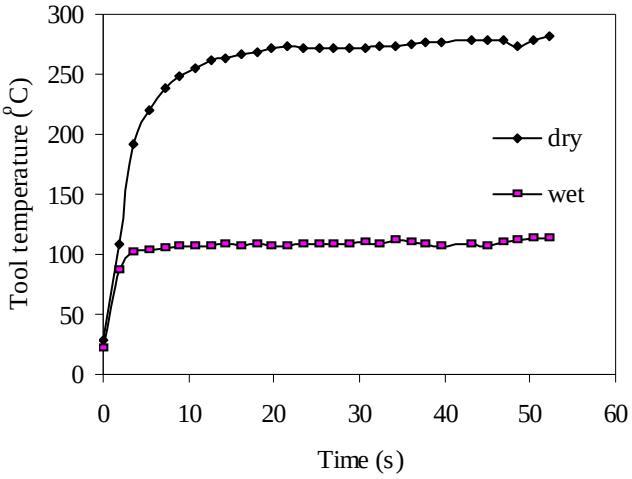

(For a cutting speed of 175 m/min, 0.23 mm/rev feed and 1 mm depth of cut.)

Figure 6.2: Temperature for wet and dry machining.

The resulting temperature difference between dry and wet cutting temperatures is found to be approximately 175 ^{o}C, indicating that air-cooling needs to be improved to remove this heat. The air-cooling performance of this process can be evaluated by determining the effect on tool life as found by Ay *et al*. [110] for the different air-cooling conditions, as the tool tip temperature is known.

6.2 Impingement Cooling During Metal Cutting

6.2.1 Experimental impingement configuration

Previous researchers have examined all of the most suitable nozzle diameters with respect to the air gap between the nozzle and the object. However, in the metal

cutting application there are other factors that have to be considered. For example, if the chosen nozzle diameter is too small it would be impossible to obtain the correct gap between the nozzle and the tool tip. If the nozzle diameter is too large then getting the correct gap between the nozzle and tool will also be impossible. The air jet must be positioned exactly at the tool tip. Basically there is a compromise between the theoretical ratio of the nozzle height and diameter to suit this application. The impingement cooling process performance during machining is determined in Section 6.2.3, and shows how the different parameters interrelate in cooling the tool tip. The impingement nozzle parameters are changed systematically as shown in Tables 6.1 to 6.4.

Table 6.1: Single jet nozzle

Jet exit diameter (mm)	Operating pressure (MPa)	Nozzle gap (mm)
1	0.6	1 to 12
1	0.8	1 to 12
1	1	1 to 12
2	0.6	1 to 12
2	0.8	1 to 12
2	1	1 to 12

Table 6.2: 1 mm Diameter multi- hole jet nozzle

Number of jet exits	Operating pressure (MPa)	Nozzle gap (mm)
4	0.8	1 to 12
4	1	1 to 12
8	0.8	1 to 12
8	1	1 to 12
16	0.8	1 to12
16	1	1 to 12

Table 6.3: Three jet nozzle

Jet exit diameter (mm)	Operating pressure (MPa)	Nozzle gap (mm)
2	0.8	1 to12
2	1	1 to 12

The three jet nozzles were positioned to cover the triangular tool tip fully during machining, similar to the position shown in Figure 6.1.

Table 6.4: 2 mm Diameter angled nozzle

Nozzle angle (deg.)	Operating pressure (MPa)	Nozzle gap (mm)
45	0.8	1 to 12
60	1	1 to 12
45	0.8	1 to12
60	1	1 to 12

The experimental test set up is illustrated in Figure 6.3 below:

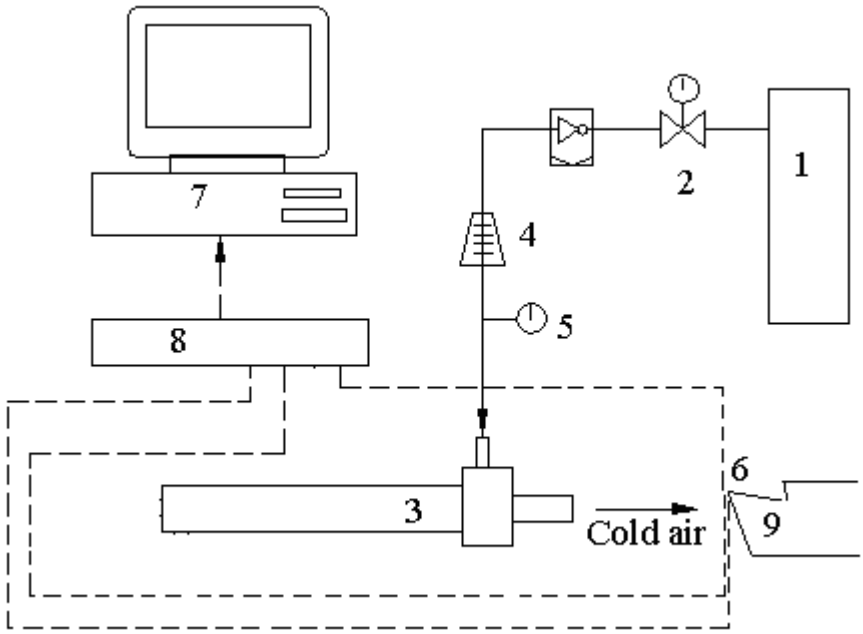

1. Supply of compressed air, 2. Control valve, 3. Impingement nozzle, 4. Flow meter, 5. Pressure gauge, 6. Thermocouples, 7. Computer, 8. Data logger, 9. Cutting tool.

Figure 6.3: Block diagram of impingement machining test apparatus

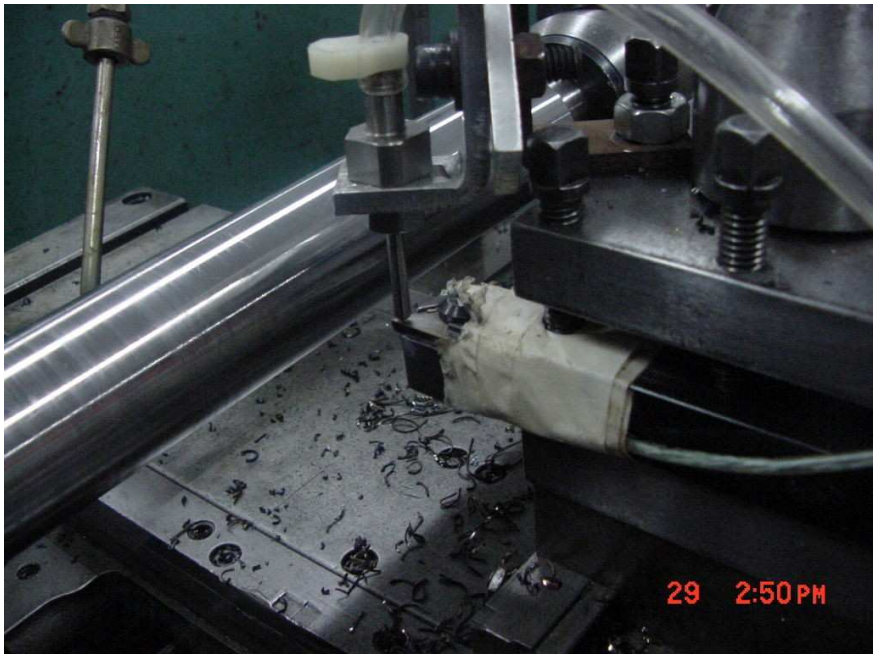

Figure 6.4: Adjustable Impingement nozzle holder

Each test parameter that is shown in Tables 6.1 to 6.4 involves a minimum of three machining tests for each set up to ensure validity of test results.

6.2.2 Impingement cooling tests

Air is directed onto the tool face as close to the tool interface as possible as shown by the arrow in Figure 6.5. It is known that the effectiveness of the air-cooling is improved by using jet-impinging jet Mao-Yu Wen *et al.*. How effective this will be in metal cutting as yet needs to be ascertained. A series of metal cutting tests were performed to determine how impingement air-cooling performed on cooling the tool tip. The most effective impingement cooling arrangement was established by changing jet parameters systematically as outlined in Appendix C, while keeping the cutting conditions constant throughout all the tests.

Previous researchers Jung-Yang San *et al.* [73] have examined the aspect of determining the most suitable jet diameter with respect to the air gap between the jet nozzle and a flat object. However, in this application there are other factors that have to be considered such as the position of the jet. Selection of the jet diameter is important, as it is usually impossible to obtain the correct gap between the jet and the tool tip with a small jet diameter.

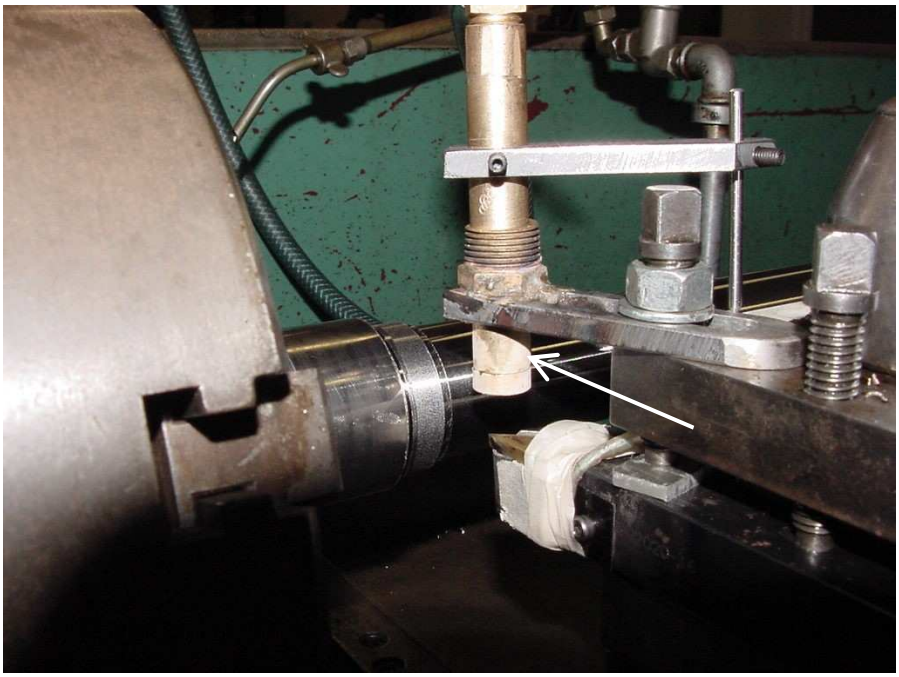

Figure 6.5: Adjustable jet-impinging jet holder.

If the diameter is large you may get the correct gap between the jet and tool, but you now cannot position the jet close to the tool tip. Basically there is a compromise between the theoretical ratio of the jet height and diameter to suit the machining application. This consideration of diameter and height has led to a jet exit diameter of 2 mm being selected for the tests, the exception being when a jet with multiple exit diameters was being tested.

Establishing a reliable method of setting the jet was essential due to the number of tests undertaken to determine the optimum supply of air pressure with respect to the gap between the tool tip and the impingement jet. This was simply achieved by sliding a height block between the tool and the nozzle jet as shown in Figure 6.6.

Figure 6.6: Height block inserted between tool tip and jet.

6.2.3 Tool tip temperature - impingement cooling

The effect of varying the jet gap, with the different supply pressures of 1 MPa, 0.8 MPa and 0.6 MPa, is shown in Figure 6.7 and 6.8, where it clearly shows that a jet height of 10 mm from the top face of the tool is the most effective cooling height. As the jet diameter is 2 mm the resulting optimum (diameter to jet gap) $\frac{G}{D}$ ratio is therefore 5 which is higher than the optimum $\frac{G}{D}$ ratio based on previous research of an impinging jet on a flat plate Lee *et al.* [113], Tong [114], proving that this previous theory may not be suitable for this machining application. A number of factors such as the shape of the surface of the tool or the effect of the rotating workpiece disturbing the air steam from the jet may have affected the performance of the impingement process.

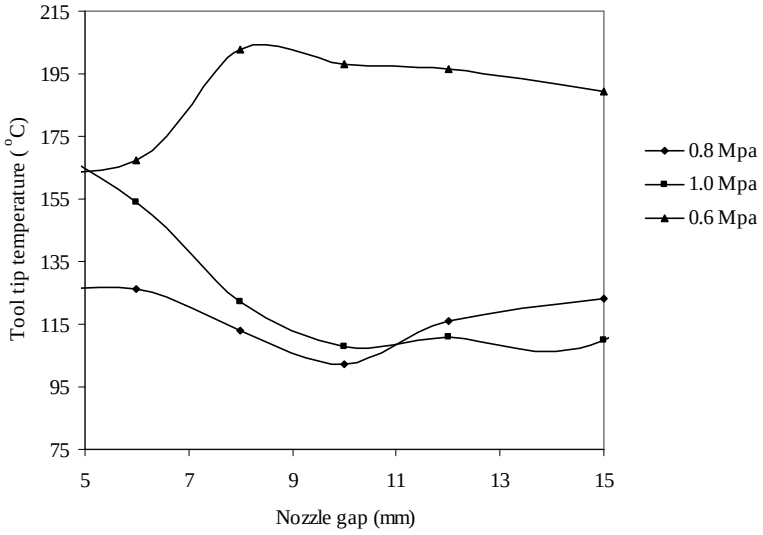

Figure 6.7: Jet optimum height from tool tip.

The temperatures of the three thermocouples in the tool tip showed the lowest temperature being recoded by channel 13 (Ch13), which is the position nearest to the tool tip, which indicates heat from the tool is being removed.

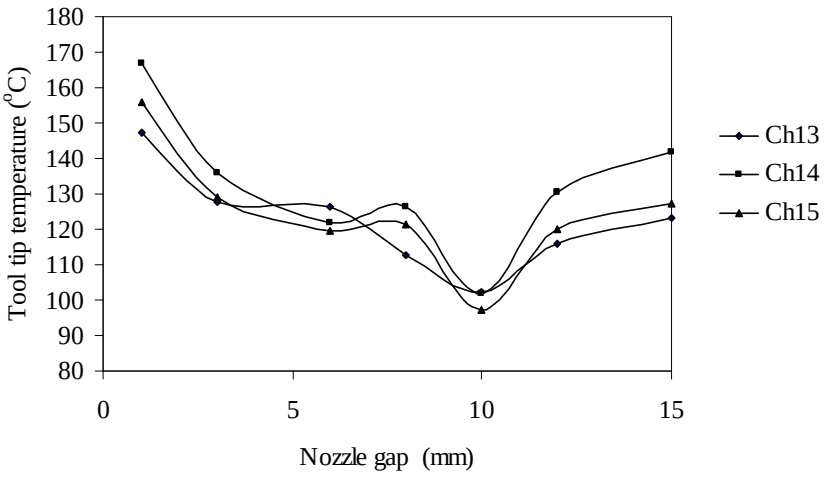

Figure 6.8:Temperatures recorded at the tool tip for a variety of air gaps at 0.8 MPa.

The results shown in Figure 6.9 when using a 2 mm diameter exit jet at 0.8 MPa illustrates that this method of air-cooling was able to cool the tool tip close to the conventional wet cooling cutting temperature (100 ^{o}C) as shown in Figure 6.2.

However, although this method is capable of cooling the tool tip, it was found that after a number of cutting tests the temperature in the workpiece became extremely hot. This therefore indicates that additional air-cooling needs to be applied to the workpiece to prevent dimensional inaccuracies occurring. Figure 6.7 showed that there was no real benefit in increasing the pressure to 1 MPa from 0.8 MPa or increasing the air gap.

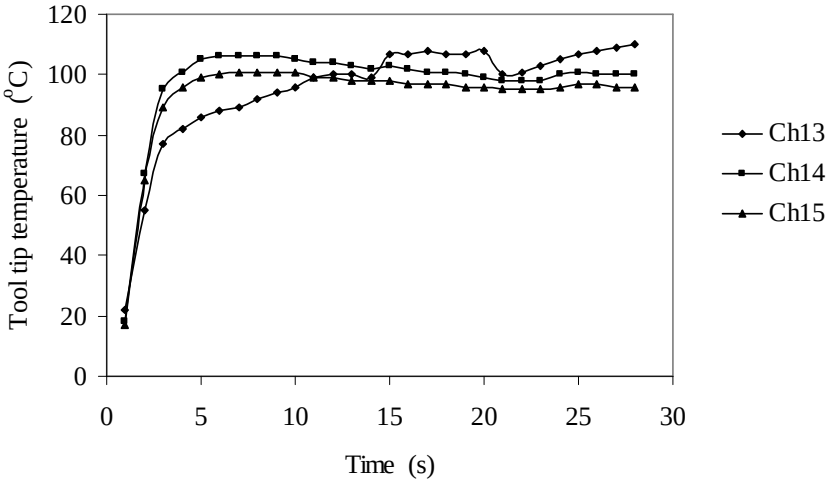

Figure 6.9: Tool tip temperatures at 0.8 MPa with an air gap of 10 mm.

The result of a cutting test at 1 MPa and 10 mm air gap is shown in Figure 6.10 which interestingly shows that the temperature channel 13 (Ch13) closest to the tool interface has increased, and the temperature further away from the tool tip has slightly decreased. This implies that air is not penetrating as close to the tool interface during the machining process, and the temperatures recoded at channel 14 (Ch14) and channel 15 (Ch15) were being cooled more efficiently due to the higher air stream velocity. The greater the fluid velocity the better the heat transfer due to the thinner boundary layer across the surface at channel 14 (Ch14) and channel 15 (Ch15), which was not occurring closer to the tool interface.

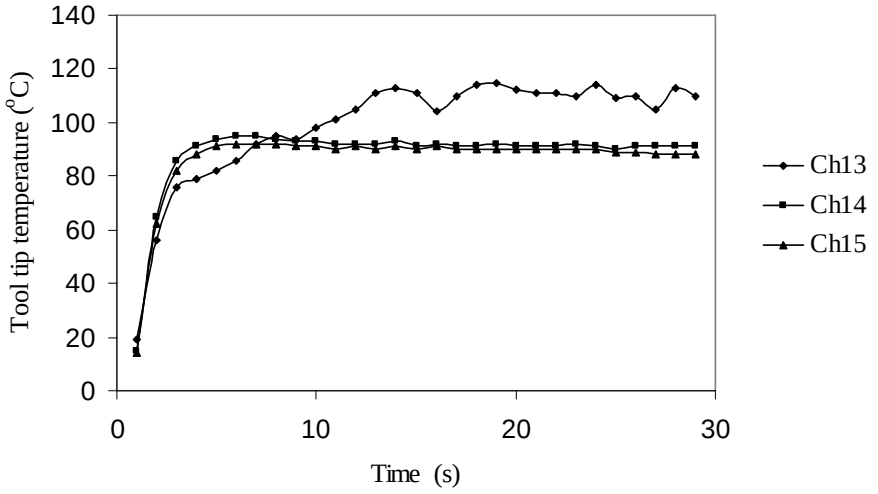

Figure 6.10: Tool tip temperatures at 1 MPa with an air gap of 10 mm.

This trend is also noted when the air gap is increased to 12 mm at 1 MPa as shown in Figure 6.11. It is well known that the flank area of the tool suffers considerable wear during machining; it suggests that the inclusion of an additional jet directed at the flank face will help reduce the temperature. The following tests were carried out with a jet directed at the flank face of the tool: the results of these tests are shown on Figure 6.12.

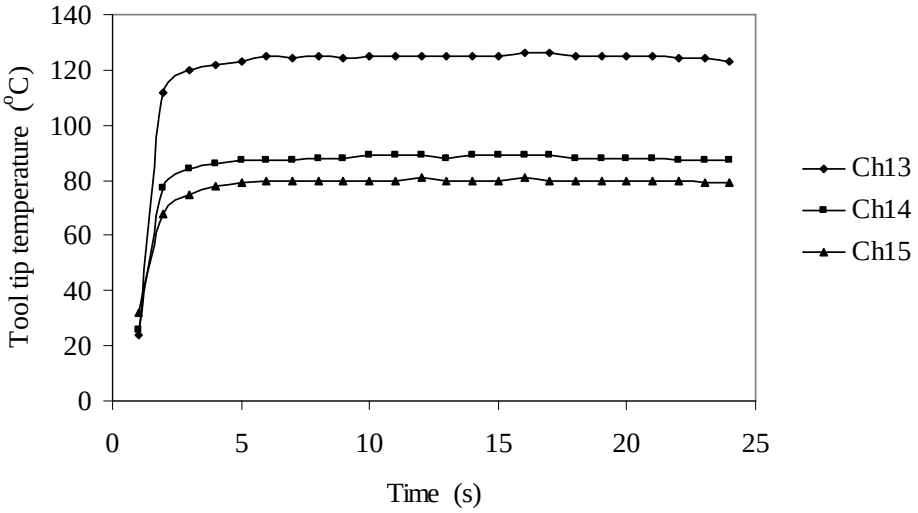

Figure 6.11: Tool tip temperatures at 1 MPa with an air gap of 12 mm.

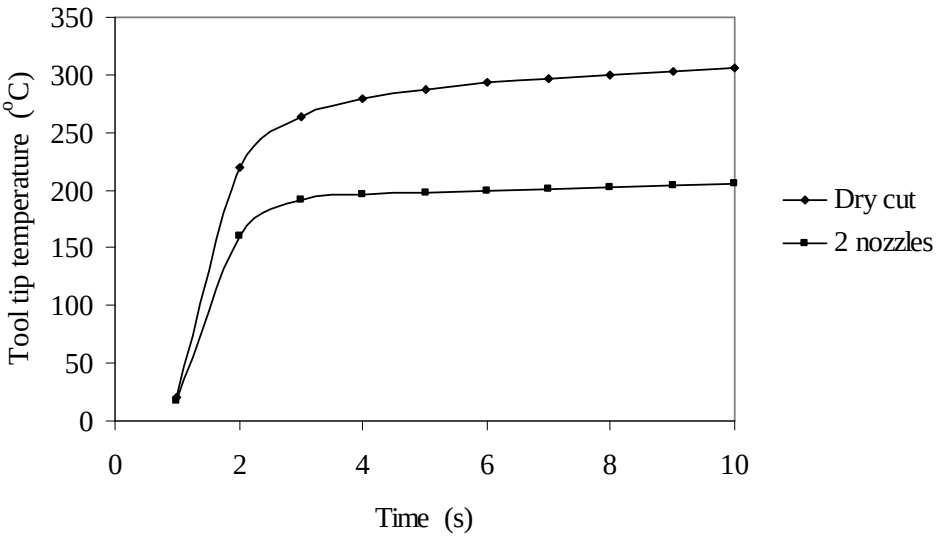

Figure 6.12: Second jet directed at flank face during machining.

Unfortunately, the results were less than promising as the jet air streams interfered with the impingement process of each of the jets. Other test configurations involved tilting the impingement jet at an angle to the top rake face to improve clearance between the workpiece and the jet. Figure 6.13 shows a jet after use where the side has worn away. The position of the jet is determined by:

- tool cutting interface;
- the diameter of the workpiece;
- and the optimum air gap.

Figure 6.13: Worn jet due to being unable to obtain correct air gap without rubbing the workpiece.

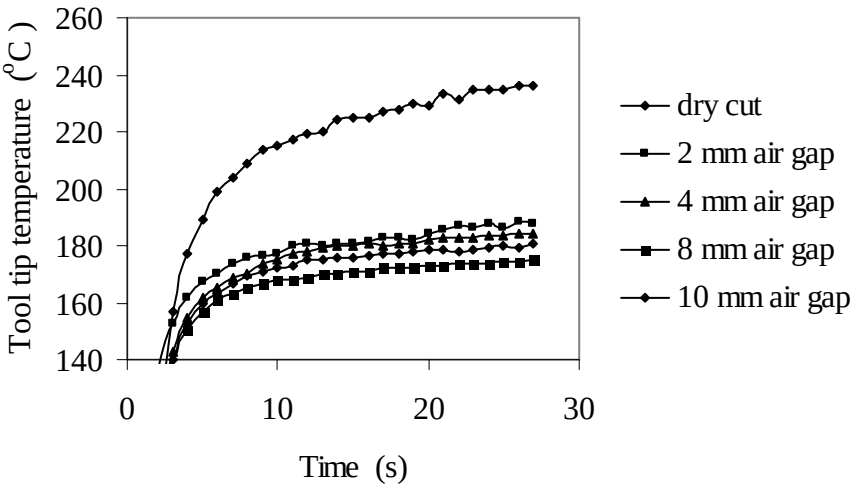

Figure 6.14: Jet angled at 45 ^{o} to the rake face at a pressure of 0.8 MPa.

Figure 6.14 indicates that the cooling efficiency of the air jet angled at 45 ^{o} to the rake face of the tool has been reduced, and also the air gap had little effect on the performance of the cooling jet. The same is also noted for the jet angled at 60 ^{o} as shown in Figure 6.15. This is what one would expect to happen due to the loss of the impingement process which is gained from using a horizontal jet. Figure 6.14 and 6.15 show that there is now no beneficial effect from the surface boundary layer breaking down and promoting a better heat transfer to the air, as both temperatures are approximately the same indicating that the tool was only being cooled by the air passing over the tool.

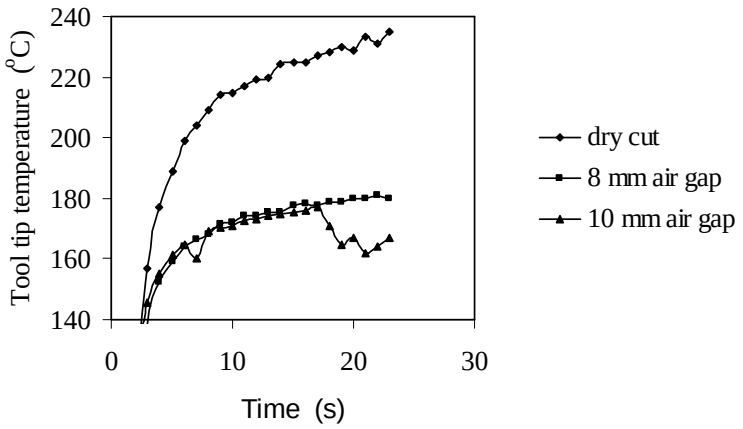

Figure 6.15: Jet angled at 60 ^{o} to the rake face at a pressure of 0.8 MPa.

Previous tests using a one exit jet, as illustrated in Figure 6.9, have demonstrated that there is an enhanced heat transfer to the air by using an impingement jet. It is then logical to think that increasing the number of exit jets directed on to the top rake face Figure 6.16 to 6.19 show multi-hole jets being used to cool the tool tip. The effectiveness of jet-to-jet spacing for confined air jets vertically impinging on a flat plate was investigated by Jung-Yang San *et. al.* [115]. As with a single exit jet it is necessary to determine the correct air gap for the jet, how many exit holes there should be, and at what diameter the exit hole should be for optimum cooling. Figure 6.16 shows the results from a four exit jet each of 1 mm diameter. Temperatures recorded are compared with the single jet in Figures 6.9 and 6.10, which has the same cross sectional area as the four exit jet.

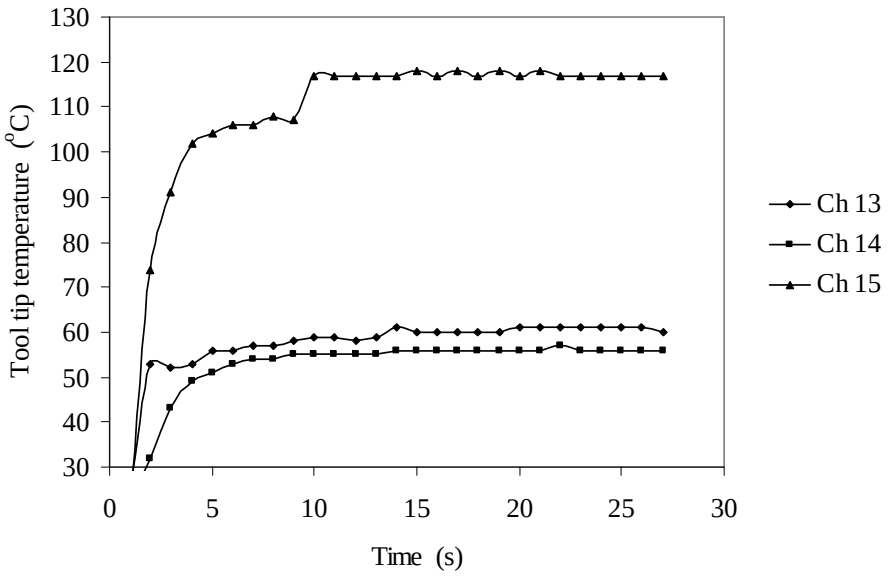

Figure 6.16: Jet with 4, 1 mm nozzles.

The interesting points to note here are that the thermocouple closest to the tool tip channel 13 (Ch13) recorded a slightly higher temperature with the four-jet than the one jet. The temperature recorded for the thermocouples on channel 14 (Ch14) and channel 15 (Ch15) were otherwise significantly reduced. This indicated that there was an increased footprint being generated by this jet due to the increased number of impingement air streams. Even though it showed that the tool interface temperature was slightly higher, the larger footprint helped with positioning the jet at the tool tip.

It was found that if the position of the jet was out by a small amount the effectiveness of cooling the tool tip interface was lost.

Further reduction in temperatures was achieved by increasing the number of jet exits to eight. Figure 6.17 shows the improved cooling effect at the tool tip, with channel 14 (Ch14) recording only 45 ^{o}C this being due to the cooling air being unimpeded. The temperatures recorded for all three thermocouples indicated a tool temperature less than those obtained for traditional coolant as shown on Figure 6.2.

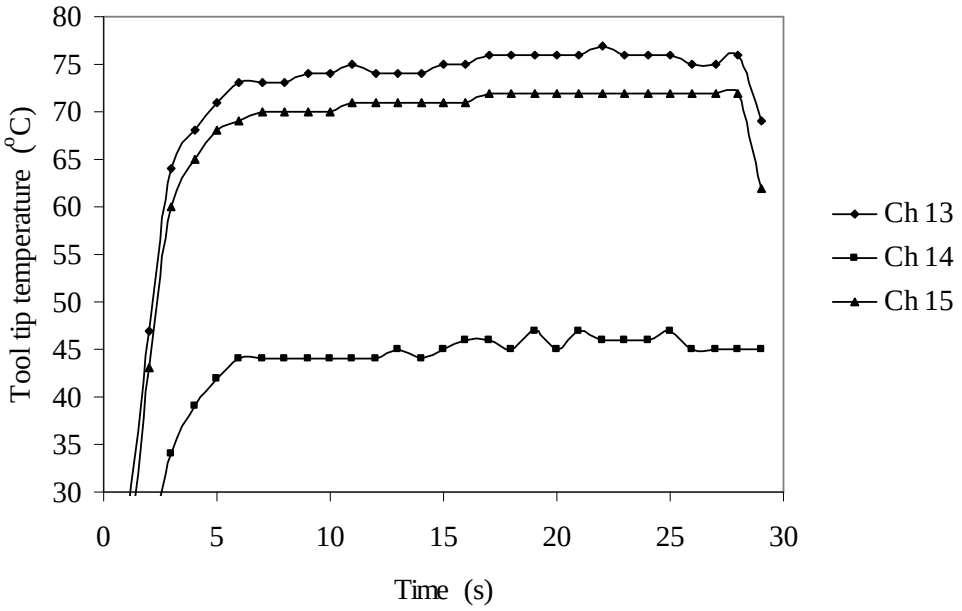

Figure 6.17: Jet with 8, 1 mm nozzles.

When the number of exit holes in the jet was increased to sixteen it was interesting to note that the thermocouple on channel 15 (Ch15) recoded temperatures below zero degrees, and that the temperatures for the other thermocouples were approximately 10 ^{o}C higher than the four exit jet Figure 6.17.

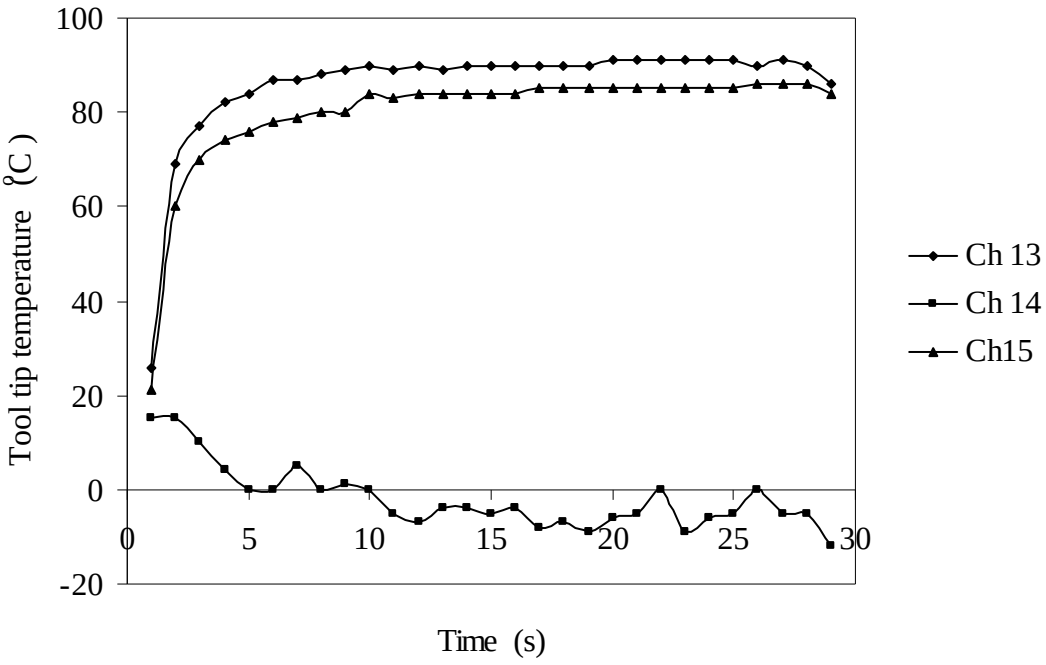

Figure 6.18: Jet with 16, 1 mm nozzles.

The trend for both of these jets is the same, in that the temperature of channel 15 (Ch15) was the lowest, and that the temperatures recorded for the other two thermocouples were quite close to each other. The reason for this improved temperature dissipation into the air can be put down to the increased footprint that is generated from the multi-exit holes used. Another advantage of the use of this multi-hole jet during machining is that the air stream is penetrating nearer to the tool tip interface. During observation of the metal cutting test it was noticed that the chips were breaking off in small regular chips which were then blown away from the cutting zone. Perhaps due to the cuttings being small and being swiftly removed from the cutting zone allowed better access of the air to the tool tip. However it must be said that any change to the cutting conditions will effect the type of chip produced during machining, as explained in Chapter 2.

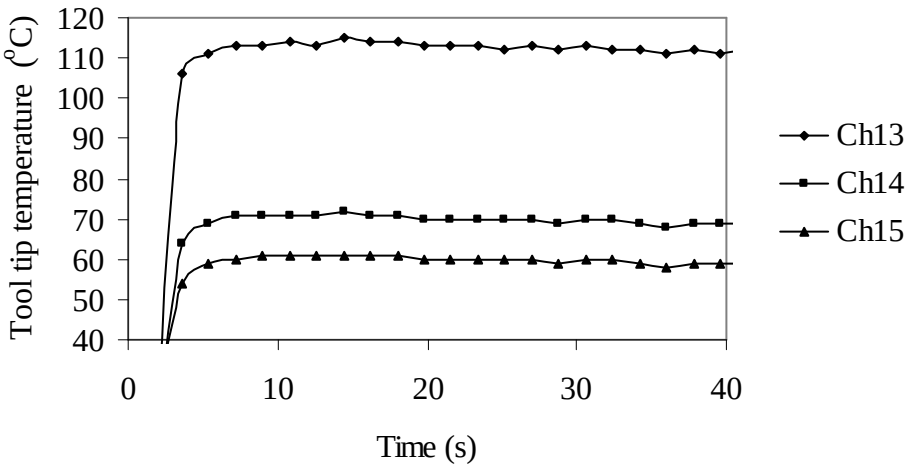

Figure 6.19: Three 2 mm diameter jets.

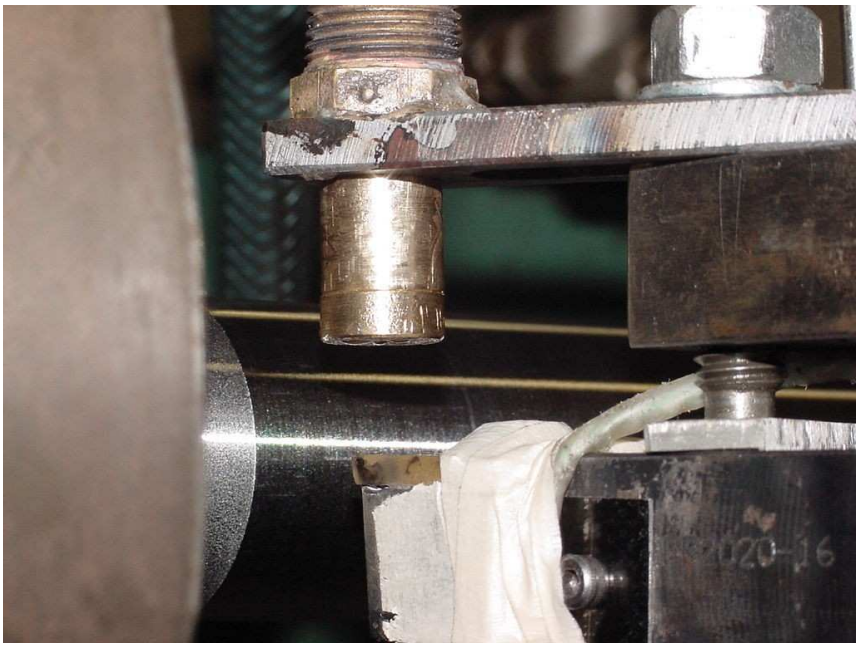

Figure 6.20: Multi-hole impinging jet nozzle.

The position of the jet relative to the tool tip is positioned to provide the maximum coverage of the air foot print during machining as shown in Figure 6.20.

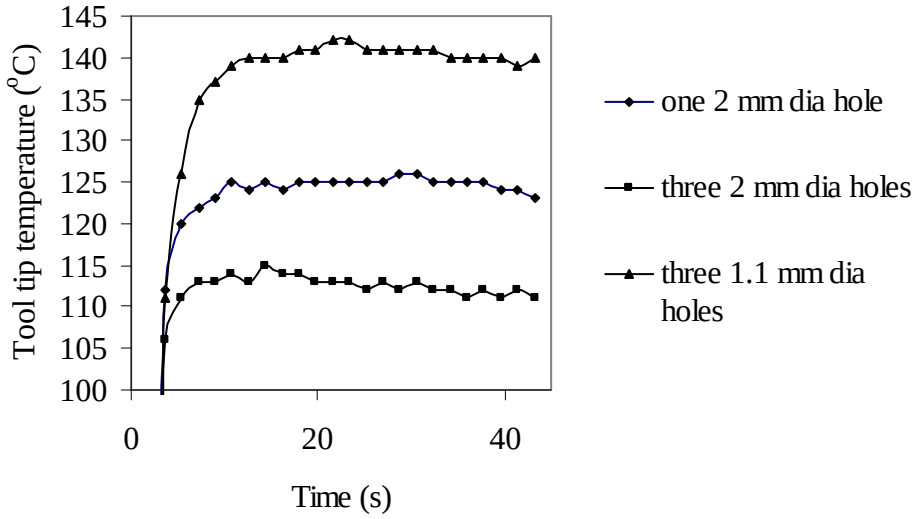

Figure 6.21: Tool temperatures for thermocouple on channel 13 (Ch13).

Figure 6.21 clearly showed that the three 2 mm diameter hole jet produced the lowest tool tip temperature closest to the tool interface during machining. The volume of air used during this test was 849 SLPM at the maximum test pressure (1MPa). This is not an extremely large supply of compressed air as a typical two-stage, two-cylinder air compressor can provide 1050 SLPM at a maximum working pressure of 1MPa with a Motor load of 7.5 kW. This would be relatively cheap to supply as can be calculated from equation 6.1. The cost of compressed air for one hour was calculated to be (AU) $1 using this compressor.

$$\text{Cost (AU) \$} = \frac{(MLxOHxCxTxFL)}{ME} \tag{6.1}$$

where ML = Motor full load in kW

OH = Number of operating hours

C = Cost per kWh

T = % of time running at this operating level

FL = % of full-load at this operating level

ME = Motor efficiency at this level

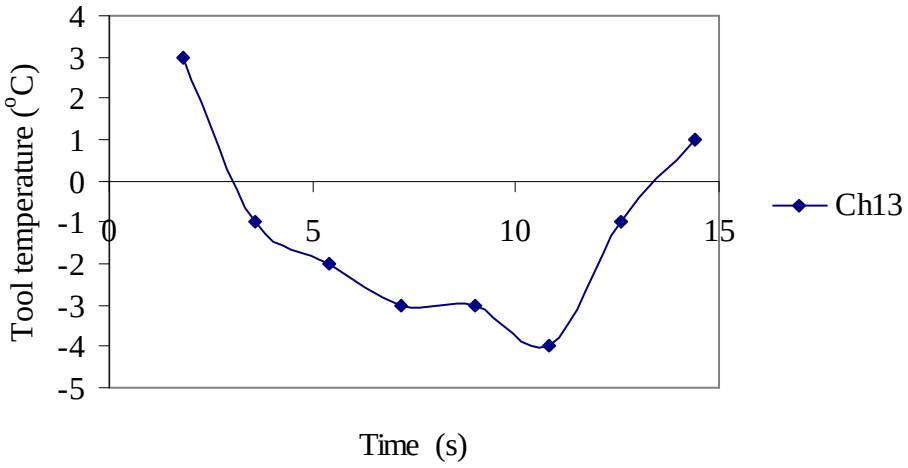

Figure 6.22: Tool temperature before cutting using three – 2 mm diameter jet.

Figure 6.23: Frost on impingement jet nozzle before machining.

The graph in Figure 6.22 was obtained before any machining had taken place and clearly indicates the effectiveness of the impingement cooling of the tool tip. Figure 6.23 shows a build up of frost on the jet nozzle. In practice, however, the efficiency of the cooling of the tool tip is reduced due to the cutting action during machining.

6.3 Vortex Tube Cooling During Metal Cutting

6.3.1 Tool tip temperature during vortex tube air-cooling

Unlike the impingement cooling process there is no difference to the cooling effect by adjusting the distance that the cold tube nozzle is from the tool tip. The nozzle does not need to be perpendicular to the rake face - unlike the impingement jet

nozzle - to be effective. Although, the closer the cold tube nozzle jet is to the tool face, the less time there is for the surrounding ambient temperature to begin to affect the cold stream of air. Figure 6.24 shows the vortex tube directing the cold airflow onto the tool face as close as the machining restraints will allow. A series of tests involving the various cutting parameters and positioning of the vortex tube were performed to determine their effects on the cooling performance. The parameters were changed systematically as outlined in Appendix D while the machining conditions were kept constant throughout the tests.

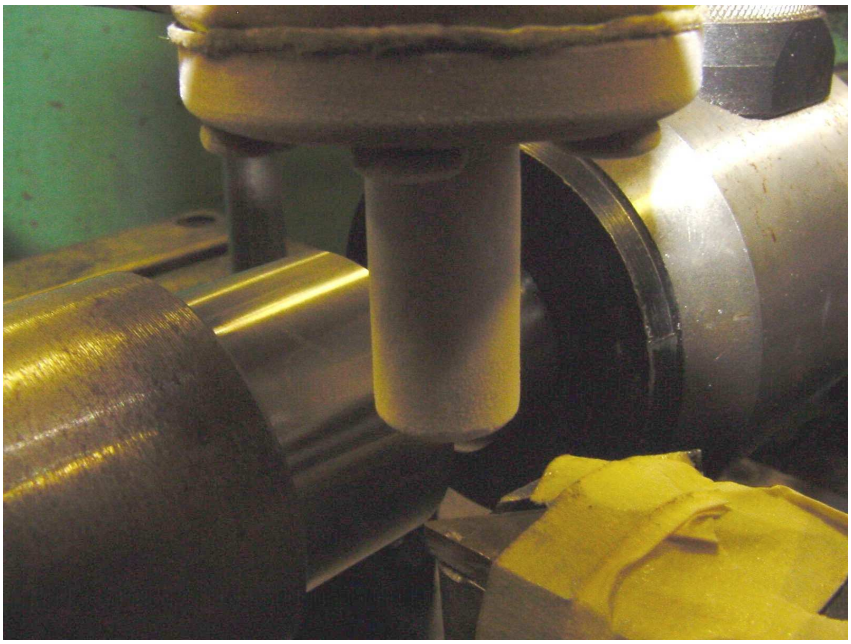

Figure 6.24: Vortex tube being positioned with respect to machining restraints.

The temperatures shown in Figure 6.25 were recorded at the tool tip during adjustment of the conical valve on the vortex tube at an inlet pressure of 0.8 MPa. Setting the valve normally takes about thirty seconds to achieve the optimum cold exit air. Having obtained the minimum air temperature, machining can commence. During this time the cold air had already started to cool the tool tip down, with two of the thermocouples recording temperatures of approximately –5 ^{o}C.

Reducing the inlet air pressure to 0.4 MPa the cold exit air temperature was approximately -15 ^{o}C, which correspondingly reduces the tool tip temperature down

to approximately -3 ^{o}C in double the time achieve by 0.8 MPa. The time factor is important in cooling the tool tip, as the rise in temperature during machining is extremely fast. It is therefore imperative to be able to dissipate the generated heat in the tool tip as quickly as possible.

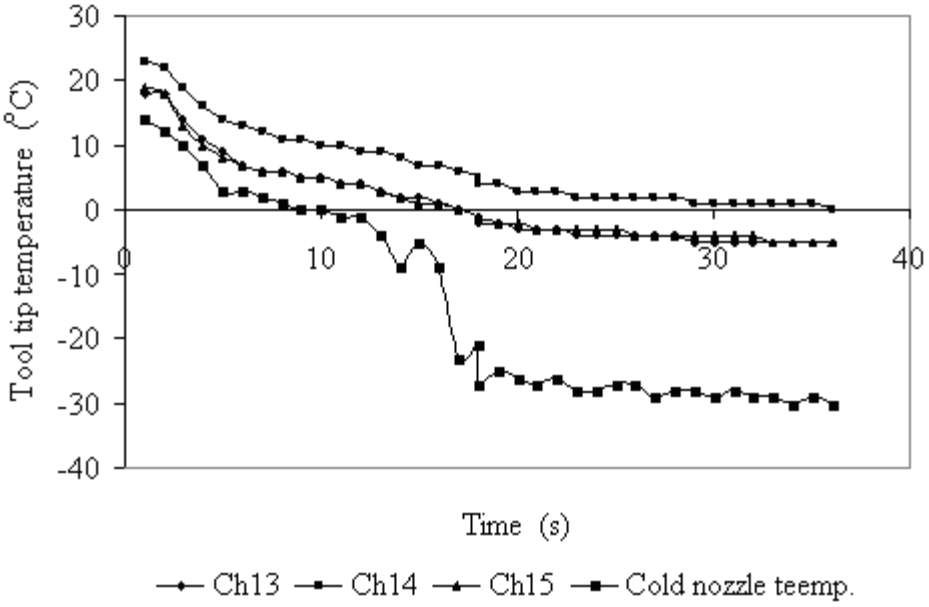

The vortex tube used a 3 mm diameter orifice plate at a pressure of 0.8 MPa

Figure 6.25: Tool tip temperatures before machining.

When the vortex exit air has reached approximately -30 ^{o}C, machining is commenced. As indicated by the rise in the tool tip temperatures, the tip rises to a steady state temperature of 60 ^{o}C channel 13 (Ch13) as shown in Figure 6.26. The temperature drop at the end indicates the point when the feed is stopped with no more chips being generated. Allowing the cooling air to flow unimpeded across the tool tip gives a better heat dissipation from the tool reducing the temperature in the tool rapidly.

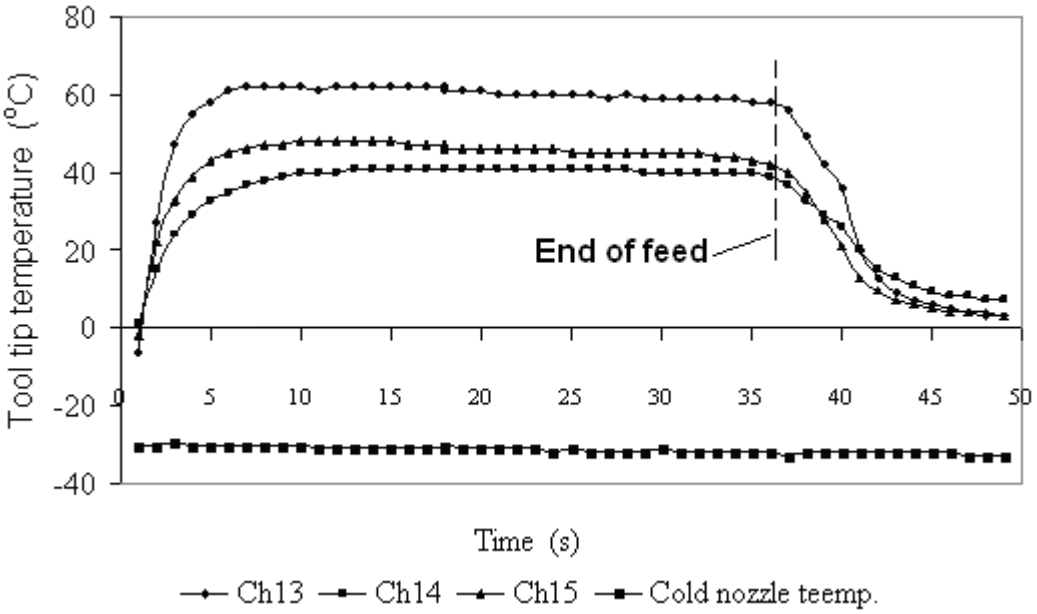

Figure 6.26: The graph shows the tool tip temperatures during machining, and after the tool feed has stoped cutting.

Figure 6.27 illustrates that a steady state temperature is reached in the tool tip in approximately 10 seconds during machining when being cooled by the vortex tube. However, it is noticeable that there is still a large temperature difference between the temperature closest to the tool interface channel 13 (Ch13), and that of the temperatures further from the tool interface channel 14 (Ch14) and channel 15 (Ch15). The inability of the air to penetrate close to the tool interface is undoubtedly due to the cold exit jet needing to be positioned away from the cutting zone due to the operating requirements. This is providing the cooled air closer to the tool interface would improve the accessibility of the air to the cutting zone, and would therefore improve further the heat dissipation at the tool tip. This challenge of improving the cold air delivery to the tool tip can be achieved by combining the cold air generated by the vortex tube with an air jet being incorporated as part of a chip breaker as shown in Figure 6.30. Even without this improved jet the reduction in temperature between dry machining and the air cooled temperature is extremely effective, and proves the case for air-cooling as shown in Figure 6.28. Appendix E gives an example of the data recorded during the tool cutting tests.

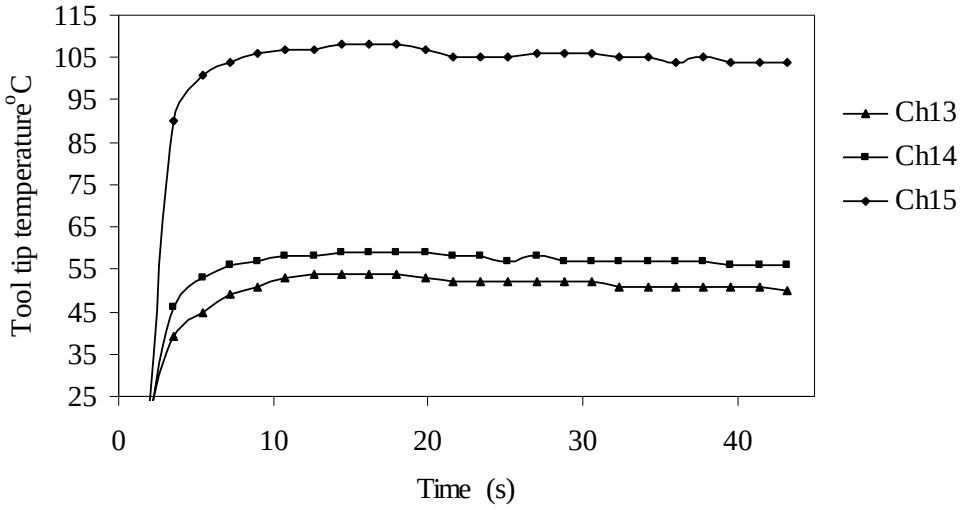

The vortex tube used a 4.5 mm diameter orifice plate at a pressure of 0.8 MPa.

Figure 6.27: Temperatures recoded at the tool tip during machining.

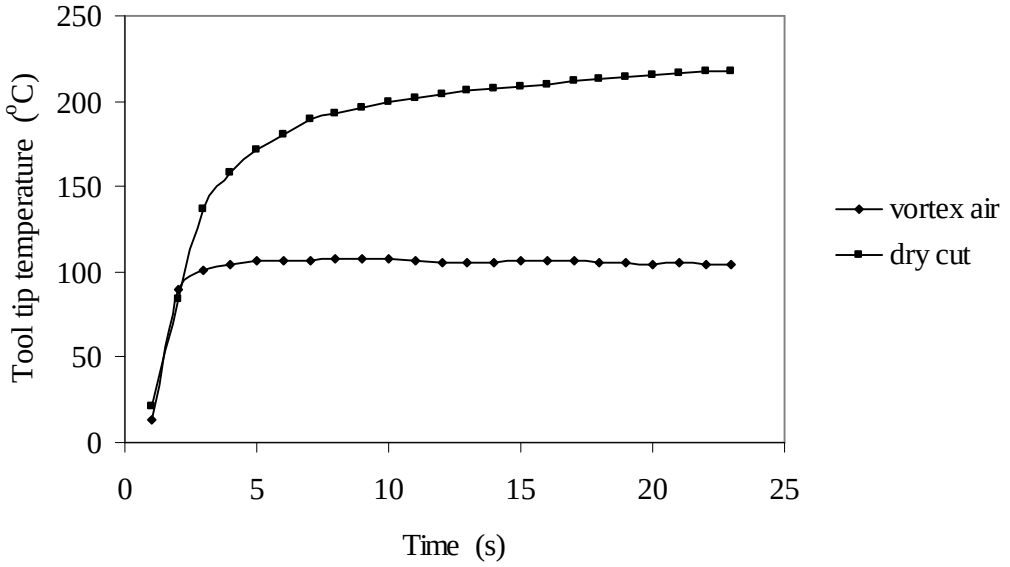

Figure 6.28: Temperatures recoded at the tool tip for dry and air-cooling.

Figure 6.29 illustrates the relationship between the hot air and the cold air generation of the vortex tube. From Chapter 4 experimental analysis of vortex tube design, it shows that the length of the hot tube has an important effect on the energy separation in the vortex tube, due to the air inner flow transfer of energy to the outer airflow. However, the vortex tube used in that tool test did not achieve the optimum

temperature difference between the hot and cold air exit. The optimum hot tube length was not used due to it being unmanageable and impractical to use on the lathe. The compromise of using a shorter vortex tube still proved to be effective as it was capable of producing cold air at -30 ^{o}C as shown on Figure 6.26.

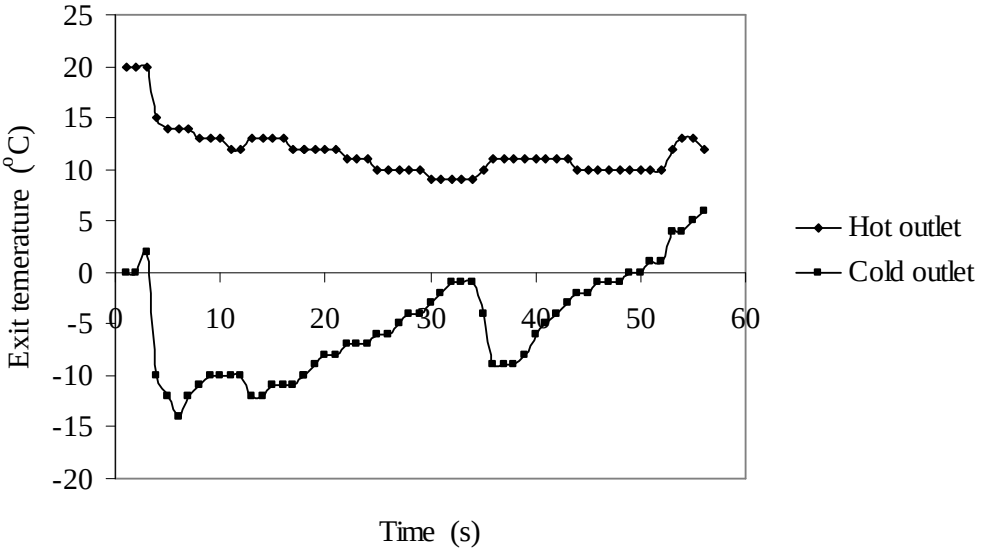

Figure 6.29: Air exit temperatures of hot and cold exit of the vortex tube.

Figure 6.30 showed that the vortex tube used in these tests was able to generate very cold air at the exit of the cold jet. A temperature of -55 ^{o}C was obtained by using an inlet pressure 1MPa to the vortex generator.

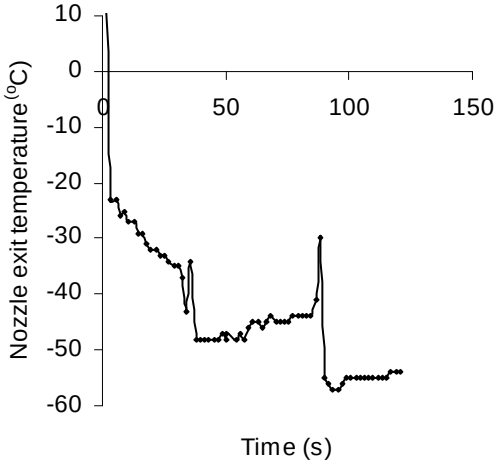

Figure 6.30: Vortex tube minimum air exit temperature.

6.3.2 Chip breaker air jet cooling

The effectiveness of air-cooling can be further improved by directing the cooled air more precisely at the tool interface during machining. To achieve this difficult task it is thought that combining an air jet nozzle, as part of a tool chip breaker, with an additional jet directing the air towards the flank face could be a possible solution to this challenge. Figure 6.31 shows the internal air channels to the tool interface jet, and Figure 6.32 & 6.33 shows the prototype lathe cutting tool directing air along the tool top rake face and flank face during machining. The cold air is supplied from the integral tool and vortex tube arrangement as shown in Figure 6.34 & 6.35.

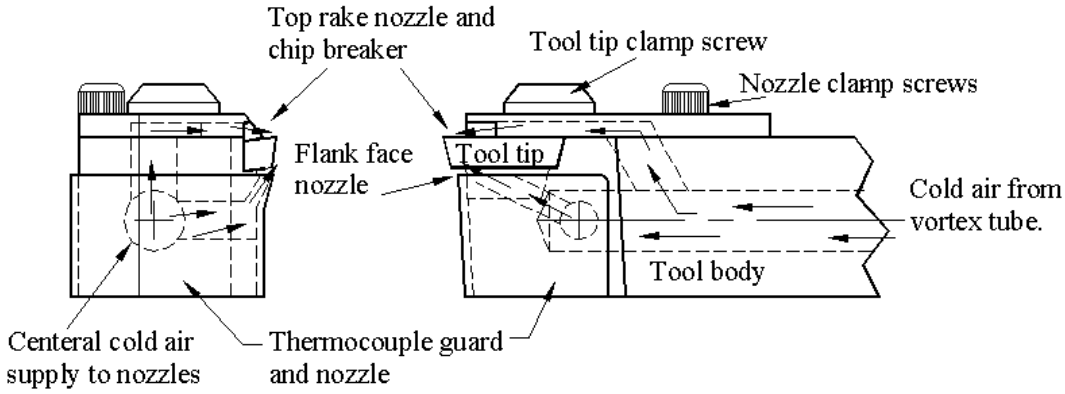

Figure 6.31: Lathe cutting tool and combined air jets and chip breaker drawing.

Figure 6.32: Top rake face air and flank face air jets.

The arrows in Figure 6.32 show the two air jets directing the cold air towards the cutting zone. In addition to the cooling effect of the air is the advantage of blowing the cuttings away from the cutting zone as can be seen from Figure 6.33. As this was

a prototype tool an additional front metal guard was employed to protect the thermocouples during machining. Close examination of the cutting process shows that the air stream is being directed underneath the chip as can be seen in Figure 6.33 promoting a better heat dissipation from the tool-cutting zone.

At a feed rate of 0.23 mm/rev and 1 mm depth of cut.
(Air being directed along top rake face and underneath the chip)

Figure 6.33: Orthogonal machining using a chip breaker incorporating air jets.

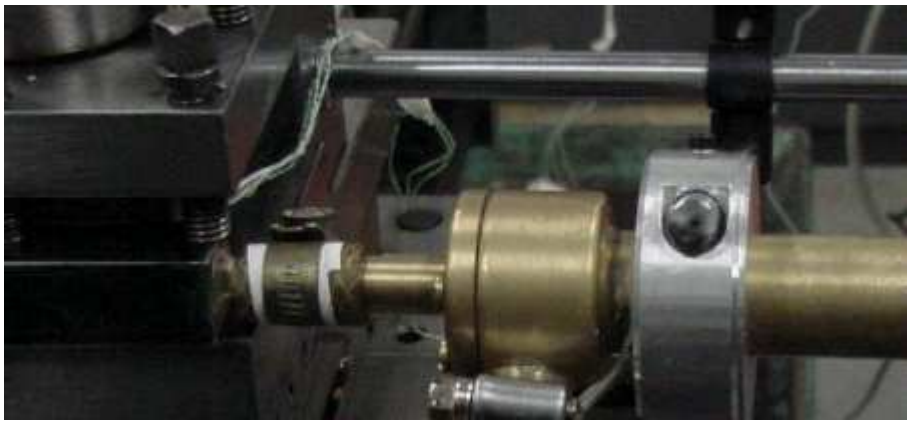

Figure 6.34: Vortex tube integral with tool body.

Figure 6.35: Continuous dark blue chip shown being produced during machining with the integral vortex tube and tool.

The temperatures recorded at the jets during machining proved to be disappointing for this prototype tool as the air never got lower than 2 ^{o}C, with the resulting tool tip temperatures during cutting being recorded hotter. Obviously, the combination of the vortex tube, lathe tool and jets was not working in this configuration. From theory and previous testing of the vortex tube the air temperature leaving the rake jet never obtained its normal cold temperature. To determine what the temperature should be in the tool body, thermocouples are inserted along an 8 mm diameter tube as shown in Figure 6.36 to record the temperatures along the tube. Being the same length and diameter that was used in the prototype tool this should measure what the temperatures should be inside the tool and as it exits the jet. The results from this test showed that the air stream leaving the jet should be approximately –16 ^{o}C. This temperature implies that the vortex cooling effect is breaking down in the prototype tool. Examination of the prototype tool shows that the jet exit area was not large enough, causing a back-pressure in the vortex generator. To improve the performance of the prototype tool the volume flow rate needs to be increased to remove the backpressure inside the cold vortex tube which is stopping the vortex cooling effect. This was achieved by increasing the size of the rake face air jet.

However, the top rake jet exit area needs to be within the physical restraints of the tool and the size should avoids chips being tangled with the jet.

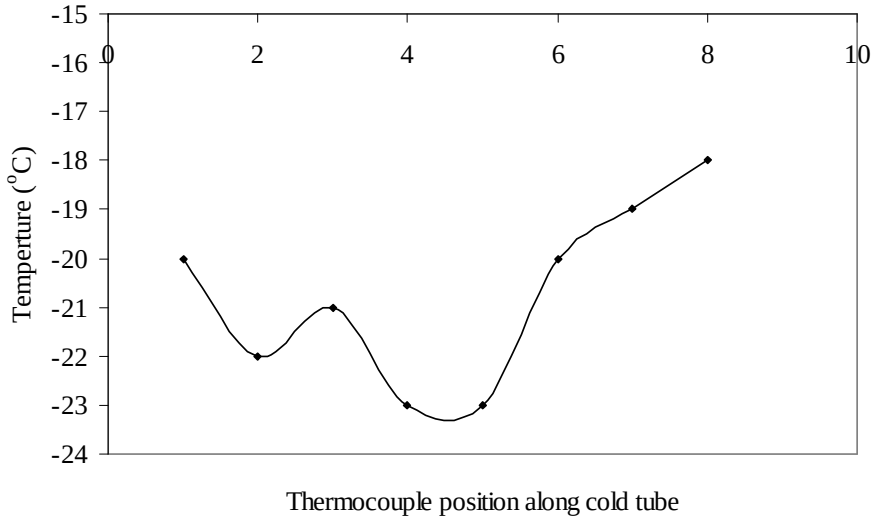

Figure 6.36: Temperatures distribution along an 8 mm diameter vortex cold exit tube.

A second prototype tool implements the increased size of top rake air jet and flank face air jet as shown in Figure 6.37. The combined cross-sectional area of the air jets must not be less than the area of the exit diameter from the vortex tube to ensure maximum air-cooling. Increasing the size of flank face jet was the most convenient way to achieve the increased jet exit area due to the physical restraints of the tool. This increased jet exit area produced the desired result, in that the recorded temperature of the air at the exits has been reduced to -6 ^{0}C as shown in Figure 6.39. Although when this temperature is compared with the temperatures recorded in Figure 6.36, it proves that there are still some improvements to be made to the combined vortex tube and tool.

Figure 6.37: Prototype tool showing increased flank face jet.

The practicability of using this tool is somewhat limited in this form due to its inability to be able to machined up to a shoulder and limited depth of cut. However, the tool did prove the benefits of providing directed cold air at the tool interface during machining.

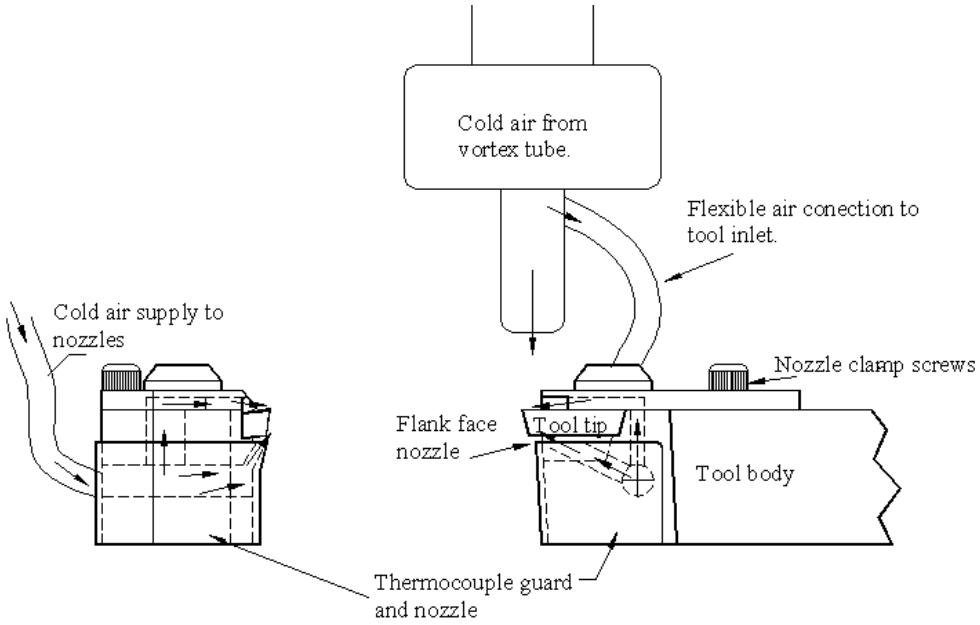

Figure 6.38: Cold air stream delivered at flank face and top rake face.

Another approach to ensure that there is no backpressure into the vortex tube is by allowing the cold air stream from the vortex to be split. The larger volume of cold air

will be directed from the vortex jet onto the tool tip as shown in Figure 6.38, with a smaller amount of cold air being delivered to the flank face of the tool.

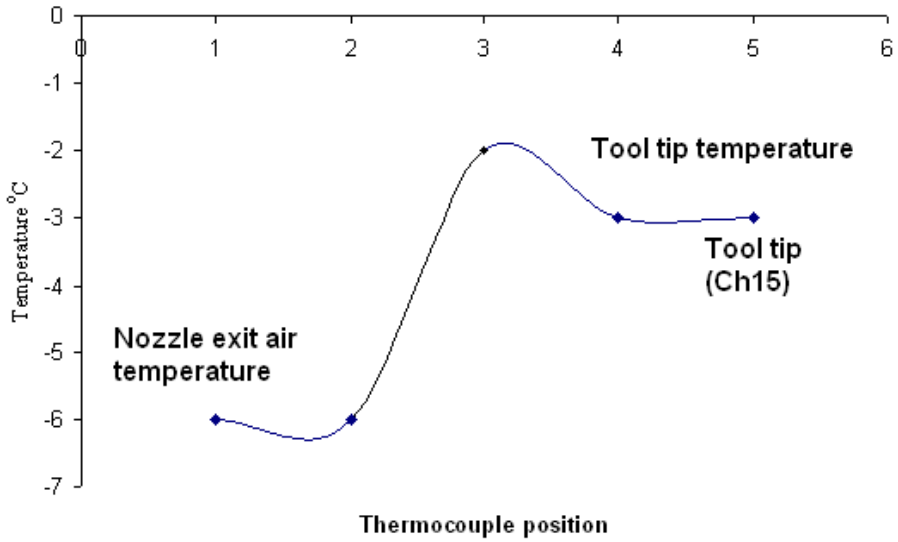

Figure 6.39: Temperature produced by the second prototype tool before machining takes place.

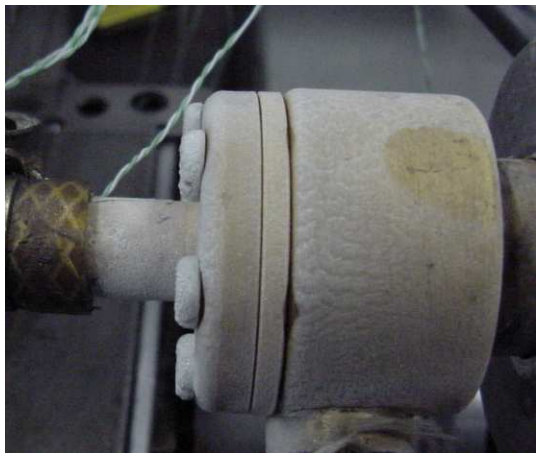

Figure 6.40: Frost on the outside of the cold tube.

The temperature that was recorded for the tool tip using the chip breaker and flank jet is similar in value to what was achieved by the previous methods of air-cooling as shown by Figures 6.22 and 6.25. However, the advantage of the chip breaker and flank jet is that the air is focused directly on to the areas of the tool that generate the most heat and where maximum wear takes place.

6.4 Tool Life

6.4.1 Effect of air-cooling on tool life

In Chapter 2 it is clearly shown that all the wear mechanisms increased at elevated temperatures, reducing the tool life. The previous sections illustrated that applying cold air to the tool tip is capable of reducing the temperature at the tool tip enabling the tool tip to have a longer tool life. The effectiveness of the air-cooled system can be shown when a comparison is made between the wear for a dry cut and an air-cooled cut for one minute and seven minutes of machining. Figure 6.41 to 6.44 shows the flank wear as seen under a microscope with a 63 optical magnification setting.

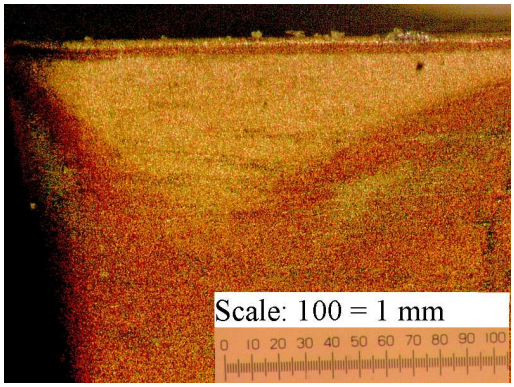

At a cutting speed of 190 m/min and feed rate of 0.23 mm/rev with a 2 mm depth of cut.

Figure 6.41: Picture showing flank wear of a dry cut after 1 minute of machining.

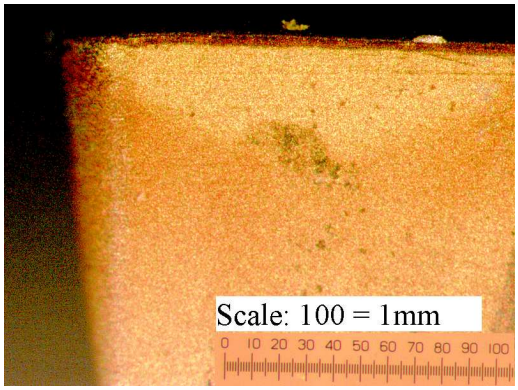

At a cutting speed of 190 m/min and feed rate of 0.23 mm/rev with a 2 mm depth of cut.

Figure 6.42: Picture showing flank wear of an air-cooled cut after 1 minute of machining.

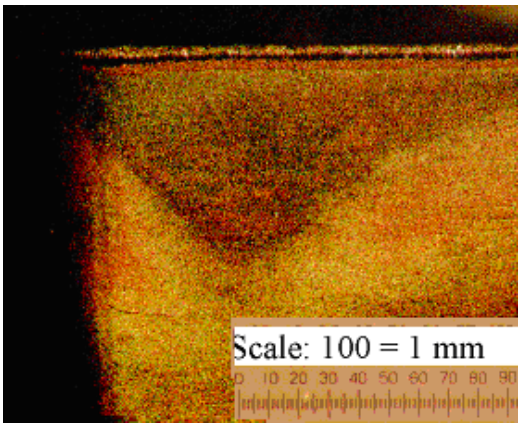

At a cutting speed of 190 m/min and feed rate of 0.23 mm/rev with a 2 mm depth of cut.

Figure 6.43: Picture showing flank wear of a dry cut after 7 minutes of machining.

The development of the flank wear was shown to take longer to develop when the cooled air was applied to the cutting zone as shown in Figure 6.44.

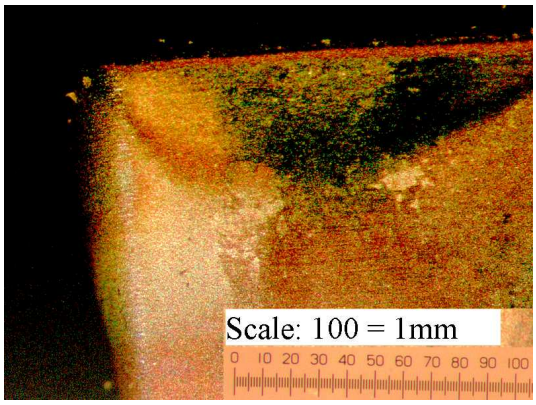

At a cutting speed of 190 m/min and feed rate of 0.23 mm/rev with a 2 mm depth of cut.

Figure 6.44: Picture showing flank wear for an air-cooled cut after 7 minutes of machining.

After seven minutes of dry machining the top rake face is starting to develop crater wear at 0.5 mm from the flank face as shown in Figure 6.45. Further dry machining will accelerate this rate of wear. At this stage the tool radius shows no sign of wear and the top flank edge has no observable notches.

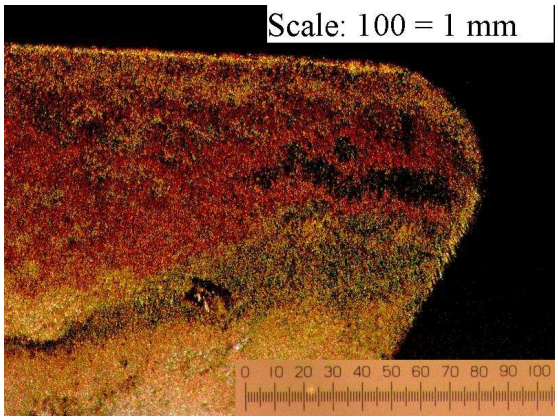

At a cutting speed of 190 m/min and feed rate of 0.23 mm/rev with a 2 mm depth of cut.

Figure 6.45: Picture showing top rake face wear for a dry cut after 7 minutes of machining.

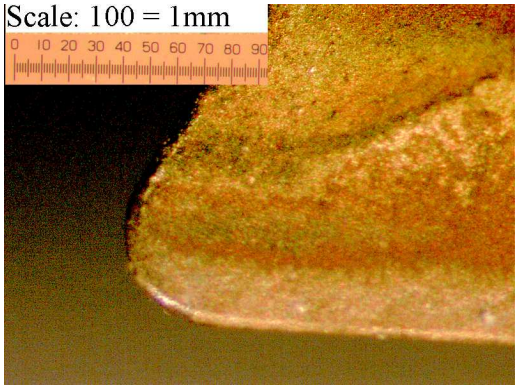

At a cutting speed of 190 m/min and feed rate of 0.23 mm/rev with a 2 mm depth of cut.

Figure 6.46: Picture showing top rake face wear for air-cooled cut after 7 minutes of machining.

With the air-cooled tool tip there are no visible signs of tool wear on the top rake face Figure 6.46, and the flank wear shown in Figure 6.41 and 6.42 is substantially reduced. Observation of the chips produced during dry and air-cooling indicated that much of the heat was being dissipated from the cutting zone. Figure 6.47 shows the chips produced during the dry and air-cooled tool tip test. From the colour of the chips a guide to the relative temperature can be made. Referring to Figure 5.2, dark blue (dry) indicates the chip temperature was approximately 750 ^{o}C, and gold indicates the chip temperature was approximately 600 ^{o}C.

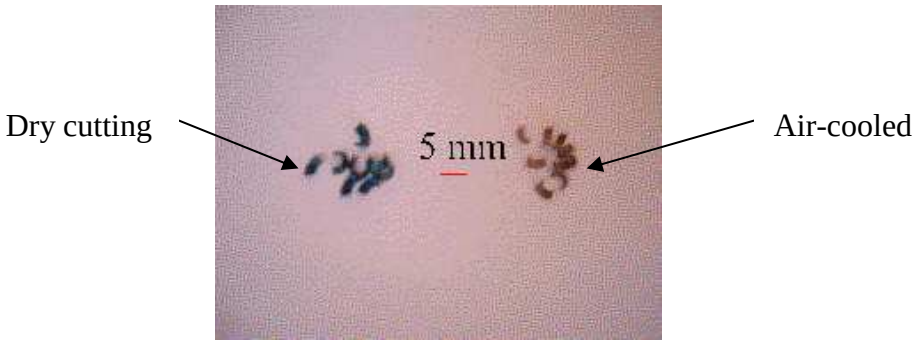

At 0.23 m/rev. feed rate, and cutting speed of 190 m/min.

Figure 6.47: Chips produced by a 2 mm depth of cut.

6.4.2 Discussion

Both the impingement and vortex tube experimental air-cooling systems have proved capable of dissipating the heat from the tool tip, proving that air-cooling is an effective method of cooling tools and increases the tool life. Whenever dry machining is considered to be the preferred method of metal cutting, it should be good practice to incorporate air-cooling. Also, air-cooling should be considered as an alternative to liquid cooling, as it was shown in this research that by reducing the temperature of the air, the tool is cooled to a point compatible with traditional coolant. Using an air-cooling system is found to be cost effective as there are no disposal costs associated with cooling, and is an environmentally friendly process. For practical operating reasons the vortex tube is the preferred option as it is more convenient for the machine operator to use as exact positioning of the cold air exit is not necessary. In addition the vortex tube is capable of cooling the air to –30 ^{o}C by a relatively low pressure supply of 0.8 MPa, which most workshops have readily available, making it convenient to use.

The most convenient method of determining tool life in this research is by using the tool tip temperature, as it has been shown that there is a relationship between the tool life and the wear mechanisms, which is shown to increase at elevated cutting temperatures. It was observed that when machining at the normal cutting speed for carbide tool tips it is not usual for the cutting tool temperatures to be above 800 ^{o}C. The result of this is the main wear mechanism is diffusion, and the temperature controls the rate of the wear process. Therefore, knowing the appropriate tool temperature, it should be possible to predict tool life when the tool life is defined in

terms of the flank ware. The relationship between tool life *L*, and the tool flank temperature, T_f can be obtained from equation (3.12) using the constants that are correct for their cutting conditions. However, equation (6.2) in the form of (3.12) has proved useful in determining the tool life, when using the temperature recorded from the imbedded thermocouple. The constants used reflect that the temperature that is measured in the tool tip is not as high as would be obtained from the tool flank face T_f.

$$L = 10^{2.974} T_{th}^{0.58} \tag{6.2}$$

The tool performance in section 6.4 examined tool tips which were tested over the same length of time and to ensure that the tool tips were being compared having completed the same amount of cutting. Even with measuring the tool tip temperature during the test there is still considerable time involved in completing all the tests to show the tool wear.

It may sound an easy challenge to measure or calculate the tool interface temperature, but as previously shown this task is fraught with difficulties. For example, there are large differences in temperature between the tool flank face and the position of the thermocouple that are measuring the tool temperature in the cutting zone. This makes it necessary to calculate the flank face temperature by using equation (3.15), which can be used to determine the tool life for the tool. If it is not possible to use the tool temperature to calculate the tool life then the only option is to carry out numerous tool cutting tests. However, to reduce the number of tool life tests it seems only logical that the factorial regression analysis method be used to determine the tool life constants for equation (3.2). Even with this method the number of required tool life tests are substantially making tool life tests time consuming and expensive, although the data that is obtained is precious in determining the performance of any cutting tool.

Previous researchers such as Liu *et al. [116], [42]* proved that compressed air did not achieve as good heat dissipation as oil water emulsion or water vapour during metal cutting as was shown in Figure 2.20. However, the results obtained from using

compressed air combined with the vortex tube have shown that this method of cooling the cutting zone is effective and compares exceedingly well with traditional methods. The effectiveness of air-cooling may be further improved by directing cold air through an air jet incorporated in the chip breaker on top of the tool.

CHAPTER 7

CONCLUSIONS

7.1 Introduction

Removing the liquid coolant from the machining process presents numerous challenges relating to machining, the primary challenges being heat dissipation from tool and workpiece, tool life, and chip removal. Certain systems and strategies can of course address these challenges. Heat removal by air requires a different approach to reduce the temperature of the tool tip compared to heat removal by liquid coolant. Special tooling using jet ducts, high-performance coated tool tips and chip evacuation systems may also be required in cooling the tool tip without the use of liquid coolant. When air-cooling is used it is necessary to show that the tool life is unchanged from wet machining and that the work piece quality is as good as, or better than, wet machining.

7.2 Significance And Outcomes

The significance of reducing the environmental burden produced by industry is now a prime objective, due to governmental registration and international regulations. For metal cutting the main source of environmental pollution is associated with traditional use of liquid coolants. This thesis has proved that air cooling can contribute to reducing or eliminating the reliance on liquid coolant used in metal cutting. Over the last few years some manufacturing industries have adopted dry machining for ductile materials which are relatively easy to machine. For harder materials coolant is found to be necessary to extend the tool life. The addition of air cooling for the machining of these materials is shown to have the same effect of extending the tool life. Therefore, for the majority of materials being machined in industry the use of air cooling is shown to be effective without adding to the cost of producing the product. In addition to the cost saving, the machine operators' health and working conditions will be improved as no liquid coolant is being used.

It has been shown that both impingement cooling and vortex tube cooling are capable of reducing the tool tip temperature during machining. The vortex tube air-cooling method has proved to be the most practical to use; it has also been found to be more robust and much easier to use. The vortex tube jet - unlike the impingement jet - had no reliance on jet operation position to produce the cooling effect on the tool tip. The vortex tube can be integral to the cutting tool because it does not have to rely on the position of the jet for the cooling. A combined vortex tube and lathe tool now has the advantage of being able to direct cold air along the rake face towards the tool cutting zone.

This thesis shows the beneficial effects of using air-cooling in metal cutting, and will help persuade the manufacturing industry to adopt this environmentally friendly air-cooling system. Worldwide saving in the amount of liquid coolant used would be enormous due to the massive amount of machining that is carried out, since metal cutting is still the primary manufacturing process used. Productivity and efficiency gains are the main advantages of having an effective air-cooling system as part of the metal cutting process: less money will be spent on tools and coolant. The goal is to keep the cutting edge "*cutting*", as productivity depends on reducing insert changing or indexing, i.e. cycle times, to produce a higher metal removal rate and consistent quality. These issues are overwhelmingly important to manufacturers, and air-cooling will help improve productivity by extending tool life when dry machining.

7.3 Recommendations And Possible Further Developments

Obtaining the temperature profiles of the tool tip allowed tool life expectancy to be determined for each of the cutting conditions. It is very important to be able to conveniently measure the tool tip temperature as this allows for an easy, reliable and quick method of determining the tool life. Recent developments in infrared measurement now allow you to measure the tool tip even more accurately than before, allowing the tool temperature to be used to give good estimates of tool life.

Future developments in this technology may be the inclusion of a very small quantity of oil to reduce the friction of the chip as it slides over the top rake face. Improving the chip removal from the cutting zone improves the air-cooling system. Materials

that create fine dust or fine cuttings need to be safely removed from the cutting area. Other machining operations such as drilling require further investigation to establish how best to provide cold air to the cutting edge of the drill.

The vortex tube method has been shown to be very effective for spot cooling, and the device itself is very simple, making it ideal for use in the workshop. Endeavour to reduce the temperature further at the cold exit jet is to take the cold exit air and pass it through a second stage vortex tube. This is only possible if there is sufficient pressure when the cold air leaves the cold exit. Another development which needs to be examined is how some other inert gas (eg. nitrogen) works with the vortex tube, as this may further improve the performance of cooling the tool tip. Carbon dioxide was tried in the mid 1950's, but was soon given up due to the cost of plant, and at that time environmental considerations were sadly of no great concern to the manufacturing industry.

7.4 Conclusion

Good classical thinking in metal cutting states that the best ratio of high productivity to low tool cost is obtained by selecting the maximum depth of cut and feed for the given situation. This thinking is correct as long as the tool tip can maintain an effective tool life, and produce the required surface finish. Using an efficient vortex tube to cool the tool during machining satisfies these conditions. This combination of air-cooling and dry machining gives an effective environmental tool cooling process. Twenty years ago the management and disposal of cutting fluids accounted for less than 3 percent of the production costs; today the cost has risen to 16 percent. Such costs explain why manufacturers are desperately looking for alternative methods to liquid coolant for cooling tool tip. This research has proven then that air-cooling using a vortex tube can certainly be considered as one of those methods.

REFERENCES

[1] M. E. Merchant, "Delphi-Type Forecast of the Future of Production Engineering," *C.I.R.P. Annals,* vol. 20, p. 213, 1971.

[2] E. J. A. Armarego and R. H. Brown, *The Machining of Metals*. New Jersey: Prentice-Hall, Inc, 1969.

[3] I. Finnie, "Review of the Metal Cutting Analyses of the Past Hundred Years," *Mechanical Engineering,* vol. 78, p. 715, 1956.

[4] W. Rosenhain and A. C. Sturney, "Report on Flow and Rupture of Metals During Cutting," *Proc. I. Mech. E.,* vol. 1, p. 141, 1925.

[5] H. Ernst, "Physics of Metals: Machining of Metals," *American Soc. for Metals,* 1938.

[6] G. C. I. Lin and P. l. B. Oxley, "Mechanics of Oblique Machining: Predicting Chip Geometry and Cutting Forces from Work Material properties and Cutting Conditions," *Proc. I. Mech. E.*, vol. 186, p. 813, 1972.

[7] M. P. Groover, *Fundamentals of Modern Manufacturing*: John Wiley and Sons. Inc, 2006.

[8] M. D. Centre, *Machine Data Handbook,* Third ed. vol. one. Cincinnati Ohio: Metcut Research Assoc. Inc, 1980.

[9] http://www.feret.com.au/c/Seco-Tools- Australia/Milling-turning-anddrilling-inserts-n689736, Uploaded on 26th January 2006.

[10] G. Boothroyd, "Temperature in Orthogonal Metal Cutting," *Proc. I. Mech. E.,* vol. 177, p. 789, 1963.

[11] H. Narita, H. Kawamura, T. Norihisa, L. Y. Chen, and H. Fujimoto, "Manufacturing Process Evaluation using Environmental Burden Analyzer

for Machine Tool Operation," in *18th International Conference on Production Research*, Salerno, Italy, 2005.

[12] D. Dudzinski, A. Devillez, A. Moufki, D. Larrouquere, V. Zerrouki, and J. Vigneau, "A review of developments towards dry and high speed machining of Inconel 718 alloy," *International Journal of Machine Tools and Manufacture,* vol. 44, pp. 439-456, 2004/3 2004.

[13] K. H. Causton, "An investigation into the suitability of dry machining automotive cylinder blocks for high volume production," in *Engineering* Bradford: University of Brdford, 2002.

[14] N. A. Abukhshim, P. T. Mativenga, and M. A. Sheikh, "Investigation of heat partition in high speed turning of high strength alloy steel," *International Journal of Machine Tools and Manufacture,* vol. In Press, Corrected Proof, 2005.

[15] B. T. Chao, H. L. Li, and K. J. Trigger, "The Influence of Tool Geometry on Interface Temperatures," *M.E. Tech. Rep.,* 1957.

[16] P. L. B. Oxley, "Mechanics of Metal Cutting for a Material of Various Flow Stress," *Trans. ASME,* vol. 85, p. p. 339, 1963.

[17] H. Ernst and M. E. Merchant, "Chip Formation, Friction and High Quality Machined Surfaces," *American Soc. for Metals,* p. 229, 1941.

[18] D. G. Christopherson, P. l. B. Oxley, and W. B. Palmer, "Orthogonal Cutting of a Work-hardened Material," *Engineering,* vol. 186, p. 623, 1959.

[19] Y. Altintas, *Manufacturing Automation*: Cambridge University Press, 2000.

[20] J. H. Weiner, "Shear Plane Temperature Distribution in Orthogonal Cutting," *Trans. ASME,* vol. 77, p. p. 1331, 1956.

[21] M. G. Steven and P. L. B. Oxley, "An Experimental Investigation of the Influence of Strain-rate and Temperature on the Flow Stress Properties of Low Carbon Steel Using a Machining Test," *Proc. I. Mech. E.,* vol. 185, p. pp. 741, 1971.

[22] N. Cook, "Tool Wear and Tool Life," *ASME Transactions,* vol. 95, pp. pp. 931-938, 1973.

[23] H. Saglam, F. Unsacar, and S. Yaldiz, "Investigation of the effect of rake angle and approaching angle on main cutting force and tool tip temperature," *International Journal of Machine Tools and Manufacture,* vol. 46, pp. 132-141, 2006/2 2006.

[24] H. A. Kishawy, M. Dumitrescu, E.-G. Ng, and M. A. Elbestawi, "Effect of coolant strategy on tool performance, chip morphology and surface quality during high-speed machining of A356 aluminum alloy," *International Journal of Machine Tools and Manufacture,* vol. 45, pp. 219-227, 2005/2 2005.

[25] M. E. Merchant, "The action of cutting fluids in machinery," *Iron and Steel Engineering,* vol. 27, pp. 101 -108, 1950.

[26] S. Kalpakjian and S. R. Schmid, *Manufacturing Engineering and Technology*, 5th ed.: Pearson Pretice Hall, 2005.

[27] M. C. Shaw, N. H. Cook, and P. A. Smith, "The Mechanics of Three-dimentional Cutting Operations," *Transactions of ASME,* pp. 1055-1064, 1962.

[28] F. Eugene, "Ann," *CIRP*, vol. 52(1), pp. 13-17, 1952.

[29] M. C. Shaw, J. D. Pigott, and L. P. Richardson, "Effect of Cutting Fluid upon Chip-Tool Interface Temperature," *Trans. Of ASME,* vol. 71, pp. 45-56, 1951.

[30] C. F. Shaw and M. Hattori, "Cost and Process Information Modelling for Dry Machining," *CiteSeer.ist,* pp. 1-8, 2004.

[31] P. Zelinski, "Where Dry Milling Makes Sense." vol. 2005: MMS Online, 2005.

[32] F. Georgia, "Near Dry Machining Means Improvements For Roof Rack Manufacturing." vol. 2005: MMS Online, 2005.

[33] A. E. Diniz and A. Jose de Oliveira, "Optimizing the use of dry cutting in rough turning steel operations," *International Journal of Machine Tools and Manufacture,* vol. 44, pp. 1061-1067, 2004/8 2004.

[34] A. E. Diniz and R. Micaroni, "Cutting conditions for finish turning process aiming: the use of dry cutting," *International Journal of Machine Tools and Manufacture,* vol. 42, pp. 899-904, 2002/6 2002.

[35] A. E. Diniz and R. Micaroni, "Influence of the direction and flow rate of the cutting fluid on tool life in turning process of AISI 1045 steel," *International Journal of Machine Tools and Manufacture,* vol. In Press, Corrected Proof.

[36] A. S. Varadarajan, P. K. Philip, and B. Ramamoorthy, "Investigations on hard turning with minimal cutting fluid application (HTMF) and its comparison with dry and wet turning," *International Journal of Machine Tools and Manufacture,* vol. 42, pp. 193-200, 2002/1 2002.

[37] M. Rahman, A. Senthil Kumar, and M. U. Salam, "Experimental evaluation on the effect of minimal quantities of lubricant in milling," *International Journal of Machine Tools and Manufacture,* vol. 42, pp. 539-547, 2002/4 2002.

[38] R. J. Piggot and A. T. Coldwell, "H-jet system for increasing tool life," *SAE Quarterly Transanction,* vol. 6, pp. 547-564, 1952.

[39] P. Dahlman and M. Escursell, "High-pressure jet-assisted cooling: a new possibility for near net shape turning of decarburized steel," *International Journal of Machine Tools and Manufacture,* vol. 44, pp. 109-115, 2004/1 2004.

[40] V. V. Podgorkov, "Method of Cutting in Application," in *Patent of USSR #1549721 MCI B23Q* Russia, 1992.

[41] V. A. Godlevski, "Water Steam Lubrication During Machining," *Tribologia,* vol. 162, pp. 890-901, 1998.

[42] J. Liu, R. Han, and Y. Sun, "Research on experiments and action mechanism with water vapor as coolant and lubricant in Green cutting," *International Journal of Machine Tools and Manufacture,* vol. 45, pp. 687-694, 2005/5 2005.

[43] S. Y. Hong and Y. Ding, "Cooling approaches and cutting temperatures in cryogenic machining of Ti-6Al-4V," *International Journal of Machine Tools and Manufacture,* vol. 41, pp. 1417-1437, 2001/8 2001.

[44] S. Y. Hong, Y. Ding, and W.-c. Jeong, "Friction and cutting forces in cryogenic machining of Ti-6Al-4V," *International Journal of Machine Tools and Manufacture,* vol. 41, pp. 2271-2285, 2001/12 2001.

[45] F. W. Taylor, "On the art of cutting metal," *Trans. ASME,* vol. 28, p. 31, 1907.

[46] J. Talylor, "The tool wear-time relationship in metal cutting," *Int. J. Mach. Tool Des. and Res.,* vol. 2, p. 119, 1962.

[47] R. Woxen, *Tool-life and Balance of Heat in lathe work* vol. 142. Stockholm: Handlingar, 1937.

[48] B. N. Colding, *A wear relationship for turning, milling and grinding*. Stockholm: Lund Press, 1959.

[49] D. A. Axinte, W. Belluco, and L. De Chiffre, "Reliable tool life measurements in turning -- an application to cutting fluid efficiency evaluation," *International Journal of Machine Tools and Manufacture,* vol. 41, pp. 1003-1014, 2001/5 2001.

[50] A. L. B. Dos Santos, M. A. V. Duarte, A. M. Abrao, and A. R. Machado, "An optimisation procedure to determine the coefficients of the extended Taylor's equation in machining," *International Journal of Machine Tools and Manufacture,* vol. 39, pp. 17-31, 1999/1 1999.

[51] K. J. Trigger and B. T. Chao, "The mechanisim of creater wear of cemented carbide tools," *Trans. ASME,* vol. 78, p. 1113, 1956.

[52] J. Sata, "Crater wear of carbide cutting tools," *Nihon Kikai Gakkai Ronbunshu,* vol. 25, p. 988, 1959.

[53] E. G. Lowen and M. C. Shaw, "On the analysis of cutting tool temperatures," *Trans. ASME,* vol. 76, p. 217, 1954.

[54] H. Takayama and R. Murata, "Basic investigation of tool wear," *Trans. ASME, J. Eng. Ind.,* vol. 85, p. 33, 1963.

[55] P. l. B. Oxley, W. F. Hastings, and M. G. Stevenson, "Predicting cutting forces, tool life,etc. using work material flow stress properties obtained from high speed compression tests," in *Proc. Int. on Prod. Eng.*, Tokyo, 1974, p. 528.

[56] G. Boothroyd, J. M. Eagle, and A. W. J. Chisholm, "Effect of tool flank wear on the temperatures generated during metal cutting," in *Proc. 8th Int. M.T.D.R. Conf.*, 1967, p. 667.

[57] W. F. Hastings and P. l. B. Oxley, "Predicting tool life from fundamental work material properties and cutting conditions," *C.I.R.P. Annals,* vol. 25/1, p. 33, 1976.

[58] B. T. Chao and K. J. Trigger, "Cutting temperatures and metal cutting phenomena," *Trans. ASME,* vol. 73, p. 777, 1951.

[59] R. N. Richardson, W. F. Hastings, and P. l. B. Oxley, "Predicting tool-life and built-up edge occurrence when machining plain carbon steel with high speed cutting tools," *I. E. Aust.,* vol. ME3, p. 50, 1978.

[60] W. F. Hastings, P. Mathew, P. l. B. Oxley, and J. Talylor, "Estimated cutting temperatures - their use as a predictor of tool performance when machining plain carbon steel," in *20th Int. M.T.D. R. conference,* 1979, p. 313.

[61] A. A. Zakaria and J. I. Gomayel, "On the reliability of the cutting temperature for monitoring tool wear," *Int. J. Mach. Tool Des. and Res.,* vol. 15, p. 195, 1975.

[62] T. N. Loladge, "Adhesion and diffussion wear in metal cutting," *Inst. Engrs. India,* vol. 43, p. 108, 1962.

[63] H. Suzuki and T. Yamamoto, "Cratering wear of cemented carbides in relation to carbon content in tools and machined steel," *Trans J.I.M.,* vol. 10, 1969.

[64] N. Narutaki and Y. Yamane, "Wear mechanism of carbide tool based on the reaction between tool and work material," *Bull. Japan Soc. Prec. Eng.,* vol. 10, pp. 95 - 133, 1976.

[65] L. Walter, "Carbon dioxide as cutting tool coolant repays research with imposing savings," *Canadian Machining and Metalworking,* vol. 76, p. 94, 1965.

[66] W. S. Hollis, "The application and effect of controlled atmosheres in the machining of metals," *Int. J. Mach. Tool Des. and Res.*, vol. 1, p. 59, 1961.

[67] G. Pahlitzsch, "Gases are good cutting coolants," *American Machinist*, vol. 97, p. 196, 1953.

[68] M. Angioletti, R. M. Di Tommaso, E. Nino, and G. Ruocco, "Simultaneous visualization of flow field and evaluation of local heat transfer by transitional impinging jets," *International Journal of Heat and Mass Transfer*, vol. 46, pp. 1703-1713, 2003/5 2003.

[69] D. H. Lee, Y. S. Chung, and M. G. Kim, "Technical NoteTurbulent heat transfer from a convex hemispherical surface to a round impinging jet," *International Journal of Heat and Mass Transfer*, vol. 42, pp. 1147-1156, 1999/3/1 1999.

[70] M. Angioletti, E. Nino, and G. Ruocco, "CFD turbulent modelling of jet impingement and its validation by particle image velocimetry and mass transfer measurements," *International Journal of Thermal Sciences*, vol. 44, pp. 349-356, 2005/4 2005.

[71] D. Hee Lee, S. Youl Won, Y. Taek Kim, and Y. Suk Chung, "Turbulent heat transfer from a flat surface to a swirling round impinging jet," *International Journal of Heat and Mass Transfer*, vol. 45, pp. 223-227, 2002/1 2002.

[72] F. P. Incropera and D. P. De Witt, *Fundamentals of Heat and Mass Transfer*: John Wiley, 1981.

[73] J.-Y. San, C.-H. Huang, and M.-H. Shu, "Impingement cooling of a confined circular air jet," *International Journal of Heat and Mass Transfer*, vol. 40, pp. 1355-1364, 1997/4 1997.

[74] G. Ranque, "Experiences sur la detente giratore avec productions simulanees d'un echappement d'air chaud et d'um echappement d'air froid," *Journal de Physique et de la Radium,* vol. 4, pp. 1125-1155, 1933.

[75] R. Hilsch, "The use of the expansion of gases in a centrifugal field as a cooling process," *The review of Sicentific Instrumets,* vol. 18(2), p. 108ff, 1947.

[76] R. G. Deissler and M. Perlmutter, "Analysis of the flow and energy separation in a turbulent vortex," *International Journal of Heat and Mass Transfer,* vol. 1, pp. 173-191, 1960/8 1960.

[77] M. Kurosaka, "Acoustic streaming in swirling flow," *Journal of Fluid Mechanics,* p. 139ff, 1982.

[78] A. I. Gulyaev, "Vortex tube and the vortex effect," *Soviet Physics: Technical Physics,* vol. 10(10), p. 1441ff, 1966.

[79] K. Stephan, S. Lin, M. Durst, F. Huang, and D. Seher, "An investigation of energy separation in a vortex tube," *International Journal of Heat and Mass Transfer,* vol. 26, pp. 341-348, 1983/3 1983.

[80] J. Lewins and A. Bejan, "Vortex tube optimization theory," *Energy,* vol. 24, pp. 931-943, 1999/11 1999.

[81] S. Eiamsa-ard and P. Promvonge, "Numerical investigation of the thermal separation in a Ranque-Hilsch vortex tube," *International Journal of Heat and Mass Transfer,* vol. In Press, Corrected Proof, 2006.

[82] M. H. Saidi and M. R. Allaf Yazdi, "Exergy model of a vortex tube system with experimental results," *Energy,* vol. 24, pp. 625-632, 1999/7 1999.

[83] M. P. Siverman, "The wirbelrohr's roar," *Cambridge University Press,* vol. 6, pp. 221-240, 1993.

[84] S. H. Yeo and S. H. Ong, "Assessment of the thermal effects on chip surfaces," *Journal of Materials Processing Technology*, vol. 98, pp. 317-321, 2000/2/14 2000.

[85] E. M. Trent, "Some factors affecting wear on cemented carbide tools," *Proc. I. Mech. E.*, vol. 166, p. 64, 1952.

[86] E. M. Trent, "Metal cutting and the tribology of seizure: I seizure in metal cutting," *Wear*, vol. 128, pp. 29-45, 1988/11/15 1988.

[87] E. M. Trent, "Metal cutting and the tribology of seizure: II movement of work material over the tool in metal cutting," *Wear*, vol. 128, pp. 47-64, 1988/11/15 1988.

[88] P. K. Wright and E. M. Trent, "Metallographic methods of determining temperature gradients in cutting tools," *Journal Iron and Steel Inst.*, vol. 211, p. 364, 1973.

[89] e. a. Chris Constable, "Up Close - new tool understanding wear processes," in *Materials World*, 2002, pp. 10 -12.

[90] D. Jianxin, L. Lili, L. Jianhua, Z. Jinlong, and Y. Xuefeng, "Failure mechanisms of TiB2 particle and SiC whisker reinforced Al2O3 ceramic cutting tools when machining nickel-based alloys," *International Journal of Machine Tools and Manufacture*, vol. 45, pp. 1393-1401, 2005/10 2005.

[91] F. Z. Schwerd, "Uber die bestimmung des terperaturfeldes beim spanablauf," *Zeitschrift des Vereines Deutscher Ingenieure*, vol. 77, pp. 211-216, 1937.

[92] Y. K. Potdar and A. T. Zehnder, "Measurements and simulations of temperature and deformation fields in transient metal cutting.," *Journal of Manufacturing Science and Engineering*, vol. 125, pp. 645-655, 2003.

[93] Y. K. Potdar and A. T. Zehnder, "Temperature and deformation measurement in transient metal cutting.," *Experimental Mechanics,* vol. 44, pp. 1-9, 2004.

[94] G. S. Reichenbach, "Experimental measurement of metal cutting temperature," *Trans ASME,* vol. 80, p. 525, 1958.

[95] B. T. Chao and K. J. Trigger, "On experimental investigation of temperature distribution at tool-flank surface," *Trans ASME,* vol. 83, p. 496, 1961.

[96] G. Arndt and R. H. Brown, "On the temperature distribution on orthogonal machining," *Int. J. Mach. Tool Des. and Res.,* vol. 7, p. 39, 1967.

[97] E.-G. Ng, D. K. Aspinwall, D. Brazil, and J. Monaghan, "Modelling of temperature and forces when orthogonally machining hardened steel," *International Journal of Machine Tools and Manufacture,* vol. 39, pp. 885-903, 1999/6 1999.

[98] E. Lenz, "Die temperaturmessung in der kontaktzone Spanwerkzeug beim drehvogang," *C.I.R.P. Annals,* vol. 13, p. 201, 1966.

[99] M. Y. Friedman and E. Lenz, "Determination of temperature field on uper chip surface," *C.I.R.P. Annals,* vol. 19, p. 395, 1971.

[100] S. Jeelani, "Measurement of temperature distribution in machining using IR photography," *Wear,* vol. 68, p. 191, 1981.

[101] P. Kwon, T. Schiemann, and R. Kountanya, "An inverse estimation scheme to measure steady-state tool-chip interface temperatures using an infrared camera," *International Journal of Machine Tools and Manufacture,* vol. 41, pp. 1015-1030, 2001/5 2001.

[102] G. Sutter, L. Faure, A. Molinari, N. Ranc, and V. Pina, "An experimental technique for the measurement of temperature fields for the orthogonal

cutting in high speed machining," *International Journal of Machine Tools and Manufacture,* vol. 43, pp. 671-678, 2003/5 2003.

[103] E. G. Herbert, "The measurement of cutting temperatures," *Proc. I. Mech. E.,* vol. 1, pp. 289-329, 1926.

[104] J. G. Balint and R. H. Brown, "A note on the investigation of rake face tool wear," *Int. J. Mach. Tool Des. and Res.,* vol. 4, p. 117, 1964.

[105] B. T. Chao and K. J. Trigger, "The influence of tool geometry on interface temperature," *M.E. Tech. Rep.,* pp. 1-50, 1957.

[106] A. C. Rapier, "A theoretical investigation of the temperature distribution in the metal cutting process," *Brit. J. Appl. Physics,* vol. 5, pp. 400-410, 1954.

[107] H. T. Young and H. Y. Liou, "On the analysis of chip temperature distribution in orthogonal machining," *International Journal of Machine Tools and Manufacture,* vol. 34, pp. 73-84, 1994/1 1994.

[108] T. Kitagawa, Kubo, and K. Maekawa, "Temperature and wear cutting tools in high-speed machining on Inconel 718 and Ti-6AI-6V-2Sn," *Wear,* vol. 202, pp. 142-148, 1997.

[109] D. O'Sullivan and M. Cotterell, "Temperature measurement in single turning point," *Journal Master. Proc. Tech.,* vol. 118, pp. 301-308, 2001.

[110] H. Ay and W.-J. Yang, "Heat transfer and life of metal cutting tools in turning," *International Journal of Heat and Mass Transfer,* vol. 41, pp. 613-623, 1998/2 1998.

[111] T. Obikawa, T. Matsumura, T. Shirakashi, and E. Usui, "Wear characteristic of alumina coated and alumina ceramic tools," *Journal of Materials Processing Technology,* vol. 63, pp. 211-216, 1997/1 1997.

[112] E. Usui, T. Shirakashi, and T. Kitagawa, "Analytical prediction of cutting tool wear," *Wear,* vol. 100, pp. 129-151, 1984/12 1984.

[113] J. Lee and S.-J. Lee, "The effect of nozzle configuration on stagnation region heat transfer enhancement of axisymmetric jet impingement," *International Journal of Heat and Mass Transfer,* vol. 43, pp. 3497-3509, 2000/9/15 2000.

[114] A. Y. Tong, "On the impingement heat transfer of an oblique free surface plane jet," *International Journal of Heat and Mass Transfer,* vol. 46, pp. 2077-2085, 2003/5 2003.

[115] J.-Y. San and M.-D. Lai, "Optimum jet-to-jet spacing of heat transfer for staggered arrays of impinging air jets," *International Journal of Heat and Mass Transfer,* vol. 44, pp. 3997-4007, 2001/11 2001.

[116] J. Liu, R. Han, L. Zhang, and H. Guo, "Study on lubricating characteristic and tool wear with water vapour as coolant and lubricant in green cutting," *Wear,* vol. In Press, Corrected Proof.

Appendix A

Parameters Investigated To Obtain The Optimum Vortex Tube

The following parameters were recorded and are taken into consideration for each test:

1. Mass flow rate of the cold and hot air $(\dot{m}_c, \dot{m}_h)$
2. Nozzle diameter of the inlet compressed air (D_i)
3. Cold nozzle diameter (D_c)
4. Hot nozzle diameter (D_h)
5. Ratio of the tube length to the tube diameter $\frac{L_t}{D_T}$
6. Pressure of the inlet compressed air (P_i)
7. Vortex generator shape
8. Valve design
9. Inlet temperature (Ti)

The thermocouple for measuring the cold air was positioned at a distance of 10 mm from the cold exit-jet, the compressed air supply temperature was measured at the air inlet to the vortex generator. The hot air temperature was measured as it escapes to the surrounding air. Conformity of each test was maintained by marking the position of the control valve allowing other variables in the system to be changed with respect to the same vortex tube control valve setting.

Test series 1 - The tests were repeated with different jet nozzle diameters to find the jet diameter with the highest efficiency (the coldest exit air): the most efficient jet nozzle was then used throughout subsequent tests. In addition to the jet nozzle the insertion of an orifice plate between the nozzle and the vortex generator can provide additional cooling of the air if required.

Test series 2 - Two different designed vortex generators are shown in Figure 4.15(c), each being tested to determine the efficiency of their vortex generating ability. The results obtained from the tests were compared, with the most efficient being selected to be used in the succeeding tests

.

Test series 3 - The most efficient nozzle jet and vortex generator is now used to determine the most efficient tube length. This configuration is now used to investigate the effect of different pressures on the performance of the vortex tube. For these tests only hot tube length is varied, as previous research by M.H. Saidi *et al.* has shown that varying the length of the cold tube does not affect the efficiency of the tube. The tube diameter is also kept constant throughout these experiments, enabling the tube length to diameter ratio to be established.

Test series 4 - The vortex tube was tested over three different pressures, with one of the pressures being above the designated pressure used in the initial experiments, while the other one is below the default pressure. The effectiveness of the vortex tube tested can be designated as that which gives the largest temperature drop, which may be obtained at the cold inlet (Ti-Tc).

For each of the test series it was necessary to ensure that the test equipment and vortex tube were properly set to the same start point for each test, and that the temperatures were recorded only when the temperatures had reached their optimum. The flowmeter was positioned in series with the pressure valve and pressure gauge in order to obtain the volumetric flow rate of the inlet compressed air. Once this was done, the compressed air was allowed to flow into the inlet by opening the pressure valve to an inlet value. The test was started with a fully closed control valve on the vortex tube, and the volumetric flow rate of the compressed air was measured using the flow meter, and the inlet flow rate and outlets temperatures was recorded.

The vortex tube control valve was slightly opened to the next position (vertical line), and the flowmeter and temperatures read at this position. During this time the supply pressure from the compressor was constantly monitored on the pressure gauge, and the pressure valve was adjusted to return the pressure to the designated value if necessary. This procedure outlined was repeated until the control valve was completely opened; this process was carried out for all tests. For all the tests the input and output temperatures were recorded on the computer for later analysis. This process was repeated three times for every test in order to get an average value from the readings which were then used for analysis.

Having completed this set of tests, the experimental setup was rearranged to enable the measurement of the volumetric flow rate of the hot outlet air. (This inconvenient rearrangement was made necessary due to having only one flow meter available for the experiment) All of the tests were repeated with the same position of the vortex control valve and the same inlet pressure of the compressed air, and the volumetric flow rate of the hot outlet air was measured and recorded. This procedure was repeated for all positions of the control valve, with the inlet pressure being kept constant throughout the experiment.

It was noticed during the temperature measurements that the temperature of the cold stream changed along the diameter of the nozzle. This meant that by changing the position of the thermocouple along the diameter of the nozzle a different temperature was measured. This problem was due to the fact that the temperature profile was not uniform inside the nozzle. Also, with regard to the high angular velocity of the swirling flow, it was not possible to put the thermocouple inside the nozzle as it started to vibrate causing fluctuations of the recorded temperature. Finally, by inserting the thermocouple inside the nozzle, it was observed that a layer of ice was created on the surface of the tip of the thermocouple due to the existence of a small amount of humidity in the air flow. This layer of ice could act as an insulator and therefore measuring the real temperature of the cold stream was more difficult to measure.

Appendix B

Thermoelectric Voltages Used For Calibration

There are a number of web addresses that give the full (mV) calibration data for thermocouples. The calibration data given in Table B.1 is for a K type thermocouple, and only shows part of the thermoelectric voltage range.

Table B.1 obtained from the web address:

http://srdata.nist.gov/its90/useofdatabase/use_of_database.html (7th December 2006)

Another suitable web address is: http://www.omega.com/temperature/Z/pdf/z204-206.pdf

Table B.1: Sample of Thermoelectric Voltage for type K thermocouple

°C	Thermoelectric Voltage in mV										
	0	-1	-2	-3	-4	-5	-6	-7	-8	-9	-10
-40	-1.527	-1.564	-1.600	-1.637	-1.673	-1.709	-1.745	-1.782	-1.818	-1.854	-1.889
-30	-1.156	-1.194	-1.231	-1.268	-1.305	-1.343	-1.380	-1.417	-1.453	-1.490	-1.527
-20	-0.778	-0.816	-0.854	-0.892	-0.930	-0.968	-1.006	-1.043	-1.081	-1.119	-1.156
-10	-0.392	-0.431	-0.470	-0.508	-0.547	-0.586	-0.624	-0.663	-0.701	-0.739	-0.778
0	0.00	-0.039	-0.079	-0.118	-0.157	-0.197	-0.236	-0.275	-0.314	-0.353	-0.392

°C	Thermoelectric Voltage in mV										
	0	1	2	3	4	5	6	7	8	9	10
0	0.000	0.039	0.079	0.119	0.158	0.198	0.238	0.277	0.317	0.357	0.397
10	0.397	0.437	0.477	0.517	0.557	0.597	0.637	0.677	0.718	0.758	0.798
20	0.798	0.838	0.879	0.919	0.960	1.000	1.041	1.081	1.122	1.163	1.203
30	1.203	1.244	1.285	1.326	1.366	1.407	1.448	1.489	1.530	1.571	1.612
40	1.612	1.653	1.694	1.735	1.776	1.817	1.858	1.899	1.941	1.982	2.023
50	2.023	2.064	2.106	2.147	2.188	2.230	2.271	2.312	2.354	2.395	2.436
60	2.436	2.478	2.519	2.561	2.602	2.644	2.685	2.727	2.768	2.810	2.851

This information was last uploaded on 7th December 2006

Appendix C

Impingement Jet Nozzle Test

The following parameters were recoded and taken into consideration for each test:

1. Mass flow rate of the air $(\dot{m}_c)$
2. Nozzle inlet pressure (P_i)
3. Atmospheric pressure (P_a)
4. Room temperature (T_r)
5. Ratio of the diameter and air gap $\frac{G}{D}$
6. Pressure of the supplied compressed air (P_s)
7. Position of nozzle.
8. Air inlet temperature (Ti)
9. Tool tip temperatures (at Ch13, Ch14 and Ch15)

To allow for the numerous changes to be made, an adjustable nozzle holder was made ensuring that the correct position was used for each test carried out as shown in Figure C.1(a)(b)&(c).

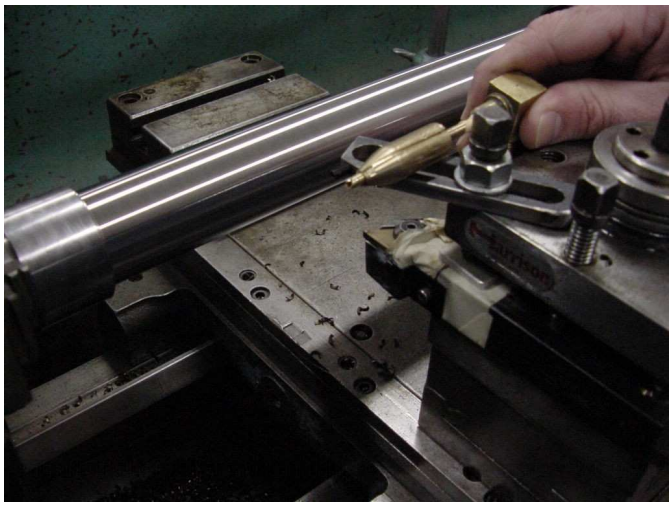

Figure C.1(a): Adjustable nozzle holder suitable for different diameter nozzles.

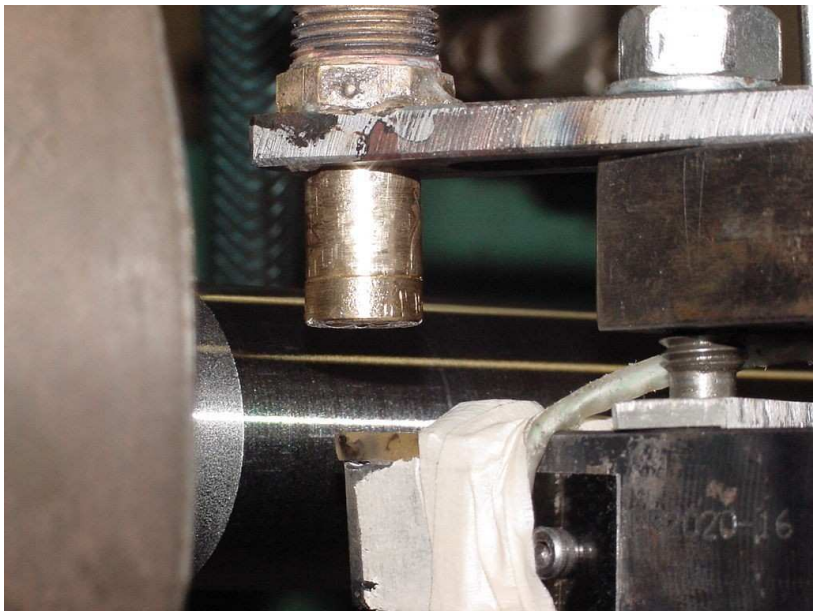

Figure C.1(b): Adjustable nozzle holder suitable for angling nozzle.

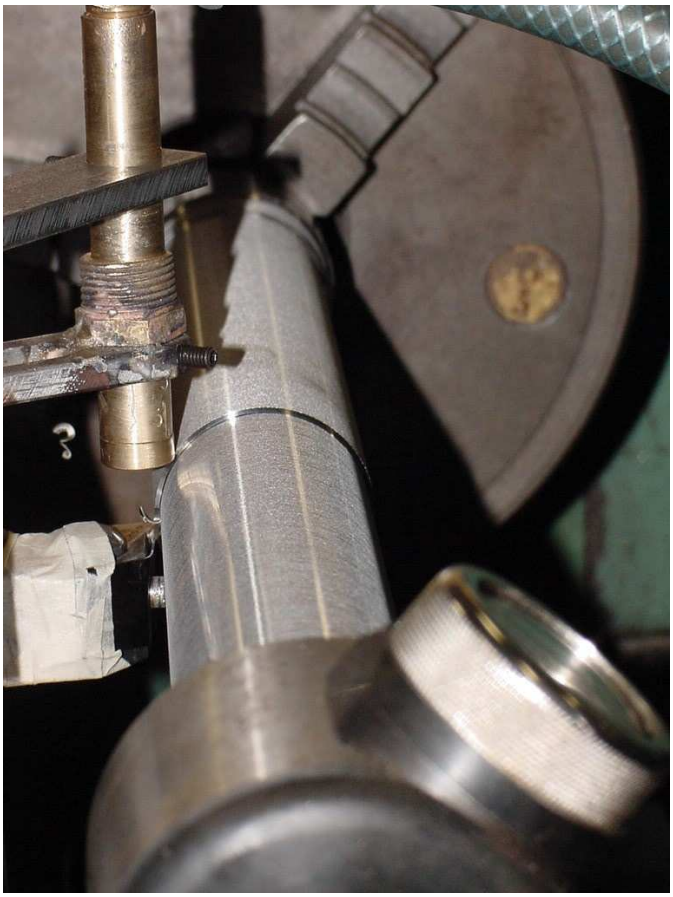

Figure C1(c):Tool tip and chips being cooled by a 3 nozzle jet

Appendix D

Vortex Tube Jet Nozzle Tests

The following parameters were recoded and taken into consideration for each test:

1. Mass flow rate of the air $(\dot{m}_c)$
2. Vortex inlet pressure (P_i)
3. Atmospheric pressure (P_a)
4. Room temperature (T_r)
5. Cold tube temperature (T_c)
6. Pressure of the supplied compressed air (P_i)
7. Position of nozzle.
8. Air inlet temperature (Ti)
9. Tool tip temperature

To allow the vortex tube to have its position adjusted, a clamp sleeve was made to hold the vortex tube on to a magnetic base. This allowed the vortex tube to be positioned appropriately for machining as shown in Figure D.1.

Figure D.1: Clamp arrangement for holding vortex tube during machining

Appendix E

Typical Temperatures Recorded During Machining

Example of a typical data logger temperatures (^{o}C), recorded during machining tests using impingement cooling method.

VIRTUALBENCH-LOGGER 2.5 REPORT
NATIONAL INSTRUMENTS
TIME CREATED 14:41:53

USER Brian Boswell

START COMMENT
Multi-hole nozzle - 4 holes 5mm gap using air bottle feed rate 0.23 rpm1400 39 dia bar
END COMMENT

START DATA

Date	Time	Ch13	Ch14	Ch15
04/22/2004	42:23.5	27	22	27
04/22/2004	42:25.3	83	36	90
04/22/2004	42:27.1	87	45	102
04/22/2004	42:28.9	92	50	107
04/22/2004	42:30.7	93	52	111
04/22/2004	42:32.5	94	53	112
04/22/2004	42:34.4	87	54	113
04/22/2004	42:36.2	84	55	114
04/22/2004	42:38.0	85	55	114
04/22/2004	42:39.8	86	56	114
04/22/2004	42:41.6	88	56	114
04/22/2004	42:43.4	89	56	114
04/22/2004	42:45.2	90	56	115

04/22/2004	42:47.0	92	56	115
04/22/2004	42:48.8	91	57	115
04/22/2004	42:50.6	87	57	116
04/22/2004	42:52.4	69	57	114
04/22/2004	42:54.2	64	57	115
04/22/2004	42:56.1	63	57	114
04/22/2004	42:57.9	63	57	114
04/22/2004	42:59.7	63	57	115
04/22/2004	43:01.5	64	58	115

Example of typical data logger report (temperatures) recorded during machining tests using a vortex cooling method.

VIRTUALBENCH-LOGGER 2.5 REPORT
NATIONAL INSTRUMENTS
TIME CREATED 11:09:24

USER Brian Boswell

START COMMENT
Orifice plate of 7 mm dia. cutting test 40 dia. bar 1400 rpm feed 0.23 mm/rev

END COMMENT

START DATA

Date	Time	Ch13	Ch14	Ch15
2/11/2005	13:11.4	21	20	20
2/11/2005	13:13.2	21	19	17
2/11/2005	13:15.0	19	16	14
2/11/2005	13:16.8	17	14	12
2/11/2005	13:18.6	16	13	11
2/11/2005	13:20.4	15	12	10
2/11/2005	13:22.2	41	71	109
2/11/2005	13:24.0	55	86	119

2/11/2005	13:25.8	78	93	124
2/11/2005	13:27.7	98	96	130
2/11/2005	13:29.5	116	92	136
2/11/2005	13:31.3	112	88	131
2/11/2005	13:33.1	107	89	127
2/11/2005	13:34.9	102	91	127
2/11/2005	13:36.7	92	91	126
2/11/2005	13:38.5	89	92	135
2/11/2005	13:40.3	86	90	130
2/11/2005	13:42.1	83	90	129
2/11/2005	13:43.9	82	90	130
2/11/2005	13:45.7	82	91	132
2/11/2005	13:47.6	83	92	134
2/11/2005	13:49.4	79	88	124
2/11/2005	13:51.2	78	88	125
2/11/2005	13:53.0	76	85	123
2/11/2005	13:54.8	75	85	122
2/11/2005	13:56.6	76	85	123
2/11/2005	13:58.4	76	85	123
2/11/2005	14:00.2	75	84	123
2/11/2005	14:02.0	74	83	120
2/11/2005	14:03.8	45	48	50
2/11/2005	14:05.6	31	31	31
2/11/2005	14:07.4	27	27	27
2/11/2005	14:09.3	25	25	25
2/11/2005	14:11.1	24	23	23
2/11/2005	14:12.9	23	22	22
2/11/2005	14:14.7	22	21	21
2/11/2005	14:16.5	22	21	21
2/11/2005	14:18.3	21	21	20
2/11/2005	14:20.1	21	20	20
2/11/2005	14:21.9	21	20	20
2/11/2005	14:23.7	21	20	20
2/11/2005	14:25.5	21	20	19

2/11/2005	14:27.3	21	20	19
2/11/2005	14:29.2	21	20	19
2/11/2005	14:31.0	21	20	19
2/11/2005	14:32.8	21	20	19
2/11/2005	14:34.6	21	20	19
2/11/2005	14:36.4	21	20	19
2/11/2005	14:38.2	21	20	19
2/11/2005	14:40.0	20	20	19

END DATA

Example of a typical infrared report (temperatures) recorded during machining tests.

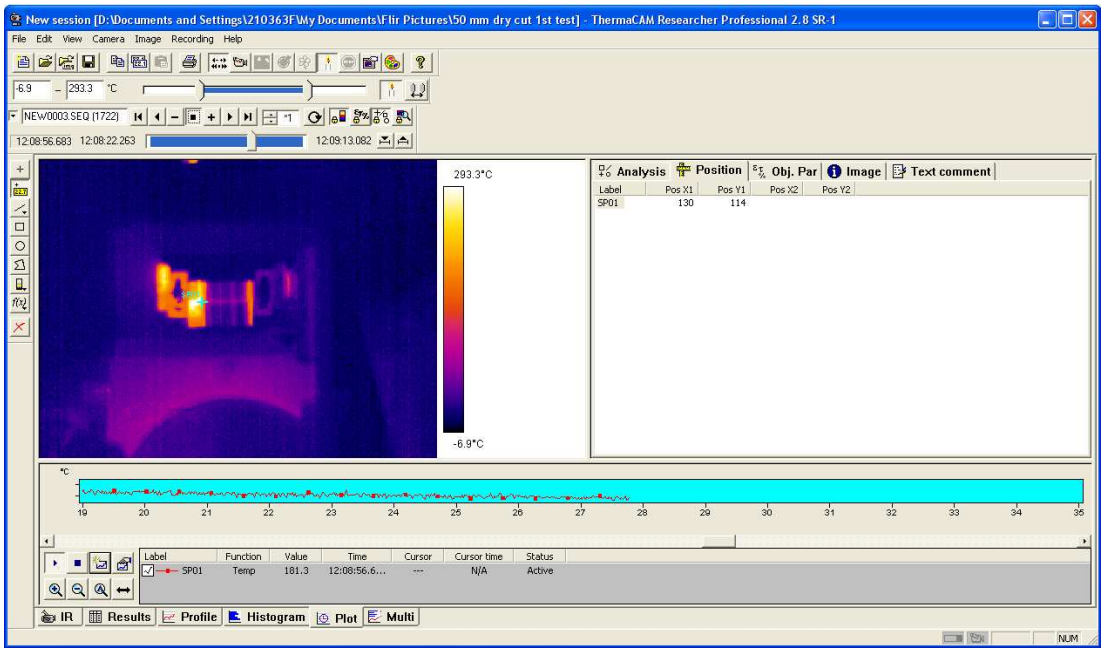

Figure E1: Shows the continuous temperature measurements for a dry cut.

The infrared software allows you to analyse any point on the tool tip after recording the machining process with the infrared camera.

Appendix F

Publications and Conference Presentations

[1] B. Boswell, T. T. Chandratilleke, “Use of Air-cooling to Reduce Tool Life Cycle Testing “, in proceedings of the International Manufacturing Leaders Forum, Adelaide, Australia, 2005.

[2] B. Boswell, T. T. Chandratilleke, “The Introduction Of An Environmental Cooling Method Is Proved By Using A Reduced Tool Life Cycle Time Method “, International Journal of Computer Integrated Manufacturing, May 2007.

[3] B. Boswell, T. T. Chandratilleke, “Improved Dry Cutting Tool Life By Air-cooling “,in proceedings of the 18th International Conference on Production Research, Salerno, Italy, 2005.

[4] B.Boswell, T. T. Chandratilleke, “Air-Cooling Used For Metal Cutting’, in proceedings of the International Manufacturing Leaders Forum, Taipei, Taiwan, 2006.

[5] B. Boswell, T. T. Chandratilleke, “Air-Cooling the Environmental Method of Metal Cutting”, in proceedings of the 4Th International Conference on Environmental, Cultural, Economic and Social Sustainability, Terengganu, Malaysia, January 2008.

[6] B. Boswell, T. T. Chandratilleke, “Air-Cooling Used For Metal Cutting“, American Journal of Applied Science, March 2008.

[7] B. Boswell, T. T. Chandratilleke, “An Environmental Friendly Method of Metal Cutting”, International Journal of Environmental, Cultural, Economic and Social Sustainability, Volume 4, Issue 3, June 2008.